



Raylane de Souza Castoldi

**Influence of surface modifications on sisal
fiber durability and interface bond towards
cement-based matrices**

Tese de Doutorado

Thesis presented to the Programa de Pós-Graduação em Engenharia Civil Department of PUC-Rio in partial fulfillment of the requirements for the degree of Doutor em Ciências – Engenharia Civil.

Advisor: Prof. Flávio de Andrade Silva

Co-advisor: Lourdes Maria Silva de Souza

Rio de Janeiro
February 2023



Raylane de Souza Castoldi

**Influence of surface modifications on sisal
fiber durability and interface bond towards
cement-based matrices**

Thesis presented to the Programa de Pós-Graduação em Engenharia Civil Department of PUC-Rio in partial fulfillment of the requirements for the degree of Doutor em Ciências – Engenharia Civil. Approved by the Examination Committee:

Prof. Flávio de Andrade Silva

Advisor

Department of Civil and Environmental Engineering – PUC-Rio

Prof. Lourdes Maria Silva de Souza

Co-advisor

Department of Civil and Environmental Engineering – PUC-Rio

Prof. Daniel Taissum Cardoso

Department of Civil and Environmental Engineering – PUC-Rio

Prof. José Roberto Moraes D’Almeida

Department of Chemical and Materials Engineering – PUC-Rio

Prof. Holmer Savastano Junior

USP

Prof. Saulo Rocha Ferreira

UFLA

Rio de Janeiro, February 10th, 2023

All rights reserved.

Raylane de Souza Castoldi

Graduated in Civil Engineering at the Federal University of Espírito Santo in 2015 and obtained her M.Sc. Degree in Civil Engineering from the Pontifical Catholic University of Rio de Janeiro in 2017.

Bibliographic data

Castoldi, Raylane de Souza

Influence of surface modifications on sisal fiber durability and interface bond towards cement-based matrices / Raylane de Souza Castoldi ; advisor: Flávio de Andrade Silva ; co-advisor: Lourdes Maria Silva de Souza. – 2023.

187 f. : il. color. ; 30 cm

Tese (doutorado)–Pontifícia Universidade Católica do Rio de Janeiro, Departamento de Engenharia Civil e Ambiental, 2023.

Inclui bibliografia

1. Engenharia Civil e Ambiental - Teses. 2. Fibra de sisal. 3. Modificação da fibra. 4. Fluência da fibra. 5. Durabilidade. I. Silva, Flávio de Andrade. II. Souza, Lourdes Maria Silva de. III. Pontifícia Universidade Católica do Rio de Janeiro. Departamento de Engenharia Civil e Ambiental. IV. Título.

CDD: 624

*To my husband, Breno, and my parents, Adilson and Angela,
for their tremendous support and encouragement.*

Acknowledgements

Many people were essential during this journey. I would like to show all my gratitude to each one of you who somehow contributed to my success.

Firstly, to God, for blessing me during all this time and for enabling me to fulfill this dream.

To my advisor, Prof. Flávio de Andrade Silva, for the trust he placed in me and my work. I am immensely grateful for the encouragement and suggestions to conclude this research.

To my co-advisor, Prof. Lourdes Maria Silva de Souza, for the incentive and partnership during these years. You were very important for my personal and professional growth, thank you for all the advice.

To my mother Angela, my father Adilson, and my husband Breno, my eternal gratitude for your support. Thank you for encouraging me to always follow my dreams, even if it meant living far away for a long time. Making you proud is my biggest motivation.

To all technicians and lab staff from the Laboratory of Structures and Materials (LEM-DEC) at PUC-Rio, Euclides, Marques, Rogério, José Nilson, Jhansen, Anderson, and Bruno. You were essential to the realization of this project. Thank you for always being willing to help me and make the days lighter.

Through the partnership between CAPES and the German Academic Exchange Service (DAAD), I had the opportunity to do a sandwich doctorate in Dresden, Germany. I am very grateful for the support of the entire research group and technical staff at the Institute of Construction Materials, at TU Dresden. The time I spent in Germany was essential for the development of my research.

To the friends that PUC-Rio gave me as a gift, thank you for having welcomed me so well during the time I was there. Having met and lived with such special people made the routine and the homesickness easier. Special thanks to Ana, Daiana, Letícia, Rebecca, and Tathiana, for all the friendship and care during this period and forever. Without you, I would not have made it this far!

To all the friends and family who in one way or another encouraged or helped me, thank you for understanding my absence and rooting for me.

I would also like to thank the Professors and members of this thesis committee, for their availability and careful reading of this study.

This study was financed in part by the Coordenação de Aperfeiçoamento de Pessoal de Nível Superior – Brasil (CAPES) – Finance Code 001.

Also, I would like to thank the financial support provided by CNPq.

Abstract

de Souza Castoldi, Raylane; de Andrade Silva, Flávio (Advisor); Silva de Souza, Lourdes Maria (Co-advisor). **Influence of surface modifications on sisal fiber durability and interface bond towards cement-based matrices.** Rio de Janeiro, 2023. 187p. Tese de Doutorado – Departamento de Engenharia Civil e Ambiental, Pontifícia Universidade Católica do Rio de Janeiro.

The use of sisal fiber in cementitious composites is a subject of current relevance, mostly as a result of the growing interest to make the construction industry more sustainable. However, there are also some drawbacks related to the use of sisal fibers as reinforcement, such as the low durability in alkaline matrices. Thus, this study aimed to investigate the changes in physical and mechanical characteristics of sisal fiber through fiber modifications, to guarantee improved performance as reinforcement in cement-based materials. Specifically, three different fiber modifications have been considered: the alkaline treatment, the use of a polymeric coating on the fiber surface, and a new technique of fiber surface functionalization based on polyphenol chemistry. The experimental program explored the modifications on treated fibers in terms of water absorption tendency, microstructural changes, fiber composition, tensile strength, and strain capacity. Additionally, a fundamental understanding of the interfacial properties between the fiber surface and the cementitious matrix was assessed. The investigations also included creep tests to evaluate the long-term performance of sisal fibers in aggressive conditions, considering different levels of sustained loads. It has been proven that all the proposed fiber modifications lead to improved physical, mechanical, durability-related, and time-dependent properties of sisal fibers, as well as enhancing fiber-matrix adhesion. Nonetheless, in terms of physico-mechanical performance and durability, the best results were reached by the polyphenol modified sisal fiber. After exposure to aggressive alkaline solution under loading, natural sisal remained only with 38% of its strength capacity, changing to approximately 55% for the modified fibers. The outcome of this study provided technical information to consolidate the use of sisal fibers as a reliable alternative to synthetic fibers for achieving structural cementitious composites.

Keywords

Sisal fiber; Fiber modification; Fiber creep; Durability.

Resumo

de Souza Castoldi, Raylane; de Andrade Silva, Flávio (Advisor); Silva de Souza, Lourdes Maria (Co-advisor). **Influência de modificações superficiais na durabilidade da fibra de sisal e aderência com matrizes cimentícias**. Rio de Janeiro, 2023. 187p. Tese de Doutorado – Departamento de Engenharia Civil e Ambiental, Pontifícia Universidade Católica do Rio de Janeiro.

A utilização da fibra de sisal em compósitos cimentícios é um tópico de relevância atual, fruto principalmente do crescente interesse em tornar a construção civil mais sustentável. No entanto, também existem algumas desvantagens relacionadas ao uso de fibras de sisal como reforço, tais como a baixa durabilidade em matrizes alcalinas. Assim, este estudo teve como objetivo avaliar a influência de alguns tratamentos nas características físicas e mecânicas da fibra de sisal, com intuito de garantir melhor desempenho como reforço em materiais cimentícios. Especificamente, três modificações foram propostas: o tratamento alcalino, o revestimento superficial polimérico e uma nova técnica de funcionalização da superfície da fibra baseada na química de polifenóis. O programa experimental avaliou a influência dos tratamentos na absorção de água das fibras, assim como mudanças microestruturais, composição química, resistência à tração e capacidade de deformação. Além disso, foram avaliadas as alterações nas características da interface fibra-matriz. As investigações também incluíram ensaios de fluência para avaliar o desempenho a longo prazo das fibras de sisal em ambientes agressivos, considerando diferentes níveis de carregamento. As modificações resultaram em melhoria de propriedades físicas, mecânicas, relacionadas à durabilidade e dependentes do tempo das fibras de sisal, além da aderência entre a fibra e a matriz. No entanto, em termos de desempenho físico-mecânico e durabilidade, os melhores resultados foram alcançados pela fibra de sisal modificada com polifenóis. Após a exposição à solução alcalina agressiva sob carregamento, a fibra de sisal natural manteve apenas 38% de sua capacidade de resistência original, modificado para aproximadamente 55% para as fibras tratadas. O resultado deste estudo forneceu embasamento técnico para que as fibras de sisal sejam consideradas como uma alternativa ao uso das fibras sintéticas em compósitos cimentícios de uso estrutural.

Palavras-chave

Fibra de sisal; Modificação da fibra; Fluência da fibra; Durabilidade.

Table of contents

Acknowledgements	5
Abstract	7
Resumo	8
Table of contents	9
List of figures	13
List of tables	19
1 Introduction	22
1.1. Motivation	22
1.2. Goals	23
1.3. Thesis organization	24
1.4. References	26
2 Literature review	27
2.1. Natural fibers	27
2.1.1. Chemical composition	30
2.1.2. Physical and mechanical properties	31
2.2. Natural fiber as reinforcement in cement-based composites	33
2.2.1. Mechanical performance	33
2.2.2. Structure of natural fiber-matrix interface	35
2.2.3. Natural fiber degradation in alkaline environment	37
2.3. Methods for improving natural fiber performance in cement-based composites	39
2.3.1. Matrix modification	39
2.3.2. Fiber modification	41
2.4. Potential applications of natural fiber cement-based composites	43

2.5. References 45

3 Effect of alkali treatment on physical-chemical properties of sisal fibers and adhesion towards cement-based matrices 55

3.1. Introduction 55

3.2. Materials 58

3.2.1. Matrix 58

3.2.2. Fiber 58

3.3. Methods 60

3.3.1. Matrix characterization 60

3.3.2. Fiber characterization 60

3.3.3. Fiber-matrix adhesion 65

3.4. Results and Discussion 66

3.4.1. Matrix characterization 66

3.4.2. Fiber characterization 68

3.4.3. Fiber-matrix adhesion 80

3.5. Conclusions 82

3.6. References 83

4 Effect of polymeric fiber coating on the mechanical performance, water absorption, and interfacial bond with cement-based matrices 87

4.1. Introduction 87

4.2. Materials and processing 89

4.2.1. Sisal fiber polymeric coating 89

4.2.2. Pullout sample preparation 90

4.2.3. Testing methods 92

4.3. Results and discussion 96

4.3.1. Scanning electron microscopy (SEM) 96

4.3.2. Thermogravimetric analysis (TGA) 98

4.3.3. Moisture affinity evaluation 100

4.3.4. Fourier transform infrared spectroscopy (FTIR) 101

4.3.5. Direct single fiber tensile test 102

4.3.6. Single-fiber pullout test 104

4.3.7. Atomic force microscope (AFM) 108

4.3.8. Stability in alkaline media	112
4.4. Conclusions	114
4.5. References	115
5 Effect of surface modification of sisal fibers with polyphenols on the mechanical properties, interfacial adhesion and durability in cement-based matrices	119
5.1. Introduction	120
5.2. Materials and methods	121
5.2.1. Fiber surface modification	121
5.2.2. Preparation of sisal fiber cementitious composite for pullout test	124
5.2.3. Fiber characterization	125
5.2.4. Fiber-matrix bond evaluation	127
5.2.5. Fiber durability evaluation	128
5.3. Results and discussion	129
5.3.1. Fiber characterization	129
5.3.2. Fiber-matrix bond evaluation	141
5.3.3. Fiber durability evaluation	144
5.4. Comparative evaluation of the proposed fiber modifications	145
5.5. Conclusions	148
5.6. References	149
6 Tensile creep behavior of sisal fibers under different environmental conditions	153
6.1. Introduction	154
6.2. Experimental methods	155
6.2.1. Materials and processing	155
6.2.2. Sisal fiber modification	156
6.2.3. Single fiber tensile test	157
6.3. Results and discussion	161
6.3.1. Quasi-static behavior of natural and modified sisal fiber	161
6.3.2. Time-dependent behavior of natural and modified sisal fiber	163
6.4. Conclusions	173
6.5. References	174

7	Conclusions and suggestions	179
7.1.	Conclusions	179
7.2.	Suggestions for future works	181
	Appendix A	182
	Different fiber treatments proposed by previous authors	182
	Appendix B	185
	Program interface developed in LabView to automatically record the fiber deformation	185

List of figures

Figure 1.1 – Organization of the experimental program.	25
Figure 2.1 – Classification of natural and synthetic fibers (Adapted from [4]).	28
Figure 2.2 – Sisal fiber: (a) <i>Agave sisalana</i> plant, (b) extraction of the leaves, (c) decortication process, and (d) bundle of fibers in poles to air dry [16,17].	29
Figure 2.3 – Current applications of sisal fibers: (a) bags, (b) carpets, (c) ropes and twines, (d) handicraft, (e) paper production, and (e) automobile parts [18].	29
Figure 2.4 – Schematic microstructural structure of sisal plant (Adapted from [25]).	31
Figure 2.5 – Influence of chemical constituents in the properties of natural fibers (Adapted from [24]).	32
Figure 2.6 – Mechanics of a deflection-softening fiber reinforced concrete (Adapted from [38]).	34
Figure 2.7 – Key factors that affect the mechanical properties of natural fiber composites (Adapted from [24]).	34
Figure 2.8 – Results from monotonic three-point bending tests performed on concrete reinforced with sisal and polypropylene fibers [45].	35
Figure 2.9 – Energy-absorbing fiber-matrix mechanisms [49].	36
Figure 2.10 – (a) Schematic illustration of the swelling process in a cell wall [52]. (b) Effect of the fiber swelling in the fiber-matrix interface [45].	37
Figure 2.11 – Results of three-point flexural tests performed on aged and non-aged concrete reinforced with sisal fiber [62].	38
Figure 2.12 – Natural fiber degradation mechanisms inside a cement-based matrix (Adapted from [61]).	39
Figure 2.13 – The use of cement-based materials reinforced with natural fibers for structural applications: (a) façade plates for building	

envelope [83], (b) comparative compressive failure of plain and sisal fiber reinforced concrete walls [106], (c) roofing system with natural fiber-cement tiles [98], (d) concrete block for one-way precast concrete slabs [102], (e) ductile break of prisms reinforced with natural fibers [105], and (f) structural beam reinforced with composite laminates [108].....	44
Figure 3.1 – (a) Picture and (b) schematic configuration of the apparatus used to keep the fibers stretched during alkalization.	59
Figure 3.2 – Chemical analysis protocol developed for chemical composition determination of lignocellulosic fibers.	62
Figure 3.3 – Schematic configuration of the sample preparation for water contact angle measurements.	63
Figure 3.4 – Schematic configuration of the (a) sample preparation and (b) setup arrangement, and (c) general view of the setup arrangement for the fiber direct tensile tests (dimensions in mm).	64
Figure 3.5 – Casting procedure of the pullout samples.	65
Figure 3.6 – (a) Detail and (b) general view of the single-fiber pullout test arrangement.	66
Figure 3.7 – TGA and DTG analysis performed for OC and 50C matrices at 28 days.....	67
Figure 3.8 – Micrograph of a typical non-circular cross-section of a sisal fiber.	68
Figure 3.9 – Micrographs in two different magnifications of the longitudinal aspect of (a, b) untreated and alkali-treated sisal fibers with (c, d) 1 wt.%, (e, f) 5 wt.% and (g, h) 10 wt.% NaOH solution concentrations.	69
Figure 3.10 – TGA and DTG analysis performed in untreated and alkali-treated sisal fibers in (a) Oxygen and (b) Nitrogen atmosphere.	71
Figure 3.11 – Chemical composition and moisture content of untreated and alkali-treated sisal fibers.	73
Figure 3.12 – (a) Water absorption curves, (b) water contact angle results, and (c) images for untreated and alkali-treated sisal fibers.	75

Figure 3.13 – Representative direct tensile stress curves of untreated and alkali-treated sisal fibers, considering the use of (a) distilled water or (b) acetic acid in the post-treatment procedure.	77
Figure 3.14 – Effect of alkali treatment on the tensile properties of sisal fibers, considering the use of (a) distilled water or (b) acetic acid in the post-treatment procedure.....	78
Figure 3.15 – Stability ratio of untreated and alkali-treated sisal fiber after exposure to pore solution and 1N NaOH solution for 28 days.	79
Figure 3.16 – Representative pullout curves of untreated and alkali-treated sisal fibers.	81
Figure 3.17 – Summary of the pullout test results of untreated and alkali-treated sisal fibers.	81
Figure 4.1 – (a) Polymer impregnation apparatus. (b) Resulted DTA curves of the thermal analysis of S and QS polymers.....	90
Figure 4.2 – Molding process of pullout samples: (a) fibers aligned in the mold, (b) casting of the specimens, and (c) mold filled with the cementitious matrix.....	91
Figure 4.3 – Testing setup for direct single fiber tensile tests: (a) general overview and (b) sample detail.	93
Figure 4.4 – Testing setup for single-fiber pullout tests: (a) general overview and (b) sample detail.	94
Figure 4.5 – Photograph of the atomic force microscope used for the measurements and the sample holder in detail.	95
Figure 4.6 – Micrographs of the longitudinal and cross-sectional aspects of (a) natural and (b-e) polymer-coated sisal fibers.	97
Figure 4.7 – TGA and DTG curves of natural sisal, (a) S50, S100, (b) QS50, and QS100 polymer-coated fibers.	99
Figure 4.8 – Water absorption test results of natural sisal and polymer-coated fibers.	100
Figure 4.9 – FTIR spectra of natural sisal, (a) S100, S50, (b) QS100, and QS50 polymer-coated fibers.	102
Figure 4.10 – Stress-strain curves of natural sisal and polymer-coated fibers.....	103

Figure 4.11 – (a) General profile of a single fiber pullout curve and (b) typical pullout load-slip curves of natural sisal and polymer-coated fibers.....	105
Figure 4.12 – AFM topography images of the surface morphology of (a) natural and (b) S50 polymer coated fibers of a representative 5 μm x 5 μm scan area.....	108
Figure 4.13 – AFM phase contrast representative images and respective histograms of the adhesion force for (a) natural and (b) S50 polymer-coated sisal fiber.....	110
Figure 4.14 – AFM phase contrast representative images and respective histograms of the stiffness for (a) natural and (b) S50 polymer-coated sisal fiber.....	111
Figure 4.15 – AFM phase contrast representative images and respective histograms of the deformation for (a) natural and (b) S50 polymer-coated sisal fiber.....	112
Figure 4.16 – Results of the mechanical evaluation of natural sisal and polymer-coated fibers after alkaline exposure, in terms of normalized tensile strength and Young’s modulus.	113
Figure 5.1 – (a) Natural sisal fiber before the modification process, (b) fiber under the TA solution, (c) fiber under the ODA solution, and (d) visual aspect of the fiber after TA-ODA modification.	122
Figure 5.2 – Scheme of the suggested fiber surface modification consisting of two steps: (a) immersion in the tannic acid solution and (b) immersion in the octadecylamine solution.	123
Figure 5.3 – Preparation of pullout samples: (a) mold and (b) casting of the specimens. (c) Schematic configuration of the pullout sample (dimensions in mm).	124
Figure 5.4 – (a) Single-fiber setup arrangement and (b) schematic configuration of the sample preparation (dimensions in mm).	127
Figure 5.5 – (a) General overview and (b) detail of the single-fiber pullout test arrangement.	128
Figure 5.6 – SEM images of the longitudinal aspect of (a) natural sisal, and (b) TA5-ODA1, (c) TA5-ODA3.75, (d) TA5-ODA5, (e) TA10-ODA3.75 modified sisal fibers.	130

Figure 5.7 – SEM images of the cross-sectional aspect of (a) natural sisal, and (b) TA5-ODA1, (c) TA5-ODA5 modified sisal fibers.....	131
Figure 5.8 – Mapping images of original and modified (TA10-ODA3.75) sisal fibers.....	133
Figure 5.9 – (a) TGA and (b) DTG curves of natural sisal and sisal fibers modified with polyphenols.	135
Figure 5.10 – Moisture content of natural sisal fiber and fibers modified with polyphenol.....	136
Figure 5.11 – Water contact angle test at 10, 20, and 30 s for (a) natural sisal and (b-f) fibers modified with polyphenols.	137
Figure 5.12 – Infrared spectroscopy of natural sisal and sisal fibers modified with polyphenols.	139
Figure 5.13 – (a) Tensile strength and (b) Young’s modulus of natural sisal and sisal fibers modified with polyphenols.....	140
Figure 5.14 – Representative direct tensile test stress-strain curves of natural sisal and sisal fibers modified with polyphenols.....	141
Figure 5.15 – Typical pullout curves of natural sisal and sisal fibers modified with polyphenols.	142
Figure 5.16 – Normalized tensile strength of natural sisal and sisal fibers modified with polyphenols before and after exposure to NaOH and Pore solutions.....	145
Figure 5.17 – Comparative graphs of fiber physical and mechanical properties considering the (a) alkali treatment, (b) polymer coating, and (c) modification with polyphenols.	146
Figure 5.18 – Comparative graph of fiber physical and mechanical properties considering the best results obtained for each treatment evaluated in this study.	147
Figure 6.1 – Setup for quasi-static single fiber tensile test.	158
Figure 6.2 – Summary of experimental conditions for time-dependent fiber tests and explanation of the sample identification in this study.	159
Figure 6.3 – Time-dependent tests: (a) Schematic configuration, (b) setup overview, (c) load application device, and (d) detail of the fibers during tests.....	160

Figure 6.4 – Quasi-static direct tensile test results of natural and modified sisal fibers.	162
Figure 6.5 – Quasi-static direct tensile test results of air-dried and saturated natural sisal fiber.	163
Figure 6.6 – Time-dependent strain test results of natural sisal fibers under “no solution”, water, and 1M NaOH conditions.	164
Figure 6.7 – The creep compliance C_c of single sisal fibers at different load levels and exposure conditions.....	165
Figure 6.8 – Four-element Burgers Model.....	166
Figure 6.9 – Typical time-dependent experimental and four-element Burgers model adjustment curves of natural sisal fibers in “no solution”, water, and 1M NaOH conditions.....	167
Figure 6.10 – Time-dependent strain test results of natural and modified sisal fibers in different environmental conditions.	169
Figure 6.11 – Normalized mechanical properties of the studied fibers after the creep tests: (a) tensile strength, (b) Young’s modulus, and (c) ultimate strain.	173

List of tables

Table 2.1 – Typical chemical composition of different natural fibers (Adapted from [4]).	30
Table 2.2 – Physical-mechanical properties of different natural and synthetic fibers.	32
Table 2.3 – Types of surface treatments in natural fibers.	41
Table 3.1 – Mixture composition of the cement-based matrix.	58
Table 3.2 – Summary of the variables related to the sample identification.	60
Table 3.3 – Amount of calcium hydroxide (CH) on the matrices.	67
Table 3.4 – Cross-sectional area of untreated and alkali-treated sisal fibers.	68
Table 3.5 – Thermogravimetric results for untreated and alkali-treated sisal fibers performed in oxygen atmosphere.	72
Table 3.6 – Tensile properties of untreated and alkali-treated sisal fibers.	76
Table 4.1 – Samples identification names related to the type of polymer and emulsion concentration adopted in the impregnation process.	90
Table 4.2 – Composition of the cement-based matrix used for the pullout tests.	91
Table 4.3 – Cross-sectional area of natural and polymer-coated sisal fibers.	98
Table 4.4 – Direct single fiber tensile test results of natural and polymer-coated sisal fibers.	104
Table 4.5 – Single-fiber pullout test results of natural and polymer-coated sisal fibers.	107
Table 5.1 – Summary of the variables related to the sample identification.	123
Table 5.2 – Mixture composition of the cement-based matrix.	124
Table 5.3 – Cross-sectional area of natural sisal and modified fibers.	132

Table 5.4 – Water contact angle data of natural sisal and sisal fibers modified with polyphenols.....	138
Table 5.5 – Summary of pullout properties of natural sisal and sisal fibers modified with polyphenols.....	143
Table 6.1 – Summary of the Four-element Burgers Model parameters for natural sisal fibers.....	168
Table 6.2 – Summary of the mechanical properties of the studied fibers after the creep tests.	171

*“I would rather have questions that can't be answered
than answers that can't be questioned.”*

Richard Feynman

1 Introduction

1.1. Motivation

In the past few decades, fibers of various materials, sizes, and geometries have been added to concrete in a variety of applications. Initially, the use of dispersed fibers in cementitious matrices was focused on the mitigation of the effects of plastic and drying shrinkage, which results in microcracks in the cementitious matrix. It was also found that, in addition to plastic and drying shrinkage control, fibers had the effect of improving some of the concrete properties such as flexural toughness, fatigue resistance, impact resistance, and post-crack strength [1–3]. Furthermore, the reduction of the crack openings due to the incorporation of fibers can improve the durability of reinforced concrete elements, reducing the entrance of aggressive agents (humidity, oxygen, and chlorides) [1]. In this context, synthetic fibers have been extensively studied, and are frequently used in building elements, added to mortars and concretes. Currently, they are widely used for floor and pavement applications, sprayed concrete, and precast elements. These fibers present good compatibility with cementitious matrices because they suffer little or no degradation in an alkaline environment [1,2].

On the other hand, natural fibers appear as a low-cost alternative, due to their natural and large-scale occurrence, mainly in developing countries and with high housing deficits [3,4]. However, these fibers are degradable in alkaline environments, resulting in changes in the mechanical performance of the composite through time, depending on the age and exposure conditions of the reinforced element [5]. Natural fibers also present high moisture absorption and subsequent swelling and interface degradation [1]. In other words, these fibers are susceptible to volume variation with the moisture presence, which results in interface degradation due to the accumulated stress in the region, leading to the formation of microcracks around the fibers. Moreover, natural fibers present a weak chemical bond to cement-based matrices, varying between 0.32 to 0.72 MPa [5,6]. Therefore, there is a gap of knowledge aiming at improving this fiber-matrix interaction

through successful physical and chemical treatments in several applications in which commonly synthetic fibers are used.

A variety of procedures has been proposed to reduce the natural fibers' volumetric instability, as well as to avoid alkaline attacks, and improve the fiber-matrix bond have been proposed [4,6], such as alkalization, acetylation, and polymer impregnation. In general, these procedures can clean the fiber surface, modify their chemical composition, reduce the moisture absorption and increase the surface roughness [7,8]. By using these treatments, some authors [8–11] affirm that it is possible to achieve a considerably enhanced performance of the composite, depending on the use of adequate fiber length and volume. However, there is still a lack of information on how the use of such treatments may interfere in the fiber-matrix bond with cement-based matrices.

Therefore, it is necessary to further investigate the influence of these treatments on the fiber properties and their adhesion to cement-based matrices. In addition, the understanding of the treatment regarding fiber resistance to alkaline attacks, in a short and long-term perspective, can encourage the use of natural fibers in applications of greater structural importance.

1.2. Goals

The objectives of the present research are related to the evaluation of the effect of different fiber treatments (alkaline treatment, polymer impregnation, and superficial modification with polyphenols) on natural fiber properties and fiber-matrix interface behavior of sisal fibers and cement mortars. Also, an investigation of the durability performance of the treated fibers was performed. These general objectives will be met by following the steps:

- i. Investigation of the proposed treatments on the physical and mechanical properties of the fibers, through evaluation of water absorption capacity, dimensional stability, and fiber direct tensile tests, covered by Chapters 3, 4, and 5;
- ii. Evaluation of fiber-matrix interface modification by pullout tests on treated and untreated fibers, also included in Chapters 3, 4, and 5;
- iii. Evaluation of time-dependent performance by studying the creep mechanical behavior effects of treated and untreated fibers, subjected

to different aggressive environmental conditions, covered in the Chapter 6.

1.3. Thesis organization

The thesis is composed of this introduction, a literature review, followed by four chapters assembled as individual full papers, conclusions, and future work suggestions, structured as follows:

- **Chapter 1:** The introduction presents the motivation, objectives, and structure of the study.
- **Chapter 2:** The literature review presents an overview of the chemical, physical and mechanical properties of natural fibers, aspects related to the fiber-matrix interface, an overview of some fiber treatments suggested in the literature to improve the natural fiber performance, and potential applications of natural fibers as reinforcement in cement-based matrices.
- **Chapter 3:** This chapter explores the effect of the alkali treatment on physico-chemical properties of sisal fibers. Also, the adhesion and durability in cement-based matrices were evaluated.

Published article: *Effect of alkali treatment on physical-chemical properties of sisal fibers and adhesion towards cement-based matrices.*

July 2nd, 2022. Construction and Building Materials.

<https://doi.org/10.1016/j.conbuildmat.2022.128363>

- **Chapter 4:** The influence of polymeric fiber coating on the mechanical performance, water absorption, and interfacial bond with cement-based matrices is exposed in this chapter.
- **Chapter 5:** A novel approach to sisal fiber modification using polyphenol chemistry is presented in this chapter. It was explored the influence on the mechanical properties, interfacial adhesion, and durability in cement-based matrices.
- **Chapter 6:** The tensile creep behavior of sisal fibers under different environmental conditions and the influence of fiber modifications on the fiber creep performance is presented in chapter 6.

- **Chapter 7:** The conclusion with the most relevant results of the previous chapters, followed by future works and suggestions.

In order to fulfill the exposed objectives, an experimental program was proposed to be mainly performed at the *Laboratório de Estruturas e Materiais* at PUC-Rio and the Institute für Baustoffe, at the Technische Universität Dresden, in Germany. This is a result of a cooperation between both universities through the Probral program nº 12/2017 and DAAD (Germany) within the research project 8887.144079/2017-00. It was also necessary to perform some specific analyses in other laboratories, which is indicated in the introductory text of the respective chapters. The flowchart of the Figure 1.1 presents an overview of the experimental program of this Thesis.

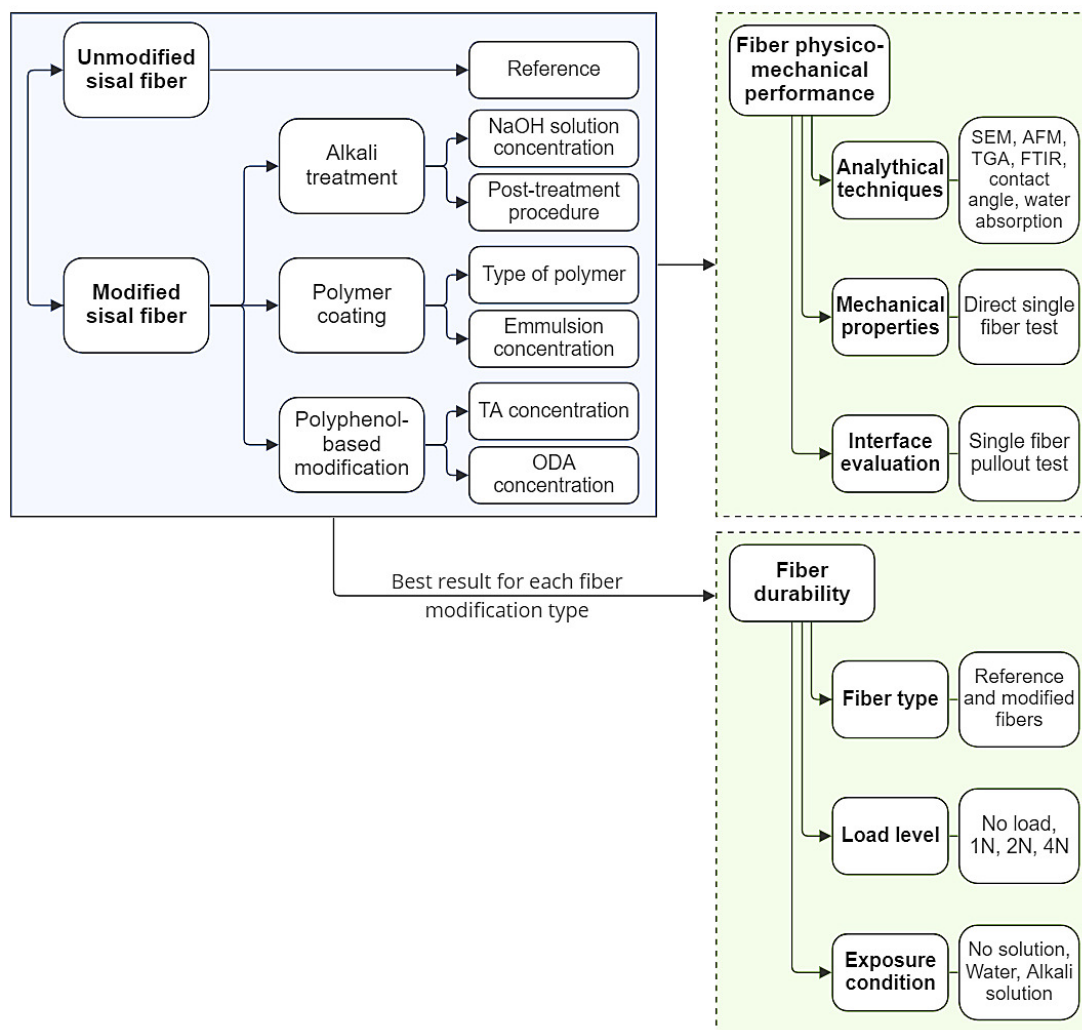


Figure 1.1 – Organization of the experimental program.

1.4. References

- 1 MUKHOPADHYAY, S.; KHATANA, S. A review on the use of fibers in reinforced cementitious concrete. **Journal of Industrial Textiles**, v.45, n.2, p.239-264, 2015.
- 2 SHAH, S. P.; KUDER, K. G.; MU, B. Fiber-Reinforced cement-based composites: A forty year odyssey. **6th RILEM Symposium Fibre-Reinforced Concretes – BEFIB**. Varenna, Italy. 2004.
- 3 ZOLLO, R. F. Fiber-reinforced concrete: an overview after 30 years of development. **Cement and Concrete Composites**, v.19, n.2, p.107-122, 1997.
- 4 AMERICAN CONCRETE INSTITUTE. **ACI 544.1R-96: State-of-the-Art Report on Fiber Reinforced Concrete**. 2002.
- 5 VO, L. T. T.; NAVARD, P. Treatments of plant biomass for cementitious building materials – A review. **Construction and Building Materials**, v.121, p.161-176, 2016.
- 6 FERREIRA, S. R.; SILVA, F. de A.; LIMA, P. R. L.; TOLEDO FILHO, R. D. Effect of fiber treatments on the sisal fiber properties and fiber-matrix bond in cement based systems. **Construction and Building Materials**, v.101, p.730-740, 2015.
- 7 LOPES, F. F. M.; ARAÚJO, T. de A.; NASCIMENTO, J. W. B.; GADELHA, T. S.; SILVA, V. R. Estudo dos efeitos da acetilação em fibras de sisal. **Revista Brasileira de Engenharia Agrícola e Ambiental**, v.14, n.17, p.783-788, 2010.
- 8 SNOECK, D.; SMETRYNS, P.-A.; BELIE, N. D. Improved multiple cracking and autogenous healing in cementitious materials by means of chemically-treated natural fibres. **Biosystems Engineering**, v.139, p.87-99, 2015.
- 9 ZUKOWSKI, B.; SILVA, F. de A.; TOLEDO FILHO, R. D. Design of strain hardening cement-based composites with alkali treated natural curauá fiber. **Cement and Concrete Composites**, v.89, p.150-159, 2018.
- 10 ZUKOWSKI, B.; SANTOS, E. R. F.; MENDONÇA, Y. G. dos S.; SILVA, F. de A.; TOLEDO FILHO, R. D. The durability of SHCC with alkali treated curauá fiber exposed to natural weathering. **Cement and Concrete Composites**, v.94, p.116-125, 2018.
- 11 SOLTAN, D. G.; NEVES, P.; OLVERA, A.; SAVASTANO JUNIOR, H.; LI, V. C. Introducing a curauá fiber reinforced cement-based composite with strain-hardening behavior. **Industrial Crops and Products**, v.103, p.1-12, 2017.

2 Literature review

2.1. Natural fibers

The growing concern with the environment encourages the search for different materials to be used as eco-friendly alternatives in several applications. Natural fibers appear as an interesting alternative, not only due to the development of new renewable materials but also to the possible generation of a non-food resource for economic development for farming and rural areas in developing countries [1]. These fibers are grown commercially in some of the poorest areas of the world, in around 100 countries [2], and are usually the only source of income and economic activity in these areas. The impact of this activity provides a livelihood for these populations as long as the use of these fibers has established their potential in different applications, such as in roping, paper products, and components in composites for automotive, sport, and construction industries.

Natural fibers are classified based on their origin: plant, mineral, or animal type (Figure 2.1). In general, natural fibers obtained from plants present a higher strength and stiffness, which makes them most suitable for use in composites with structural requirements [3]. These fibers are extracted from different parts of the plants: from the leaves (sisal, curauá), the seeds/fruit (coir, coconut, kapok), the grass/reed (bagasse, bamboo), the wood (softwood, hardwood), the stalk (rice, oat, wheat), and the bast/stem (kenaf, jute, hemp, flax) [4,5]. Generally, natural fibers derived from both leaf and stem seem to provide better mechanical properties than the ones derived from fruits [6]. However, as these fibers grow in a natural environment, their performance is highly influenced by several aspects, such as the species, climatic conditions, variety of the plant, and some agricultural variables, which include the soil quality, weathering conditions, and the level of plant maturity [4,7,8].

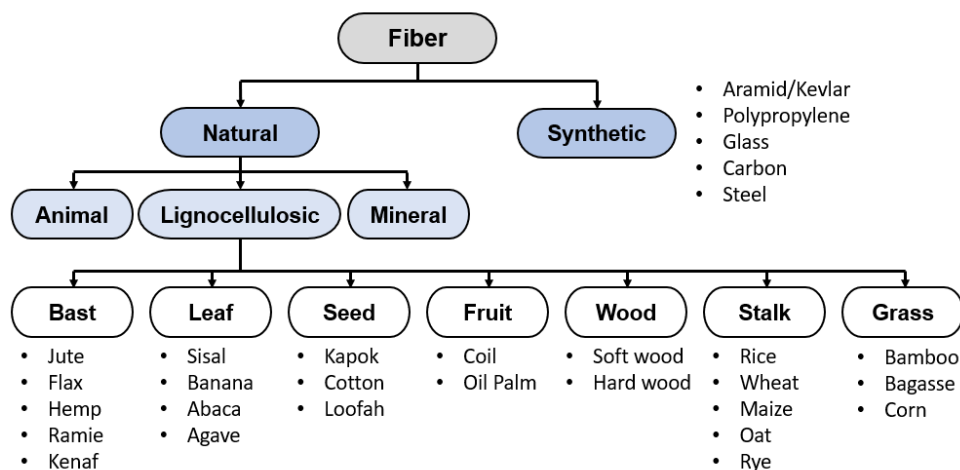


Figure 2.1 – Classification of natural and synthetic fibers (Adapted from [4]).

Given its abundance and excellent properties, the sisal fiber is considered an ideal candidate for reinforcement in composites in a series of applications [4,9–11]. The production of these fibers originated in Mexico and was introduced into Brazil in 1900, with the first commercial production starting in 1930 [2]. Nowadays, Brazil is the largest producer and exporter of sisal fiber in the world. The fibers are produced especially in the State of Bahia, where about 90% of the total Brazilian sisal is obtained [12].

The sisal fibers are extracted from the leaves of the *Agave sisalana* plant (Figure 2.2). The raw sisal fiber is obtained through the mechanical decortication process, which requires a low amount of energy [13]. In this process, the leaves are crushed by a rotating wheel with blunt knives, separating the fibers from the leaves [11]. The resulting fibers represent only 3-5% of the weight of the processed leaves. After the defibration, the fibers are placed in poles to air dry.

Traditionally, the main uses of the sisal fibers are focused on non-structural applications, such as carpets, ropes, twines, and paper production (Figure 2.3). Also, these fibers can be extruded in sheet form for use in automotive interior components, such as door panels, trunk liners, seatbacks, packages, and speaker trays [11,14]. However, there is the possibility of opening new markets for these fibers. Sisal has a promising future not only because of the new uses but also because of growing public awareness that natural fibers are environmentally friendly. In the construction sector, sisal fiber is gaining attention for other applications, such as in residential houses as reinforcement in composites, as well as in the replacement of asbestos in the composition of tiles and roofing materials

[15]. Some sisal fiber properties such as biodegradable and renewable features, high availability, low cost, and specific mechanical properties also make them a convenient material to be adopted as reinforcement for cement-based matrices [4].

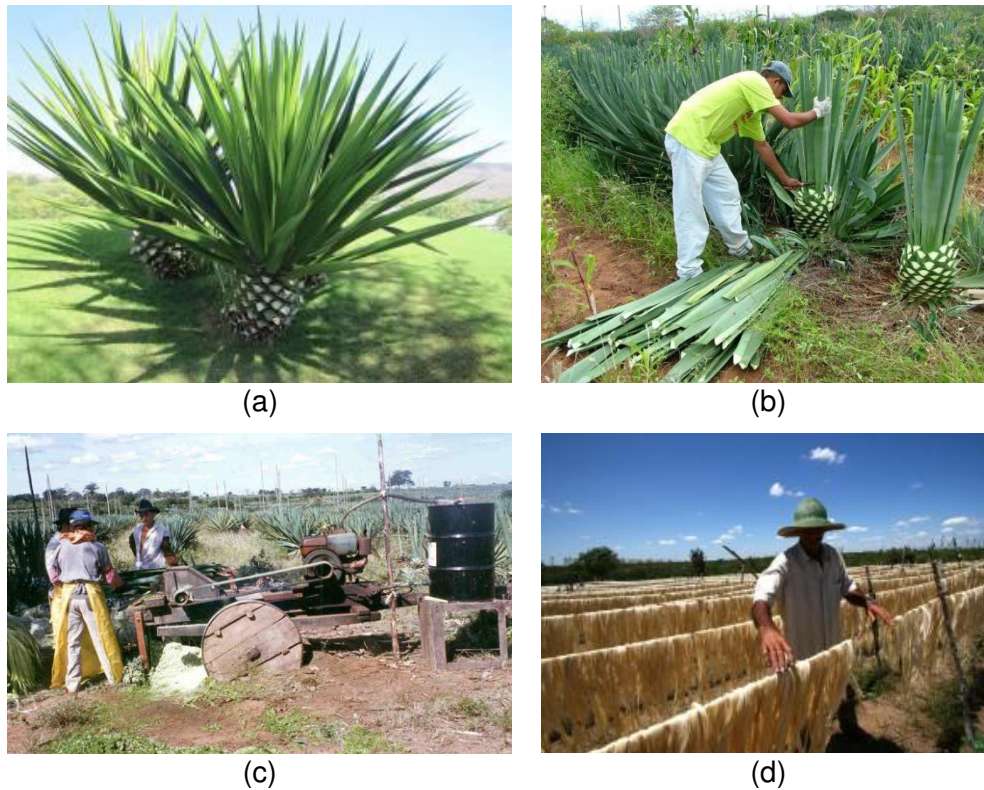


Figure 2.2 – Sisal fiber: (a) *Agave sisalana* plant, (b) extraction of the leaves, (c) decortication process, and (d) bundle of fibers in poles to air dry [16,17].

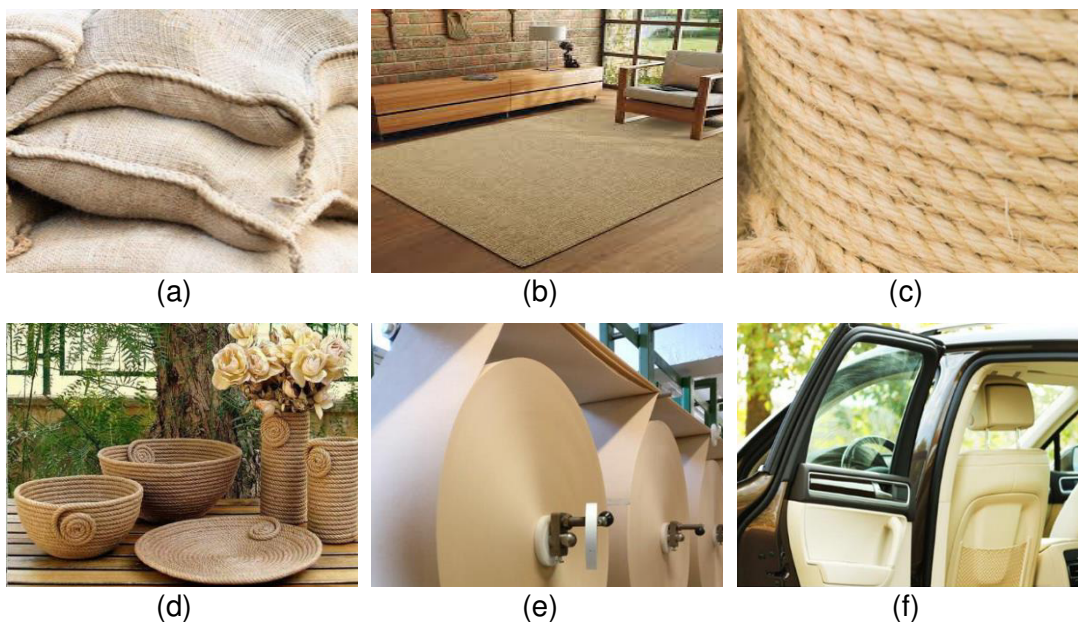


Figure 2.3 – Current applications of sisal fibers: (a) bags, (b) carpets, (c) ropes and twines, (d) handicraft, (e) paper production, and (e) automobile parts [18].

2.1.1. Chemical composition

Plant fibers are also known as cellulosic/lignocellulosic fibers, name attributed to their composition. These fibers can be considered itself a composite material [4], made up mainly of cellulose fibrils, immersed in a matrix of hemicellulose, lignin, wax, pectin, and minor amounts of sugars and other water-soluble components [3,19]. Table 2.1 lists the typical chemical composition of different types of natural fibers. As vegetal fiber grows naturally, their properties are heterogeneous. The chemical composition of natural fibers is directly influenced by geographical and climatic variations, type of soil, extraction method, and other non-controlled conditions [7]. This composition is usually expressed as the percentage of each constituent in terms of maximum and minimum values, which generally vary in a wide range. Also, the sum of all percentages may not be 100%, which is explained by the fact that it is not possible to measure the quantity of some minor constituents [7]. The mechanical and physical characteristics of natural fibers are directly correlated to the fiber composition and the proportion between the components. Thus, the combined effect of cellulose, hemicelluloses, and lignin dictates the overall properties of fiber plants.

Table 2.1 – Typical chemical composition of different natural fibers (Adapted from [4]).

Fiber	Cellulose (%)	Hemicellulose (%)	Pectin (%)	Lignin (%)	Wax (%)
Bagasse	37	21	10	22	-
Banana	62.5	12.5	4	7.5	-
Bamboo	34.5	20.5	-	26	-
Coir	46	0.3	4	45	-
Cotton	86	4	6	0.75	0.6
Curauá	73.6	5	-	7.5	-
Flax	72.5	14.5	0.9	2.5	-
Hemp	81	20	0.9	4	0.8
Jute	67	16	0.2	9	0.5
Sisal	60	11.5	1.2	8	-

Figure 2.4 shows a typical natural fiber structure covering the three main structural components of natural fibers: cellulose, hemicellulose, and lignin. Basically, they present crystalline (cellulose) and amorphous (non-crystalline cellulose, hemicellulose, and lignin) fractions [20]. The fiber structure is composed of individual cellulose fiber cells, held together by a lignin and hemicellulose matrix, named middle lamella [21]. Each fiber cell is composed of a primary cell

wall, three secondary walls, and the lumen [22]. In the cell walls, the hemicellulose molecules are hydrogen-bonded to cellulose to form the supportive matrix for the microfibrils, which are the main structural components of the fiber cell [23]. On the primary cell wall, the cellulose crystalline microfibrils are randomly oriented, while in the secondary walls the cellulose crystalline microfibrils are arranged helically, with the main direction of the fiber [22]. The angle between the fiber axis and the microfibrils is known as the microfibrillar angle, and it governs the tensile properties of natural fibers [19]. Fibers are rigid and have a high tensile strength if the microfibrils are aligned to the fiber axis [7,24].

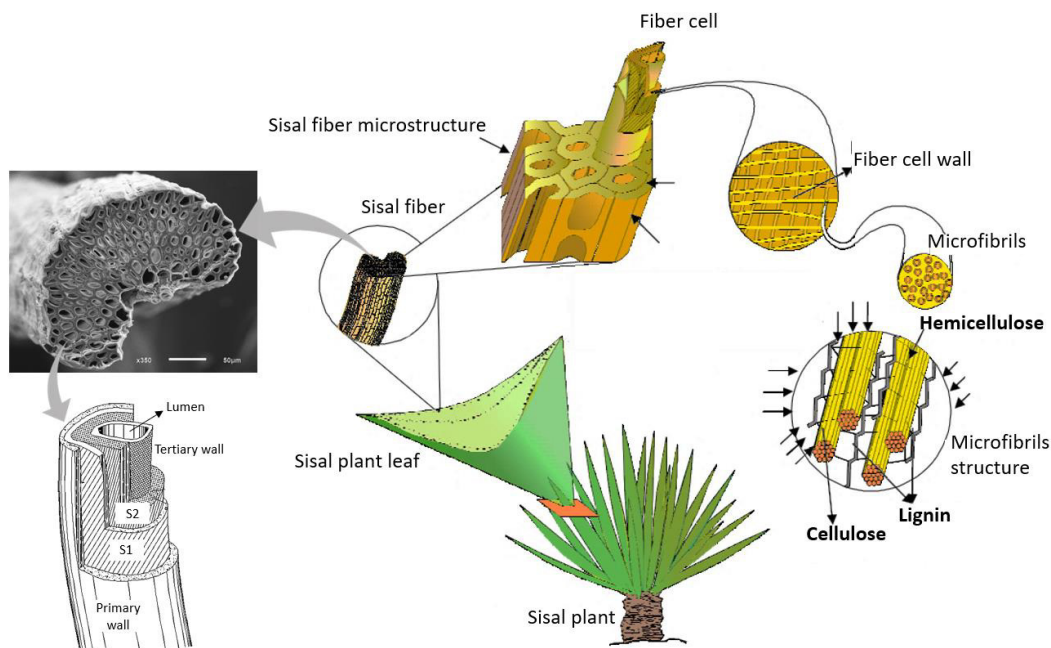


Figure 2.4 – Schematic microstructural structure of sisal plant (Adapted from [25]).

2.1.2. Physical and mechanical properties

The physical characteristics and mechanical performance of natural fibers are highly dependent on their chemical composition. Figure 2.5 summarizes the correlation between some properties of natural fibers and the influence of the chemical constituents. Cellulose is the basic structural component of all natural fibers and provides strength, stiffness, and stability to them [5,7]. Generally, tensile strength and Young's modulus of fibers increase with the increase of the cellulose content [7,19]. Hemicelluloses are very hydrophilic in nature, and are mainly responsible for the moisture absorption, thermal, and biodegradation characteristics of natural fibers [26]. The lignin content mostly controls the thermal stability and

gives rigidity to the plants [13,19]. Lignin is totally amorphous and acts as an encrusting agent in the cellulose/hemicellulose matrix [7,19]. Among them, the amount of organic and inorganic substances is responsible for the color, odor, decay resistance, and abrasive nature of these fibers [27].

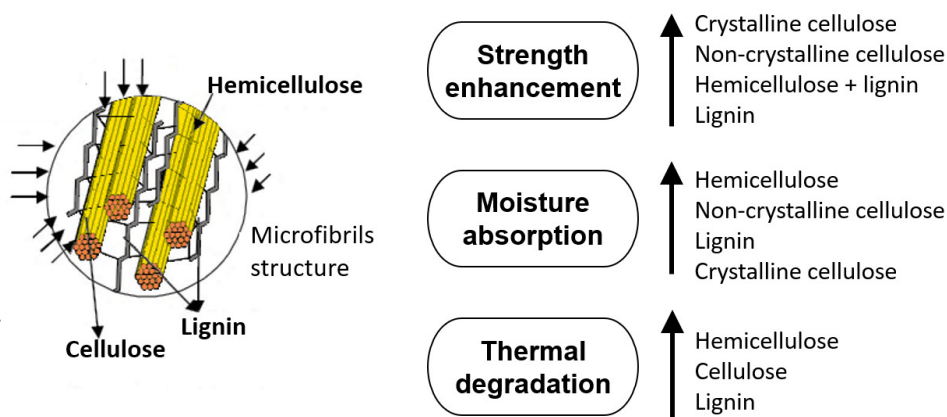


Figure 2.5 – Influence of chemical constituents in the properties of natural fibers (Adapted from [24]).

Table 2.2 presents typical values of some physical-mechanical properties of different natural and synthetic fibers. Given their excellent mechanical properties, sisal fiber is one of the most widely used natural fibers [4,9,10]. It is considered an attractive option to be used as an alternative for synthetic fiber applications, having specific mechanical properties comparable to synthetic ones (e.g. polypropylene) [28]. Besides that, sisal fiber has a low density, abundant availability worldwide, and is a non-hazardous and non-abrasive alternative [4,13]. However, the presence of hemicellulose content is a key reason for the high moisture susceptibility of these fibers. During water absorption, the hydrophilic structure of this constituent allows the moisture to penetrate and results in fiber dimensional instability, named the swelling process.

Table 2.2 – Physical-mechanical properties of different natural and synthetic fibers.

Fiber	Density (g/cm ³)	Tensile Strength (MPa)	Young's modulus (GPa)	Ref.
Coir	0.67-1.46	95-230	2.8-6	[4,29,30]
Curauá	1.4	87-1150	11.8-96	[4]
Hemp	1.2-1.5	270-900	23.5-90	[4,24,31]
Jute	1.3-1.5	320-800	13-27	[4,24,29]
Sisal	1.33-1.5	347-800	9-38	[4,24,28,31]
Aramid	1.4	3000-3150	63-67	[24,29]
Glass (E)	2.5	1200-1500	63-83	[24,29]
Polypropylene	0.91	250	2	[30,31]

2.2. Natural fiber as reinforcement in cement-based composites

Fibers of different types of materials and geometries have been used as reinforcement for fragile cement-based matrices in several applications. The main focus is the mitigation of the microcracks in the matrix as a result of the shrinkage phenomena, where commonly synthetic fibers are used. Thus, the presence of these fibers controls the plastic and drying shrinkage but can also provide improvements to the matrix, including flexural toughness, fatigue, impact resistance, and post-cracking strength [32–35]. On the other hand, the cracking control also improves the composite durability, avoiding the entrance of aggressive agents [32].

With a promising range of mechanical and physical properties, natural fibers have become potential alternative materials to use as reinforcement in cement-based matrices, especially in developing countries with housing deficits as a consequence of their large occurrence and relatively low cost [34,36]. An increase in research activities in this direction is driven by several promising features of these fibers such as reasonable mechanical strength and biodegradability of these fibers in comparison to synthetic fibers [4]. The properties of these composites composed of the natural fiber and cementitious matrix are dependent on the component's properties and the interaction between them. Therefore, in order to analyze the resulting composite material and predict its behavior under different loading conditions, three main phases must be considered: the matrix, the fibers, and the fiber-matrix interface.

2.2.1. Mechanical performance

The use of natural fibers in cement-based composite enhances the overall mechanical properties of the composite [10]. The presence of these fibers in cementitious composites has been found to result in improvements in properties such as shrinkage resistance, toughness, and ductility [35,37]. The general purpose is to improve the post-cracking toughness of building materials, such as cement, mortar, or concrete. The fibers act as a bridge in this region, allowing stress transfer, reducing crack propagation, and resulting in residual strength after the crack formation (Figure 2.6). Moreover, the presence of natural fibers can reduce free plastic and drying shrinkage and thermal conductivity, improve sound absorption

and vibration properties of cementitious materials [4]. However, these improvements depend on some key factors, listed in Figure 2.7.

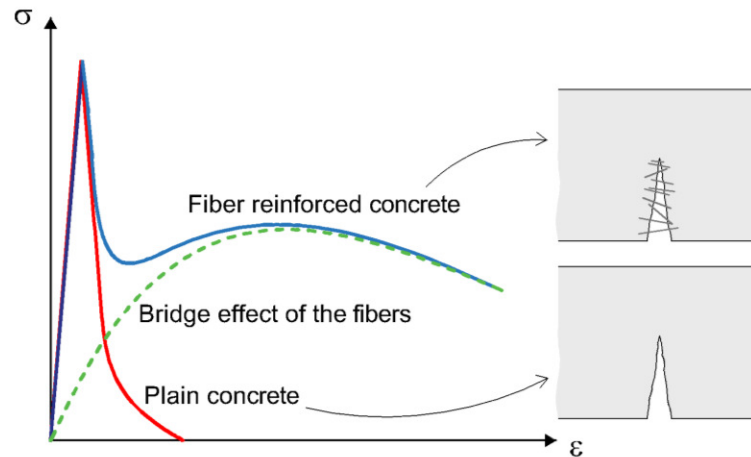


Figure 2.6 – Mechanics of a deflection-softening fiber reinforced concrete (Adapted from [38]).

In general, the natural fiber can assume two different geometries in cement-based composites: continuous reinforcement in the form of long fibers, with lengths between 200 mm to 1 m [11,39–41], or discrete short fibers [11,42,43] (Figure 2.7). In the form of continuous reinforcement, the fibers can be aligned in a preferred orientation, which results in a composite with enhanced mechanical properties in the considered direction. In this case, it is possible to obtain a structural reinforcement and the mechanical properties of the composite are considerably improved [39]. Composites reinforced with aligned natural fibers can achieve extraordinary mechanical behavior, with strength levels comparable to synthetic ones [34]. However, the production process may be a limitation for the use on large scale for structural elements.



Figure 2.7 – Key factors that affect the mechanical properties of natural fiber composites (Adapted from [24]).

On the other hand, the use of short-dispersed fibers in the matrix results in random orientation of the fibers. The incorporation of these fibers can be made during the mixing process, a less complex process than the one required for continuous fibers. In this case, fibers are usually adopted as a secondary reinforcement, controlling the opening and propagation of cracks. In a previous work [45], it was proven that the addition of 10 kg/m³ of short sisal fiber (50 mm length) as reinforcement was sufficient to provide ductility to concrete with the same level of residual strength as the concrete reinforced with 6 kg/m³ of polypropylene fiber (Figure 2.8), resulting in a deflection-softening behavior concrete. However, some authors [26,46,47] proposed fiber treatments to enhance adhesion with the matrix to obtain strain-hardening composites reinforced with discrete natural fibers, reaching elevated mechanical performance – deflection-hardening composites.

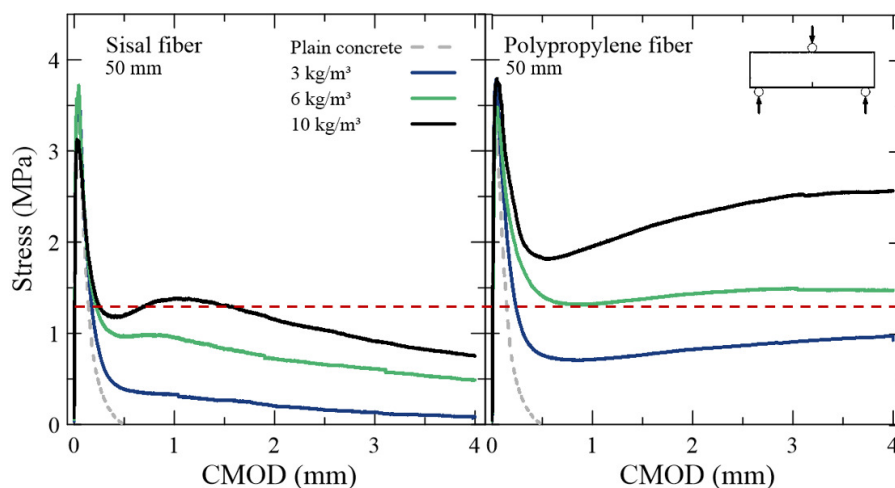


Figure 2.8 – Results from monotonic three-point bending tests performed on concrete reinforced with sisal and polypropylene fibers [45].

2.2.2. Structure of natural fiber-matrix interface

The mechanical performance of the composites depends not only on the matrix and fiber characteristics but also on the interface properties [44,48]. Thus, the mechanical properties of natural fiber composites are directly governed by the interfacial bonding properties between the natural fiber and its surrounding matrix. The fiber-matrix interaction involves chemical and physical mechanisms, which lead to energy absorption in the cracked zone. These interactions include fiber

failure, fiber pullout, and fiber bridging [49]. In addition, the possibility of fiber/matrix debonding and matrix cracking is considered (Figure 2.9).

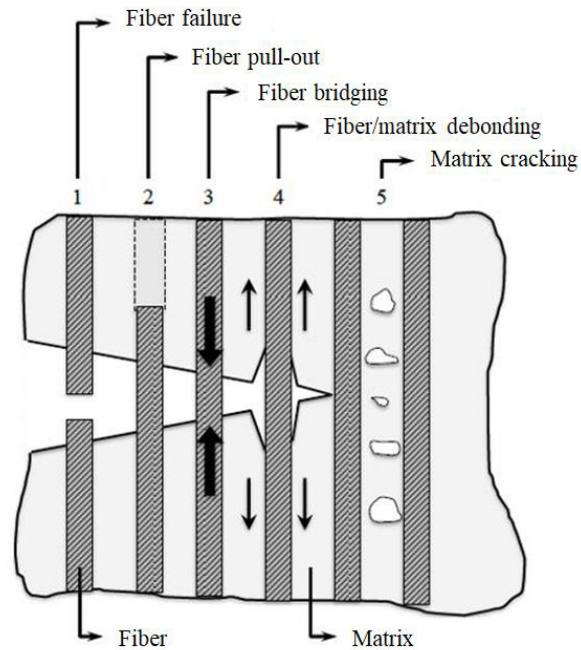


Figure 2.9 – Energy-absorbing fiber-matrix mechanisms [49].

Natural fibers present a weak chemical bond to cement-based matrices [37,50,51], resulting from Van der Waals forces and -OH interactions of the cellulosic molecules and the calcium hydroxide of the matrix. In addition, another key barrier in the extensive use of natural fibers is their affinity towards moisture and water in service environments. The hydroxyl groups in the cellulose, hemicellulose, and lignin build a large number of hydrogen bonds between the macromolecules of cellulose and the fiber cell wall [52]. However, the crystalline hydrophilic cellulose structures allow the moisture to penetrate through the amorphous region, composed of hemicellulose and lignin [53]. The presence of humidity breaks these hydrogen bonds, and the hydroxyl groups form new hydrogen bonds with the water molecules, which induce fiber swelling (Figure 2.10.a) [54]. This dimensional instability leads to the formation of microcracks in the fiber-matrix surrounding, corroborating to the poor physical adhesion between the fiber and the matrix (Figure 2.10.b) [30,41,54].

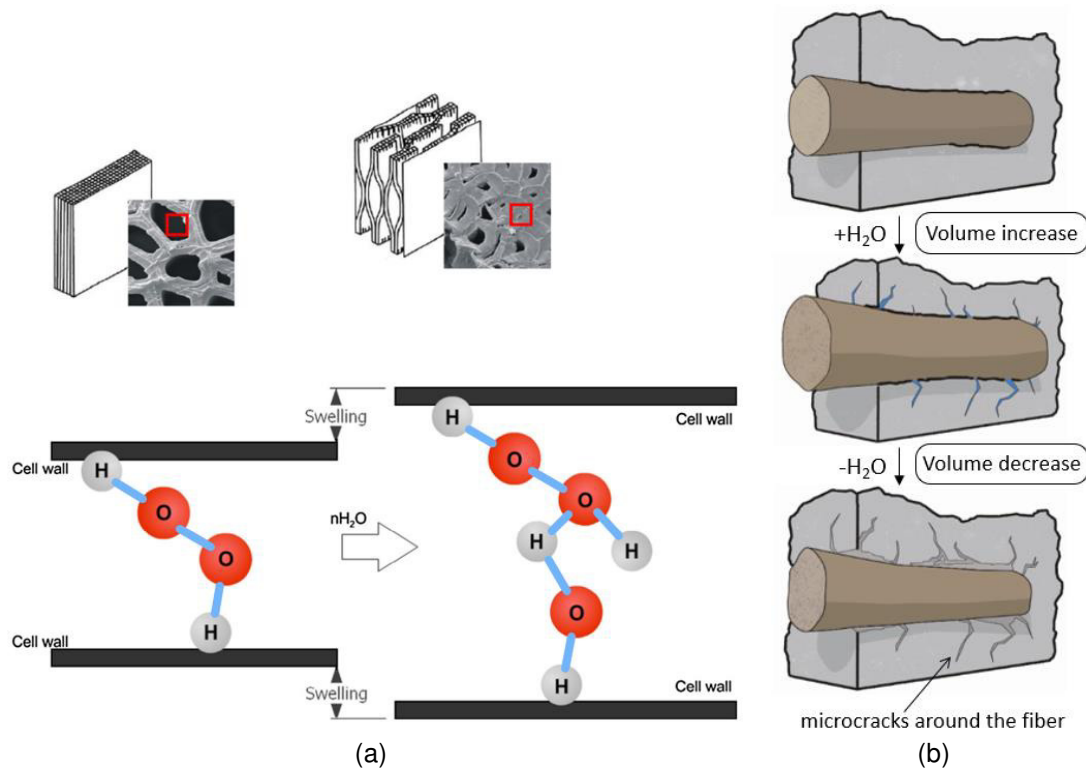


Figure 2.10 – (a) Schematic illustration of the swelling process in a cell wall [52]. (b) Effect of the fiber swelling in the fiber-matrix interface [45].

Natural fibers are, therefore, usually subjected to treatments/modifications to improve their adhesion properties, simultaneously reducing the water absorption tendency and improving their durability [55]. Therefore, there is a huge concern to modify these fibers to overcome these limitations and successfully utilize these materials in several applications in which commonly synthetic fibers are used.

2.2.3. Natural fiber degradation in alkaline environment

Although the several advantages of the use of natural fibers as reinforcement of cement-based composites, some deficiencies were found in their long-term durability [4,45,56–58]. The durability issues are associated with an increase in fiber failure and a decrease in fiber pullout over time, resulting in a reduction in the post-cracking strength and toughness of composites reinforced with these fibers. [10,45,57–61]. Gram [56] was one of the first authors to study the durability of sisal and coir fiber-reinforced concrete. The fiber degradation was evaluated by exposing them to alkaline solutions and then measuring the variations in tensile strength. He observed a deleterious effect of Ca^{2+} elements on fiber degradation. In a previous work [62], it was demonstrated that sisal fibers were completely degraded inside an

alkaline concrete, resulting in the loss of the concrete ductility after an accelerated aging test, with 10 wetting and drying cycles (Figure 2.11). This degradation in the alkaline environment of cementitious matrices depletes their reinforcing effect, which is a challenge that should be addressed before the widespread acceptance and implementation of cement-based composites in practical engineering.

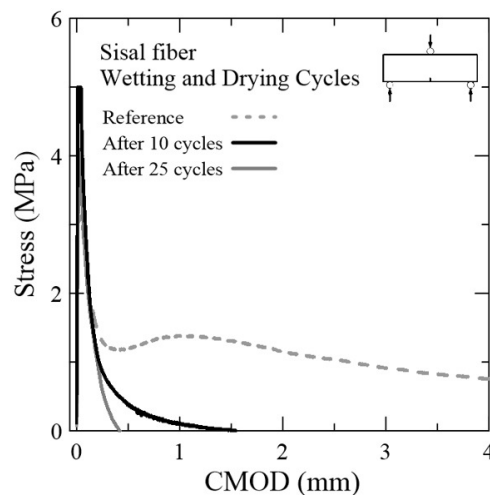


Figure 2.11 – Results of three-point flexural tests performed on aged and non-aged concrete reinforced with sisal fiber [62].

Cement-based matrices have high alkalinity due to the presence of calcium hydroxide [10], resulting in the degradation of natural fibers associated with two major mechanisms: alkaline hydrolysis and mineralization [56,60] (Figure 2.12). The alkaline hydrolysis consists of the dissolution of lignin and hemicellulose by means of diving up their molecular chains, reducing the polymerization degree [32,60,63]. As lignin and hemicellulose compose the middle lamella, their degradation by alkaline hydrolysis breaks the links between the individual cellulosic fiber cells, resulting in the loss of the reinforcing capacity of the fibers [10,59,60]. As a consequence, the fiber cells become dispersed in the pore alkaline solution of the matrix, which accelerates cellulose degradation [60]. As the degradation proceeds, the cement hydration products could gradually infiltrate into the fiber cell wall and lumens, leading to the mineralization of the natural fiber [44,61]. This process results in the embrittlement of the fiber, and also in the reduction of the strength and strain capacity [60].

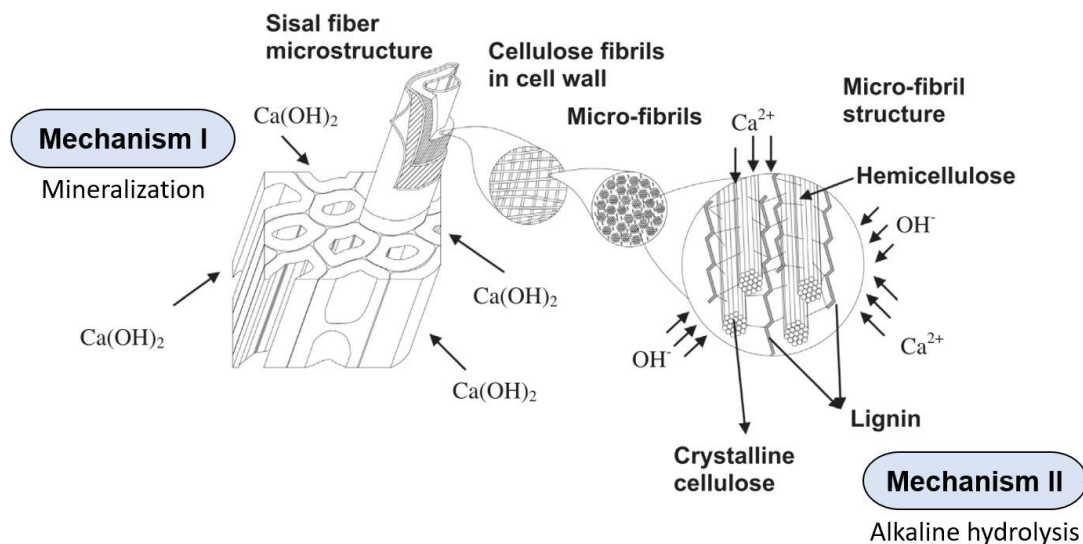


Figure 2.12 – Natural fiber degradation mechanisms inside a cement-based matrix (Adapted from [61]).

2.3. Methods for improving natural fiber performance in cement-based composites

Despite all the aforementioned advantages of the use of natural fibers, it was exposed that there are some limitations of their use as reinforcement in cementitious matrices, mainly associated with the long-term durability of this material. Therefore, there is an increasing interest in developing methods to overcome this condition, combining an adequate manner to enhance the interfacial fiber-matrix bond and ensure natural fiber durability. The developed methods can be divided into two different strategies: i) matrix modification, to reduce the alkalinity of the pore solution in cementitious composites; ii) fiber modification/treatment through physical or chemical protocols, in order to increase their stability and reduce water affinity.

2.3.1. Matrix modification

It is known that the high alkalinity of the pore solution in cementitious composites results in natural fiber degradation [31,37]. Thus, finding ways to reduce this alkalinity could help conserving the fibers. The use of supplementary cementitious materials as a partial replacement for Portland cement is a promising strategy to guarantee fiber integrity [31]. During the hydration process of ordinary Portland cement, pozzolanic reactions occur, that is, calcium hydroxide reacts with

amorphous silica and alumina, producing C-S-H/C-A-S-H. However, these reactions are not enough to consume all the calcium hydroxide content, leading to the enhancement of the matrix alkalinity. Thus, the addition of pozzolans promotes the reaction of the remaining calcium hydroxide, reducing the matrix alkalinity that weakens natural fibers [44]. Consequently, the alkaline hydrolysis and mineralization phenomena, discussed in the previous sections, are avoided.

Several pozzolanic materials have already been successfully applied for this purpose, such as silica fume, metakaolin, blast furnace slag, fly ash, and calcined clay, among others [45,59,61,64–66]. The partial replacement of Portland cement by silica fume and blast furnace slag (10% and 40% by mass, respectively) was proposed by Toledo Filho et al. [65]. The results indicated that the addition of silica fume was effective for preventing natural fiber degradation, while the blast furnace was less effective. By the replacement of 50% of cement with calcined clay, Toledo Filho et al. [59] achieved a CH-free matrix and the long-term embrittlement of the composite was completely avoided. These authors also reached good results by developing a low alkaline matrix with 50% partial cement replacement by metakaolin [61]. According to Silva et al. [64], a proportion of 30% of metakaolin and 20% of calcined clay was also effective to obtain a CH-free matrix. In a previous work [45], it was evaluated the efficacy of 50% by mass of cement replacement by metakaolin and fly ash. The results demonstrated that the degradation of sisal fiber was completely avoided by the reduction of the matrix alkalinity.

Therefore, the use of pozzolanic materials to obtain a low alkaline matrix seems to be a promising alternative for increasing the long-term durability of natural fiber cement-based composites. Besides that, Wei et al. [66] reported that cement substitution resulted in increased interfacial bond properties between natural fiber and cementitious matrix, as more cement hydration products adhered to the natural fiber surface, and a thicker transition zone was reached. Also, it is important to highlight that there is a potential reduction in the CO₂ emissions associated with cement production as a consequence of the partial replacement by pozzolanic materials, resulting in a more economical and sustainable material [67].

2.3.2. Fiber modification

Natural fibers can easily be modified to improve the interface bonding with the cementitious matrix. To minimize the dimensional changes of the fibers, chemical or physical modifications can be carried out [22,26,27,52,54,68,69]. Several treatments were proposed and successfully tested by some authors such as acetylation [26,70], hornification [50,51,71,72], polymer impregnation [52,73–76], and alkaline treatment [26,54,68,77,78]. Some treatments/modifications proposed in the literature are enlisted in Appendix A. It is important to highlight that studies on the influence of natural fiber treatments in cementitious matrices have been rare and are not exhaustive. Besides that, most of the studies are focused on polymeric matrices.

Physical modifications on natural fibers enhance their mechanical adhesion to the matrix as a result of the fiber roughness increase, without changing the chemical properties of the fibers [79]. On the other hand, chemical modifications improve fiber-matrix adhesion via chemical reactions [26,52,54,55]. Also, the chemical modification decreases the inherent hydrophilic behavior of the fibers, improving the fiber's volumetric stability and adhesion properties. A summary of different fiber modification procedures is presented in Table 2.3.

Table 2.3 – Types of surface treatments in natural fibers.

Fiber modification	Overall procedure	Ref.
Alkalization	Immersion of the fibers in alkaline solutions to remove hydrophilic constituents.	[42]
Acetylation	Change of the surface of the fibers through the application of acetic and propionic anhydrides.	[80]
Silanization	Application of silicon compounds that transform the surface of the fibers into hydrophobic.	[81]
Polymer impregnation	Creates a hydrophobic layer on the fiber surface, reducing fiber wettability.	[82]
Hornification	Subject the fibers to wetting and drying cycles in water, forcing the controlled shrinkage of the fibers.	[71]

Hornification is considered a simple and eco-friendly treatment, which uses water as the reagent, and has been successfully used to obtain durable cement composites reinforced with natural fibers [83]. The reduction in the water absorption capacity for the hornified fibers can be explained as follows: after several cycles of wetting and drying, there is an increased packing of the fiber cells

and a reduction of the lumen, which consequently reduces the capacity of water absorption of the fiber. According to Ferreira [50,71], the cycles promoted an increase in fiber stiffness and also reduced the water absorption tendency and dimensional variation [50]. Consequently, it was observed an increase in fiber-matrix adhesion.

Acetylation of natural fibers is a well-known esterification method causing the plasticization of cellulosic fibers [84]. The mechanism of the acetylation process is based on the reaction of the hydrophilic hydroxyl groups from hemicellulose and lignin of the natural fibers with acetyl groups ($\text{CH}_3\text{COO}-$) from acetic anhydride, therefore rendering the fiber surface more hydrophobic [84]. It has been reported that the acetylation treatment of plant fibers resists up to 65% moisture absorption depending on the degree of acetylation [84–86]. This treatment also provides a rough surface to the fibers with fewer void contents, improving the adhesion of the fiber with the matrix [85].

Among the various treatments cited, alkali treatment is considered one of the cheapest and less aggressive to the environment alternative, because it does not need any toxic organic chemicals [79,87]. Alkali treatment consists of fiber immersion on solutions of Calcium hydroxide ($\text{Ca}(\text{OH})_2$) [46,52,88] or Sodium hydroxide (NaOH) [54,55,74,87,89–91]. It results in the removal of some fiber constituents, including hemicellulose, lignin, pectin, waxy substances, and natural oils that cover the external surface of the fiber cell wall [68]. As a consequence, there is an improvement in the fiber's dimensional stability, reducing water absorption capacity, and also enhancing the resistance to the fiber against deterioration [22,68]. Besides the concern about the optimal solution concentration and period of exposure, the application of load during this treatment was also studied by some authors [87,92,93]. It has been found that load application can improve the alignment of the micro-fibrils along the fiber axis, resulting in higher strength and stiffness [87].

Polymer coating results in a reduction of water absorption by sealing the fiber surface [82]. The use of styrene-butadiene polymer latex as a surface treatment was evaluated by previous authors [52,73–76,94]. The improvement of the interfacial adhesion is a result of the chemical reactions of the polymer with calcium hydroxide and silicates, resulting in a polymer film that acts as a bridge between the fiber and the cementitious matrix, improving the interfacial bonding [52]. Chakraborty et al.

[95] suggested that a polymer modification enhanced the interfacial bond of jute fibers with a cementitious mortar. According to Fidelis et al. [76], this treatment also improves the volumetric stability of the fiber.

Although widely implemented in research works, many available methods have limitations for widespread large-scale implementation, such as the use of expensive and non-sustainable materials, the requirement of fiber separation during modification, complex instrumentation, and the need for multistep procedures. Therefore, the development of new innovative methods is still highly desired to encourage the use of dispersed natural fibers in cementitious composites.

2.4. Potential applications of natural fiber cement-based composites

Natural fibers can be added to cement-based matrices to act as a primary or secondary reinforcement, depending on the building component [96]. These fibers can work as primary reinforcement in thin products in which conventional reinforcing bars cannot be used. In these applications, the fibers could act to increase both the strength and toughness of the composite. In components such as slabs and pavements, fibers can be added to control cracking induced by humidity or temperature variations, working as secondary reinforcement.

The construction industry is considered the second largest sector employing natural fibers, second only to the automobile sector [11]. The production of composites with natural fibers was already investigated by different authors for a range of construction products, including tiles and sheets for roofing [15,97–104], wall panels [15,83,104], load-bearing hollowed walls [105–107], and paver blocks [94] (Figure 2.13). Savastano and his research group [15,100,101] focused on the use of natural fibers in building materials such as wall panels and roofing tiles. It was found that plant fiber composites based on brittle matrices are suitable as low-cost materials, with enough performance. Nevertheless, as durability is a major concern, each type of component must be well evaluated before widespread commercial use.

Roma et al. [98] evaluated the mechanical, physical, and thermal performance of cement-based tiles reinforced with sisal and eucalyptus fibers. The thermal performance of roofing tiles reinforced with vegetable fibers is acceptable as substitutes for conventional sheets. However, exposure to tropical climates caused

a severe reduction in the mechanical properties of the composites. Lertwattanaruk and Suntijitto [97] showed that 5% by weight of 10-mm-length coir fiber in cement-based roof sheets was sufficient to achieve the mechanical and thermal properties required for this application. Agopyan et al. [15] developed hollowed load-bearing wall panels with a composite reinforced with 2% of coir fibers, reaching an increase in the impact strength by two times more if compared to the unreinforced matrix. The panels also presented good thermal performance. Claramunt et al. [83] conducted experimental research to analyze the mechanical performance and durability of façade pieces of cement-based composites reinforced with treated flax nonwovens. The composite was considered a potential material for building envelopes with high strength and durability.

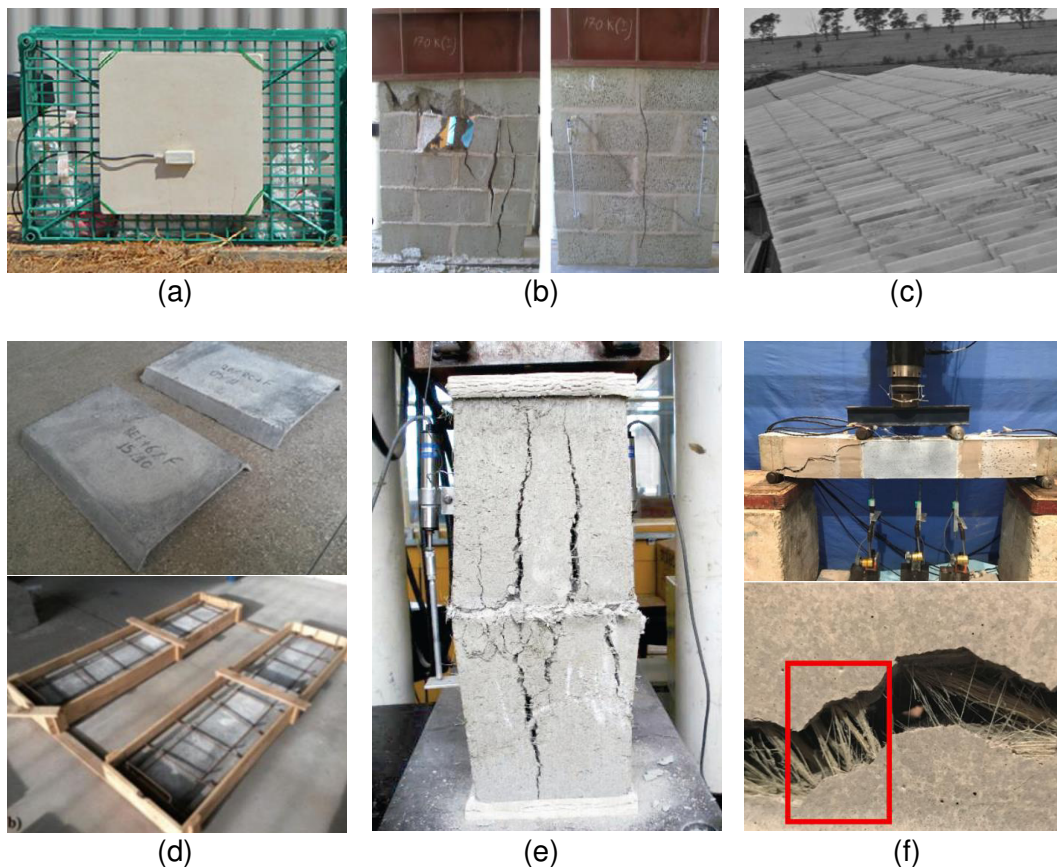


Figure 2.13 – The use of cement-based materials reinforced with natural fibers for structural applications: (a) façade plates for building envelope [83], (b) comparative compressive failure of plain and sisal fiber reinforced concrete walls [106], (c) roofing system with natural fiber-cement tiles [98], (d) concrete block for one-way precast concrete slabs [102], (e) ductile break of prisms reinforced with natural fibers [105], and (f) structural beam reinforced with composite laminates [108].

It is also possible to use sisal fibers in SHCC composites to be applied to several structural applications, which include structural elements from the bridge deck, columns and beams, building dampers, and repair of aging infrastructures, water channels, and other hydraulic structures [46]. These composites are usually reinforced with synthetic fibers, such as polyvinyl alcohol (PVA), polyethylene (PE), poly(p-phenylene-terephthalamide) (aramid), or high-tenacity polypropylene (HTPP). However, there is a recent effort to evaluate the use of natural fibers instead of synthetic ones [26,46,47,88]. Also, studies on the fracture and impact properties of short discrete natural fiber-reinforced cementitious composites by Zhou et al. [109] and Fujiyama et al. [110] confirmed that such composites can be effectively used for high-strength applications or where higher impact resistance is required. The use of aligned fibers results in an even better performance [39,111]. According to Teixeira et al. [39], the use of curauá fiber composite as a structural reinforcement provided an increase of about 16% in the ultimate strength of a concrete beam. However, the production of laminated panels with aligned fibers requires an onerous process to be executed.

Using natural fibers in engineering applications is challenging due to extensive issues addressed in previous sections. The high degree of moisture absorption, consistency of raw materials and their properties, and bonding characteristics between the natural fibers and cement-based matrices are the major issues that resist the popularity of using these composites in large-scale applications.

2.5. References

- 1 SATYANARAYANA K. G.; ARIZAGA, G. G. C.; WYPYCH, F. Biodegradable composites based on lignocellulosic fibers - An overview. **Progress in Polymer Science**, v.34, n.9, p.982-1021, 2009.
- 2 TOWNSEND, T. World natural fibre production and employment. In:___ **Handbook of Natural Fibres**. Elsevier, 2020. p.15-36.
- 3 BOURMAUD, A.; BEAUGRAND, J.; SHAH, D. U.; PLACET, V.; BALEY, C. Towards the design of high-performance plant fibre composites. **Progress in Materials Science**, v.97, p.347-408, 2018.
- 4 YAN, L.; KASAL, B.; HUANG, L. A review of recent research on the use of cellulosic fibres, their fibre fabric reinforced cementitious, geo-polymer and polymer composites in civil engineering, **Composites Part B: Engineering**, v.92, p.94-132, 2016.

- 5 MISRA, M.; PANDEY, J. K.; MOHANTY, A. K. **Biocomposites: Design and Mechanical Performance**. Elsevier, 2017.
- 6 FERREIRA, S. R. **Effect of surface treatments on the structure, mechanical, durability and bond behavior of vegetable fibers for cementitious composites**. Rio de Janeiro, 2016. 259p. Tese de Doutorado – COPPE, Universidade Federal do Rio de Janeiro.
- 7 KOMURAIHAH, A.; KUMAR, N. S.; PRASAD, B. D. Chemical Composition of Natural Fibers and its Influence on their Mechanical Properties. **Mechanics of Composite Materials**, v.50, n.3, p.359-376, 2014.
- 8 ROWELL, R. M.; HAN, J. S.; ROWELL, J. S. Characterization and Factors Effecting Fiber Properties. **Natural Polymers an Agrofibers Composites**. São Carlos, 2000. p.115-134.
- 9 SILVA, F. de A.; CHAWLA, N.; TOLEDO FILHO, R. D. Mechanical behavior of natural sisal fibers. **Journal of Biobased Materials and Bioenergy**, v.4, n.2, p.106-113, 2010.
- 10 KLERK, M. D.; KAYONDO, M.; MOELICH, G. M.; VILLIERS, W. I.; COMBRINCK, R.; BOSHOFF, W. P. Durability of chemically modified sisal fibre in cement-based composites. **Construction and Building Materials**, v.241, p.117835, 2020.
- 11 BARROS, J. A. O.; FERRARA, L.; MARTINELLI, E. **Recent Advances on Green Concrete for Structural Purposes**. The Contribution of the EU-FP7 Project EnCoRe. Springer, 2017.
- 12 CANTALINO, A.; TORRES, E. A.; SILVA, M. S. Sustainability of Sisal Cultivation in Brazil Using Co-Products and Wastes. **Journal of Agricultural Science**, v.7, n.7, p.64-74, 2015.
- 13 GAUAV; GOHAL, H.; KUMAR, V.; JENA, H. Study of natural fibre composite material and its hybridization techniques. **Materials Today: Proceedings**, v.26, n.2, p.1368-1372, 2020.
- 14 LEAO, A. L.; ROWELL, R.; TAVARES, N. Applications of Natural Fibers in Automotive Industry in Brazil - Thermoforming Process. In: **Fourth International Conference on Frontiers of Polymers and Advanced Materials**. Springer Science & Business Media, 1997. p.755-761.
- 15 AGOPYAN, V.; SAVASTANO JUNIOR, H.; JOHN, V. M.; CINCOTTO, M. A. Developments on vegetable fibre-cement based materials in São Paulo, Brazil: An overview. **Cement & Concrete Composites**, v.27, n.5, p.527-536, 2005.
- 16 SILVA, O. R.; COUTINHO, W. M.; CARTAXO, W. V.; CARVALHO, O. S.; SOFFIATI, V.; SILVA FILHO, J. L.; COSTA, L. B. Equipamentos. **Sisal**, 2021. Available in: <<https://www.embrapa.br/agencia-de-informacao-tecnologica/cultivos/sisal/pre-producao/equipamentos>> Accessed in: December 23, 2022.
- 17 S.A.A.S. FIBER. O Sisal. **Sisall: All About Sisal Fiber**, 2022. Available in: <<http://www.sisall.com.br/o-sisal/>>. Accessed in: December 23, 2022.
- 18 PALMFIL. Applications and Industries. **Reinforce Sustainably With**

- PalmFil**, 2020. Available in: <<https://www.palmfil.com/>>. Accessed in: December 23, 2022.
- 19 JOHN, M. J.; THOMAS, S. Biofibres and biocomposites. **Carbohydrate Polymers**, v. 71, n.3, p.343-364, 2008.
 - 20 GANAPATHY, T.; SATHISKUMAR, R.; SENTHAMARAIKANNAN, P.; SARAVANAKUMAR, S. S.; KHAN, A. Characterization of raw and alkali treated new natural cellulosic fibres extracted from the aerial roots of banyan tree. **International Journal of Biological Macromolecules**, v.138, p.573-581, 2019.
 - 21 SILVA, F. de A.; MOBASHER, B.; TOLEDO FILHO, R. D. Cracking mechanisms in durable sisal fiber reinforced cement composites. **Cement & Concrete Composites**, v.31, n.10, p.721-730, 2009.
 - 22 SANJAY, M. R.; SIENGCHIN, S.; PARAMESWARANPILLAI, J.; JAWAID, M.; PRUNCU, C. I.; KHAN, A. A comprehensive review of techniques for natural fibers as reinforcement in composites: Preparation, processing and characterization. **Carbohydrate Polymers**, v.207, p.108-121, 2019.
 - 23 JOHN, M. J.; ANANDJIWALA, R. D. Polyvinyl Alcohol-Modified Pithecellobium Clypearia Benth Herbal Residue FiberPolypropylene Composites. **Polymer Composites**, v.37, n.1, p.915-924, 2016.
 - 24 TAK LAU, K.; YAN HUNG, P.; ZHU, M. H.; HUI, D. Properties of natural fibre composites for structural engineering applications. **Composites Part B: Engineering**, v.136, p.222-233, 2018.
 - 25 MELO FILHO, J. de A. **Durabilidade química e térmica e comportamento mecânico de compósitos de alto desempenho reforçados com fibras de sisal**. Rio de Janeiro, 2012. 200p. Tese de Doutorado – COPPE, Universidade Federal do Rio de Janeiro.
 - 26 SNOECK, D.; SMETRYNS, P.-A.; BELIE, N. D. Improved multiple cracking and autogenous healing in cementitious materials by means of chemically-treated natural fibres. **Biosystems Engineering**, v.139, p.87-99, 2015.
 - 27 SOOD, M.; DWIVEDI, G. Effect of fiber treatment on flexural properties of natural fiber reinforced composites: A review. **Egyptian Journal of Petroleum**, v.27, n.4, p.775-783, 2018.
 - 28 CASTOLDI, R. de S.; SOUZA, L. M. S.; SILVA, F. de A. Comparative study on the mechanical behavior and durability of polypropylene and sisal fiber reinforced concretes. **Construction and Building Materials**, v.211, p.617-628, 2019.
 - 29 SHAHINUR, S.; HASAN, M. Natural Fiber and Synthetic Fiber Composites: Comparison of Properties, Performance, Cost and Environmental Benefits. In: **Encyclopedia of Renewable and Sustainable Materials**. Elsevier, 2019. p.794-802.
 - 30 SAVASTANO JUNIOR, H.; AGOPYAN, V. Transition zone studies of vegetable fibre-cement paste composites. **Cement and Concrete**

- Composites**, v.21, n.1, p.49-57, 1999.
- 31 PACHECO-TORGAL, F.; JALALI, S. Cementitious building materials reinforced with vegetable fibres: A review. **Construction and Building Materials**, v.25, n.2, p.575-581, 2011.
- 32 MUKHOPADHYAY, S.; KHATANA, S. A review on the use of fibers in reinforced cementitious concrete. **Journal of Industrial Textiles**, v.45, n.2, p.239-264, 2015.
- 33 SHAH, S. P.; KUDER, K. G.; MU, B. Fiber-Reinforced cement-based composites: A forty year odyssey. **6th RILEM Symposium Fibre-Reinforced Concretes – BEFIB**. Varenna, Italy. 2004.
- 34 ZOLLO, R. F. Fiber-reinforced concrete: an overview after 30 years of development. **Cement and Concrete Composites**, v.19, n.2, p.107-122, 1997.
- 35 VEIGAS, M. G.; NAJIMI, M.; SHAFEI, B. Cementitious composites made with natural fibers: Investigation of uncoated and coated sisal fibers. **Case Studies in Construction Materials**, v.16, e00788, 2022.
- 36 AMERICAN CONCRETE INSTITUTE. **ACI 544.1R-96**: State-of-the-Art Report on Fiber Reinforced Concrete. 2002.
- 37 ADESINA, A. Challenges and solutions for the use of natural fibers in cementitious composites. In: __ **Advances in Bio-Based Fiber: Moving Towards a Green Society**. Elsevier, 2022. p.675-685.
- 38 LI, V. C.; STANG, H.; KRENCHER, H. Micromechanics of crack bridging in fibre-reinforced concrete. **Materials and Structures**, v.26, n.8, p.486-494, 1993.
- 39 TEIXEIRA, F. P.; SILVA, F. de A. On the use of natural curauá reinforced cement based composites for structural applications. **Cement and Concrete Composites**, v.114, p.103775, 2020.
- 40 SOUZA, L. O.; SOUZA, L. M. S.; SILVA, F. de A. Study of Cracking Pattern and Its Evolution on Natural Textile Reinforced Concrete By Image Analysis. **4th Brazilian Conference on Composite Materials – BCCM4**. Rio de Janeiro, Brazil. 2018.
- 41 SILVA, F. de A.; MOBASHER, B.; SORANAKOM, C.; TOLEDO FILHO, R. D. Effect of fiber shape and morphology on interfacial bond and cracking behaviors of sisal fiber cement based composites. **Cement & Concrete Composites**, v.33, n.8, p.814-823, 2011.
- 42 CASTOLDI, R. de S.; SOUZA, L. M. S.; SOUTO, F.; LIEBSCHER, M.; MECHTCHERINE, V.; SILVA, F. de A. Effect of alkali treatment on physical–chemical properties of sisal fibers and adhesion towards cement-based matrices. **Construction and Building Materials**, v.345, p.128363, 2022.
- 43 CASTOLDI, R. de S.; SOUZA, L. M. S.; SILVA, F. de A. Cyclic Flexural Behavior of Polypropylene and Sisal Fiber Reinforced Concrete. **4th Brazilian Conference on Composite Materials – BCCM4**. Rio de Janeiro, Brazil. 2018.

- 44 ARDANUY, M.; CLARAMUNT, J.; TOLEDO FILHO, R. D. Cellulosic fiber reinforced cement-based composites: A review of recent research. **Construction and Building Materials**, v. 79, p.115-128, 2015.
- 45 CASTOLDI, R. de S.; SOUZA, L. M. S.; SILVA, F. de A. Comparative study on the mechanical behavior and durability of polypropylene and sisal fiber reinforced concretes. **Construction and Building Materials**, v.211, p.617-628, 2019.
- 46 ZUKOWSKI, B.; SILVA, F. de A.; TOLEDO FILHO, R. D. Design of strain hardening cement-based composites with alkali treated natural curauá fiber. **Cement and Concrete Composites**, v.89, p.150-159, 2018.
- 47 SOLTAN, D. G.; NEVES, P.; OLVERA, A.; SAVASTANO JUNIOR, H.; LI, V. C. Introducing a curauá fiber reinforced cement-based composite with strain-hardening behavior. **Industrial Crops and Products**, v.103, p.1-12, 2017.
- 48 DRECHSLER, A.; FRENZEL, R.; CASPARI, A.; MICHEL, S.; HOLZSCHUH, M.; SYNYSKA, A.; CUROSU, I.; LIEBSCHER, M.; MECHTCHERINE, V. **Surface modification of poly(vinyl alcohol) fibers to control the fiber-matrix interaction in composites**. *Colloid and Polymer Science*, v.297, n.7-8, p.1079-1093, 2019.
- 49 SINGH, S.; SHUKLA, A.; BROWN, R. Pullout behavior of polypropylene fibers from cementitious matrix. **Cement and Concrete Research**, v.34, n.10, p.1919-1925, 2004.
- 50 FERREIRA, S. R.; LIMA, P. R. L.; SILVA, F. de A.; TOLEDO FILHO, R. D. Effect of Sisal Fiber Hornification on the Fiber-Matrix Bonding Characteristics and Bending Behavior of Cement Based Composites. **Key Engineering Materials**, v. 600, p.421-432, 2014.
- 51 BALLESTEROS, J. E. M.; DOS SANTOS, V.; MÁRMOL, G.; FRÍAS, M.; FIORELLI, J. Potential of the hornification treatment on eucalyptus and pine fibers for fiber-cement applications. **Cellulose**, v.24, n.5, p.2275-2286, 2017.
- 52 FERREIRA, S. R.; SILVA, F. de A.; LIMA, P. R. L.; TOLEDO FILHO, R. D. Effect of fiber treatments on the sisal fiber properties and fiber-matrix bond in cement based systems. **Construction and Building Materials**, v.101, p.730-740, 2015.
- 53 JAIN, D.; KAMBOJ, I.; BERA, T. K.; KANG, A. S.; SINGLA, R. K. Experimental and numerical investigations on the effect of alkaline hornification on the hydrothermal ageing of Agave natural fiber composites. **International Journal of Heat and Mass Transfer**, v.130, p.431-439, 2019.
- 54 MWAIKAMBO, L. Y.; ANSELL, M. P. Chemical modification of hemp, sisal, jute, and kapok fibers by alkalization. **Journal of Applied Polymer Science**, v.84, n.12, p.2222-2234, 2002.
- 55 MWAIKAMBO, L. Y.; ANSELL, M. P. The effect of chemical treatment on the properties of hemp, sisal, jute and kapok for composite reinforcement. **Die Angewandte Makromolekulare Chemie**, v.272, n.1, p.108-116, 2002.

- 56 GRAM, H. **Durability of natural fibres in concrete**. Stockholm: CBI Forskning research, 1983. 255p.
- 57 RAMAKRISHNA, G.; SUNDARARAJAN, T. Studies on the durability of natural fibres and the effect of corroded fibres on the strength of mortar. **Cement and Concrete Composites**, v.27, n.5, p.575-592, 2005.
- 58 TOLEDO FILHO, R. D.; SCRIVENER, K.; ENGLAND, G. L.; GHAVAMI, K. Durability of alkali-sensitive sisal and coconut fibres in cement mortar composites. **Cement & Concrete Composites**, v.22, p.127-143, 2000.
- 59 TOLEDO FILHO, R. D.; SILVA, F. de A.; FAIRBAIRN, E. M. R.; MELO FILHO, J. de A. Durability of compression molded sisal fiber reinforced mortar laminates. **Construction and Building Materials**, v.23, n.6, p.2409-2420, 2009.
- 60 WEI, J.; MEYER, C. Degradation mechanisms of natural fiber in the matrix of cement composites. **Cement and Concrete Research**, v. 73, p.1-16, 2015.
- 61 MELO FILHO, J. de A.; SILVA, F. de A.; TOLEDO FILHO, R. D. Degradation kinetics and aging mechanisms on sisal fiber cement composite systems. **Cement & Concrete Composites**, v.40, p.30-39, 2013.
- 62 CASTOLDI, R. de S. **Propriedades mecânicas e durabilidade de concretos reforçados com fibras de polipropileno e sisal**. Rio de Janeiro, 2018. 147p. Dissertação de Mestrado – Programa de Pós-Graduação em Engenharia Civil, PUC-Rio.
- 63 SILVA, F. de A.; PELED, A.; ZUKOWSKI, B.; TOLEDO FILHO, R. D. Fiber Durability. In: __ **A Framework for Durability Design with Strain-Hardening Cement-Based Composites (SHCC)**. RILEM State-of-the-Art Reports 22, 2017. p. 59–78.
- 64 SILVA, F. de A.; TOLEDO FILHO, R. D.; MELO FILHO, J. de A.; FAIRBAIRN, E. de M. R. Physical and mechanical properties of durable sisal fiber-cement composites. **Construction and Building Materials**, v.24, n.5, p.777-785, 2010.
- 65 TOLEDO FILHO, R. D.; GHAVAMI, K.; ENGLAND, G. L.; SCRIVENER, K. Development of vegetable fibre-mortar composites of improved durability. **Cement & Concrete Composites**, v.25, n.2, p.185-196, 2003.
- 66 WEI, J.; MA, S.; THOMAS, D. G. Correlation between hydration of cement and durability of natural fiber-reinforced cement composites. **Corrosion Science**, v.106, p.1-15, 2016.
- 67 SILVA, G.; KIM, S.; AGUILAR, R.; NAKAMATSU, J. Natural fibers as reinforcement additives for geopolymers – A review of potential eco-friendly applications to the construction industry. **Sustainable Materials and Technologies**, v.23, p.e00132, 2020.
- 68 LI, X.; TABIL, L. G.; PANIGRAHI, S. Chemical treatments of natural fiber for use in natural fiber-reinforced composites: A review. **Journal of Polymers and the Environment**, v.15, n.1, p.25-33, 2007.
- 69 BECKERMANN, G. W.; PICKERING, K. L. Engineering and evaluation of

- hemp fibre reinforced polypropylene composites: Fibre treatment and matrix modification. **Composites Part A: Applied Science and Manufacturing**, v.39, n.6, p.979-988, 2008.
- 70 HILL, C. A. S.; KHALIL, H. P.; HALE, M. D. A study of the potential of acetylation to improve the properties of plant fibres. **Industrial Crops and Products**, v.8, n.1, p.53-63, 1998.
- 71 FERREIRA, S. R.; SILVA, F. de A.; LIMA, P. R. L.; TOLEDO FILHO, R. D. Effect of hornification on the structure, tensile behavior and fiber matrix bond of sisal, jute and curauá fiber cement based composite systems. **Construction and Building Materials**, v.139, p.551-561, 2017.
- 72 CLARAMUNT, J.; ARDANUY, M.; GARCÍA-HORTAL, J. A.; TOLEDO FILHO, R. D. The hornification of vegetable fibers to improve the durability of cement mortar composites. **Cement and Concrete Composites**, v.33, n.5, p.586-595, 2011.
- 73 LOPES, F. F. M.; ARAÚJO, T. de A.; NASCIMENTO, J. W. B.; GADELHA, T. S.; SILVA, V. R. Estudo dos efeitos da acetilação em fibras de sisal. **Revista Brasileira de Engenharia Agrícola e Ambiental**, v.14, n.17, p.783-788, 2010.
- 74 KUNDU, S. P.; CHAKRABORTY, S.; ROY, A.; ADHIKARI, B.; MAJUMDER, S. B. Chemically modified jute fibre reinforced non-pressure (NP) concrete pipes with improved mechanical properties. **Construction and Building Materials**, v.37, p.841-850, 2012.
- 75 FIDELIS, M. E. A.; SILVA, F. de A.; TOLEDO FILHO, R. D. The Influence of Fiber Treatment on the Mechanical Behavior of Jute Textile Reinforced Concrete. **Key Engineering Materials**, v.600, p.469-474, 2014.
- 76 FIDELIS, M. E. A.; TOLEDO FILHO, R. D.; SILVA, F. de A.; MOBASHER, B.; MÜLLER, S.; MECHTCHERINE, V. Interface characteristics of jute fiber systems in a cementitious matrix. **Cement and Concrete Research**, v.116, p.252-265, 2019.
- 77 GOMES, A.; MATSUO, T.; GODA, K.; OHGI, J. Development and effect of alkali treatment on tensile properties of curaua fiber green composites. **Composites Part A: Applied Science and Manufacturing**, v.38, n.8, p.1811-1820, 2007.
- 78 MANNA, S.; SAHA, P.; CHOWDHURY, S.; THOMAS, S. Alkali Treatment to Improve Physical, Mechanical and Chemical Properties of Lignocellulosic Natural Fibers for Use in Various Applications. In:___ **Lignocellulosic Biomass Production and Industrial Applications**. Scrivener Publishing LLC, 2017. p.47-64.
- 79 GHOLAMPOUR, A.; OZBAKKALOGLU, T. A review of natural fiber composites: properties, modification and processing techniques, characterization, applications. **Journal of Materials Science**, v.55, n.3, p.829-892, 2020.
- 80 TSERKI, V.; ZAFEIROPOULOS, N. E.; SIMON, F.; PANAYIOTOU, C. A study of the effect of acetylation and propionylation surface treatments on

- natural fibres. **Composites Part A: Applied Science and Manufacturing**, v.36, n.8, p.1110-1118, 2005.
- 81 GAÑAN, P.; GARBIZU, S.; LLANO-PONTE, R.; MONDRAGON, I. Surface modification of sisal fibers: Effects on the mechanical and thermal properties of their epoxy composites. **Polymer Composites**, v.26, n.2, p.121-127, 2005.
- 82 FERREIRA, S. R.; SENA NETO, A. R.; SILVA, F. de A.; SOUZA JUNIOR, F. G.; TOLEDO FILHO, R. D. The influence of carboxylated styrene butadiene rubber coating on the mechanical performance of vegetable fibers and on their interface with a cement matrix. **Construction and Building Materials**, v.262, p.120770, 2020.
- 83 CLARAMUNT, J.; FERNÁNDEZ-CARRASCO, L. J.; VENTURA, H.; ARDANUY, M. Natural fiber nonwoven reinforced cement composites as sustainable materials for building envelopes. **Construction and Building Materials**, v.115, p.230-239, 2016.
- 84 BLEZKI, A. K.; MAMUN, A. A.; LUCKA-GABOR, M.; GUTOWSKI, V. S. The effects of acetylation on properties of flax fibre and its polypropylene composites. **Express Polymer Letters**, v.2, n.6, p.413-422, 2008.
- 85 ZHOU, Y.; FAN, M.; CHEN, L. Interface and bonding mechanisms of plant fibre composites: An overview. **Composites Part B: Engineering**, v.101, p.31-45, 2016.
- 86 BLEZKI, A. K.; GASSAN, J. Composites reinforced with cellulose based fibres. **Progress in Polymer Science**, v.24, p.221-274, 1999.
- 87 KIM, J. T.; NETRAVALI, A. N. Mercerization of sisal fibers: Effect of tension on mechanical properties of sisal fiber and fiber-reinforced composites. **Composites Part A: Applied Science and Manufacturing**, v.41, n.9, p.1245-1252, 2010.
- 88 ZUKOWSKI, B.; SANTOS, E. R. F.; MENDONÇA, Y. G. dos S.; SILVA, F. de A.; TOLEDO FILHO, R. D. The durability of SHCC with alkali treated curaua fiber exposed to natural weathering. **Cement and Concrete Composites**, v.94, p.116-125, 2018.
- 89 MOKALOBA, N.; BATANE, R. The effects of mercerization and acetylation treatments on the properties of sisal fiber and its interfacial adhesion characteristics on polypropylene. **International Journal of Engineering, Science and Technology**, v.6, n.4, p.83-97, 2014.
- 90 MOHAN, T. P.; KANNY, K. Chemical treatment of sisal fiber using alkali and clay method. **Composites Part A: Applied Science and Manufacturing**, v.43, n.11, p.1989-1998, 2012.
- 91 SREEKUMAR, P. A.; THOMAS, S. P.; SAITER, J. M.; JOSEPH, K.; UNNIKRISHNAN, G.; THOMAS, S. Effect of fiber surface modification on the mechanical and water absorption characteristics of sisal/polyester composites fabricated by resin transfer molding. **Composites Part A: Applied Science and Manufacturing**, v.40, n.11, p.1777-1784, 2009.

- 92 GODA, K.; SREEKALA, M. S.; GOMES, A.; KAJI, T.; OHGI, J. Improvement of plant based natural fibers for toughening green composites-Effect of load application during mercerization of ramie fibers. **Composites Part A: Applied Science and Manufacturing**, v.37, n.12, p.2213-2220, 2006.
- 93 SUIZU, N.; UNO, T.; GODA, K.; OHGI, J. Tensile and impact properties of fully green composites reinforced with mercerized ramie fibers. **Journal of Materials Science**, v.44, n.10, p.2477-2483, 2009.
- 94 KUNDU, S. P.; CHAKRABORTY, S.; CHAKRABORTY, S. Effectiveness of the surface modified jute fibre as fibre reinforcement in controlling the physical and mechanical properties of concrete paver blocks. **Construction and Building Materials**, V.191, P.554-563, 2018.
- 95 CHAKRABORTY, S.; KUNDU, S. P.; ROY, A.; ADHIKARI, B.; MAJUMDER, S. B. Polymer modified jute fibre as reinforcing agent controlling the physical and mechanical characteristics of cement mortar. **Construction and Building Materials**, v.49, p.214-222, 2013.
- 96 TOLEDO FILHO, R. D.; JOSEPH, K.; GHAVAMI, K.; ENGLAND, G. L. The use of sisal fibre as reinforcement in cement based composites. **Revista Brasileira de Engenharia Agrícola e Ambiental**, V.3, N.2, P.245-256, 1999.
- 97 LERTWATTANARUK, P.; SUNTIJITTO, A. Properties of natural fiber cement materials containing coconut coir and oil palm fibers for residential building applications. **Construction and Building Materials**, v.94, p.664-669, 2015.
- 98 ROMA, L. C.; MARTELLO, L. S.; SAVASTANO JUNIOR, H. Evaluation of mechanical, physical and thermal performance of cement-based tiles reinforced with vegetable fibers. **Construction and Building Materials**, v.22, n.4, p.668-674, 2008.
- 99 ARSÈNE, M.; SAVASTANO JUNIOR, H.; ALLAMEH, S. M.; GHAVAMI, K.; SOBOYEJO, W. O. Cementitious composites reinforced with vegetable fibers. **Proceedings of the 1st Interamerican Conference on Non-conventional Materials and Technologies in the Eco-construction and Infrastructure – IAC-NOCMAT**. 2003.
- 100 SAVASTANO JUNIOR, H.; AGOPYAN, V.; NOLASCO, A. M.; PIMENTEL, L. Plant fibre reinforced cement components for roofing. **Construction and Building Materials**, v.13, n.8, p.433-438, 1999.
- 101 TONOLI, G. H.; SANTOS, S. F.; RABI, J. A.; SANTOS, W. N.; SAVASTANO JUNIOR, H. Thermal performance of sisal fiber-cement roofing tiles for rural constructions. **Scientia Agrícola**, v.68, n.1, p.1-7, 2011.
- 102 LIMA, P. R.; BARROS, J. A.; ROQUE, A. B.; FONTES, C. M.; LIMA, J. M. Short sisal fiber reinforced recycled concrete block for one-way precast concrete slabs. **Construction and Building Materials**, v.187, p.620-634, 2018.

- 103 LIMA, P. R.; ROQUE, A. B.; FONTES, C. M.; LIMA, J. M.; BARROS, J. A. Potentialities of cement-based recycled materials reinforced with sisal fibers as a filler component of precast concrete slabs. In: __ **Sustainable and Nonconventional Construction Materials using Inorganic Bonded Fiber Composites**. Elsevier, 2017. p.399-428.
- 104 LIMA, P. R.; BARROS, J. A. Exploring the Use of Cement Based Materials Reinforced with Sustainable Fibres for Structural Applications. In: __ **Recent Advances on Green Concrete for Structural**. Springer, 2017. p.403-424.
- 105 SOTO, I. I.; RAMALHO, M. A.; IZQUIERDO, O. S. Post-cracking behavior of blocks, prisms, and small concrete walls reinforced with plant fiber. **IBRACON Structures and Materials Journal**, v.6, n.4, p.598-612, 2013.
- 106 IZQUIERDO, S. I.; IZQUIERDO, O. S.; RAMALHO, M. C.; TALIERCIO, A. Sisal fiber reinforced hollow concrete blocks for structural applications: Testing and modeling. **Construction and Building Materials**, v.151, p.98-112, 2017.
- 107 ABDULLAH, A. C.; LEE, C. C. Effect of Treatments on Properties of Cement-fiber Bricks Utilizing Rice Husk, Corncob and Coconut Coir. **Procedia Engineering**, v.180, p.1266-1273, 2017.
- 108 TEIXEIRA, F. P.; CARDOSO, D. C. T.; SILVA, F. de A. On the shear behavior of natural curauá fabric reinforced cement-based composite systems. **Engineering Structures**, v.246, p.113054, 2021.
- 109 ZHOU, X.; GHAFAR, S. H.; DONG, W.; OLADIRAN, O.; FAN, M. Fracture and impact properties of short discrete jute fibre-reinforced cementitious composites. **Materials and Design**, v.49, p.35-47, 2013.
- 110 FUJIYAMA, R.; DARWISH, F.; PEREIRA, M. V. Mechanical characterization of sisal reinforced cement mortar. **Theoretical & Applied Mechanics Letters**, v.4, n.6, p.061002, 2014.
- 111 SOUZA, L. O.; SOUZA, L. M. S.; SILVA, F. de A. Mechanics of natural curauá textile-reinforced concrete. **Magazine of Concrete Research**, v.73, p.135-146, 2021.

3 Effect of alkali treatment on physical-chemical properties of sisal fibers and adhesion towards cement-based matrices

This chapter aims to evaluate the effect of an alkali treatment on sisal fibers to improve the fiber properties and the effectiveness of their use as reinforcement in cement-based matrices. Alkaline solution concentration (1, 5, and 10 wt.% NaOH) and different post-treatment protocols (use of distilled water or acetic acid) influence were evaluated. The physical, chemical, thermal, wettability, and surface characteristics were analyzed. Also, single-fiber direct tensile and pullout tests were performed. Results showed an increase in cellulose proportion with a reduction in hemicellulose and lignin content upon alkali treatment. Consequently, enhanced thermal stability and a decrease in the water uptake tendency were reached. Additionally, improved tensile properties, as well as an enhanced bond with the cementitious matrix, were found for alkali-treated fibers. Also, fibers became more stable when subjected to alkaline aggressive conditions. Thus, the alkali-treated sisal fiber seems to be an adequate and sustainable alternative as reinforcement for cement-based matrices.

The mechanical tests of the experimental program presented in this chapter were performed at PUC-Rio. The TGA and SEM images were obtained at TU Dresden, Germany, and the chemical composition analysis and water contact angle were executed at the Thermoanalysis and Rheology Laboratory at UFRJ.

Published article: July 2nd, 2022 – *Construction and Building Materials*

<https://doi.org/10.1016/j.conbuildmat.2022.128363>

3.1. Introduction

In recent years, there is a growing concern about environmental awareness, resulting in increased interest in the development of sustainable materials to replace the use of conventional synthetic ones. In this context, natural fibers are gaining

importance as a potential alternative to synthetic fibers to be used as reinforcement in composites. Several studies have been conducted to expose the benefits of using natural fibers, including their low density, low environmental impact, and adequate mechanical properties [1–8]. A variety of natural fibers are available for this purpose, such as jute, hemp, sisal, coir, flax, and others [1,9–14]. Those fibers are abundant in tropical climate zones and available at relatively low cost, mainly in developing countries. Also, they are biodegradable and obtained from natural sources, which may reduce the dependence on non-renewable material sources [1–3]. Their specific mechanical properties are comparable to those of synthetic fibers when used as reinforcement material [2,7,8,15,16].

Given its excellent mechanical properties, sisal fiber is one of the most widely used natural fibers [2,17,18]. This type of fiber is abundant and can be easily extracted from the leaves of the *Agave sisalana*. Even though they have the potential to be used in cement-based matrices, most of the studies are related to polymeric matrices [16]. On cement-based matrices, the use of dispersed fibers is focused on the mitigation of the shrinkage effects, improvement in the composite ductility and post-cracking toughness, and enhancement of fatigue and impact properties [18–20]. In addition, the ability of these fibers to reduce the propagation of cracks can improve the durability of reinforced concrete elements, avoiding the entrance of aggressive agents [11,20].

The physical and mechanical properties of these fibers are highly dependent on their chemical composition which consists of cellulose, hemicellulose, lignin, and a small amount of other soluble substances [2,16,21]. Cellulose is a component that provides fiber strength, stiffness, and stability [2,21]. It is a natural polymer that presents glucose units linked together in long chains, aligned in bundles named microfibrils. These microfibrils are embedded in a matrix of hemicellulose and lignin, bonded to the fibrils by hydrogen bonds [2,22]. The large number of hydroxyl groups in these bonds results in the hydrophilic nature of these fibers, leading to water movement through them [12,22,23]. Moisture absorption is responsible for the fiber dimensional variation, resulting in microcracks around the fiber-matrix interface and poor interfacial bond [2,7,23,24]. Besides that, these fibers are susceptible to degradation in an alkaline environment, resulting in changes to the mechanical performance of the composite depending on the age and exposure conditions of the reinforced element [1,2,16,23]. The high alkalinity

present in cement-based composites is a consequence of the presence of the calcium hydroxide formed during the cement hydration and is responsible for the loss of reinforcing capacity of sisal fibers due to the reaction named alkaline hydrolysis [25,26].

To inhibit or reduce the mentioned phenomena, several approaches have been proposed in the literature, mainly related to fiber or matrix modification. The matrix modification aims to reduce the calcium hydroxide content, responsible for the matrix alkalinity. The replacement of cement with pozzolanic materials has been studied by several researchers [12,15,27,28], and is shown to be a good alternative to guarantee the integrity of natural fibers. Another proposed technique is to subject the fiber to chemical or physical treatments to modify its chemical composition and/or surface properties to reach a more stable structure with enhanced bond properties [5,7,12,18,22,24,29–32]. Some examples of these treatments are acetylation [31,33], hornification [34,35], polymer impregnation [7,10,24,36,37], and alkali treatment [6,21,22,30,31,38–40]. These treatments can provide a reduction of the water absorption capacity, increased dimensional stability of natural fibers, and also resistance to alkaline attack [4,22,30,32].

Among the several approaches abovementioned, alkalization is considered one of the least expensive and most environmental-friendly methods considering that it does not need any toxic organic chemicals [6,41,42]. In addition, it is considered a simple procedure, possible to be implemented on an industrial scale. Alkali treatment consists of fiber immersion on controlled solutions of calcium hydroxide ($\text{Ca}(\text{OH})_2$) or sodium hydroxide (NaOH) [22,24,36,39,41,43–46]. The treatment results in the controlled removal of some fiber constituents, including hemicellulose, lignin, pectin, waxy substances, and natural oils that cover the external surface of the fiber cell wall [30]. As a consequence, fiber dimensional stability is improved by reducing water absorption capacity and increasing the fiber resistance against deterioration [29,30,42]. Besides the concern about the optimal solution concentration, the stretch of the fibers during the alkali exposure was found to improve the alignment of the microfibrils along the fiber axis, resulting in higher strength and stiffness on the alkali-treated fibers [41,42,47,48].

Even though there are studies on alkali treatment, most of them are focused on the application of these treated fibers in polymeric matrices [5,12,29,30,46,49,50]. Moreover, if the alkaline solution concentration is higher

than the optimum, excessive fiber degradation may occur, resulting in weakening or damaging the fibers [30,39,51]. However, fewer studies report the evaluation of the influence of this parameter on the fiber and cement-based composites properties. In this framework, the present work aims to clarify the effect of alkali treatment on sisal fibers' performance, focusing on the impact of the NaOH solution concentration, load application, and post-treatment procedure. Investigations in terms of fiber's physical aspect, mechanical properties, adhesion properties with cement-based matrix, and the changes in the stability of these fibers when exposed to an aggressive alkaline media were carried out.

3.2. Materials

3.2.1. Matrix

The cement-based matrix composition is presented in Table 3.1. The water/binder ratio adopted was 0.51. The binder material was composed of 50 wt.% of CP-II-F32 defined by the Brazilian standard ABNT NBR 16697 [1], 30 wt.% of metakaolin supplied by BASF, and 20 wt.% of fly ash supplied by Pozo Fly. The fine aggregate adopted was natural river sand with a fineness modulus of 3.02 mm and a maximum particle size of 4.75 mm. A proportion of 0.25 wt.% of Superplasticizer Glenium 51 supplied by BASF (solids content of 31 wt.%) was used to ensure good workability for the mixture. The mixture was produced in a cement mixer with 5 dm³ of capacity by first blending the dry materials for 1 minute and then adding the water and superplasticizer and mixing for 10 minutes.

Table 3.1 – Mixture composition of the cement-based matrix.

Components	Cement	Metakaolin	Fly Ash	Natural Sand	Water	Super-plasticizer
Dosage (kg/m ³)	190	114	76	535	195	0.95

3.2.2. Fiber

The sisal fibers used in this study were obtained from the sisal plant cultivated in farms located in the city of Valente, the state of Bahia, Brazil. The fibers were received in the form of bundles with approximately one meter in length. To remove surface residues and impurities, the fibers were submerged in hot water (70 ± 5 °C)

for one hour and then air-dried for 48 h. After this preliminary treatment, the fibers were subjected to the alkalization process, by immersing them in NaOH solution at a laboratory environmental controlled temperature of 22 ± 3 °C. A chemical treatment apparatus was developed to perform the alkali treatment on single-fiber monofilaments. This device allows for keeping the fiber stretched during the immersion of NaOH solution to minimize fiber shrinkage (Figure 3.1). The fibers were subjected to alkali treatment, considering the following variables:

- NaOH solution concentrations of 1, 5, and 10 wt.%;
- Immersion in the alkali solution for 1 h;
- Post-treatment procedure by washing with distilled water or by neutralizing with 1 wt.% of acetic acid (CH_3COOH) solution.

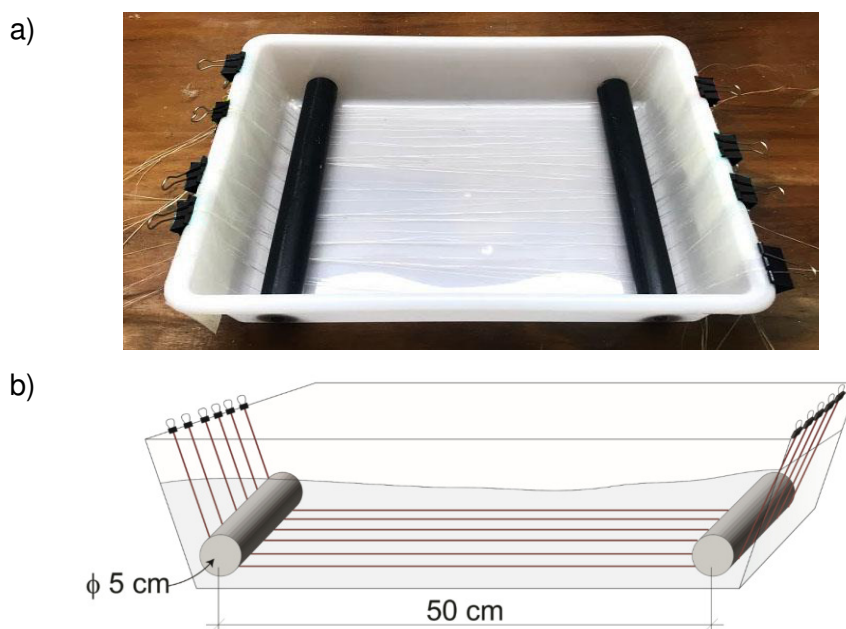


Figure 3.1 – (a) Picture and (b) schematic configuration of the apparatus used to keep the fibers stretched during alkalization.

Table 3.2 presents the summary of the variables and respective sample identification. For comparison, a fiber immersed in 5 wt.% NaOH solution in a non-stretched condition (5wt.%-A-NS) was also investigated in the mechanical evaluation. After the alkalization, the fibers were washed with distilled water or neutralized with an acetic acid solution. In the second case, fibers were thoroughly washed with distilled water after exposure to an acetic acid solution. The washed samples were then air-dried and prepared for the evaluations.

Table 3.2 – Summary of the variables related to the sample identification.

Sample identification	Solution Concentration	Post-treatment
Natural Sisal	-	-
1wt.%-W	1 wt.%	Water
1wt.%-A	1 wt.%	Acetic acid
5wt.%-W	5 wt.%	Water
5wt.%-A	5 wt.%	Acetic acid
10wt.%-W	10 wt.%	Water
10wt.%-A	10 wt.%	Acetic acid

3.3. Methods

3.3.1. Matrix characterization

It is well known that a partial cement replacement by pozzolanic materials results in more consumed calcium hydroxide, reaching a lower alkaline matrix and then preventing the degradation of lignocellulosic fibers [2–4]. Therefore, to evaluate the presence of calcium hydroxide in the matrix, the cement hydration products were determined through thermogravimetric analysis (TGA) using an STA 409 cell (Netzsch, Germany). The analysis was performed under an oxygen atmosphere in a constant flow of 60 ml/min, with a heating range of 10 K/min from room temperature until reaching 1000 °C.

3.3.2. Fiber characterization

3.3.2.1. Morphological characterization

The microstructure of the untreated and treated fibers was evaluated using an environmental scanning electron microscope (ESEM) model Quanta 250 FEG, FEI (The Netherlands). The ESEM was operated between 5 and 7 kV under low vacuum mode (40-110 Pa) without any additional sample coating.

3.3.2.2. Thermal stability

The thermal stability of the untreated and treated sisal fibers was evaluated by thermogravimetric analysis (TGA) using an STA 409 cell (Netzsch, Germany). The analysis was performed under oxygen as well as nitrogen atmosphere in a constant gas flow of 60 ml/min, with a heating rate of 10 K/min. Samples were previously weighed at 50 mg and then cut with a scissor into small fibers (approximately 1 mm in length) to carry out the analyses.

3.3.2.3. Chemical composition determination

The major components of the fibers were determined by a chemical analysis protocol (Figure 3.2). Before the chemical analysis, samples were grounded to powder, and the moisture content was obtained through an Electronic Moisture Analyzer (Ohaus, model MB27) by subjecting the fibers to the temperature of 105 °C. The dried samples were then enclosed in a sealed bag to avoid environmental moisture absorption.

The proportions of cellulose, hemicellulose, soluble and non-soluble lignin, extractives, and ash were determined by different processes. Firstly, the fiber extractives were removed with a Soxhlet extractor following the recommendations of Taylor [5,6]. Then, extractive-free samples were used for the subsequent analyses. The ash proportion, related to the inorganic portion of the lignocellulosic fiber, was obtained by igniting the organic material, following an adaptation of the procedures recommended by ABNT NBR 13999 [7]. The cellulose and hemicellulose contents were determined based on the total reducing sugar and glucose measured by the DNS (3,5-Dinitrosalicylic acid) protocol and GOD (Glucose oxidase) method. Both constituents were obtained following Maeda protocol [8]. Procedures presented by Gomide and Demuner [9] and Goldschmidt [10] were employed to measure the content of Klason lignin (non-soluble lignin) and soluble lignin, respectively. All the absorbance determinations in the process were measured in a UV spectrophotometer UV-2700 Shimadzu in the specific wavelengths presented in Figure 3.2.

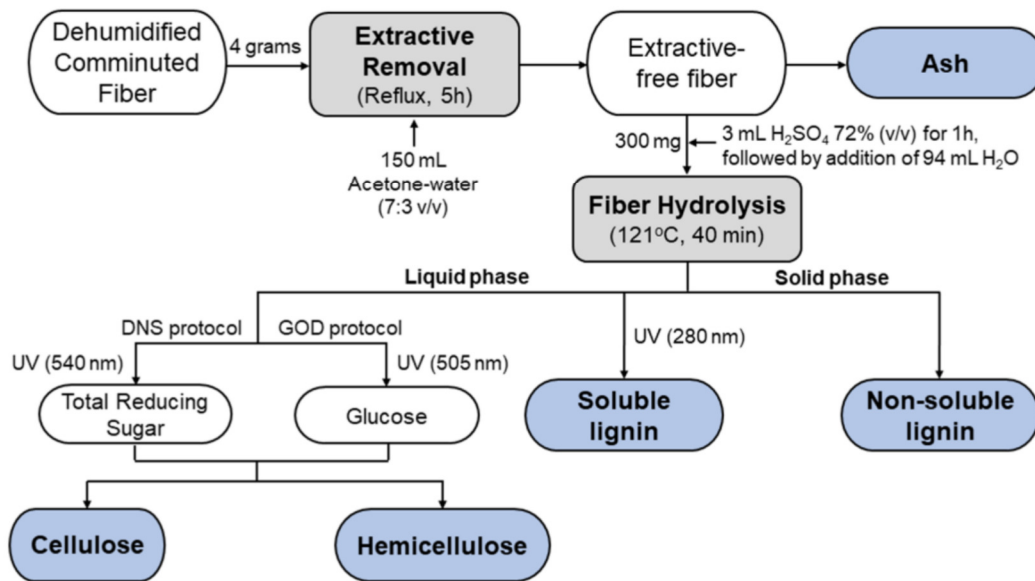


Figure 3.2 – Chemical analysis protocol developed for chemical composition determination of lignocellulosic fibers.

3.3.2.4. Water absorption capacity

The influence of the treatment on the fiber water absorption capacity was assessed by gravimetric analysis. Therefore, the samples of untreated and treated fibers were first subjected to a drying process with a constant temperature of 50 °C. Then, an amount of 0.1 g of fiber was immersed in distilled water to reach the maximum absorption capacity. After 10 and 30 minutes, 1, 2, 3, 4, 5, 6, 7, 8, and 24 hours the fibers were removed from the water, the excess water was eliminated with an absorbent paper, and then weighed. The water absorption of each sample was defined as an increase in weight percent according to Equation 3.1 as follows:

$$\text{Water absorption (\%)} = \left(\frac{\text{Saturated weight} - \text{Dry weight}}{\text{Dry weight}} \right) \times 100 \quad (\text{Eq. 3.1})$$

3.3.2.5. Water contact angle

Sisal fibers' wettability was also assessed through water contact angle measurements. A flat sheet of approximately 1 mm was prepared as a result of four alternate layers of fibers on a glass slide, resulting in a square sample of 1 cm x 1 cm, as presented in Figure 3.3. The water contact angle of these sheets was then measured by the sessile drop technique, in a DSA 100 Drop Shape Analyzer

System. A single 5 μl droplet of distilled water was placed on the surface of the sample at a rate of 100 $\mu\text{l}/\text{min}$ by using a pipette. Images were taken at each 1s until the test reached 30s. The contact angle values were then measured on both sides of the drop profile by using ImageJ software, and the final value corresponds to the average. This procedure was repeated at least 5 times for each condition.

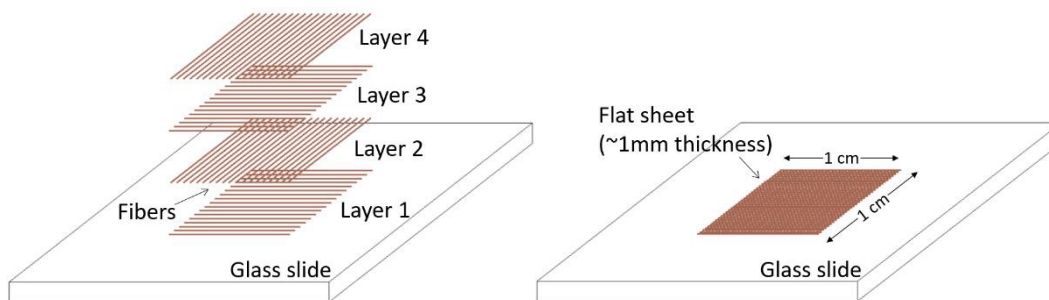


Figure 3.3 – Schematic configuration of the sample preparation for water contact angle measurements.

3.3.2.6. Mechanical properties

The sisal fibers' mechanical properties were measured by single-fiber direct tensile tests following the recommendations of ASTM C1557 [11]. Figure 3.4 shows the test arrangement and the detail of the specimen prepared for the test. Firstly, the fibers were fixed on a stiff paper frame (120 g/cm^2) using epoxy resin, with a gauge length of 20 mm. Then the frame was clamped on the testing machine and both edges of the paper frame were cut into two parts to allow the deformation of the fiber during the test. The tests were performed on a servo-hydraulic mechanical testing system model MTS-810 with a load capacity of 250 kN using a displacement rate of 0.1 mm/min . A load cell of 100 N was used to obtain the applied load with better resolution, and a linear variable differential transformer (LVDT) was coupled to the grips to record the displacement of the fiber. To ensure that the fibers were completely stretched at the beginning of the test, a pre-load of 0.5 N was applied to the fibers.

Ten samples of each condition presented in Table 3.2 were tested. To obtain the tensile stresses, an adjacent piece of the fiber was kept before each test and the fiber cross-sectional image was obtained from an optical microscope. Then, the images were post-processed using ImageJ software. A contour line was drawn to delineate the fiber perimeter, and the cross-sectional area of each tested fiber was

estimated. It is well known that the tensile strength of natural fibers is directly related to the orientation of the microfibrils compared to the load application axis, known as the microfibrillar angle (α). So, the microfibrillar angles were also obtained, following Equation 3.2 [12] as follows:

$$\varepsilon = \ln\left(1 + \frac{\Delta L}{L_0}\right) = -\ln(\cos \alpha) \quad (\text{Eq. 3.2})$$

Where α is the microfibrillar angle in degrees, ε is the strain, ΔL is the elongation at break in mm and L_0 is the gauge length in mm.

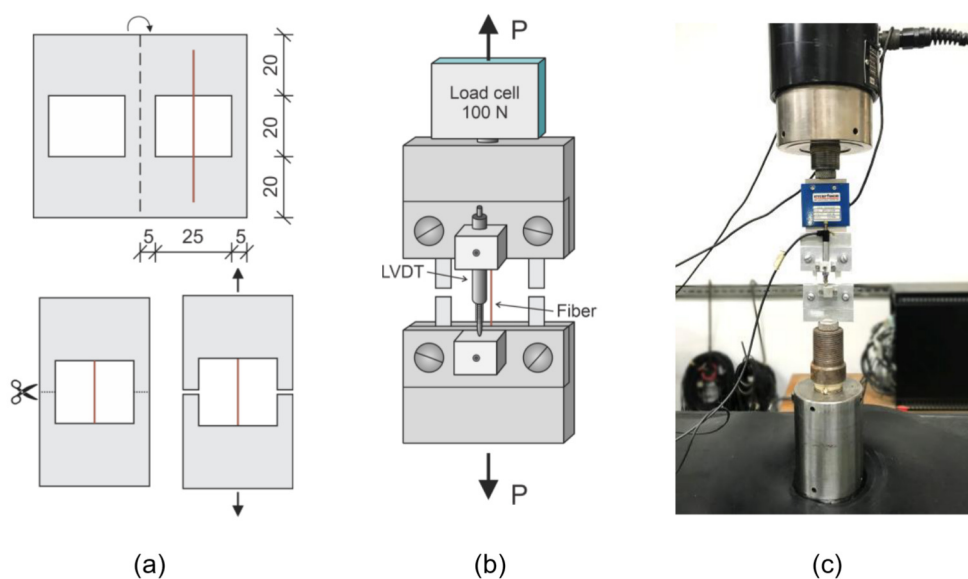


Figure 3.4 – Schematic configuration of the (a) sample preparation and (b) setup arrangement, and (c) general view of the setup arrangement for the fiber direct tensile tests (dimensions in mm).

3.3.2.7. Stability in alkaline media

The influence of the treatment on fiber stability in alkaline media was assessed. The main idea was to simulate the alkaline environment of cementitious matrices and evaluate if the treatment was effective to enhance fiber stability in these conditions. The procedure started with the exposure of discrete fibers for 28 days to two different aggressive alkaline solutions: 1N NaOH aqueous solution and pore solution, which consisted of a filtrated Portland cement solution made by mixing 1.25 kg of CEM I 32.5 R in 6.5 l of water and filtration after 24h. The pH values of the NaOH and Pore solutions were respectively 13.6 and 12.8. After the exposure interval, fibers were washed to remove the excess solution, dried for 24h,

and prepared for mechanical evaluation. Then, direct tensile tests were performed following the procedure explained for the evaluation of mechanical properties. To assess the effect of the alkaline exposure in terms of fiber strength, the Stability Ratio was obtained as defined in Equation 3.3.

$$\begin{aligned} \text{Stability Ratio} & \qquad \qquad \qquad \text{(Eq. 3.3)} \\ & = \frac{\text{Tensile strength after exposure to aggressive solution}}{\text{Tensile strength before exposure to aggressive solution}} \end{aligned}$$

3.3.3. Fiber-matrix adhesion

Single-fiber pullout tests were executed to evaluate the treatment influence on the adhesion with a cement-based matrix. The schematic configuration of the pullout specimens is shown in Figure 3.5. A special mold was produced to prepare them, consisting of acrylic plates connected by pins, with a specific dimension to ensure an embedded length of 25 mm. Firstly, the fibers were fixed transversely between the plates with 25 mm of spacing between them. Then, the superior plate was connected to the arrangement to maintain the alignment of the fibers and to not allow the fiber movement during casting. Finally, the mold was filled with the matrix. The demolding process involved the extraction of a long matrix beam with the fibers. Before testing the samples were cut between the neighboring fibers with a saw disc for having the 10 distinct specimens, with the dimensions of 25 mm by 25 mm. The specimens were cured for 28 days in a curing chamber with standard climate conditions until the fiber pullout tests.

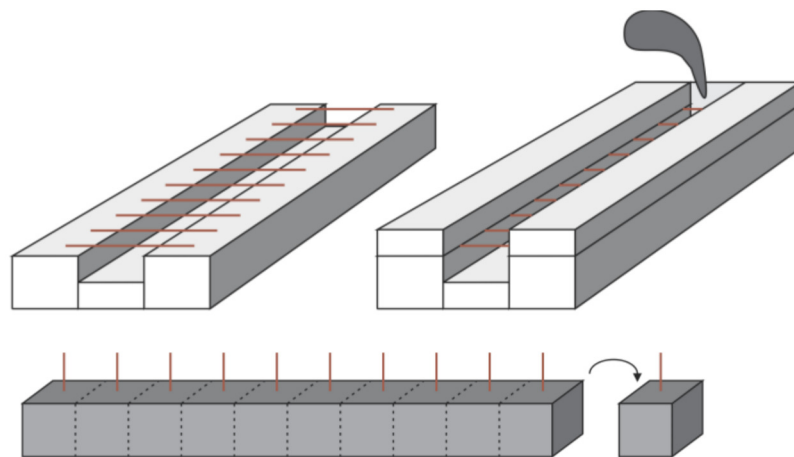


Figure 3.5 – Casting procedure of the pullout samples.

Figure 3.6 shows the setup configuration of the pullout tests. The test setup consisted of a metallic frame with two parallel aluminum plates. The distance between the plates is adjustable to the height of the sample to test. Tests were performed on a servo-hydraulic mechanical testing system model MTS-810 with a load capacity of 250 kN. A load cell of 100 N was attached to the arrangement to obtain the applied load. The test was conducted under constant crosshead displacement control at a rate of 1 mm/min. A total of 10 samples of each condition were tested. The cross-sectional area of each fiber was estimated before the tests from optical microscope images, as described for the single-fiber tensile tests. The average interfacial shear stress (τ) was obtained by a relation of the load immediately before the initiation of debonding (P_{max}) and the contact surface area of the fiber, i.e. the cross-sectional perimeter times the embedded length (Equation 3.4). To obtain the cross-sectional perimeter, the equivalent radius (r) was obtained from the fiber cross-sectional area before each test and the parameter L_c is equivalent to the embedded length, equal to 25 mm.

$$\text{Interfacial shear stress } (\tau) = \frac{P_{max}}{2\pi r L_c} \quad (\text{Eq. 3.4})$$

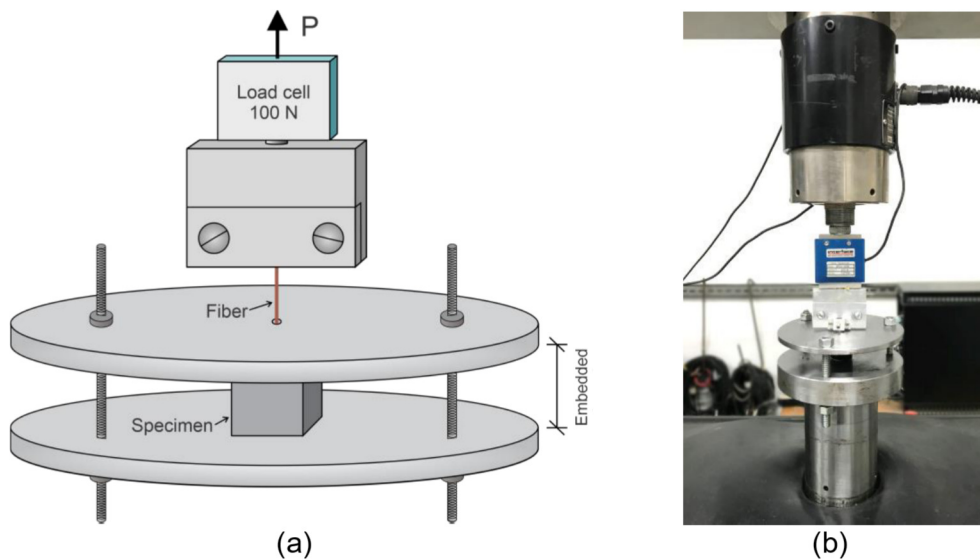


Figure 3.6 – (a) Detail and (b) general view of the single-fiber pullout test arrangement.

3.4. Results and Discussion

3.4.1. Matrix characterization

The matrix proposed in this study (Matrix 50C) and a matrix with 100% of cement as a binder (Matrix OC) were evaluated, for comparison. Figure 3.7 presents the TGA and DTG curves obtained after 28 days of curing. The results can be better visualized from the DTG curves, in which each peak corresponds to a mass loss related to the degradation of a specific hydration product. It can be noticed that the replacement of 50 wt.% of Portland cement with metakaolin and fly ash decreased the calcium hydroxide content of the matrix, evidenced by the elimination of the DTG peak between 450 and 550 °C, which is related to its dehydroxylation. The content of $\text{Ca}(\text{OH})_2$ (C_{CH}), expressed as a percentage of the dry sample weight at 550 °C [13,14], was also obtained (see Table 3.3). There was a reduction of around 75% in the $\text{Ca}(\text{OH})_2$ content for the 50C matrix in comparison to the OC Matrix. Furthermore, the amount of calcium-silicate-hydrate (C-S-H) gel was increased, indicated by a more pronounced peak around 130 °C. This mechanism is related to the reaction of the pozzolanic materials, rich in amorphous silica, with the $\text{Ca}(\text{OH})_2$ formed during cement hydration, generating more C-S-H [15]. Therefore, it is expected that this reduction in the matrix alkalinity avoids the degradation of the natural fiber.

Table 3.3 – Amount of calcium hydroxide (CH) on the matrices.

	Matrix OC	Matrix 50C
C_{CH} (wt.%)	13.62	3.34

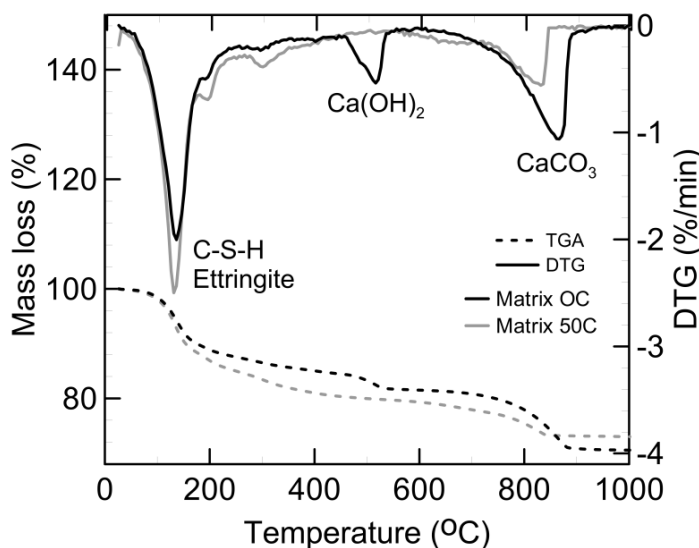


Figure 3.7 – TGA and DTG analysis performed for OC and 50C matrices at 28 days.

3.4.2. Fiber characterization

3.4.2.1. Morphological characterization

Table 3.4 present the average results of the cross-sectional area from untreated and alkali-treated sisal fibers. These fibers present a characteristic non-circular cross-section, as presented in Figure 3.8. The area of each fiber was obtained using ImageJ software, from an outline traced around each fiber. For the lowest NaOH solution concentration of 1wt.%, the cross-section area did not change considerably. However, with increasing NaOH concentration, the cross-sectional area of individual sisal fiber decreased. A similar result was also reported for other natural fibers [16,17]. This dimensional change could be related to the loss of matrix and microfibril aggregations with the treatment.

Table 3.4 – Cross-sectional area of untreated and alkali-treated sisal fibers.

	Natural Sisal	1wt.%-A	5wt.%-A	10wt.%-A
Cross-sectional area (mm²)	0.030 ± 0.008	0.032 ± 0.007	0.028 ± 0.010	0.023 ± 0.008

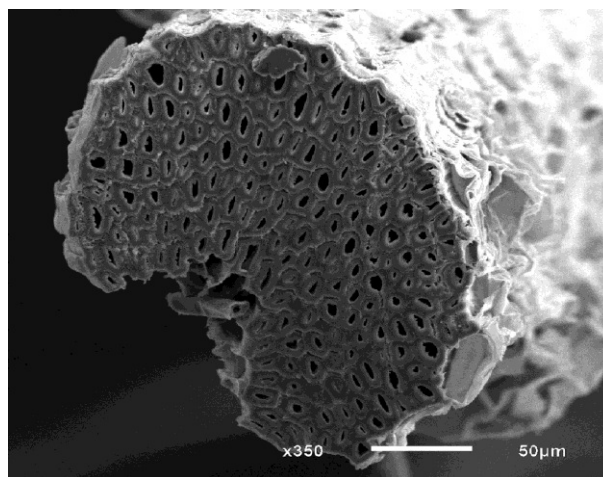
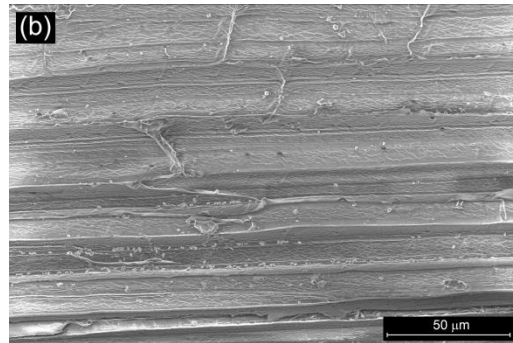
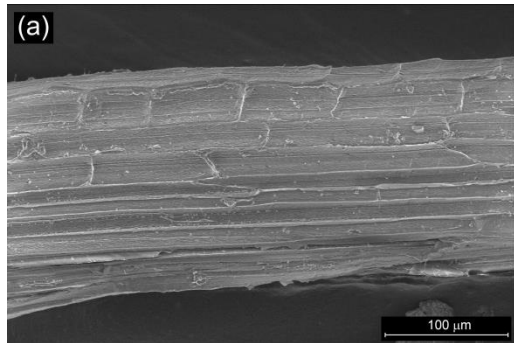


Figure 3.8 – Micrograph of a typical non-circular cross-section of a sisal fiber.

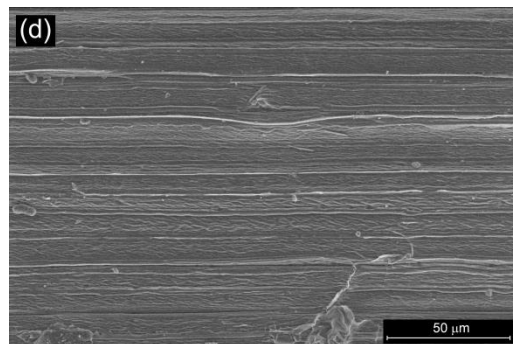
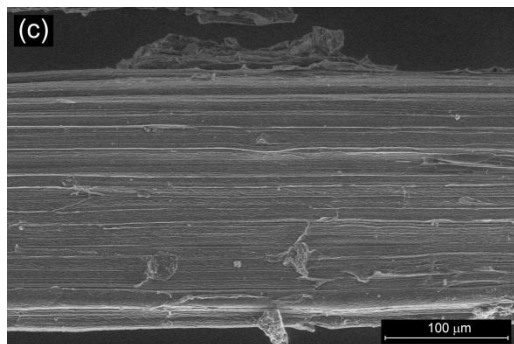
The ESEM micrographs of the longitudinal aspect of untreated and treated sisal fibers at two different magnifications are presented in Figure 3.9. From Figures 3.9.a and b, it can be observed that untreated sisal fibers are characterized by cellulose microfibrils, longitudinally oriented and parallel to the fiber axis, bonded together by a layer of hemicellulose, lignin, and waxes. However, alkali-treated

sisal fibers showed a different longitudinal aspect. The micrographs demonstrated that the increment in the solution concentration used in the alkali treatment resulted in a progressive increase in fiber deterioration.

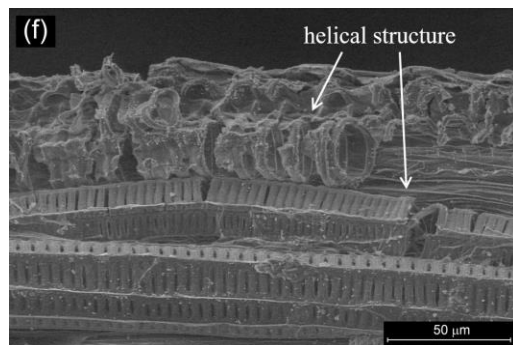
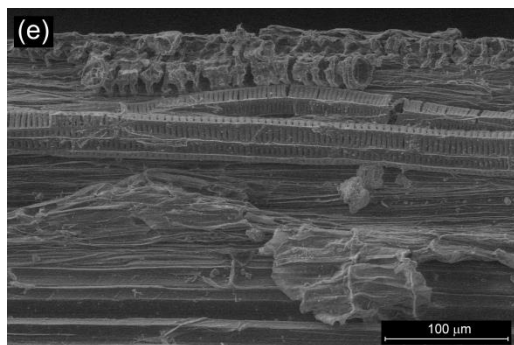
Natural Sisal



1 wt.% NaOH



5 wt.% NaOH



10 wt.% NaOH

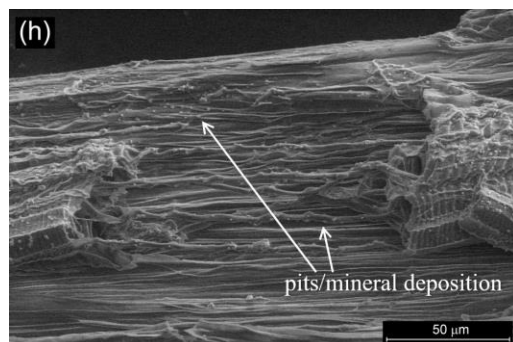
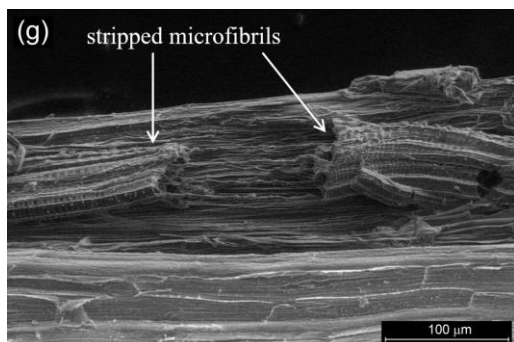


Figure 3.9 – Micrographs in two different magnifications of the longitudinal aspect of (a, b) untreated and alkali-treated sisal fibers with (c, d) 1 wt.%, (e, f) 5 wt.% and (g, h) 10 wt.% NaOH solution concentrations.

It is well known that alkaline deterioration consists of different steps, which are related to the time of exposure and also the environment's aggressiveness [18]. The first step consisted of the lignin degradation and part of the hemicellulose content, followed by the stripping of the cellulose microfibrils and finally the alkaline hydrolysis of the amorphous regions in cellulose chains [19]. In this sense, in the less aggressive condition with 1 wt% NaOH solution a low level of fiber deterioration was observed (Figures 3.9.c and d), and there is a removal of some surface constituents of the fiber, resulting in a relatively smooth surface compared to the natural sisal.

On the other hand, in a more aggressive environment with 5 wt% NaOH solution concentration, the degradation was more evident (Figures 3.9.e and f). The protective barriers of lignin and hemicellulose were destroyed, evidenced by fibril separation and the exposure of the helical structure of the cellulose microfibrils, composed of square-shaped spirals. This partial degradation of the matrix of lignin and hemicellulose, resulted in a rougher surface, which may enhance the available contact area and adhesion between fiber and the cementitious matrix.

The micrographs of 10 wt% alkali-treated sisal fiber (Figure 3.9.g and h) showed that at the higher degree of alkalization, the fibrillation increased but fiber damage was also observed. It is possible to notice the stripping of the microfibrils, which resulted from the partial removal of the non-cellulosic materials from the outer layer, revealing the inner cellulose microfibrils and resulting in the separation of fibrils as seen in detail in Figure 3.9.h. The removal of the outer layer is in accordance with the reduction of the cross-section area values observed from the alkali-treated fibers. Also, Figure 3.9.h shows many pits on the surface and mineral deposition. From this analysis, it was concluded that alkalization resulted in considerable modification of the surface of the fibers.

3.4.2.2. Thermal stability

The thermogravimetric (TGA) and differential thermogravimetry (DTG) curves of the untreated and alkali-treated sisal fibers in oxygen and nitrogen atmospheres are shown in Figure 3.10. The untreated fiber shows in both atmospheres three main decomposition steps, while the treated fibers presented only two clearly. The first mass loss starts at around 100 °C and is related to the loss of

free or weakly bonded water. A second peak at 270 °C appears only for the untreated fibers, and is associated with the thermal decomposition of hemicellulose. For all alkali-treated samples, this peak is not detected, evidencing a reduction of the hemicellulose content.

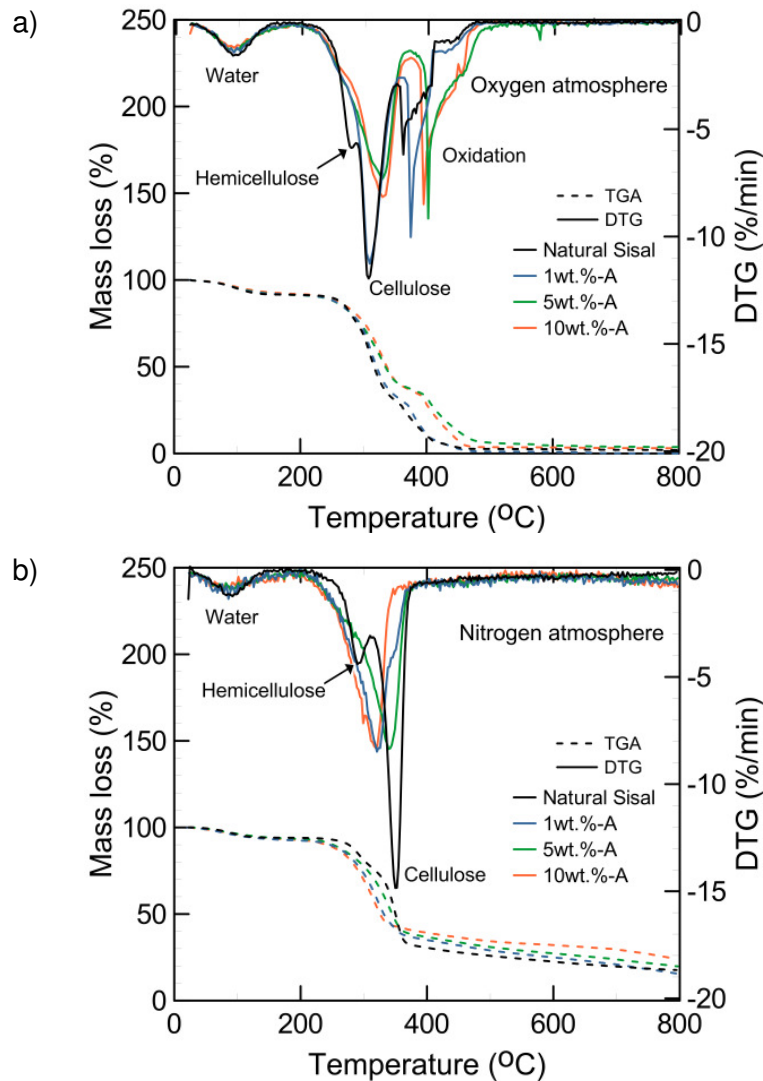


Figure 3.10 – TGA and DTG analysis performed in untreated and alkali-treated sisal fibers in (a) Oxygen and (b) Nitrogen atmosphere.

The maximum degradation rate occurs between 280 to 350 °C and is associated with the thermal decomposition of cellulose. For the alkali-treated fibers, this peak decreases in intensity. The evaluation of lignin degradation is more complex, as it extends to the whole temperature range (from 200 to 700 °C), due to different activities of the chemical bonds present in its structure [20]. In the oxidative atmosphere, a decomposition peak from 360 to 460 °C is seen, which only

happens as a result of the oxidation of volatile products formed due to reactions that involve cellulose [21,22]. In summary, all degradation peaks from hemicellulose and cellulose were shifted slightly to smaller temperatures in the oxidative atmosphere, as sisal fibers are more stable in nitrogen than air [21].

From Table 3.5, it is clear that the alkali treatment increased the main peak degradation temperature, and hence improved their thermal stability, which is in line with previous research works [21,23,24]. This behavior is mainly attributed to the reduced hemicellulose content, which does have a lower thermal resistance [22,25], and potentially by restricted molecules mobility due to the presence of new chemical groups on the fibers' surface [24].

Table 3.5 – Thermogravimetric results for untreated and alkali-treated sisal fibers performed in oxygen atmosphere.

	Peak degradation temperature (°C)	Temperature (°C)						
		10 wt.% mass loss	20 wt.% mass loss	30 wt.% mass loss	40 wt.% mass loss	50 wt.% mass loss	60 wt.% mass loss	70 wt.% mass loss
Natural Sisal	304.89	244.9	277.4	294.9	304.9	314.9	327.4	349.9
1wt.%-A	306.64	236.6	281.6	296.6	306.6	316.6	331.6	361.6
5wt.%-A	324.30	231.8	279.3	301.8	316.8	331.8	354.3	401.8
10wt.%-A	327.09	242.1	287.1	307.1	322.1	337.1	357.1	397.1

3.4.2.3. Chemical composition and water absorption measurements

The chemical composition of sisal fibers is fundamental to understanding the influence of the alkali treatment on the fiber structure and predicting their performance as reinforcement in cementitious composites. Figure 3.11 presents the measured chemical composition of the fibers, showing the concentration of cellulose, hemicellulose, lignin, ash, and extractives. It can be seen that the content of cellulose is much higher than hemicellulose, lignin, and other components, which is in agreement with previously reported results [26–29].

Comparing alkali-treated fibers to untreated fibers, cellulose was not consumed by the alkalization, proving that it is more stable to alkaline attack than the other components. Precisely, the alkali treatment did not consume the cellulose but modified the cellulose structure [16,30,31]. The native cellulose present in the untreated sisal fiber shows a monoclinic crystalline lattice of cellulose-I. After alkali treatment, it is possible that it converted to a new crystalline structure,

cellulose-II, which is thermodynamically more stable [16,30]. Since the strength and stiffness of natural fibers mainly depend on their cellulose content, as it is the only component that can exist in the crystalline form [32], increasing the cellulose content is important to improve fiber properties.

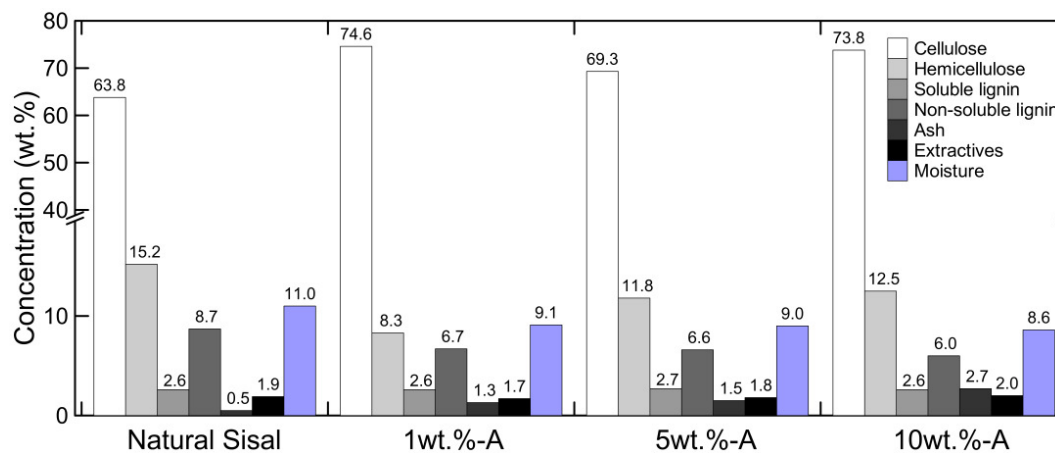


Figure 3.11 – Chemical composition and moisture content of untreated and alkali-treated sisal fibers.

However, the alkalization influences the non-crystalline components – hemicellulose, lignin, and ash, which are situated in between the cellulose region [23,33]. As shown in Figure 3.11, hemicellulose and lignin are more sensitive to the alkali attack, leading to a higher level of degradation, increasing the cellulose proportion on the fiber composition. The hemicellulose content is found in the non-crystalline regions of the fiber structure and has a lower average molar mass than those of cellulose, resulting in improved degradation [34]. Approximately 45 wt.%, 23 wt.%, and 18 wt.% of hemicellulose were removed from the natural fiber due to alkali treatment with 1, 5, and 10 wt.% solution of NaOH respectively, thus confirming TGA findings. The dissolution of hemicellulose may contribute to a closer packing of the cellulose chains and higher freedom for the fibrils, which can be reoriented along the direction of the tensile force and could enhance the mechanical performance of the fiber.

The NaOH solution is also responsible for the removal of lignin through a separation of the structural linkages between lignin and cellulose, and the disintegration of the lignin structure [35]. During the process of obtaining the Klason lignin (non-soluble), some amount of lignin is not accounted for, as it is partially soluble in acid. So, the content of the soluble lignin was also obtained. Concerning the soluble lignin, the results did not show significant changes in the

content after treatment. However, the non-soluble lignin presented considerable degradation after alkalization. The content was reduced from 8.7 wt.% to 6.7 wt.%, 6.6 wt.%, and 6.0 wt.% with alkali treatment with 1, 5, and 10 wt.% NaOH solutions, respectively. In consequence, a total lignin amount reduction was observed, reaching a loss of 24 % with the higher NaOH concentration treatment. The removal of lignin may be associated with the increase in fiber surface roughness (Figure 3.9), which is expected to lead to better interlocking with the matrix [36].

Another important point to notice is that treated sisal fibers presented a reduction in the water absorption capacity. In comparison to the untreated fiber, the moisture content on the fiber was reduced by 17%, 18%, and 22% for the 1, 5, and 10 wt.% NaOH-treated fiber, respectively (Figure 3.11). The same behavior was observed from the water absorption curves for the untreated and treated fibers as shown in Figure 3.12.a. The moisture absorption of the fiber was reduced drastically upon alkali treatment, which agrees with a previous report [36]. Also, the moisture absorption of the treated fibers decreased with an increase in NaOH concentration. The sisal fiber treated with 5 wt.% of alkali solution concentration reached about 70% lower moisture absorption than the untreated sisal fiber, while the treatment with 10 wt.% of alkali solution concentration resulted in approximately 90% of reduction. However, treatment with 1 wt.% of the alkali solution concentration was not efficient in the reduction of the water absorption capacity.

These results were also confirmed by water contact angle measurements (Figure 3.12.b and c). Untreated and alkali-treated sisal fibers did not present any considerable change in the contact angle result until 10s of the water droplet was placed onto the sample surface. However, after 20s it was completely absorbed by the untreated and 1wt.% alkali-treated fiber, which confirms that the treatment with low NaOH solution concentration was not efficient to reduce the water uptake tendency of sisal fibers. On the other hand, 5 and 10wt.% NaOH solution concentrations changed this behavior, with a slight decrease in water contact angle measurements, evidencing the increased hydrophobic behavior of alkali-treated fibers.

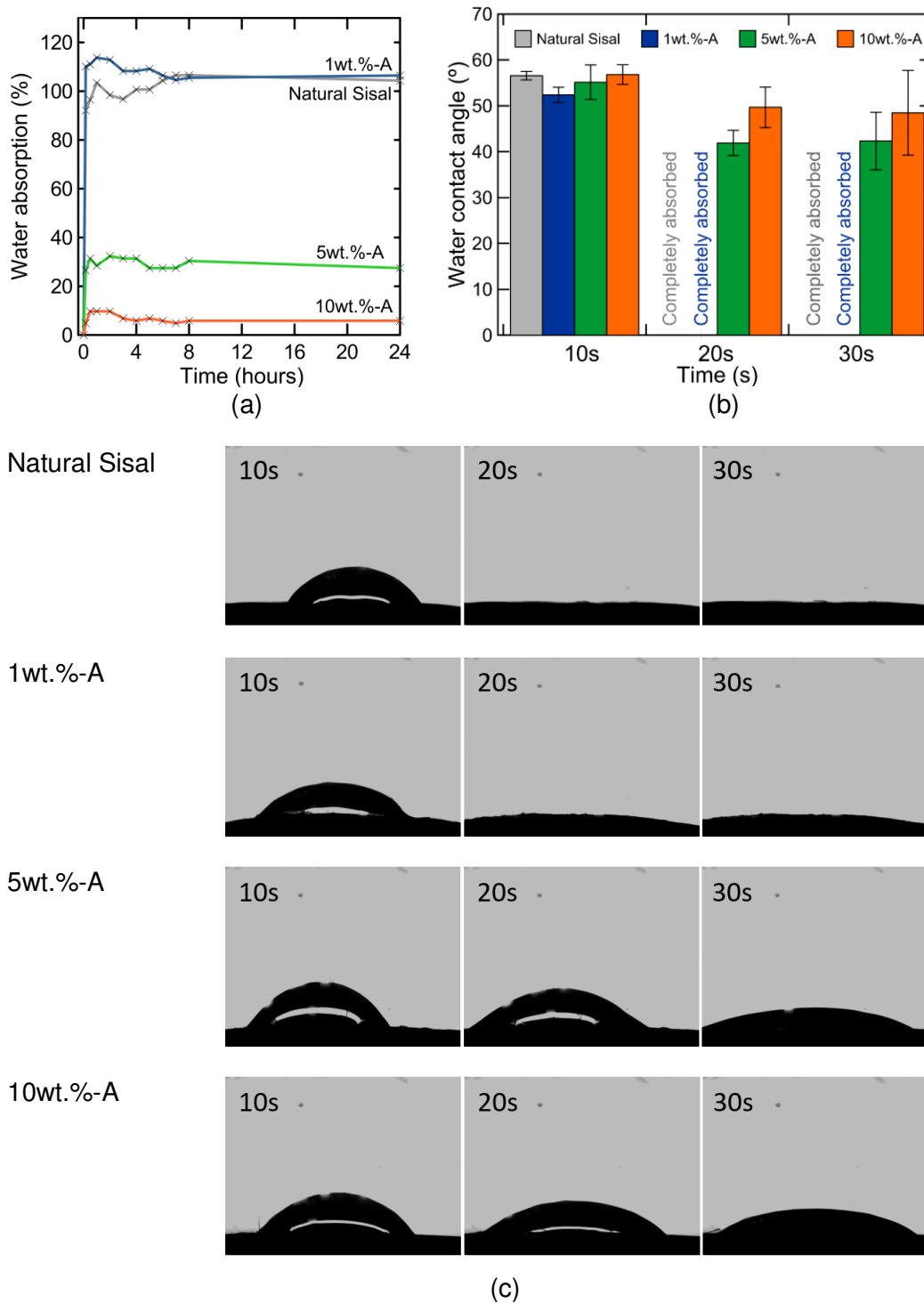


Figure 3.12 – (a) Water absorption curves, (b) water contact angle results, and (c) images for untreated and alkali-treated sisal fibers.

Hemicelluloses are highly hydrophilic [37], which justifies the reduction in moisture absorption with the reduction of the hemicellulose content observed for 5 and 10 wt.% NaOH solutions. Regarding cellulose, the conversion of cellulose from cellulose-I to cellulose-II type results in a more stable crystalline structure [16,30,38]. In the presence of NaOH, the OH^- groups present in cellulose molecules

react with water molecules and move out from the fibers, reducing the hydrophilic hydroxyl groups and, as a consequence, reducing the moisture tendency of the fiber [38]. In addition, it is expected that the cross-section of alkali-treated fibers presented a more compressed structure with a reduced void area of the fiber, which also can contribute to lower capillary water absorption [31,39]. It can be said that the hydrophilic nature of fiber had changed into a more hydrophobic character by alkali treatment. This fact could enhance the durability and dimensional stability of these fibers, resulting in less damage of the interfacial zone with cement-based matrices.

3.4.2.4. Mechanical properties

Table 3.6, Figures 3.13 and 3.14 show the direct tensile test results of untreated and treated sisal fibers in terms of average tensile properties values and typical tensile stress-strain curves for each condition. The effects of the exposure to alkali solutions with concentrations of 1, 5, and 10 wt.% and after treatment procedure by washing with distilled water or by neutralizing with acetic acid were evaluated. In addition, the non-stretched condition for the 5 wt.% NaOH solution concentration (5wt.%-A-NS) was evaluated for comparison. Untreated fibers presented a uniaxial tensile strength of 277.7 ± 28.9 MPa and a strain capacity of 10.6 ± 1.3 %, similar to previous studies [3,40–42].

Table 3.6 – Tensile properties of untreated and alkali-treated sisal fibers.

	Tensile Strength (MPa)	Young's Modulus (GPa)	Elongation at break (%)	Microfibrillar angle (°)
Natural Sisal	277.6 (28.9)	2.5 (0.3)	10.6 (1.3)	25.8 (1.5)
1wt.%-W	328.6 (28.7)	6.7 (0.8)	4.9 (0.5)	17.7 (1.0)
1wt.%-A	393.9 (65.3)	7.1 (0.9)	5.6 (1.0)	18.9 (1.6)
5wt.%-W	386.2 (53.2)	8.4 (1.4)	4.7 (1.0)	17.3 (1.8)
5wt.%-A	383.2 (54.7)	8.1 (1.1)	4.8 (1.0)	17.5 (1.8)
5wt.%-A-NS	215.8 (19.6)	5.6 (1.2)	4.2 (0.7)	16.5 (1.4)
10wt.%-W	365.9 (45.1)	5.8 (1.0)	6.0 (0.6)	19.6 (1.0)
10wt.%-A	314.6 (36.8)	7.0 (1.0)	4.5 (0.6)	17.1 (1.2)

From Table 3.6 it can be seen that all alkali-treated sisal fibers showed an increase in the tensile strength and Young's modulus up to 42% and 237%, respectively, and a decrease up to 60% on the elongation at break compared to the untreated fiber. As seen in the chemical composition determination, typically, the alkali treatment reduced the hemicellulose and lignin content while enhancing the cellulose proportion. Since the strength and stiffness of natural fibers are directly dependent on the cellulose content [32,36], as it is the only crystalline component in the fiber composition, it is expected that the enhancement of the cellulose proportion increases the tensile properties of alkali-treated fibers [43]. Also, the dissolution of amorphous components allows the cellulose fibrils reorientation along the direction of the tensile force, resulting in enhanced mechanical performance.

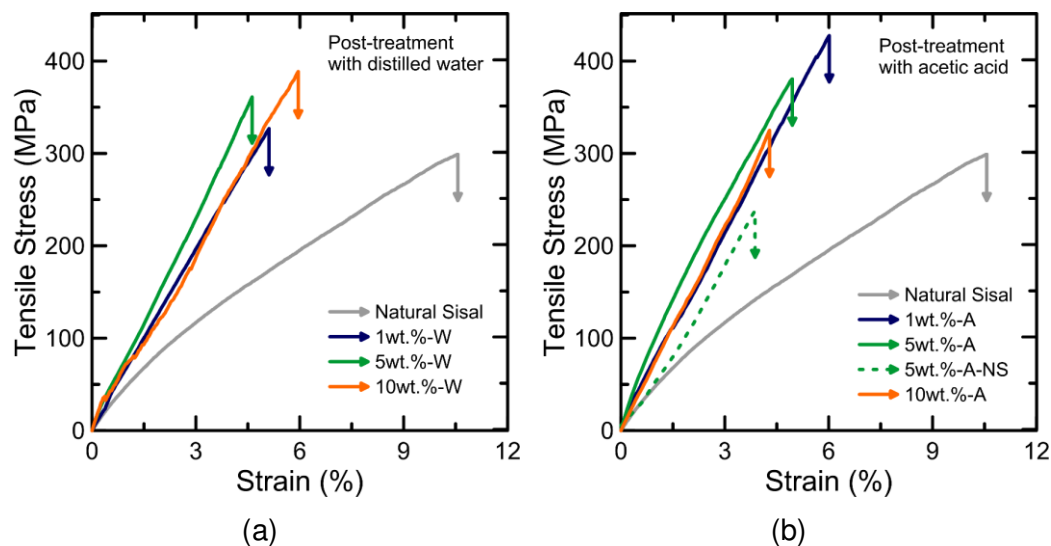


Figure 3.13 – Representative direct tensile stress curves of untreated and alkali-treated sisal fibers, considering the use of (a) distilled water or (b) acetic acid in the post-treatment procedure.

The effect of the alkali solution concentration on the fiber's mechanical properties is also shown in Figures 3.13 and 3.14. Considering the use of distilled water in the post-treatment procedure (Figures 3.13.a and 3.14.a), the increase in the alkali solution concentration resulted in a progressive increase in tensile strength, until 5 wt.% NaOH concentration. In the case of 10 wt.% concentration, it can be seen a decrease in tensile properties. Similar behavior was found in the case of the use of the acid acetic solution in the neutralizing procedure after

treatment (Figures 3.13.b and 3.14.b). In this case, a decrease in tensile properties was observed for the 5 wt.% solution concentration. However, it was more evident for the highest solution concentration. This reduction of strength due to alkali treatment was also reported in previous research [34], and should be attributed to enhanced degradation of fiber components and destruction of the links between the fiber cells, indicating that the treatment with higher alkali solution concentrations resulted in excessive damage of the fiber. However, the fracture stress and Young's modulus were still higher than those of untreated fibers.

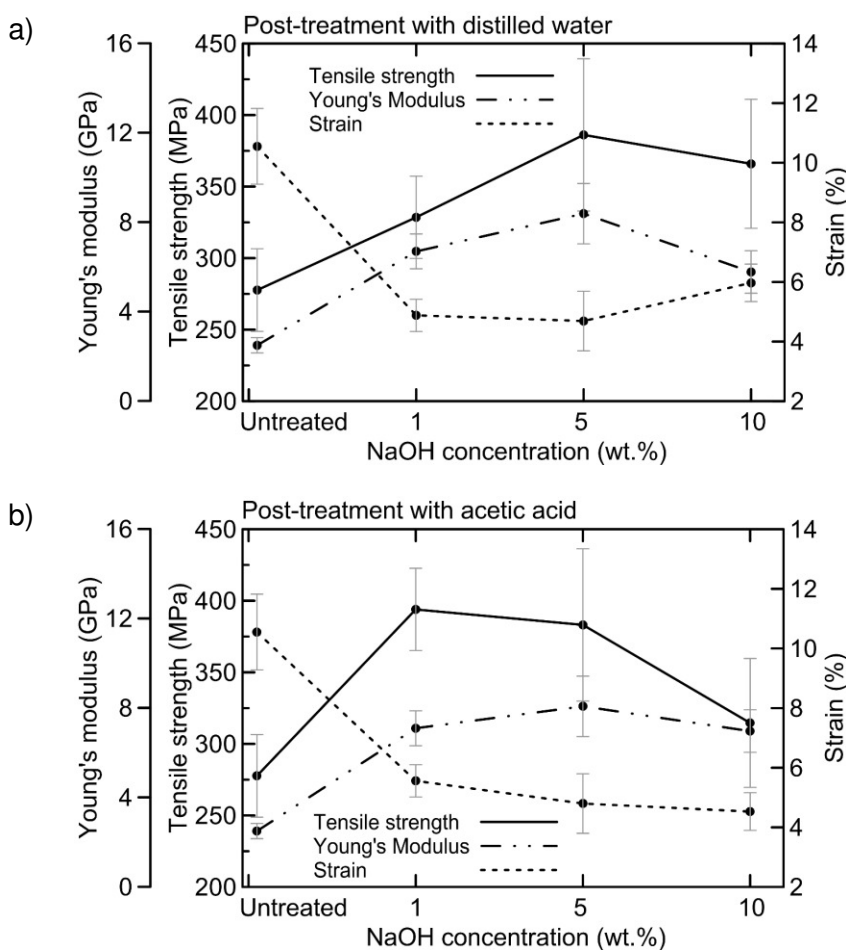


Figure 3.14 – Effect of alkali treatment on the tensile properties of sisal fibers, considering the use of (a) distilled water or (b) acetic acid in the post-treatment procedure.

From Figure 3.13.b it is also possible to compare the typical tensile stress-strain curves of sisal fibers treated with 5 wt.% alkali solution concentration under two different load conditions: (i) non-stretched condition, as discrete fibers of 50 mm simply soaked in the alkaline solution during fiber treatment (5wt.%-A-NS); and (ii) stretched condition, with the fibers aligned during treatment (5wt.%-A).

From the curves, it is clear that simply soaking discrete fibers in the solution results in a reduction of around 45% in the fiber tensile strength. In this condition, it is expected to occur the shrinkage of the fibers, which can directly influence their tensile properties.

On the other hand, the stretch of the fibers during alkalization avoids the shrinkage effect and allows the arrangement of the microfibrils, becoming relatively parallel and aligned along the fiber axis. The microfibrillar angle was directly proportional to the elongation at break and inverse proportional to the tensile strength and Young's modulus. This reduction in the microfibrillar angle can be related to the increase in fiber strength and stiffness and a decrease in strain. The current results are similar to those found in the literature [32,44–47].

3.4.2.5. Stability in alkaline media

To evaluate the effect of the alkaline exposure on untreated and treated fiber mechanical strength, the stability ratio (SR) was obtained as a comparison of the tensile strength of the fiber before and after the degradation procedure. The results are presented in Figure 3.15. Higher ratios of SR mean that the fibers have greater stability in an alkaline environment.

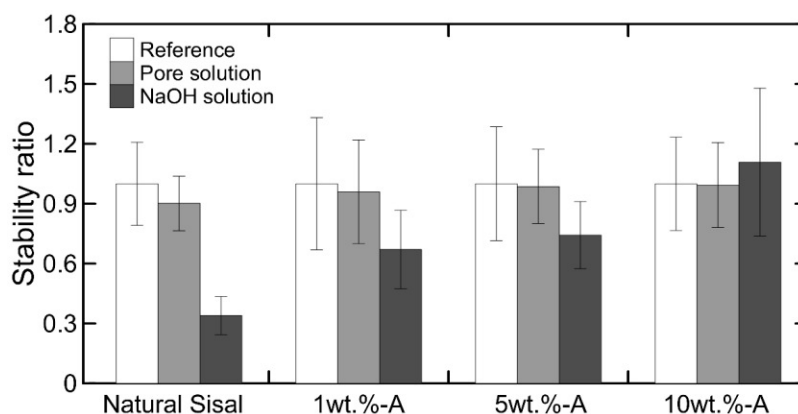


Figure 3.15 – Stability ratio of untreated and alkali-treated sisal fiber after exposure to pore solution and 1N NaOH solution for 28 days.

From Figure 3.15, it is clear that there is a degradation of the natural sisal fiber tensile strength for both alkaline solutions adopted in this study. For natural sisal, after 28 days a SR of 0.90 ± 0.14 and 0.34 ± 0.09 was obtained for the pore and NaOH solutions, respectively. As mentioned before, in aggressive alkaline media lignin and hemicellulose are gradually destroyed, followed by the

deterioration of cellulose. As a consequence, there is a reduction in the mechanical properties of these fibers [18,43]. It should be mentioned that 1N NaOH solution is more alkaline than a typical cementitious matrix, and thus represents a severe condition. For this reason, increased degradation was observed in this aggressive solution in comparison to the pore solution.

On the other hand, the alkaline treatment was efficient to guarantee more stable fibers in sodium hydroxide solution. After exposure to aggressive solutions, SR of 0.67 ± 0.19 and 0.74 ± 0.17 in the highly aggressive NaOH solution for 1wt.%-A and 5wt.%-A fibers, respectively. It means that they became more resistant to the alkaline attack in comparison to the natural fiber subjected to the same conditions. The best results were achieved by the 10wt.%-A treated fiber, which presented higher ratios of stability ratio, 0.99 ± 0.21 in pore solution and 1.11 ± 0.37 in NaOH solution. Similar results were obtained in a previous study [43]. Therefore, alkali-treated sisal fibers have potential use in cementitious composites in terms of improved stability in alkaline conditions.

3.4.3. Fiber-matrix adhesion

Figure 3.16 shows the typical pullout curves of untreated and treated sisal fibers in a low alkaline cement-based matrix with 25 mm of embedment length. The pullout curve of natural sisal fiber is characterized by an initial linear range with a rapid rate of ascending load, followed by a nonlinearity, corresponding to the initial point of fiber debonding. The load at this point is known as the peak debonding load (P_{max}), equivalent to the maximum value reached under partial debonding conditions. After this peak load, there is a progressive failure of the chemical bond, propagating toward the embedded end of the fiber. At this moment, the pullout behavior is governed by the frictional interaction and mechanical interlock of the fiber-matrix interface until the complete debonding of the fiber. From Figure 3.16 it is possible to notice that all the evaluated fibers presented a debonding process with a constant slip behavior, with the complete fiber pullout and no occurrence of fiber failure.

Figure 3.17 summarizes the fiber-matrix interfacial characteristics expressed in terms of peak debonding load, interfacial bond strength, and total energy until 1 mm of displacement. As sisal fibers present a significant variability in geometric

properties, the pullout results are presented in terms of the average interfacial bond strength (τ), obtained as the peak load divided by the embedment surface area of the respective tested fiber. It is assumed a uniform bond shear stress over the length of the embedded part of the fiber. The total energy was evaluated by computing the area under pullout curves until the slip value of 1 mm. From Figure 3.16 it is possible to note that, at 5 wt.% NaOH solution concentration, treated fibers had significantly enhanced pullout properties than untreated fiber. Compared to natural sisal, there is an increase of approximately 118%, 67%, and 90% on the peak debonding load, interfacial bond strength, and energy until 1 mm, respectively. However, the alkali modification with 1 wt.% and 10 wt.% does not significantly affect the interaction of sisal fibers with a cementitious matrix.

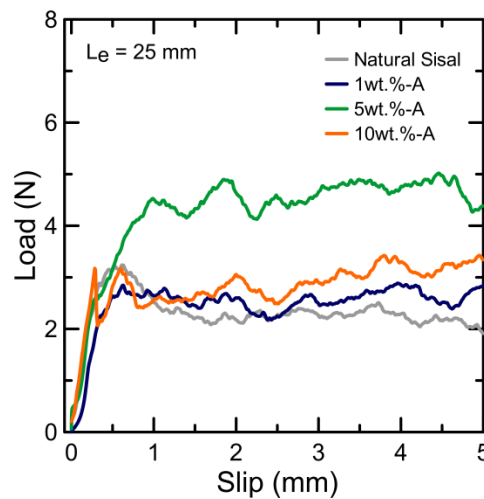


Figure 3.16 – Representative pullout curves of untreated and alkali-treated sisal fibers.

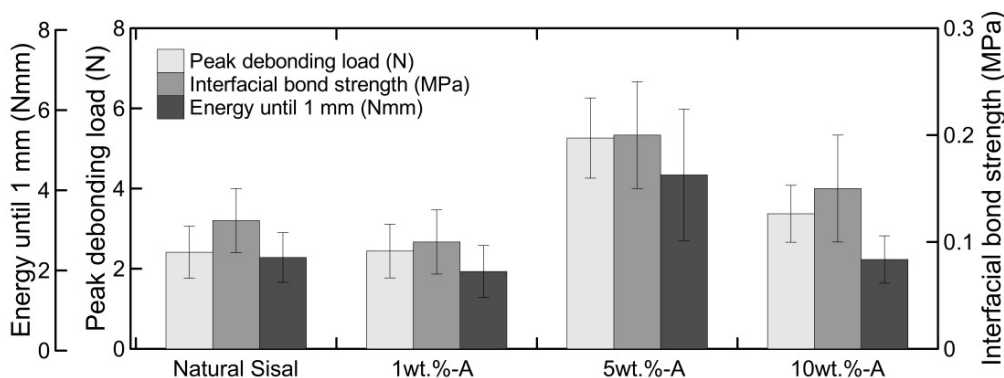


Figure 3.17 – Summary of the pullout test results of untreated and alkali-treated sisal fibers.

The bond improvement observed for the 5 wt.% alkali-treated fiber could be related to the removal of fiber constituents that cover the external surface of the

fiber cell wall by the alkalization. The reaction of NaOH with cellulose depolymerizes the fiber and this fibrillation gives a rough surface topography to the fiber, increasing the superficial roughness and leading to a better interlocking with the matrix. Even though, the calcium hydroxide deposition on the fiber surface could also have increased the roughness of the fiber surface. However, in the case of 1 wt.% alkali-treated fiber, the improvement of roughness was not sufficient to enhance the fiber's interfacial characteristics. This is further confirmed through observation of the microscope images in Figure 3.9. Besides that, the higher water uptake observed in the water absorption evaluation should decrease the fiber-matrix bond, even for the alkali-treated fiber. On the other hand, the excessive damage of the fiber surface observed for 10 wt.% treated fibers could be the explanation for the low pullout resistance obtained.

3.5. Conclusions

Based on the results obtained in the present research, the following conclusions can be drawn:

- Alkali treatment reduced the fiber cross-sectional area, thereby indicating the removal of some constituents of the fiber, such as hemicellulose and lignin, especially for higher NaOH solution concentrations of 5 and 10wt.%. It was confirmed by the chemical composition determination. This may also have enhanced the cellulose proportion in comparison to the amorphous compounds of the fiber, resulting in a considerable decrease in the water uptake tendency and an increase in the thermal stability of the alkali-treated sisal fiber;
- Enhancement in tensile strength and stiffness for the alkali-treated fibers was observed from the single fiber tensile test results. Also, the stretch of the fibers during the treatment procedure allows a much greater improvement in fiber strength as it avoids fiber shrinkage and improves the orientation of the fibrils, reducing the microfibrillar angle;
- The SEM analysis showed an increased roughness on the longitudinal surface of the fiber, especially for 5wt.%-A treated fiber, which could

be related to the removal of hemicellulose and lignin. This enhancement in roughness resulted in an increased bond with the cementitious matrix, confirmed by the single-fiber pullout test.

Thus, from the results, it is concluded that alkali treatment is efficient to enhance sisal fiber properties to encourage its use as reinforcement in cement-based matrices.

3.6. References

- 1 ASSOCIAÇÃO BRASILEIRA DE NORMAS TÉCNICAS. **NBR 16697**: Cimento Portland – Requisitos. Rio de Janeiro, 2018.
- 2 SILVA, F. de A.; TOLEDO FILHO, R. D.; MELO FILHO, J. de A.; FAIRBAIRN, E. de M. R. Physical and mechanical properties of durable sisal fiber-cement composites. **Construction and Building Materials**, v.24, n.5, p.777-785, 2010.
- 3 CASTOLDI, R. de S.; SOUZA, L. M. S.; SILVA, F. de A. Comparative study on the mechanical behavior and durability of polypropylene and sisal fiber reinforced concretes. **Construction and Building Materials**, v.211, p.617-628, 2019.
- 4 MELO FILHO, J. de A.; SILVA, F. de A.; TOLEDO FILHO, R. D. Degradation kinetics and aging mechanisms on sisal fiber cement composite systems. **Cement & Concrete Composites**, v.40, p.30-39, 2013.
- 5 TAYLOR, A. M.; BROOKS, J. R.; LACHENBRUCH, B.; MORRELL, J. J. Radial patterns of carbon isotopes in the xylem extractives and cellulose of Douglas-fir. **Tree Physiology**, v.27, n.6, p.921-927, 2007.
- 6 MORAIS, J. P. S.; ROSA, M. de F.; MARCONCINI, J. M. **Procedimentos para análise lignocelulósica**, Embrapa Algodão. Campina Grande, 2010. 58p.
- 7 ASSOCIAÇÃO BRASILEIRA DE NORMAS TÉCNICAS, **NBR 13999**: Paper, board, pulps and wood - Determination of residue (ash) on ignition at 525 °C. Rio de Janeiro, 2017.
- 8 MAEDA, R. N. **Produção de celulose por *Penicillium funiculosum* em fermentação submersa de bagaço de cana pré-tratado e sua aplicação na produção de etanol de segunda geração**. Rio de Janeiro, 2010. 243p. Tese de Doutorado – Programa de Pós- Graduação em Tecnologia de Processos Químicos e Bioquímicos, Universidade Federal do Rio de Janeiro.
- 9 GOMIDE, J. L.; DEMUNER, B. J. Determinação do teor de lignina em material lenhoso – Método klason modificado. **O papel**, v.47, p.36-38, 1986.
- 10 SARKANEN, K. V.; LUDWIG, C. H. Lignins: Occurrence, formation, structure and reactions. **World Information on Earthquake Engineering**, v.22, n.2, p.110-113, 2006.
- 11 AMERICAN SOCIETY FOR TESTING AND MATERIALS. **ASTM**

- C1557**: Standard Test Method for Tensile Strength and Young's Modulus of Fibers. United States, 2020.
- 12 GANAPATHY, T.; SATHISKUMAR, R.; SENTHAMARAIKANNAN, P.; SARAVANAKUMAR, S. S.; KHAN, A. Characterization of raw and alkali treated new natural cellulosic fibres extracted from the aerial roots of banyan tree. **International Journal of Biological Macromolecules**, v.138, p.573-581, 2019.
 - 13 WEERDT, D. K.; HAHA, M. B.; SAOUT, G. L.; KJELLEN, K. O.; JUSTNES, H.; LOTHENBACH, B. Hydration mechanisms of ternary Portland cements containing limestone powder and fly ash. **Cement and Concrete Research**, v.41, n.3, p.279-291, 2011.
 - 14 SOUZA, L. M. S.; FAIRBAIRN, E. de M. R.; TOLEDO FILHO, R. D.; CHAGAS, G. Influence of initial CaO/SiO₂ ratio on the hydration of the rice husk ash-Ca(OH)₂ and sugar cane bagasse ash-Ca(OH)₂ pastes. **Química Nova**, v.37, n.10, p.1600-1605, 2014.
 - 15 WEI, J.; MA, S.; THOMAS, D. G. Correlation between hydration of cement and durability of natural fiber-reinforced cement composites. **Corrosion Science**, v.106, p.1-15, 2016.
 - 16 CHEN, H.; YU, Y.; ZHONG, T.; WU, Y.; LI, Y.; WU, Z.; FEI, B. Effect of alkali treatment on microstructure and mechanical properties of individual bamboo fibers. **Cellulose**, v.24, n.1, p.333-347, 2017.
 - 17 BAHJA, B.; ELOUAFI, A.; TIZLIOUINE, A.; OMARI, L. H. Morphological and structural analysis of treated sisal fibers and their impact on mechanical properties in cementitious composites. **Journal of Building Engineering**, v.34, p.102025, 2021.
 - 18 WEI, J.; MEYER, C. Degradation mechanisms of natural fiber in the matrix of cement composites. **Cement and Concrete Research**, v. 73, p.1-16, 2015.
 - 19 WEI, J. Degradation behavior and kinetics of sisal fiber in pore solutions of sustainable cementitious composite containing metakaolin. **Polymer Degradation and Stability**, v.150, p.1-12, 2018.
 - 20 MARTIN, A. R.; MARTINS, M. A.; SILVA, O. R. R.; MATTOSO, L. H. C. Studies on the thermal properties of sisal fiber and its constituents. **Thermochimica Acta**, v.506, n.1-2, p.14-19, 2010.
 - 21 BARRETO, A. C. H.; ROSA, D. S.; FECHINE, P. B. A.; MAZZETTO, S. E. Properties of sisal fibers treated by alkali solution and their application into cardanol-based biocomposites. **Composites Part A: Applied Science and Manufacturing**, v.42, n.5, p.492-500, 2011.
 - 22 CANDAMANO, S.; CREA, F.; COPPOLA, L.; DE LUCA, P.; COFFETTI, D. Influence of acrylic latex and pre-treated hemp fibers on cement based mortar properties. **Construction and Building Materials**, v.273, p.121729, 2021.
 - 23 ORUE, A.; JAUREGI, A.; PEÑA-RODRIGUEZ, C.; LABIDI, J.; ECEIZA, A.; ARBELAIZ, A. The effect of surface modifications on sisal fiber

- properties and sisal/poly (lactic acid) interface adhesion. **Composites Part B: Engineering**, v.73, p.132-138, 2015.
- 24 HAJIHA, H.; SAIN, M.; MEI, L. H. Modification and Characterization of Hemp and Sisal Fibers. **Journal of Natural Fibers**, v.11, n.2, p.144-168, 2014.
- 25 GAÑAN, P.; GARBIZU, S.; LLANO-PONTE, R.; MONDRAGON, I. Surface modification of sisal fibers: Effects on the mechanical and thermal properties of their epoxy composites. **Polymer Composites**, v.26, n.2, p.121-127, 2005.
- 26 RAY, D.; SARKAR, B. K. Characterization of alkali-treated jute fibers for physical and mechanical properties. **Journal of Applied Polymer Science**, v.80, n.7, p.1013-1020, 2001.
- 27 LACERDA, T. M.; PAULA, M. P.; ZAMBON, M. D.; FROLLINI, E. Saccharification of Brazilian sisal pulp: Evaluating the impact of mercerization on non-hydrolyzed pulp and hydrolysis products. **Cellulose**, v.19, n.2, p.351-362, 2012.
- 28 WEI, J.; MEYER, C. Degradation rate of natural fiber in cement composites exposed to various accelerated aging environment conditions. **Corrosion Science**, v.88, p.118-132, 2014.
- 29 RAMAKRISHNA, G.; SUNDARARAJAN, T. Studies on the durability of natural fibres and the effect of corroded fibres on the strength of mortar. **Cement and Concrete Composites**, v.27, n.5, p.575-592, 2005.
- 30 VAN DE WEYENBERG, I.; CHI TRUONG, T.; VANGRIMDE, B.; VERPOEST, I. Improving the properties of UD flax fibre reinforced composites by applying an alkaline fibre treatment. **Composites Part A: Applied Science and Manufacturing**, v.37, n.9, p.1368-1376, 2006.
- 31 REDDY, K. O.; REDDY, K. R. N.; ZHANG, J.; ZHANG, J.; RAJULU, V. Effect of Alkali Treatment on the Properties of Century Fiber. **Journal of Natural Fibers**, v.10, n.3, p.282-296, 2013.
- 32 KIM, J. T.; NETRAVALI, A. N. Mercerization of sisal fibers: Effect of tension on mechanical properties of sisal fiber and fiber-reinforced composites. **Composites Part A: Applied Science and Manufacturing**, v.41, n.9, p.1245-1252, 2010.
- 33 GOMES, A.; MATSUO, T.; GODA, K.; OHGI, J. Development and effect of alkali treatment on tensile properties of curaua fiber green composites. **Composites Part A: Applied Science and Manufacturing**, v.38, n.8, p.1811-1820, 2007.
- 34 ZWANE, P. E.; NDLOVU, T.; MKHONTA, T. T.; MASARIRAMBI, M. T.; THWALA, J. M. Effects of enzymatic treatment of sisal fibres on tensile strength and morphology. **Scientific African**, v.6, p.e00136, 2019.
- 35 BECKERMANN, G. W.; PICKERING, K. L. Engineering and evaluation of hemp fibre reinforced polypropylene composites: Fibre treatment and matrix modification. **Composites Part A: Applied Science and Manufacturing**, v.39, n.6, p.979-988, 2008.

- 36 FERREIRA, S. R.; SILVA, F. de A.; LIMA, P. R. L.; TOLEDO FILHO, R. D. Effect of fiber treatments on the sisal fiber properties and fiber-matrix bond in cement based systems. **Construction and Building Materials**, v.101, p.730-740, 2015.
- 37 ZHOU, Y.; FAN, M.; CHEN, L. Interface and bonding mechanisms of plant fibre composites: An overview. **Composites Part B: Engineering**, v.101, p.31-45, 2016.
- 38 MANNA, S.; SAHA, P.; CHOWDHURY, S.; THOMAS, S. Alkali Treatment to Improve Physical, Mechanical and Chemical Properties of Lignocellulosic Natural Fibers for Use in Various Applications. In:___ **Lignocellulosic Biomass Production and Industrial Applications**. Scrivener Publishing LLC, 2017. p.47-64.
- 39 CAO, Y.; SHIBATA, S.; FUKUMOTO, I. Mechanical properties of biodegradable composites reinforced with bagasse fibre before and after alkali treatments. **Composites Part A: Applied Science and Manufacturing**, v.37, n.3, p.423-429, 2006.
- 40 TEIXEIRA, F. P.; GOMES, O. da F. M.; SILVA, F. de A. Degradation Mechanisms of Curaua, Hemp, and Sisal Fibers Exposed to Elevated Temperatures. **BioResources**, v.14, n.1, p.1494-1511, 2019.
- 41 LI, Y.; MAI, Y.-W.; YE, L. Sisal fibre and its composites: a review of recent developments. **Composites Science and Technology**, v.60, n.11, p.2037-2055, 2000.
- 42 F. de A. Silva, N. Chawla, R.D. de T. Filho, Tensile behavior of high performance natural (sisal) fibers. **Composites Science and Technology**, v.68, n.15-16, p.3438-3443, 2008.
- 43 KLERK, M. D.; KAYONDO, M.; MOELICH, G. M.; VILLIERS, W. I.; COMBRINCK, R.; BOSHOFF, W. P. Durability of chemically modified sisal fibre in cement-based composites. **Construction and Building Materials**, v.241, p.117835, 2020.
- 44 GODA, K.; SREEKALA, M. S.; GOMES, A.; KAJI, T.; OHGI, J. Improvement of plant based natural fibers for toughening green composites- Effect of load application during mercerization of ramie fibers. **Composites Part A: Applied Science and Manufacturing**, v.37, n.12, p.13-20, 2006.
- 45 PATIL, N. V.; RAHMAN, M. M.; NETRAVALI, A. N. "Green" composites using bioresins from agro-wastes and modified sisal fibers. **Polymer Composites**, v.40, n.1, p.99-108, 2019.
- 46 PLACET, V.; BOUALI, A.; PERRÉ, P. The possible role of microfibril angle of Hemp fibre during fatigue tests and its determination using Wide-Angle X-ray diffraction. **Materiaux et Techniques**, v.99, n.6, p.683-689, 2011.
- 47 BOURMAUD, A.; MORVAN, A.; BOUALI, A.; PLACET, V.; PERRÉ, P.; BALEY, C. Relationships between micro-fibrillar angle, mechanical properties and biochemical composition of flax fibers. **Industrial Crops and Products**, v.44, p.343-351, 2013.

4 Effect of polymeric fiber coating on the mechanical performance, water absorption, and interfacial bond with cement-based matrices

In this chapter, the use of carboxylate styrene-butadiene polymer as a coating for sisal fibers is proposed. Different XSBR polymers and emulsions concentrations were adopted. The effects of this treatment on physical, chemical, and mechanical properties were studied. The physical properties of the modified fibers were investigated by means of SEM and AFM analyses. Also, changes in the moisture absorption capacity of the coated fibers were evaluated. To study the chemical influence of the polymer coating in the modified fibers, TGA and FTIR techniques were adopted. Direct tensile and pullout tests were also performed in natural and coated sisal fibers, to mechanically evaluate the modification in terms of fiber strength and adherence, respectively. The results evidenced the formation of a new polymeric layer around the fiber, responsible for reducing the water absorption tendency of the natural fiber. The increase in the fiber-matrix adhesion obtained in the pullout evaluation was attributed to the rougher superficial aspect of the modified fibers and increased chemical interaction between the polymer and the cementitious matrix. Moreover, it was proven that the polymeric layer reduced the fiber's alkaline degradation susceptibility resulting in a more stable sisal fiber.

Most of the experimental program presented in this chapter was developed at TU Dresden, Germany. However, the AFM analysis was performed at the Nanoscopy Lab, at PUC-Rio. Also, the SEM images and FTIR spectra were obtained at the Center of Mineral Technology (CETEM) and Analytical Central Laboratory of Analysis (PUC-Rio), respectively.

4.1. Introduction

Due to the current effort to develop alternative sustainable building materials for the modern construction industry, several studies are seeking new environmentally friendly materials that can replace synthetic ones [1–3]. In this regard, natural fibers are gaining importance as reinforcement for cement-based matrices, where synthetic fibers are commonly used [4,5]. Several studies have

been conducted to prove the potential of these fibers to reinforce cement-based composites [3,5–10]. However, it is well-known that there are some limitations to the use of natural fibers in cement-based matrices, such as the high water absorption tendency and susceptibility to alkaline attack. Despite these challenges, many researchers have tried to improve the natural fiber performance with different chemical and physical methods of surface modification [5].

In general, chemical treatments are focused on changing fiber composition by partially removing some hydrophilic constituents, such as hemicellulose and lignin. On the other hand, physical modifications change the surface properties of the fibers to influence the fiber's stability and bonding to the matrix [5]. The impregnation of the fibers with polymer compatible with cement-based materials is a promising alternative. Chakraborty et al. [4] suggested that a polymer modification helped the reinforcing jute fiber to enhance the interfacial bond with a cementitious mortar. Ferreira et al. [9] studied the effect of carboxylate styrene-butadiene rubber latex (XSBR) coating on the mechanical performance of curauá, jute, and sisal fibers and found that it was very effective in reducing the water absorption of these fibers. They achieved a significant improvement in the fiber mechanical performance and higher chemical and physical bonding with the matrix. Fidelis et al. [11] also performed treatment in jute fibers with styrene-butadiene polymer and found a stronger chemical adhesion of the fibers to the matrix.

The carboxylate styrene-butadiene rubber latex is usually applied to paper coating, carpet adhesives, and impregnations. It was also investigated the use of this material for the impregnation of glass and carbon fibers [12–15]. Scheffler et al. [14] observed an improvement in the durability of glass fibers impregnated with styrene-butadiene, and also an improved the mechanical behavior of cementitious composites with these coated fibers. Mäder et al. [13] reported an increase in fiber-matrix adhesion in composites with glass and carbon fibers impregnated with this polymer. In this context, it is also considered a promising material to be used as a coating for natural fibers [9,16,17]. It is expected that the polymer modification enhances fiber performance creating a linkage between the polymeric compounds and the active regions of the cellulosic fibers [5]. The chemical and mechanical anchorage to a cement-based matrix could be enhanced by the reduction of the fiber dimensional variation and roughness increase [9].

Even though previous researchers presented improvements in mechanical performance and bonding of different polymer-coated synthetic fibers with cement-based matrices, there is still a lack of knowledge of the influence of this modification in natural fibers, in terms of the fiber performance and fiber-matrix interlock improvements. Given this background, the present work aims to study the effect of XSBR polymer coating in sisal fibers to be used as reinforcement in cement-based matrices. Therefore, the effect of surface modification on the physical and mechanical properties of sisal fibers was investigated. Moreover, the effectiveness of this coating on the sisal fiber interaction with a cement-based matrix was evaluated. Finally, polymer-coated sisal fiber durability in a highly alkaline environment was also investigated.

4.2. Materials and processing

4.2.1. Sisal fiber polymeric coating

The sisal fibers used in this study were the same detailed in Chapter 3. Also, the fibers were cleaned before treatment, as mentioned in Section 3.2.2. Three different polymers (XSBR) were used in the sisal fiber polymer coating process, Litex™ Quickshield 1545, Litex™ S 9076, and Litex™ S 10656, all purchased from Synthomer (Germany). The Litex™ Quickshield 1545 is an aqueous emulsion of a self-crosslinking copolymer of butadiene and styrene, with a solid content of 50% and viscosity of 100 mPa.s. The Litex™ S 9076 and 10656 were used together as a blend. The Litex™ S 9076 is classified as an aqueous, anionic dispersion of a self-crosslinking butadiene styrene copolymer while Litex™ S 10656 is a carboxylated self-crosslinking butadiene styrene methacrylate copolymer. A hand-mixed 1:1 binder solution was prepared with Litex™ S 9076 (soft stiff, solid content 47% and viscosity < 300 mPa.s) and Litex™ S 10656 (medium stiff, solid content 50% and viscosity < 500 mPa.s), based on supplier recommendations and previous research [11,18].

To ensure the uniformity of the impregnation process for coating the sisal fibers, a two-roller apparatus was developed to guide the fiber in the polymer emulsions and a sponge was used to remove the polymer excess in the final step, as shown in Figure 4.1.a. The fibers were subjected to two different polymer solutions, QS (Litex™ Quickshield 1545) and S (Litex™ S 9076 + S 10656), considering two

different aqueous emulsion concentrations, 50 and 100% v/v (Table 4.1). After the impregnation process, fibers were kept in the oven for 4 minutes at 140 ± 5 °C, to ensure polymer crosslinking. The optimum value of temperature was determined by thermal analysis (Figure 4.1.b). From the DTA curve, at around 140 °C the crosslinking reaction already occurred for both emulsions, which is in accordance with the recommendations in the technical data sheet. Also, following the supplier's instructions, 4 minutes was chosen as the temperature exposure time.

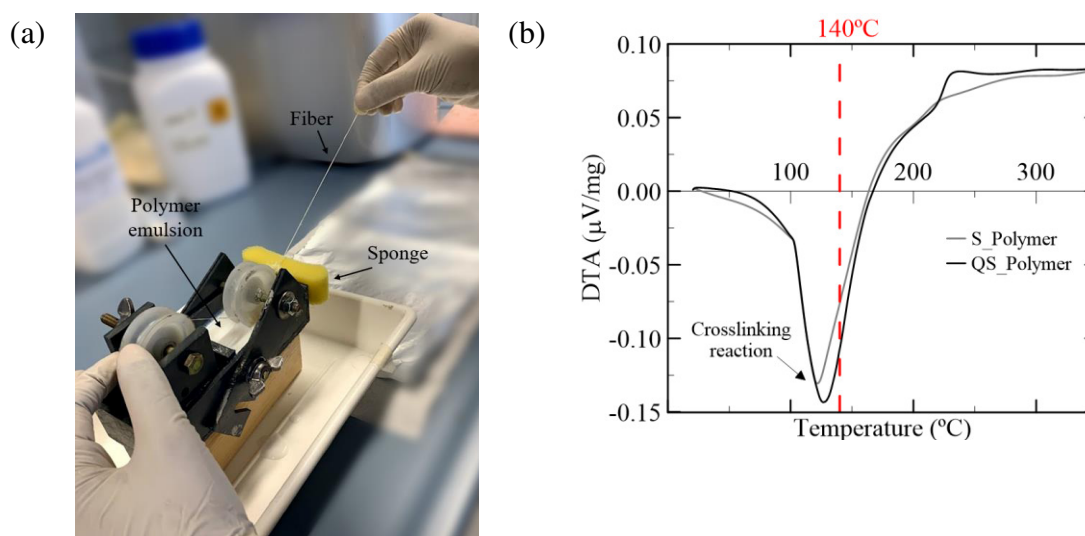


Figure 4.1 – (a) Polymer impregnation apparatus. (b) Resulted DTA curves of the thermal analysis of S and QS polymers.

Table 4.1 – Samples identification names related to the type of polymer and emulsion concentration adopted in the impregnation process.

Sample's identification	Type of polymer	Emulsion concentration
QS50	Litex™ Quickshield 1545	50% v/v
QS100	Litex™ Quickshield 1545	100% v/v
S50	1:1 Litex™ S 9076 + S 10656	50% v/v
S100	1:1 Litex™ S 9076 + S 10656	100% v/v

4.2.2. Pullout sample preparation

The cement-based matrix was produced with CEM II/A-M (S-LL) 52.5 R cement type, commercially available in Germany. Metakaolin (MetaMax® BASF) and fly ash (Steament H4) were also used as binder materials, to obtain a low-alkaline cementitious matrix [6]. The binder materials were firstly dry mixed with natural river sand (0-2 mm), and then the water and superplasticizer (BASF

MasterGlenium SKY 593) were added. The mixture was mixed for 10 minutes, using an IKA T50 digital Ultra-Turrax disperser. The cement-based matrix composition is presented in Table 4.2.

Table 4.2 – Composition of the cement-based matrix used for the pullout tests.

Material	[kg/m ³]
Cement	190
Metakaolin	114
Fly ash	76
Natural Sand	536
Water	246
Superplasticizer	1.12

Prismatic specimens with 8x10 mm² section and 25 mm high were produced for pullout tests. The preparation of the specimens followed the procedure described: (i) fibers were cut into 50 mm segments; (ii) fibers were then fixed in the bottom plate of the pullout mold; (iii) fibers were straightened and then fixed to the upper acrylic plate of the pullout mold, to ensure fiber alignment; (iv) the mixture was placed into the molds. After filling the mold, it was vibrated for 1 minute to remove possible voids in the matrix. After 24 hours, the pullout specimens were demolded, sealed in plastic bags, and stored in a climatic chamber with standard conditions of temperature and humidity for 28 days until the pullout tests. All the specimens were prepared in embedded lengths of 25 mm for each fiber. For each fiber type, 10 specimens were prepared. Figure 4.2 presents the molding process of the pullout specimens.

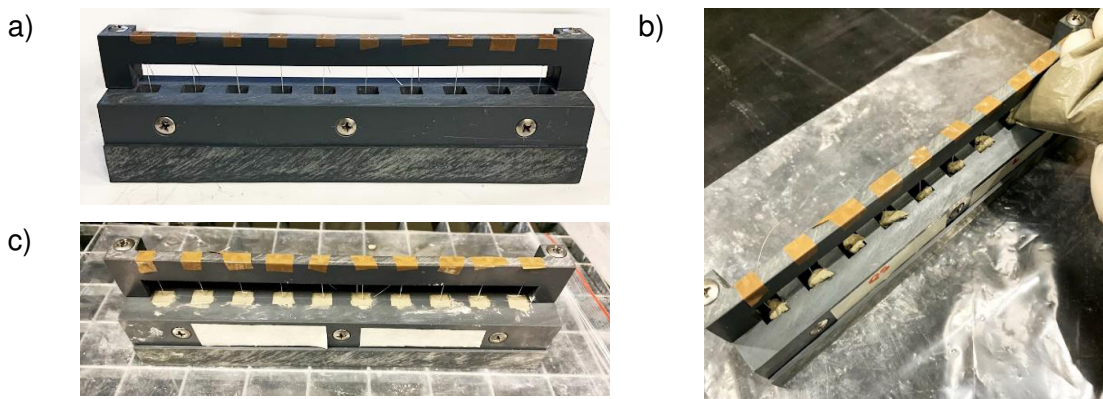


Figure 4.2 – Molding process of pullout samples: (a) fibers aligned in the mold, (b) casting of the specimens, and (c) mold filled with the cementitious matrix.

4.2.3. Testing methods

4.2.3.1. Scanning electron microscopy (SEM)

The scanning electron microscopy technique was used to perform a microstructural evaluation of the longitudinal and cross-sectional surfaces of polymer-coated sisal fibers. For the longitudinal images, a Quanta 250 FEG Environmental Scanning Microscope (ESEM) equipment was used. It was operated at 5 to 7 kV, in a low vacuum environment. Sample coating was not necessary for the sample preparation. For the cross-sectional images, a TM3030Plus Hitachi Scanning Electron Microscope (SEM) was used. It was operated at 15 kV, in a high vacuum mode. The samples were sputter coated with a layer of gold to ensure conductivity and to prevent polymer or fiber degradation.

4.2.3.2. Thermogravimetric analysis (TGA)

Thermogravimetric analysis (TGA) was employed to investigate the thermal stability of fibers before and after modification. The thermal analysis was carried out by an STA 409 cell thermal analyzer (Netzsch, Germany). Fibers were first cut into small segments of approximately 1 mm in length. About 50 mg of fiber was placed in an aluminum pan and warmed from 20 to 800 °C at a rate of 10 K/min. A nitrogen environment with a rate flow of 60 ml/min was maintained during the analysis. The mass loss was recorded for every 2.5 °C temperature rise.

4.2.3.3. Moisture affinity evaluation

The water absorption capacity of natural and polymer-coated sisal fibers was evaluated in terms of two different parameters: moisture absorption percentage and water contact angle. For the moisture absorption percentage calculation, it followed the same procedure presented in Section 3.3.2.4. The moisture content (MC%) was evaluated according to the following expression:

$$\text{MC}\% = \frac{(W_t - W_0)}{W_0} \times 100 \quad (\text{Eq. 4.1})$$

Where W_0 is the dry weight of the samples after 24 hours in the oven and W_t is the weight of the samples after a defined time interval under distilled water.

4.2.3.4. Fourier transform infrared spectroscopy (FTIR)

FTIR was performed to determine the chemical changes in functional groups of fibers before and after polymer coating. A Bruker FTIR Spectrometer Alpha II equipment using an ATR accessory (Bruker ATR module) was used for the analysis. The spectra were recorded with 32 scans within the wavenumber range between 4000 and 400 cm^{-1} , with a resolution of 2 cm^{-1} . Each sample was measured three times.

4.2.3.5. Direct single fiber tensile test

The influence of the polymer coating on the fiber mechanical performance was evaluated through direct single fiber tensile tests, following recommendations of ASTM C1557 [19]. Figure 4.3 presents the experimental setup used for the tensile tests. A Zwick Roell 1445 testing machine was used, coupled with an additional load cell with a capacity of 50 N. A displacement rate of 0.1 mm/min was adopted. A pre-load of 0.2 N was applied to ensure that the fibers were completely stretched at the beginning of the test. Before the tests, fiber samples were prepared by gluing them into a paper frame template, for better alignment inside the grips.

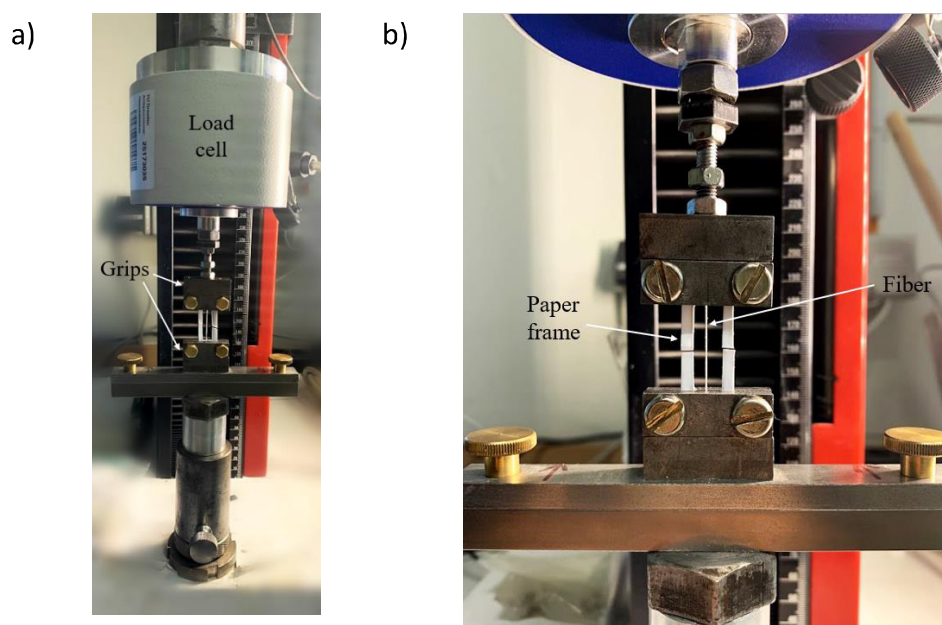


Figure 4.3 – Testing setup for direct single fiber tensile tests: (a) general overview and (b) sample detail.

The tests were performed with a free fiber length of 20 mm and, for each fiber type, 10 specimens were tested. It is important to highlight that, as the fibers are obtained from a natural source, the cross-sectional area may considerably change. So, the cross-sectional area of each fiber tested was measured from SEM images.

4.2.3.6. Single-fiber pullout test

Single-fiber pullout tests were performed to investigate the influence of the polymeric coating on the fiber-matrix interaction. A Zwick Roell 1445 testing machine was used for the tests, equipped with a 50 N load cell. The bottom part of the specimen (mortar) was clamped in the machine, while the fiber was clamped in the superior grip of the setup, connected to the load cell. The grip consisted of two plates connected with two bolts each to avoid the slip of the fiber from the grip – the only allowed slip is of the fiber from the matrix. A tensile force was applied to the specimen at a constant rate of 1 mm/min. For each fiber type, 10 specimens were tested. Figure 4.4 presents the experimental setup used for the single-fiber pullout tests.

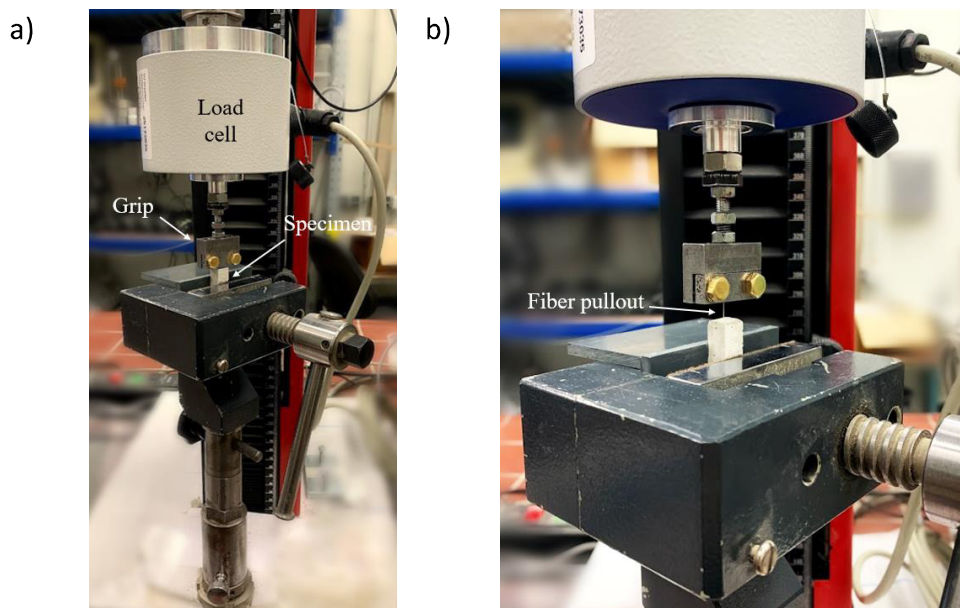


Figure 4.4 – Testing setup for single-fiber pullout tests: (a) general overview and (b) sample detail.

4.2.3.7. Atomic force microscope (AFM)

An atomic force microscope was used for the quantitative measurements of the changes in terms of surface roughness in a nanoscale resolution for the natural

and polymer-coated fibers. Other superficial physical properties such as adhesion, stiffness, and deformation were also investigated. It is expected that the observations collected by means of the AFM technique should be related to the results obtained from the macroscale evaluation, involving the direct single fiber tensile and pullout tests. This technique allows the determination of surface profiles of heterogeneous materials with a sub-nanometer level resolution, and without any specific sample preparation [20].

Fibers of ~1cm in length were first fixed on a sample holder with a double-sided adhesive tape (Figure 4.5). Then, the samples were placed in the microscope, under ambient conditions (21 ± 1 °C and $50 \pm 5\%$ RH). The AFM analysis was performed with a Park NX10 Atomic Force Microscope, using a non-contact and tapping mode operation. A Tap300Al-G tapping mode AFM probe with Aluminum Reflective Coating was adopted (AFM Tip rotated, 17 μm height, 15 μm setback, and 10 nm radius), with a cantilever spring constant k of 40 N/m. For superficial roughness analysis, a topography image was obtained mapping a selected 5 μm x 5 μm area. The tapping mode also allowed to record phase contrast images, detecting variations in adhesion, stiffness, and deformation levels in the defined fiber surface area. To ensure reproducibility, the analyses were performed in two replicated for each fiber type. Also, for each replica, 5 different zones in the fiber surface were considered.

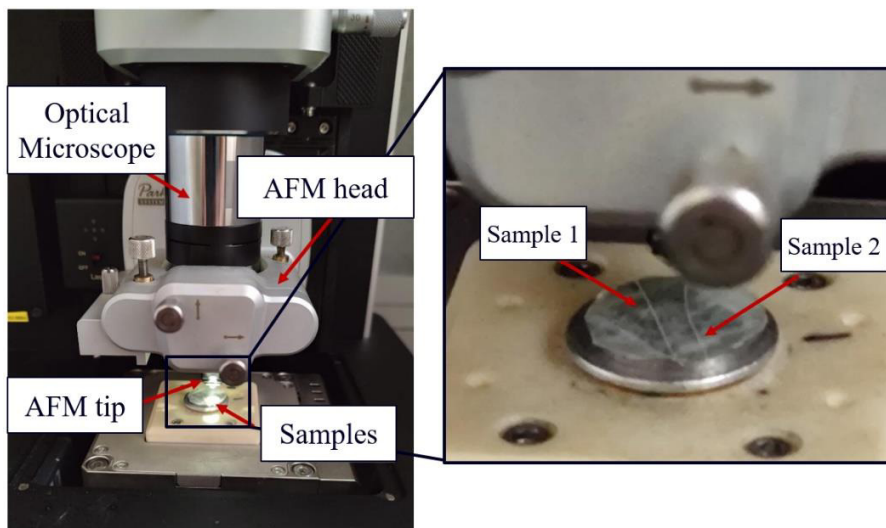


Figure 4.5 – Photograph of the atomic force microscope used for the measurements and the sample holder in detail.

4.2.3.8. Stability in alkaline media

In order to evaluate the durability of polymer-coated sisal fibers in cement-based matrices, fibers were subjected to alkaline media exposure. It is well known that cement-based matrices are alkaline in nature [5]. So, it is important to enhance sisal fiber's alkaline resistance to make them suitable for use as reinforcement in cementitious composites. In this sense, an alkaline solution was used to model the effect of alkalinity on natural and polymer-coated sisal fibers. In this research, 1M NaOH solution was chosen, with 13.6 pH. Although this alkali concentration is higher than usual cement-based matrices (pH of approximately 12.7 at the fresh state [16,21]), stronger pH provides an increased degradation in a short time of exposure.

The natural and polymer-coated fibers were immersed in the solution and were kept there for 28 days. After the exposure interval, fibers were taken, washed with water, and air-dried. Then, single fibers direct tests were performed to investigate the fiber degradation in terms of mechanical performance. The sample preparation and test parameters followed the same presented in Section 4.2.3.5.

4.3. Results and discussion

4.3.1. Scanning electron microscopy (SEM)

Figure 4.6 shows SEM images of the fiber surface and cross-section of all evaluated fibers. Also, the cross-sectional area of the fibers was measured and it is reported in Table 4.3. Figure 4.6.a shows a typical natural sisal fiber microstructure, characterized by an irregular cross-section, with a known horseshoe shape [22]. These fibers are composed of numerous individual cellulosic fiber cells of about 6-30 μm in equivalent diameter that are linked together by means of the middle lamella, composed of hemicellulose and lignin. Each fiber cell is formed by primary, secondary, and tertiary walls, and the lumens, which are placed in the center of the fiber cells [18,23].

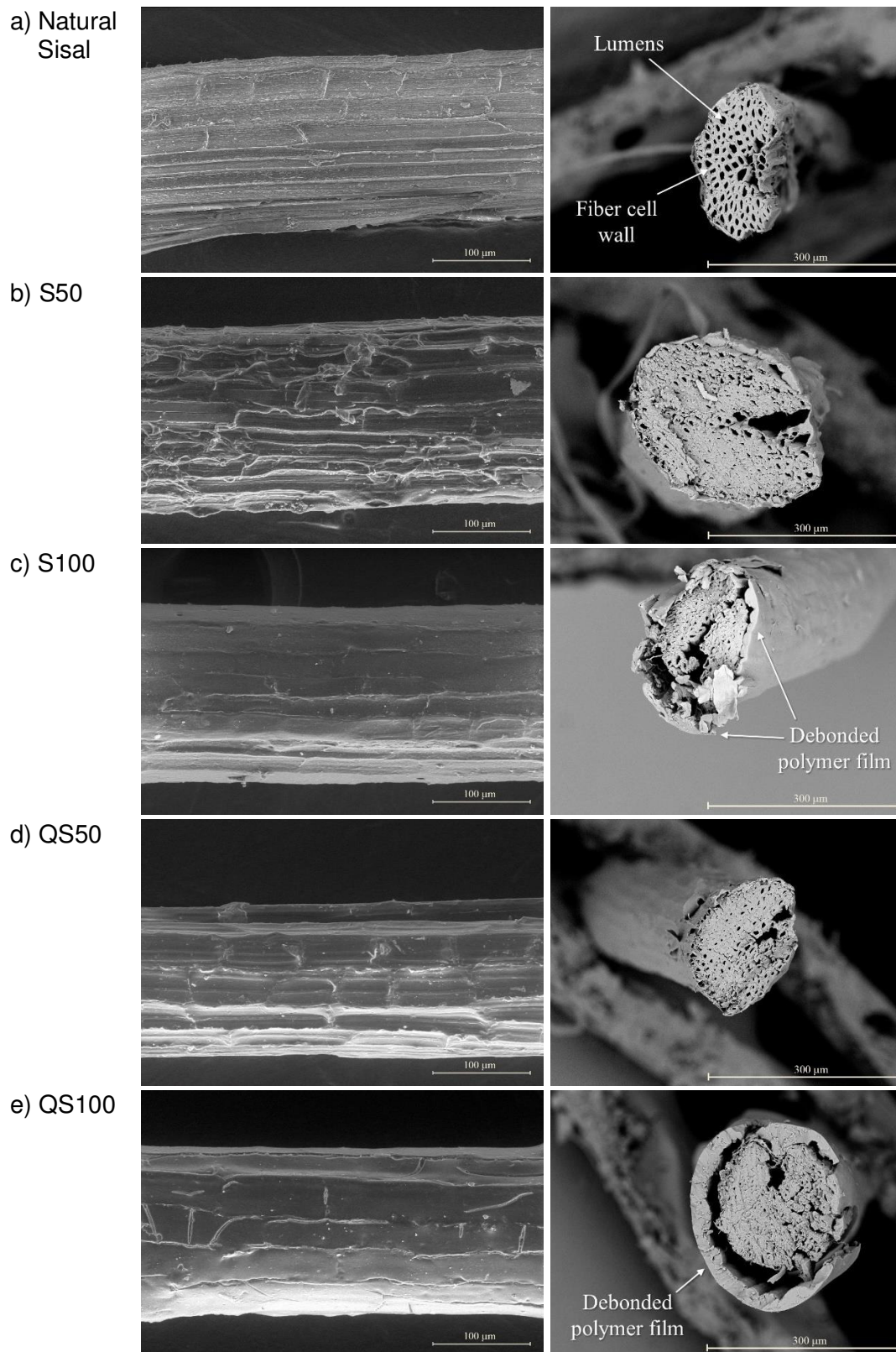


Figure 4.6 – Micrographs of the longitudinal and cross-sectional aspects of (a) natural and (b-e) polymer-coated sisal fibers.

Table 4.3 – Cross-sectional area of natural and polymer-coated sisal fibers.

	Cross-sectional area (mm ²)
Natural Sisal	0.030 ± 0.008
S50	0.036 ± 0.009
S100	0.046 ± 0.011
QS50	0.031 ± 0.013
QS100	0.046 ± 0.011

From the longitudinal fiber images of the polymer-coated fiber, it is clear the formation of a new layer on the fiber surface, with different superficial aspects. For the 50% emulsion polymer-coated fibers (S50 and QS50), a thin coating and a comparatively rougher surface were observed. Comparing the two different polymers, a more irregular surface was reached by the S50 coated fiber, which could result in a higher mechanical interlock with the matrix. Also, from the cross-sectional surface aspect, it is possible to note that the lumens are not empty, which could be an indication that the polymer was capable to penetrate the fiber structure and occupy the voids.

However, the use of high emulsion polymers (S100 and QS100) resulted in a smoother surface, in comparison to natural sisal. From the cross-sectional micrographs, it was also observed the lumens filled by the polymer presence. Also, there was a formation of a wider coating around the fiber, confirmed by the enhanced cross-sectional area reported in Table 4.3. However, it was observed lower adherence of the polymer to the fiber structure, as the polymer film is partially debonded from the fiber surface, as shown in Figures 4.6.c and 4.6.e.

4.3.2. Thermogravimetric analysis (TGA)

Figure 4.7 presents the TGA/DTG curves of natural and polymer-coated fibers. From the DTG curves, it is clear that natural sisal is characterized by three significant mass losses. The mass loss at 60–200 °C is attributed due to the water release [24]. The significant mass losses at the temperature ranges of 220–300 °C and 300–400 °C are attributed to the decomposition of hemicellulose and cellulose, respectively. This result was in accordance with several previous research works that evaluated the thermal stability of sisal fibers [24–26]. As lignin loses mass

steadily across all the temperature ranges, it is not possible to identify this compound from TGA/DTG curves.

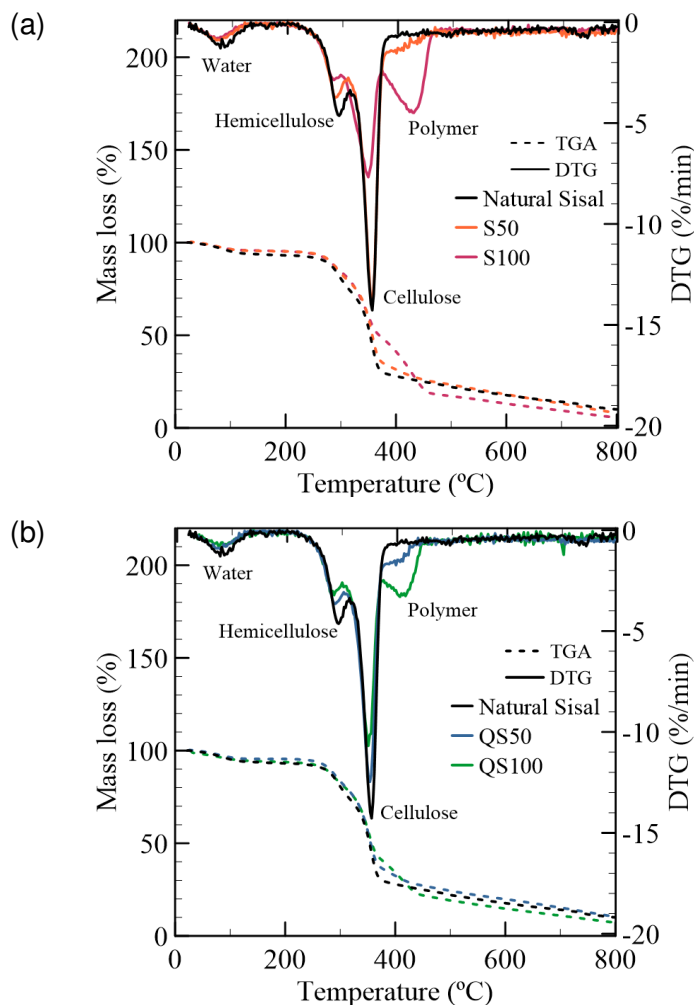


Figure 4.7 – TGA and DTG curves of natural sisal, (a) S50, S100, (b) QS50, and QS100 polymer-coated fibers.

On the other hand, polymer-coated fibers presented peaks in the same temperature range as natural sisal, with some minor modifications related to the peak shape. The cellulose DTG peak presented the more pronounced modification for the polymer-coated fiber in comparison to natural sisal. As reported by previous authors [9,27], the polymer covering results in the presence of vapor pressure during thermogravimetric analysis, leading to changes in the cellulose peak. The decrease in the cellulose peak is not related to the reduction of the cellulose proportion, but to the fact that the initial mass of the sample is not only the fiber but the fiber and polymer. Also, a new DTG peak at the temperature range of 400–500 °C is related to the simultaneous decomposition of butadiene and styrene [8,9,28]. The presence of this peak in the DTG curves for polymer-coated fibers is evidence of the polymer

present in the modified fibers. Finally, it should be not that the fibers modified with the not diluted polymer systems show the highest mass losses, indicating a considerable amount of applied coating layer onto the fiber surfaces, which corresponds to the previously shown ESEM analysis.

4.3.3. Moisture affinity evaluation

Figure 4.8 presents the water absorption test results for natural and polymer-coated sisal fibers. The moisture content percentage was observed to increase with increasing immersion time for all samples until reaching the saturation point at around 2 hours. For natural sisal, the saturation point corresponds to water absorption of around 100% of its weight in the natural form. However, a significant decrease in the water absorption was observed for polymer-coated fibers. Polymer-coated fibers presented a decrease of approximately 80% in moisture content compared to non-coated fibers. This is attributed to the hydrophobic nature of the SBR polymers used in the coating process. The occupation of the lumens with the polymer emulsion, evidenced in Figure 4.6, works as a barrier for the water absorption by the fiber structure. Also, the polymeric layer around the fibers acts as a protective layer, avoiding moisture absorption.

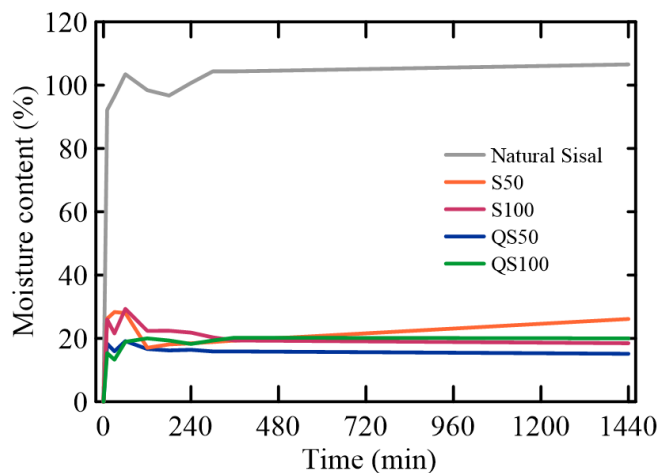


Figure 4.8 – Water absorption test results of natural sisal and polymer-coated fibers.

The high-water absorption capacity of natural fibers has a direct influence on their reinforcing performance and durability in cement-based composites. The reduction in the moisture absorption tendency of coated fibers could be beneficial for the fiber-matrix transition zone since it avoids the occurrence of fiber swelling,

characterized by the volume variation in these fibers due to the water absorption tendency [6,29]. Consequently, an improved fiber-matrix interface could be reached, providing better reinforcing performance of these fibers. Also, it avoids the fiber mineralization process, which occurs due to the migration of calcium hydroxide from the cementitious matrix to the fibers [6,21,29]. As a result, it is expected increased fiber durability within cementitious composites.

4.3.4. Fourier transform infrared spectroscopy (FTIR)

Figure 4.9 presents the FTIR spectra of natural and polymer-coated sisal fibers. The significant changes observed in FTIR spectra for the modified fibers compared to natural sisal are highlighted. The obtained spectrum of natural sisal is in agreement with the literature [8,30], and the basic fiber components can be identified from the peaks. It is well known that sisal fiber is mainly composed of cellulose, hemicellulose, and lignin, related to the peaks in the region between 800 and 2000 cm^{-1} . The natural sisal FTIR spectra exhibited C=O stretching of carboxylic acid or ester of hemicelluloses [8,30], C=C benzene stretching ring of lignin [8,30,31], and C–OH stretching absorption of lignin [30,31] at around 1739 cm^{-1} , 1608 cm^{-1} , and 1026 cm^{-1} wavenumber, respectively. Also, a distinct broad peak centered at around 3315 cm^{-1} represents the stretching vibration of the hydroxyl group from moisture due to the intramolecular hydrogen bonding in cellulose [32].

After the polymer coating, sisal fibers presented some different peaks. Firstly, the peak at 3315 cm^{-1} reduced considerably, evidencing the change in the water uptake tendency for the polymer-coated fibers (Section 4.3.3). Among them, the absorption bands at around 2850 and 2920 cm^{-1} in polymer-treated fibers appear due to the C-H stretching of aromatic rings [4,9,28]. The peaks at ~966 and ~699 cm^{-1} are correlated with the styrene absorption for the SBR, attributed to aromatic C-C stretching [9,28]. Also, the trans-1,4-configuration and vinyls' content of the butadiene is related to the 912, 757, and 3032 cm^{-1} peaks, observed for the polymer-coated fibers [9,28,33]. These mentioned peaks presented higher intensity for the 100% polymer emulsion fibers (S100 and QS100), which may indicate a higher amount of polymer content on the fiber surface. It is also important to highlight that the absorption band at 1739 cm^{-1} appears only in the S100 polymer-modified fiber.

This mode is assigned to be due to the C=O stretching of ester linkage, which is indicative of a more evident interaction between the polymer and the sisal fiber [4]. Hence, in conclusion, the FTIR analysis indicates the formation of a polymer coating on the sisal fiber surface.

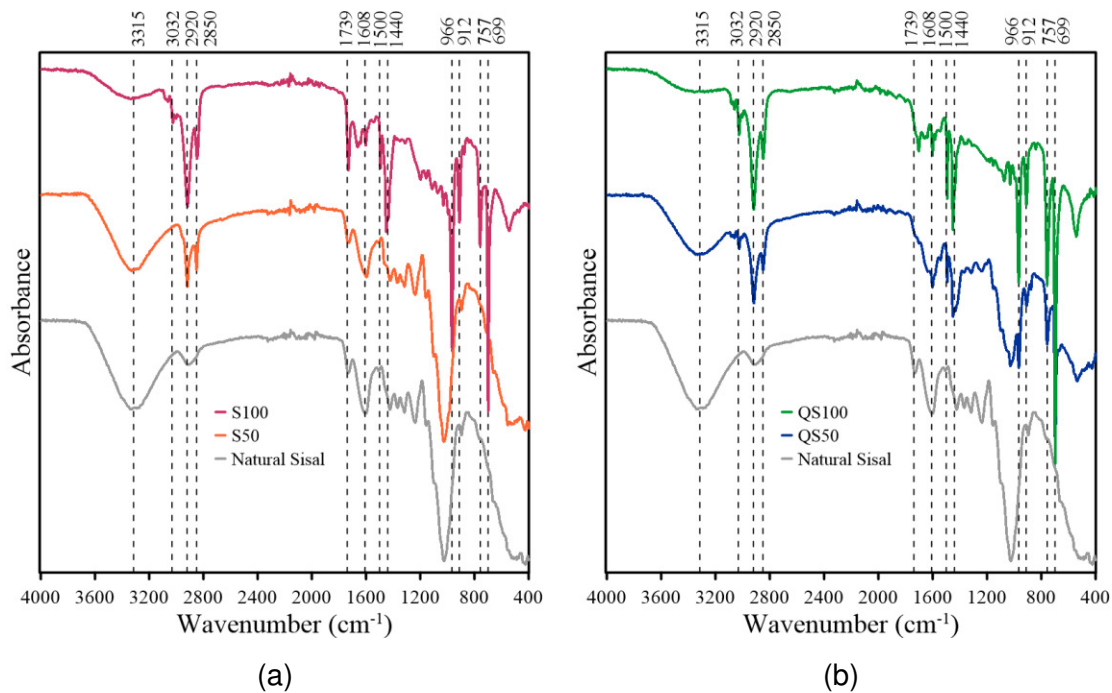


Figure 4.9 – FTIR spectra of natural sisal, (a) S100, S50, (b) QS100, and QS50 polymer-coated fibers.

4.3.5. Direct single fiber tensile test

The direct single fiber tensile test results of natural and polymer-coated fibers, in terms of typical stress-strain curves, are presented in Figure 4.10. Tensile strength, Young's modulus, and elongation at break obtained from the experimental curves are presented in Table 4.4. The typical stress-strain curve of natural sisal fibers shows a linear elastic deformation until fiber rupture. The ultimate tensile strength of natural sisal fiber found was 441.1 ± 9.3 MPa and Young's modulus of 12.8 ± 1.5 GPa, which is in accordance with previous studies [9,34].

Before discussing the polymer-coated fiber results, the influence of the temperature should be evaluated, as the exposure of the fiber to temperature is a step of the procedure. As explained in Section 4.2.1, to ensure the polymer crosslinking, fibers were put in the oven at 140 ± 5 °C for 4 minutes. After exposing the natural sisal fiber to this temperature, it was found a decrease in terms of

mechanical properties values, presenting 358.3 ± 30.0 MPa and 10.9 ± 0.9 GPa for tensile strength and Young's modulus, respectively. Even though there is a slight decrease in tensile behavior ($\sim 19\%$ for tensile strength and $\sim 15\%$ for Young's modulus), the fibers are not mechanically compromised. According to Martin et al. [24], an expressive degradation of sisal fiber components starts at 186 °C, which means that the use of temperatures under 185 °C does not compromise the structure of the fiber. Also, Teixeira et al. [34] found that severe losses in tensile strength only start at 150 °C for sisal fiber.

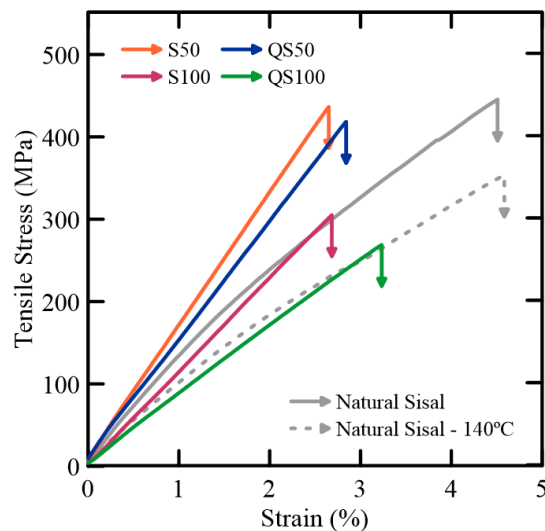


Figure 4.10 – Stress-strain curves of natural sisal and polymer-coated fibers.

All polymer-coated fibers exhibited the same linear behavior under tension, until the fiber rupture. The S50 and QS50 fibers showed a stiffer behavior, with increased ultimate tensile strength and lower deformation capacity. As mentioned in Section 4.3.1, it was observed the polymer penetration between fiber cells and internal lumen walls, resulting in stiffening and making the fiber structure rigid and dense. This is attributed to the fact that the polymer could act as a stabilizing agent for the fiber structure, preventing deformation and subsequent collapse of the cellulose microfibrils, increasing the rigidity of the fiber structure. The same was found in previous studies [9,11].

On the opposite, S100 and QS100 fibers presented a decrease in the ultimate tensile strength capacity. For higher polymer emulsion, it is expected a formation of a thicker layer around the fibers, as was exposed in the SEM images (Figure 4.6), with a poor interlock with the fiber surface. Therefore, the outer layer fibrils of the

fiber structure are free to deform during tensile and may collapse prematurely compared to the S50 and QS50 fibers. According to the literature [16], the styrene-butadiene copolymer consists of rigid styrene and flexible butadiene, with particular mechanical properties. In this context, the coated fibers are considered a composite itself, with properties linearly proportional to the properties of each component material – the fiber and the polymeric layer. So, as the polymeric layer is not completely adhered to the fiber surface, the S100 and QS100 polymer-coated fibers did not work as a composite material, and the tensile strength and Young's modulus of the coated fibers are reduced.

Table 4.4 – Direct single fiber tensile test results of natural and polymer-coated sisal fibers.

	Tensile Strength (MPa)	Young's Modulus (GPa)	Elongation at break (%)
Natural Sisal	441.1 ± 9.3	12.8 ± 1.5	4.1 ± 0.6
Natural Sisal (140 °C)	358.3 ± 30.0	10.9 ± 0.9	4.9 ± 0.8
S50	390.4 ± 52.4	15.0 ± 1.9	2.6 ± 0.2
S100	306.5 ± 46.2	11.1 ± 1.1	2.8 ± 0.2
QS50	396.8 ± 42.9	14.4 ± 2.2	2.8 ± 0.5
QS100	279.3 ± 54.9	8.8 ± 1.1	3.1 ± 0.3

4.3.6. Single-fiber pullout test

The pullout load versus slip typical curve is schematically presented in Figure 4.11.a. According to the theoretical background [35], the pullout curves can be divided into two different regions, considering the debonding and pullout stages. At the beginning of the debonding stage, there is an elastic-linear range with a rapid load increase. At this moment, the fiber and the matrix work together through adhesion and static friction, and there is no relative slip between these two components. Before reaching the peak debonding load, the debonding process starts, and the curve slope becomes lower, with a gradual ascending stage. Then, in the post-peak region, the pullout process takes place, and the behavior is governed by kinetic friction. With the increase of the slip, the interfacial area decreases, leading to a reduction in the load until the complete fiber pullout, characterizing a slip-softening behavior. Thus, it is expected that the polymer modification change

the pullout performance of sisal fibers, in terms of modification in the chemical and mechanical interaction of the fiber with the matrix.

From the direct tensile test results (Section 4.3.5), it was observed a considerable loss in the mechanical performance of S100 and QS100 polymer-coated fibers. Therefore, pullout tests were performed only on the natural sisal and S50 and QS50 polymer-coated fibers. Typical load versus slip curves of the tested fibers are shown in Figure 4.11.b. The natural sisal presented a typical slip-softening behavior, characterized by a drop in the load-slip curve after reaching the peak load. Until the P_{max} point, the chemical adhesion between the fiber surface and the matrix governs the pullout behavior, until the complete fiber debonding. After this point, the residual pullout force is governed by the frictional shear strength of the interface, and it continues until the complete fiber pullout. Similar behavior has been observed in previous studies [6,22].

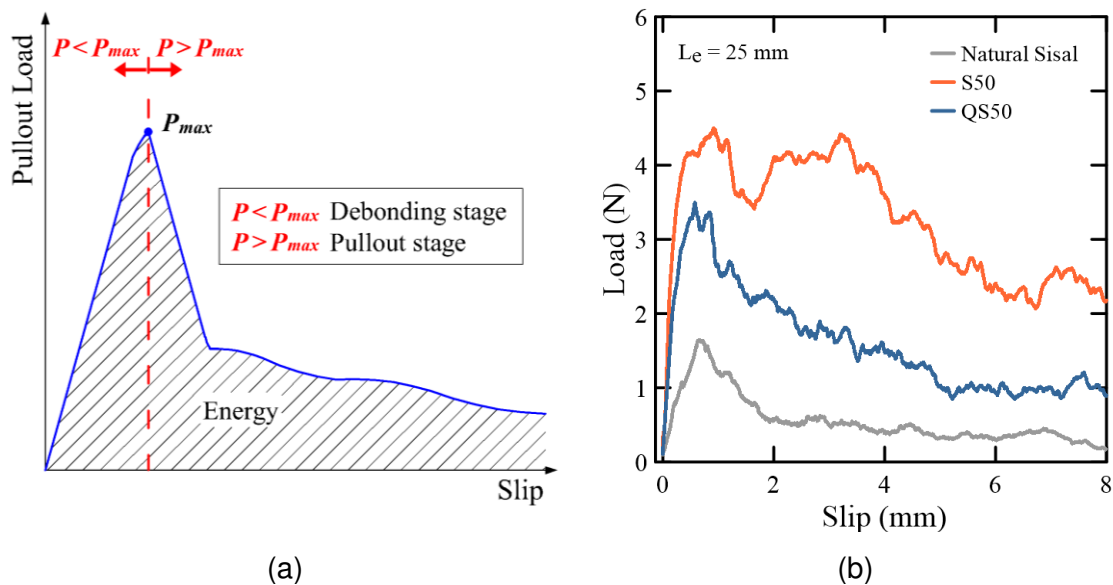


Figure 4.11 – (a) General profile of a single fiber pullout curve and (b) typical pullout load-slip curves of natural sisal and polymer-coated fibers.

The presence of a polymeric layer on the fiber surface resulted in changes in the load-slip curves. According to Lima et al. [10], the pullout behavior of polymer-coated fiber can be influenced by three factors: the polymer-matrix interface, the fiber-polymer interface, and the polymer film stiffness under loading. It was reported in Section 4.3.3 that sisal fibers are highly hydrophilic. The absorption of water by the fibers inside the matrix results in expansion and consequently

microcracking in the matrix interface. A subsequent possible water loss may result in fiber shrinkage, reducing the contact area in the fiber-matrix interface. On the other hand, the presence of a polymeric layer resulted in protection against the water uptake tendency of the fibers (Section 4.3.3), avoiding the fiber swelling process, which is favorable for the formation of a denser fiber-matrix interface. Moreover, from the SEM images evaluation (Section 4.3.1) it was reported a rougher surface for the polymer-treated fibers in comparison to the natural sisal, which may contribute to enhancing the mechanical interlocking in the interfacial transition zone. Also, the interface between the polymer film and the sisal fiber plays an important role in stress transfer. During the pullout test, the fiber is loaded and the load transfer to the matrix depends on the efficiency of the adhesion between the sisal fiber and the polymeric film. Asprone et al. [3] stated that the bond between the polymer coating and the matrix is generally higher than the bond between the polymer and the fibers.

Another important change in the pullout curves is related to the initial linear slope. In comparison to natural sisal, S50 and QS50 pullout samples presented a significant increase in the linear slope of the initial portion of the curves, related to the debonding stage. From the single fiber tensile test results (Section 4.3.5), an increase in Young's modulus was reported for S50 and QS50 fibers. In this sense, the presence of the polymer film contributed to the increase in the rigidity of the load-slip curve, and also the load level before the initiation of the pullout stage. Furthermore, in addition to polymer stiffness, the polymer coating promotes enhanced chemical bonds to the cement-based matrix. It is known that the SBR polymer coating act as a bridge between the fiber and cementitious matrices [7,36]. The existing carboxylic groups in the XSBR polymers eventually interact with the hydroxyl groups present in the fiber structure, mainly presented in the cellulose. Also, another part of these copolymers is able to form bonds with the calcium ions of the hydrated cement, providing chemical adhesion with the cement-based matrix [7].

Some fiber-matrix interfacial parameters were also obtained from the load versus slip curves and are presented in Table 4.5. The *peak debonding load* corresponds to the maximum load before the pullout process begins. The *pullout energy* is obtained by the integration of the area under the load versus slip curves and is related to the energy consumption to pull out the fiber. In this study, the

pullout energy was calculated considering the maximum slip of 1 mm. According to the Model Code 2010 [37], a crack opening of 0.5 mm characterizes the serviceability limit state for fiber-reinforced concretes for structural uses. So, the consideration of 1 mm maximum slip for the energy calculation guarantee that this limit is covered and ensures the consideration of the peak debonding load for the energy calculation [38]. Finally, the *interfacial bond strength* between the fiber and the matrix was obtained from Equation 4.2:

$$\tau = \frac{P_{max}}{\pi d L_c} \quad (\text{Eq. 4.2})$$

Where τ is the interfacial bond strength in the peak debonding load P_{max} , d is the equivalent diameter related to the fiber cross-sectional area, and L_c is the embedded length, adopted as 25 mm in this study.

Table 4.5 – Single-fiber pullout test results of natural and polymer-coated sisal fibers.

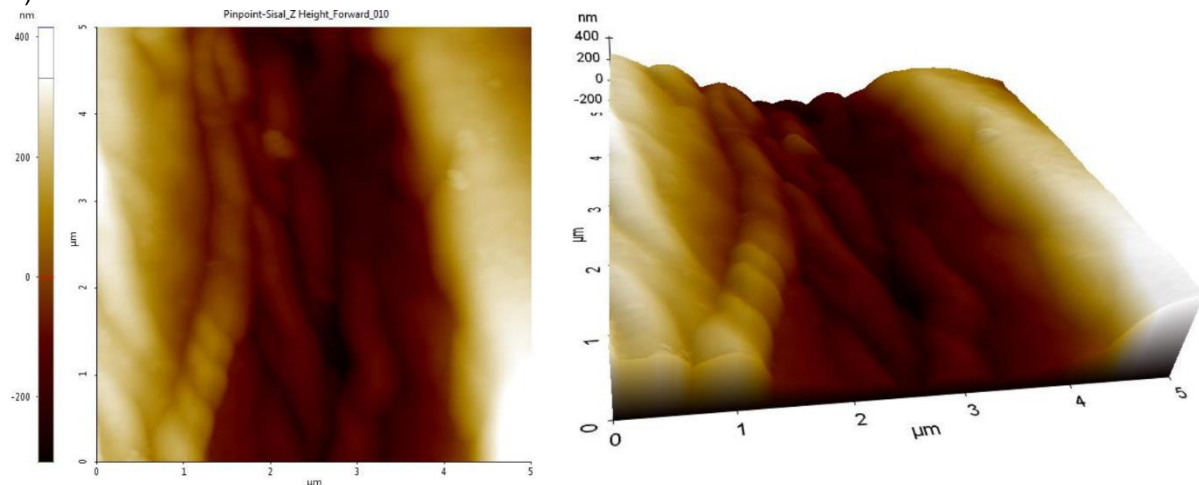
	Peak debonding load (N)	Interfacial bond strength (MPa)	Energy until 1 mm (N.mm)
Natural Sisal	2.08 ± 0.61	0.14 ± 0.04	1.67 ± 0.59
S50	4.74 ± 1.42	0.31 ± 0.09	3.65 ± 1.07
QS50	3.51 ± 0.90	0.23 ± 0.06	2.19 ± 0.78

From the results presented in Table 4.5, the polymer coating promoted an increase in all evaluated parameters. The interfacial bond strength changed from 2.08 ± 0.61 MPa for natural sisal to 4.74 ± 1.42 MPa and 3.51 ± 0.90 MPa for S50 and QS50 fiber, respectively. Moreover, the pullout energy increased by ~120% for S50 and ~31% for QS50 polymer-coated fibers, compared to natural sisal. These increments can be attributed to the enhanced contact area along the fiber length due to the polymer film layer, which leads to higher interfacial bond stress values as a result of the mechanical anchoring contribution. As mentioned in Section 4.3.1, the micrographs of the longitudinal aspect of polymer-coated fibers showed an increased roughness in the S50 fiber, which can, in turn, improve the mechanical interlock with the matrix and chemical interact, resulting in enhanced pullout parameters compared to the QS50 fiber. In addition, the chemical adhesion between the matrix and the new polymeric layer on the surface of the fiber also contributes to the improvement of interfacial properties. The same improvement was reported by previous studies [3,7,9,11].

4.3.7. Atomic force microscope (AFM)

AFM topographic 2D and 3D images of the natural and S50 polymer-coated fibers are shown in Figure 4.12.a and 4.12.b, respectively. Although natural fibers present a high variation in a micro-nanoscale property, and the statistical analysis is considerably unfeasible with the AFM technique [39], it is still possible to perform a comparative investigation between the natural and polymer-coated sisal fibers. The S50 polymer-coated sisal fiber was chosen as it presented the best results for direct tensile strength and pullout tests (Sections 4.3.5 and 4.3.6).

a) Natural Sisal



b) S50 polymer coated fiber

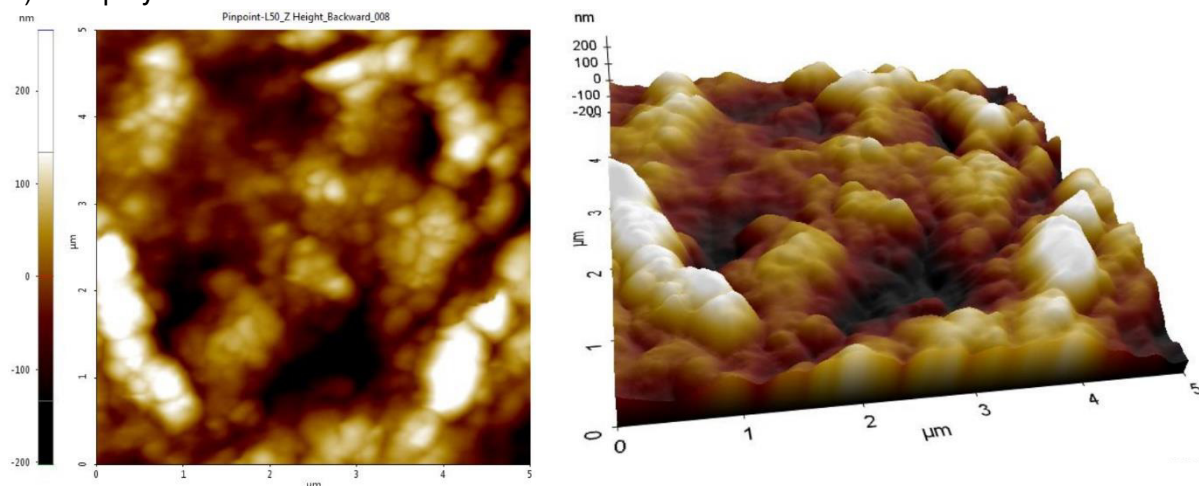


Figure 4.12 – AFM topography images of the surface morphology of (a) natural and (b) S50 polymer coated fibers of a representative 5 μm x 5 μm scan area.

From Figure 4.12 it is clear that natural sisal fibers present pronounced peaks and valleys, characterized by high hills and deep valleys, varying from approximately -250 to 400 nm in the representative scan area presented in Figure

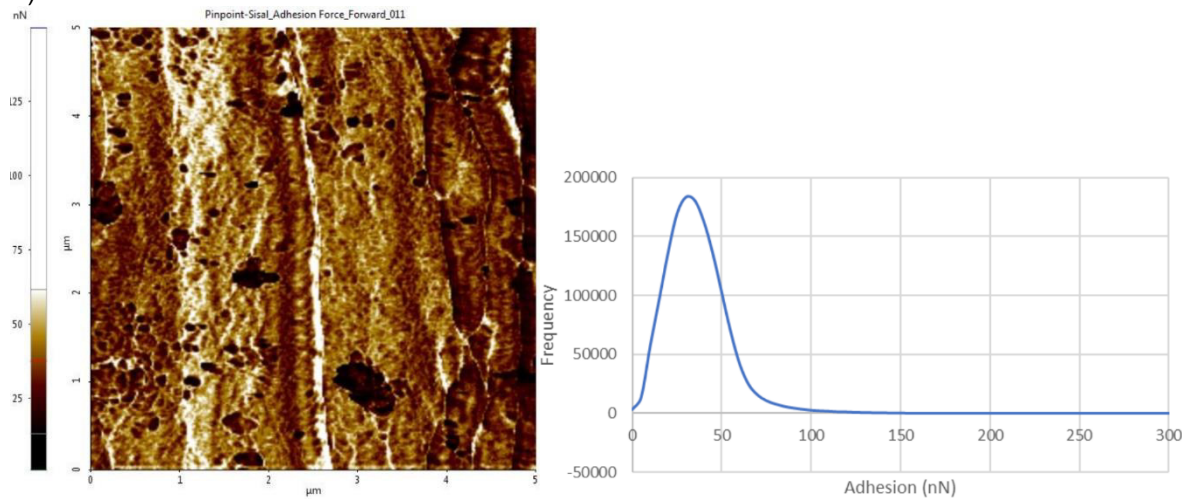
4.12.a. The longitudinal line aspect observed in the images could be related to the presence of the cellulose fibrils that compose the fiber structure [40,41], which were also observed in a lower magnification on the SEM observations (Section 4.3.1). Meanwhile, S50 polymer coated fibers presented a flat and smoother surface, with a granular aspect. In this case, the height variation between the deepest valley and highest hill was around 450 nm (from -200 to 250 nm), representing a reduction of about 30% compared to the natural sisal. The modification in the fiber's superficial aspect evidences the presence of the new polymeric layer around the fiber. Thus, the polymer coating presence did not increase the maximum peak-to-valley height, however, the irregularity of the surface is increased, which can in turn improve the mechanical interlock between the single fiber and the matrix.

Beyond the roughness observations, the AFM analysis allows simultaneous measurement of the load and penetration depth of the tip, obtaining the adhesion forces, contact stiffness, and contact modulus of a thin layer on the fiber surface. Phase contrast imaging was also investigated, as it is considered one of the most common AFM imaging methods to obtain contrast based on material properties. The phase images reveal differences in these surface mechanical properties in a graphic approach [15]. AFM phase images and histograms of the adhesion force, stiffness, and deformation data for natural sisal and S50 polymer-coated fibers are presented in Figures 4.13, 4.14 and 4.15, respectively.

Figure 4.13 showed that the adhesion forces were found to vary according to the fiber type. The polymer coating was found to increase the adhesion force between the fiber and the AFM tip whereas the lowest mean adhesion force was found for the natural sisal fiber. From the phase images of the adhesion force evaluation, it is possible to observe a more uniform grain structure on the polymer-coated fiber. However, on the untreated surface, black patches were observed, which could be correlated with different surface properties. The mean values of adhesion force were ~40 nN and ~60 nN for natural and S50 sisal fiber, respectively. In this sense, it is expected enhanced mechanical adhesion of the polymer-coated fibers with another surface. This finding corroborates with the pullout results (Section 4.3.6), where the polymer-coated fiber showed greater adhesion with the cement-based matrix in comparison to natural sisal.

Adhesion force

a) Natural sisal fiber



b) S50 polymer-coated fiber

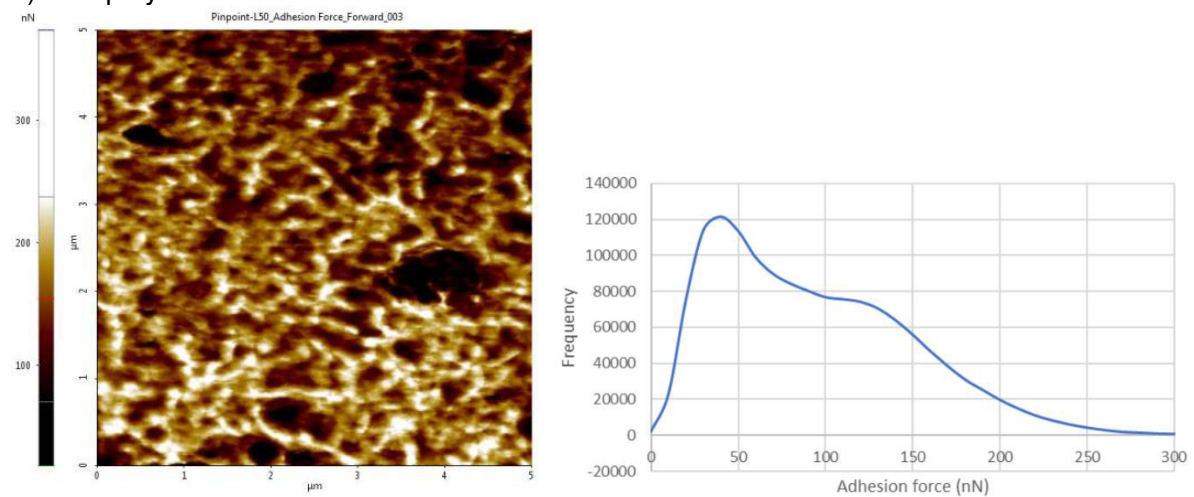
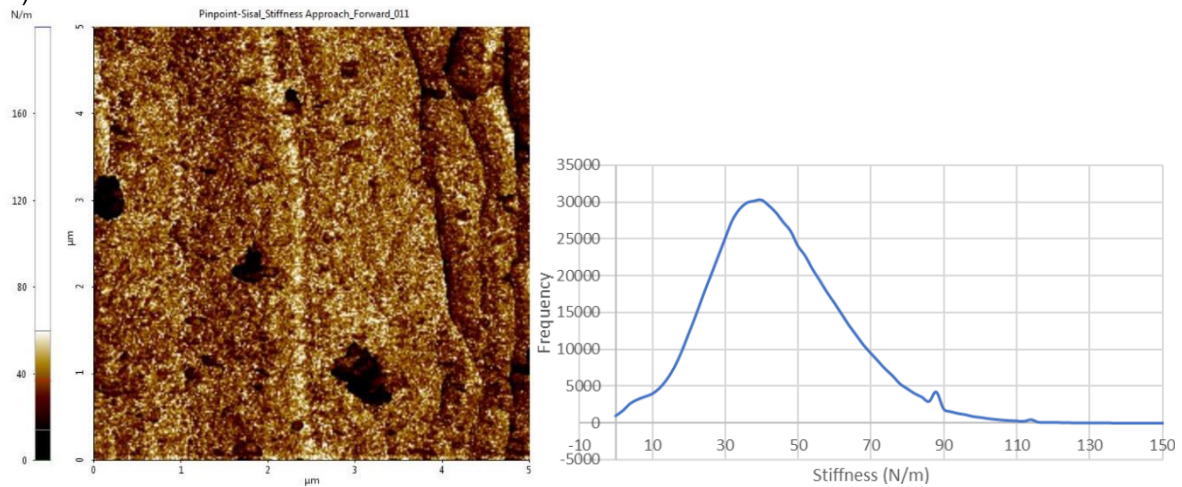


Figure 4.13 – AFM phase contrast representative images and respective histograms of the adhesion force for (a) natural and (b) S50 polymer-coated sisal fiber.

Following the same reasoning, the mean value of deformation measured from the natural sisal histogram was ~ 2 nm (Figure 4.15.a), which is not related to the fiber surface deformation. As the stiffness of the fiber surface was higher than the cantilever tip material (spring constant k of 40 N/m), this deformation is associated with the cantilever deformation (see Figure 4.14).

Stiffness

a) Natural sisal fiber



b) S50 polymer-coated fiber

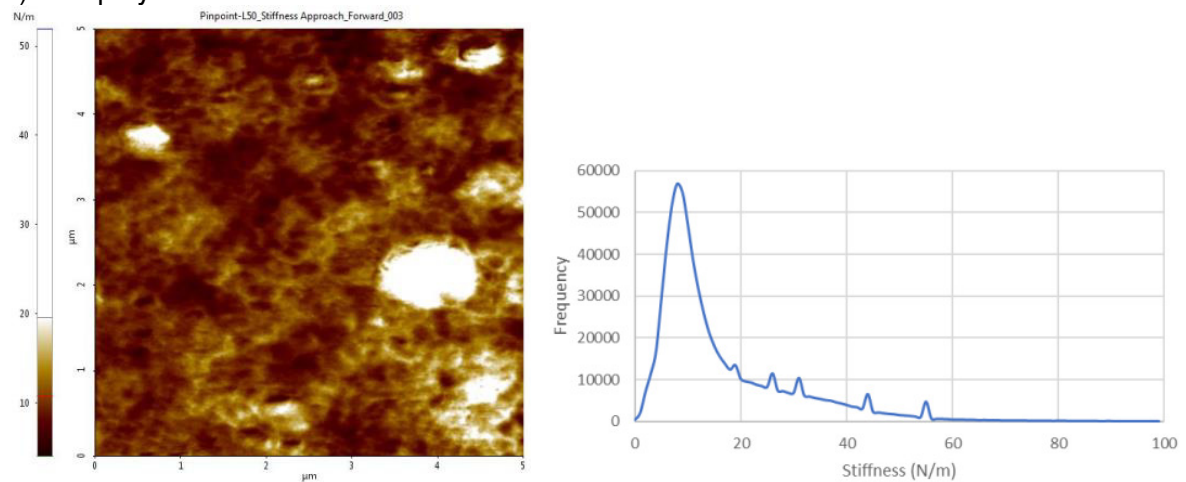
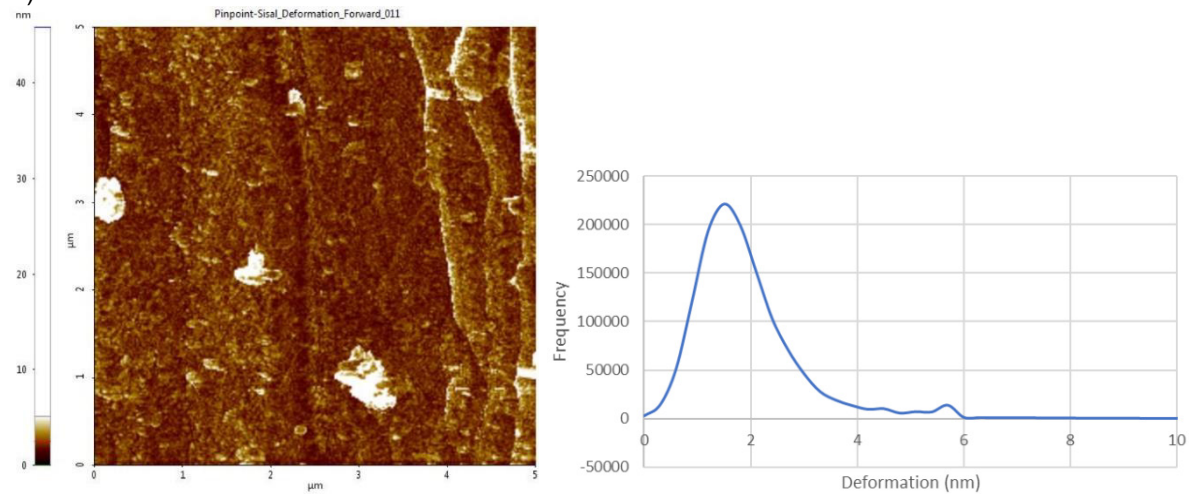


Figure 4.14 – AFM phase contrast representative images and respective histograms of the stiffness for (a) natural and (b) S50 polymer-coated sisal fiber.

On the other hand, the histogram of S50 coated fiber (Figure 4.15.b), showed a range of 0 to 40 nm, with a mean value of ~ 11 nm. In this case, it could be related to the fiber surface deformation, more specifically to the deformation of the superficial polymeric layer. As expected, lower stiffness resulted in higher deformation, as these properties are directly correlated.

Deformation

a) Natural sisal fiber



b) S50 polymer-coated fiber

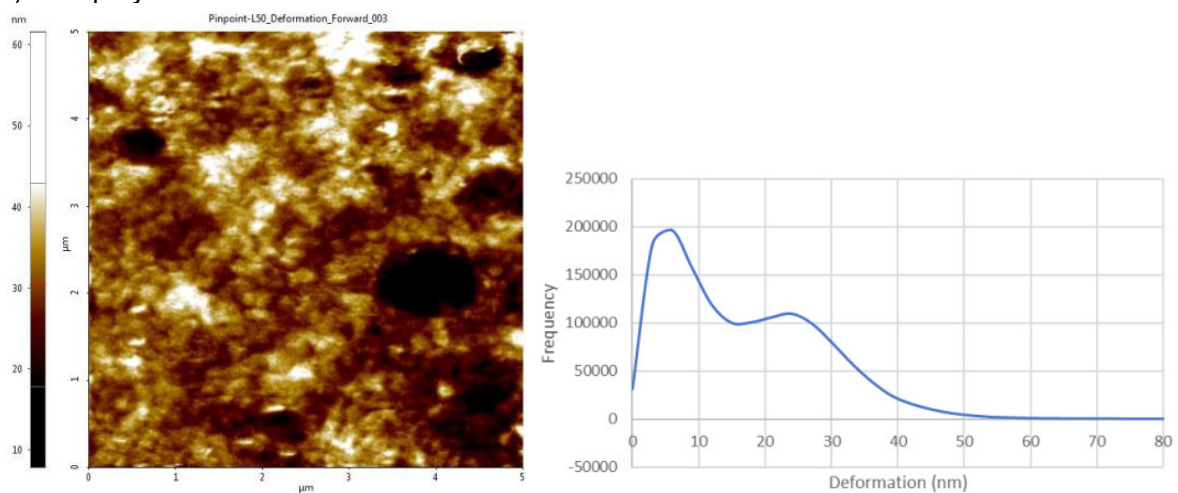


Figure 4.15 – AFM phase contrast representative images and respective histograms of the deformation for (a) natural and (b) S50 polymer-coated sisal fiber.

4.3.8. Stability in alkaline media

In this study, fibers were exposed to 1M NaOH solution for 28 days, followed by the measurement of the tensile strength and Young's modulus of the fibers to evaluate durability performance. Figure 4.16 depicts the results in terms of normalized tensile strength and Young's modulus of natural and polymer-coated fibers. The normalized value corresponds to the ratio between the Tensile strength value after and before alkaline exposure. The same was considered for the normalized values Young's modulus. Consequently, values closer to 1 indicate that the fiber presented greater stability in the alkaline environment, with similar mechanical property values before and after alkaline exposure.

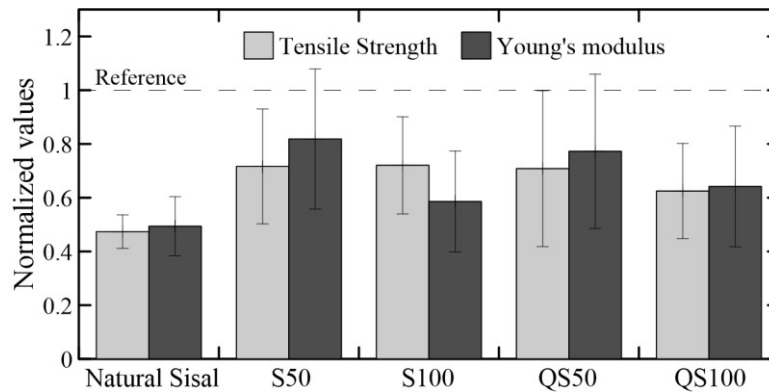


Figure 4.16 – Results of the mechanical evaluation of natural sisal and polymer-coated fibers after alkaline exposure, in terms of normalized tensile strength and Young's modulus.

In the alkaline environment, a similar trend in the tensile strength deterioration of natural and polymer-coated sisal fibers was observed, with a decrease in tensile strength after the alkaline exposure. However, results revealed that a significantly lesser degradation takes place for polymer-modified fibers than that for natural sisal. Natural sisal retains only 47% of its original tensile strength, while polymer-modified fibers presented better tensile strength retention, with approximately 72% for S50, S100, and QS50 fibers, and 62% for the QS100 fiber. Results for polymer-coated fibers presented higher deviation, which is related to fiber heterogeneity as a result of the coating methodology adopted. Hence, it is considered that the polymer-modified sisal fibers are more durable as compared to natural sisal in NaOH alkaline media.

In terms of Young's modulus degradation evaluation, the results followed a similar trend to those for ultimate tensile strength, with lower degradation for polymer-coated fibers. The loss corresponds to approximately 50% for natural sisal, while 18% loss was observed for the QS50 fiber. The Young's modulus decrease in the natural sisal fiber may be attributed to the dissolution of some fiber components, such as cellulose, hemicellulose, or lignin, and also to a decrease in density in general [21]. Since the effect was more pronounced for natural sisal fiber, it indicates that the polymer coating process produced a protective layer around the fibers, avoiding fiber compound degradation.

In conclusion, the results indicated that the presence of a polymeric layer in the fiber surface prevents the NaOH alkaline attack and a more stable fiber was reached. Consequently, it is expected that cementitious matrices reinforced with

polymer-coated sisal fibers became more stable and possessed improved service life.

4.4. Conclusions

The experimental investigation of the performance of natural sisal and polymer-coated fibers leads to the following conclusions:

- Natural sisal fibers present a considerable water absorption capacity, increasing 100% of their own weight after 2 hours of immersion in water. Also, the natural sisal fiber exposure to an alkaline environment resulted in a decrease of ~50% in tensile strength and Young's modulus after 28 days;
- The polymer coating procedure proposed in this study was considered efficient as a new layer formation was confirmed by SEM and AFM images, with a rougher surface aspect compared to natural sisal. Also, TGA and FTIR analyses indicated the presence of new chemical structures in the fiber surface, related to the polymer presence;
- The 50% polymer emulsion (S50 and QS50) was capable to create an external layer around the fiber and also penetrate the fiber lumens, resulting in a stiffer fiber with increased ultimate tensile strength and lower deformation capacity. On the other hand, 100% polymer emulsions (S100 and QS100) presented a lower adherence to the fiber surface with partial debonding from the substrate, resulting in a loss in terms of mechanical properties;
- The polymer presence in the fiber structure was responsible for a considerable reduction in the water absorption capacity of sisal fibers. Also, increased fiber durability was reached, as the new layer acted as a protective barrier against alkaline attack;
- The pullout performance of polymer-coated sisal fibers was enhanced by the chemical and mechanical interactions of the polymeric layer and the cementitious matrix. The denser matrix interface and the rougher surface contributed to the enhancement of the initial rigidity of the load-slip curve and increase load level before fiber debonding.

In conclusion, the polymer coating was considered an effective alternative to modify sisal fibers and make them suitable for use in cement-based matrices. It reached a stronger sisal fiber, with increased fiber-matrix adhesion parameters and enhanced stability in an alkaline environment.

4.5. References

- 1 SHAHINUR, S.; HASAN, M. Natural Fiber and Synthetic Fiber Composites: Comparison of Properties, Performance, Cost and Environmental Benefits. In: **Encyclopedia of Renewable and Sustainable Materials**. Elsevier, 2019. p.794-802.
- 2 TOWNSEND, T. World natural fibre production and employment. In: **Handbook of Natural Fibres**. Elsevier, 2020. p.15-36.
- 3 ASPRONE, D.; DURANTE, M.; PROTA, A.; MANFREDI, G. Potential of structural pozzolanic matrix-hemp fiber grid composites. **Construction and Building Materials**, v.25, n.6, p.2867-2874, 2011.
- 4 CHAKRABORTY, S.; KUNDU, S. P.; ROY, A.; ADHIKARI, B.; MAJUMDER, S. B. Polymer modified jute fibre as reinforcing agent controlling the physical and mechanical characteristics of cement mortar. **Construction and Building Materials**, v.49, p.214-222, 2013.
- 5 AKINYEMI, B. A.; ADESINA, A. Utilization of polymer chemical admixtures for surface treatment and modification of cellulose fibres in cement-based composites: a review. **Cellulose**, v.28, p.1241-1266, 2021.
- 6 CASTOLDI, R. de S.; SOUZA, L. M. S.; SILVA, F. de A. Comparative study on the mechanical behavior and durability of polypropylene and sisal fiber reinforced concretes. **Construction and Building Materials**, v.211, p.617-628, 2019.
- 7 KUNDU, S. P.; CHAKRABORTY, S.; ROY, A.; ADHIKARI, B.; MAJUMDER, S. B. Chemically modified jute fibre reinforced non-pressure (NP) concrete pipes with improved mechanical properties. **Construction and Building Materials**, v.37, p.841-850, 2012.
- 8 FERREIRA, S. R.; SILVA, F. de A.; LIMA, P. R. L.; TOLEDO FILHO, R. D. Effect of fiber treatments on the sisal fiber properties and fiber-matrix bond in cement based systems. **Construction and Building Materials**, v.101, p.730-740, 2015.
- 9 FERREIRA, S. R.; SENA NETO, A. R.; SILVA, F. de A.; SOUZA JUNIOR, F. G.; TOLEDO FILHO, R. D. The influence of carboxylated styrene butadiene rubber coating on the mechanical performance of vegetable fibers and on their interface with a cement matrix. **Construction and Building Materials**, v.262, p.120770, 2020.
- 10 LIMA, P. R. L.; SANTOS, H. M.; CAMILLOTO, G. P.; CRUZ, R. S. Effect of Surface Biopolymeric Treatment on Sisal Fiber Properties and Fiber-

- Cement Bond. **Journal of Engineered Fibers and Fabrics**, v.12, n.2, p.59-71, 2018.
- 11 FIDELIS, M. E. A.; TOLEDO FILHO, R. D.; SILVA, F. de A.; MOBASHER, B.; MÜLLER, S.; MECHTCHERINE, V. Interface characteristics of jute fiber systems in a cementitious matrix. **Cement and Concrete Research**, v.116, p.252-265, 2019.
- 12 WEN, S.; CHUNG, D. D. L. Carbon fiber-reinforced cement as a strain-sensing coating. **Cement and Concrete Research**, v.31, n.4, p.665-667, 2001.
- 13 MÄDER, E.; PLONKA, P.; SCHIEKEL, M.; HEMPEL, R. Coatings on alkali-resistant glass fibres for the improvement of concrete. **Journal of Industrial Textiles**, v.33, n.3, p.191-207, 2004.
- 14 SCHEFFLER, C.; GAO, S. L.; PLONKA, R.; MÄDER, E.; HEMPEL, S.; BUTLER, M.; MECHTCHERINE, V. Interphase modification of alkali-resistant glass fibres and carbon fibres for textile reinforced concrete I: Fibre properties and durability. **Composites Science and Technology**, v.69, n.3-4, p.531-538, 2009.
- 15 GAO, S. L.; MÄDER, E.; PLONKA, R. Nanocomposite coatings for healing surface defects of glass fibers and improving interfacial adhesion. **Composites Science and Technology**, v.68, n.14, p.2892-2901, 2008.
- 16 KUNDU, S. P.; CHAKRABORTY, S.; MAJUMDER, S. B.; ADHIKARI, B. Effectiveness of the mild alkali and dilute polymer modification in controlling the durability of jute fibre in alkaline cement medium. **Construction and Building Materials**, v.174, p.330-342, 2018.
- 17 FIDELIS, M. E. A.; SILVA, F. de A.; TOLEDO FILHO, R. D. The Influence of Fiber Treatment on the Mechanical Behavior of Jute Textile Reinforced Concrete. **Key Engineering Materials**, v.600, p.469-474, 2014.
- 18 TRINDADE, A. C. C.; BORGES, P. H. R.; SILVA, F. de A. Evaluation of Fiber–Matrix Bond in the Mechanical Behavior of Geopolymer Composites Reinforced with Natural Fibers. **Advances in Civil Engineering Materials**, v.8, n.3, p.20180136, 2019.
- 19 AMERICAN SOCIETY FOR TESTING AND MATERIALS. **ASTM C1557**: Standard Test Method for Tensile Strength and Young’s Modulus of Fibers. United States, 2020.
- 20 BALNOIS, E.; BUSNEL, F.; BALEY, C.; GROHENS, Y. An AFM study of the effect of chemical treatments on the surface microstructure and adhesion properties of flax fibres. **Composite Interfaces**, v.14, n.7-9, p.715-731, 2007.
- 21 STAPPER, J. L.; GAUVIN, F.; BROUWERS, H. J. H. Influence of short-term degradation on coir in natural fibre-cement composites. **Construction and Building Materials**, v.306, p.124906, 2021.
- 22 SILVA, F. de A.; MOBASHER, B.; SORANAKOM, C.; TOLEDO FILHO, R. D. Effect of fiber shape and morphology on interfacial bond and cracking behaviors of sisal fiber cement based composites. **Cement & Concrete**

- Composites**, v.33, n.8, p.814-823, 2011.
- 23 SILVA, F. de A.; CHAWLA, N.; TOLEDO FILHO, R. D. Mechanical behavior of natural sisal fibers. **Journal of Biobased Materials and Bioenergy**, v.4, n.2, p.106-113, 2010.
- 24 MARTIN, A. R.; MARTINS, M. A.; SILVA, O. R. R.; MATTOSO, L. H. C. Studies on the thermal properties of sisal fiber and its constituents. **Thermochimica Acta**, v.506, n.1-2, p.14-19, 2010.
- 25 HAJIHA, H.; SAIN, M.; MEI, L. H. Modification and Characterization of Hemp and Sisal Fibers. **Journal of Natural Fibers**, v.11, n.2, p.144-168, 2014.
- 26 SILVA, C. C.; LIMA, A. de F.; MORETO, J. A.; DANTAS, S.; HENRIQUE, M. A.; PASQUINI, D.; RANGEL, E. C.; SCARMÍNIO, J.; GELAMO, R. V. Influence of plasma treatment on the physical and chemical properties of sisal fibers and environmental application in adsorption of methylene blue. **Materials Today Communications**, v.23, p.101140, 2020.
- 27 VÁRHEGYI, G.; SZABÓ, P.; MOK, W. S. L.; ANTAL, M. J. Kinetics of the thermal decomposition of cellulose in sealed vessels at elevated pressures. Effects of the presence of water on the reaction mechanism. **Journal of Analytical and Applied Pyrolysis**.v.26, n.3, p.159-174, 1993.
- 28 BAETA, D. A.; ZATTERA, J. A.; OLIVEIRA, M. G.; OLIVEIRA, P. J. The use of styrene-butadiene rubber waste as a potential filler in nitrile rubber: Order of addition and size of waste particles. **Brazilian Journal of Chemical Engineering**, v.26, n.1, p.23-31, 2009.
- 29 WEI, J.; MEYER, C. Degradation mechanisms of natural fiber in the matrix of cement composites. **Cement and Concrete Research**, v. 73, p.1-16, 2015.
- 30 SANJAY, M. R.; SIENGCHIN, S.; PARAMESWARANPILLAI, J.; JAWAID, M.; PRUNCU, C. I.; KHAN, A. A comprehensive review of techniques for natural fibers as reinforcement in composites: Preparation, processing and characterization. **Carbohydrate Polymers**, v.207, p.108-121, 2019.
- 31 SIVA, J.; RAJU, N.; VICTOR, M.; KUMARAN, P. Comprehensive characterization of raw and alkali (NaOH) treated natural fibers from *Symphirema involucreatum* stem. **International Journal of Biological Macromolecules**, v.186, p.886-896, 2021.
- 32 BARRETO, A. C. H.; ROSA, D. S.; FECHINE, P.B.A.; MAZZETTO, S. E. Properties of sisal fibers treated by alkali solution and their application into cardanol-based biocomposites. **Composites Part A: Applied Science and Manufacturing**, v.42, n.5, p.492-500, 2011.
- 33 MARTÍNEZ-BARRERA, G.; LÓPEZ, H.; CASTAÑO, V. M.; RODRÍGUEZ, R. Studies on the rubber phase stability in gamma irradiated polystyrene-SBR blends by using FT-IR and Raman spectroscopy. **Radiation Physics and Chemistry**, v.69, n.2, p.155-162, 2004.
- 34 TEIXEIRA, F. P.; GOMES, O. da F. M.; SILVA, F. de A. Degradation

- Mechanisms of Curaua, Hemp, and Sisal Fibers Exposed to Elevated Temperatures. **BioResources**, v.14, n.1, p.1494-1511, 2019.
- 35 REN, G.; YAO, B.; HUANG, H.; GAO, X. Influence of sisal fibers on the mechanical performance of ultra-high performance concretes. **Construction and Building Materials**, v.286, p.122958, 2021.
- 36 FERREIRA, S. R.; SILVA, F. de A.; LIMA, P. R. L.; TOLEDO FILHO, R. D. Effect of hornification on the structure, tensile behavior and fiber matrix bond of sisal, jute and curauá fiber cement based composite systems. **Construction and Building Materials**, v.139, p.551-561, 2017.
- 37 INTERNATIONAL FEDERATION FOR STRUCTURAL CONCRETE. **Model Code 2010: Final Draft**. Switzerland, 2012.
- 38 CASTOLDI, R. de S.; SOUZA, L. M. S.; SOUTO, F.; LIEBSCHER, M.; MECHTCHERINE, V.; SILVA, F. de A. Effect of alkali treatment on physical–chemical properties of sisal fibers and adhesion towards cement-based matrices. **Construction and Building Materials**, v.345, p.128, 2022.
- 39 PRAVEEN, K. M.; THOMAS, S.; GROHENS, Y.; MOZETIČ, M.; JUNKAR, I.; PRIMC, G.; GORJANC, M. Investigations of plasma induced effects on the surface properties of lignocellulosic natural coir fibres. **Applied Surface Science**, v.368, p.146-156, 2016.
- 40 PENG, X.; ZHONG, L.; REN, J.; SUN, R. Laccase and alkali treatments of cellulose fibre: Surface lignin and its influences on fibre surface properties and interfacial behaviour of sisal fibre/phenolic resin composites. **Composites Part A: Applied Science and Manufacturing**, v.41, n.12, p.1848-1856, 2010.
- 41 MACHADO JUNIOR, M.; SOUZA, S. M. A.; MORGADO, A. F.; CALDAS, P. G.; PTAK, F.; PRIOLI, R. Influence of cellulose fibers and fibrils on nanoscale friction in kraft paper. **Cellulose**, v.23, n.4, p.2653-2661, 2016.

5 Effect of surface modification of sisal fibers with polyphenols on the mechanical properties, interfacial adhesion and durability in cement-based matrices

This chapter aims to describe a facile approach for sisal fiber surface functionalization based on polyphenol chemistry, and to study fiber-matrix bonding performances as well as durability behavior in highly alkaline conditions. The modification process was accomplished through a two-step procedure including immersion in tannic acid (TA) solution (5 and 10 g/L) followed by treatment with octadecylamine (ODA) solution (1, 2.5, 3.75, and 5 g/L). Different analytical techniques were employed to examine the effect of the treatment, including Fourier transform infrared spectroscopy (FTIR) and thermogravimetric analysis (TGA). SEM images along with mapping analyses were obtained to evaluate the formation, chemical composition, and distribution of TA-ODA layer on modified fibers. Changes in terms of water uptake ability were studied by water absorption and contact angle measurements. Fiber-matrix interactions were also evaluated throughout single fiber pullout tests from a cement-based matrix. To characterize the mechanical properties of the fibers before and after the modification, single fiber direct tensile tests were applied. Moreover, the stability in alkaline environments (NaOH and Pore solutions) was investigated in terms of mechanical properties degradation after fiber exposure for 28 days. The results showed that modification with a low concentration of TA and ODA solutions was efficient to reduce the hydrophilic tendency of these fibers while enhancing fiber roughness and interlock with the cement-based matrix. In addition, the modified fiber presented improved stability in an aggressive alkaline environment.

Most of the experimental program presented in this chapter was developed at TU Dresden, Germany. However, the SEM images and FTIR spectra were obtained at the Center of Mineral Technology (CETEM) and Analytical Central Laboratory of Analysis (PUC-Rio), respectively. Also, the water contact angle analysis was performed at the Thermoanalysis and Rheology Laboratory at UFRJ.

5.1. Introduction

The existing alternatives for fiber modification include various physical and chemical approaches, including hornification, alkaline, silane, acetylation, plasma treatment, among others [1–7]. Although widely implemented in research works, many of the aforementioned methods have limitations for widespread large-scale implementation, such as the use of expensive and non-sustainable materials, the requirement of fiber separation during modification, complex instrumentation, and the need of multistep procedures. Therefore, the development of a simple and low-cost method for surface modification of natural fibers is still highly desired to encourage the use of dispersed natural fibers in cementitious composites.

To change fiber surface wettability, the catechol chemistry has been served recently as one of the most effective techniques based on using the dopamine (DA) modification approach [8–12]. For instance, Bashiri Rezaie et al. [10] applied polydopamine as a surface modifier for PE fibers, focusing on the enhancement of interfacial bonding with cementitious matrices. After the evaluation through single-fiber pullout tests, a noticeable increase in the maximum pullout load, interfacial shear strength, and fiber pullout energy was achieved for the modified fibers.

Recently, as an alternative to the use of dopamine, a low-cost plant-based polyphenol has attracted attention: tannic acid (TA). This plant polyphenol is a compound with galloyl units of up to 12, having three hydroxyl groups in each unit [13]. It is capable of cross-linking molecules with different interactions, such as hydrogen/ionic bonding and hydrophobic interactions through secondary reactions with amine compounds [13,14]. According to Gu et al. [8], the fabrication of highly hydrophobic cotton fabrics via coordination assembly of tannic acid (TA) and Fe(III) followed by treatment with 1-octadecylamine was efficient to control the fabric wettability, and increased the resistance to acid, alkaline, and salt corrosion. Hu et al. [9] proposed an environmentally friendly procedure for surface modification of cellulose nanocrystals (CNCs) through a two-step procedure, using tannic acid and decylamine. As a result, the modified CNC particles presented increased contact angle and ability to be redispersed in organic solvents, evidencing the increased hydrophobicity of the modified particles. Hence, TA surface modification can be regarded as a proper candidate for diminishing the wettability of natural fibers, however, it has not been applied to sisal fibers yet.

On the other hand, the weak alkaline stability of cellulosic fibers is another challenging issue, especially when used in cementitious composites with a high alkali environment [15,16]. It means that the degradation of these fibers can gradually happen inside of compendious matrix which results in a relatively reduced reinforcing capacity in the later stage of service life [17]. To mitigate this defect, graphene oxide-based membrane coating, as an example, was suggested by Zhao et al. [18] for sisal fibers, and an improved deterioration resistance under the environment of cement hydration was observed through the formation of a protective layer on the fiber surface. TA functionalization, therefore, can affect the alkaline degradation process of sisal fibers in cementitious matrices which has not been studied in the literature.

With the above background in mind, the objective of the current research work is to evaluate the influence of TA surface treatment of sisal fibers on fiber-cementitious matrix interactions and the fiber alkaline stability. To the best of the authors' knowledge, this is the first example of assessing the interfacial properties of TA-modified sisal fibers embedded into cementitious composites as well as their stability in such alkaline medium.

5.2. Materials and methods

5.2.1. Fiber surface modification

The sisal fibers used in this study were the same detailed in Chapter 3. Also, the fibers were cleaned before modification, as mentioned in Section 3.2.2. Surface modification of sisal fibers was carried out via a two-step process by using tannic acid (ACS reagent) and octadecylamine ($\geq 99.0\%$, GC), both purchased from Sigma-Aldrich. Tannic acid is a type of polyphenol extracted from plants, known as a commercial form of Tannin and Gallotannin, with the empirical formula $C_{76}H_{52}O_{46}$. It is a naturally occurring organic compound characterized by multiple phenol units, which present one or more hydroxyl groups bonded directly to an aromatic hydrocarbon group. The octadecylamine, on the other hand, presents the empirical formula $CH_3(CH_2)_{17}NH_2$, and it is also known as 1-Aminooctadecane and Stearylamine. In short, the two-step process consisted of the use of tannic acid acting as a primer to form an active polymeric layer on the sisal fiber surface, which

is then reacted with the octadecylamine (ODA), reaching a proper hydrophobic surface.

Figure 5.1 presents some photographs of the procedure. In the first step, a 200 mL tannic acid (TA) aqueous solution was prepared with deionized water and different TA concentrations (5 and 10 g/L). The solution was stirred intensely at room temperature and then the pH value was adjusted to 8.0 by adding 0.55 M NaOH solution to initiate a self-polymerization process according to the literature [8]. It was previously reported [9,19] that, under alkaline conditions and in the presence of available dissolved oxygen, there is the occurrence of plant polyphenol oxidation and oligomerization, resulting in the formation of higher molecular weight species with decreased solubility [19]. Subsequently, 1.0 g of cleaned sisal fiber was immersed in the solution and the mixture was mechanically stirred at room temperature for 12 hours (Figure 5.1.b). After this period, the fibers were removed and washed several times with deionized water to remove the excess of TA solution.

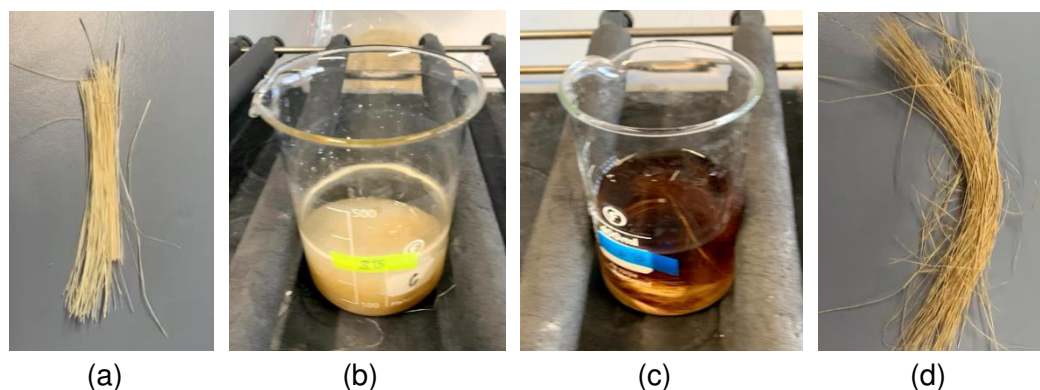


Figure 5.1 – (a) Natural sisal fiber before the modification process, (b) fiber under the TA solution, (c) fiber under the ODA solution, and (d) visual aspect of the fiber after TA-ODA modification.

In the second step, fibers were immersed in 200 mL of octadecylamine (ODA) solution, prepared with 120 mL of isopropanol, 80 mL of deionized water, and different ODA concentrations (1, 2.5, 3.75, and 5 g/L). The solution with the fibers was then stirred for 12 hours at room temperature (Figure 5.1.c). Then, the resultant TA-ODA coated fibers were washed several times with deionized water and air-dried for 24 hours at room temperature. By the end of the process, the modified fibers changed from a light-yellow color to a dark brownish color, as a result of the self-polymerization (Figure 5.1.d). A summary of the TA-ODA coated fibers

obtained according to the combination of TA and ODA concentration is presented in Table 5.1.

Table 5.1 – Summary of the variables related to the sample identification.

Sample identification	TA concentration (g/L)	ODA concentration (g/L)
Natural Sisal	0	0
TA5-ODA1	5	1
TA5-ODA2.5	5	2.5
TA5-ODA3.75	5	3.75
TA5-ODA5	5	5
TA10-ODA3.75	10	3.75

The scheme of the steps involved in the fiber surface modification in this study is presented in Figure 5.2.

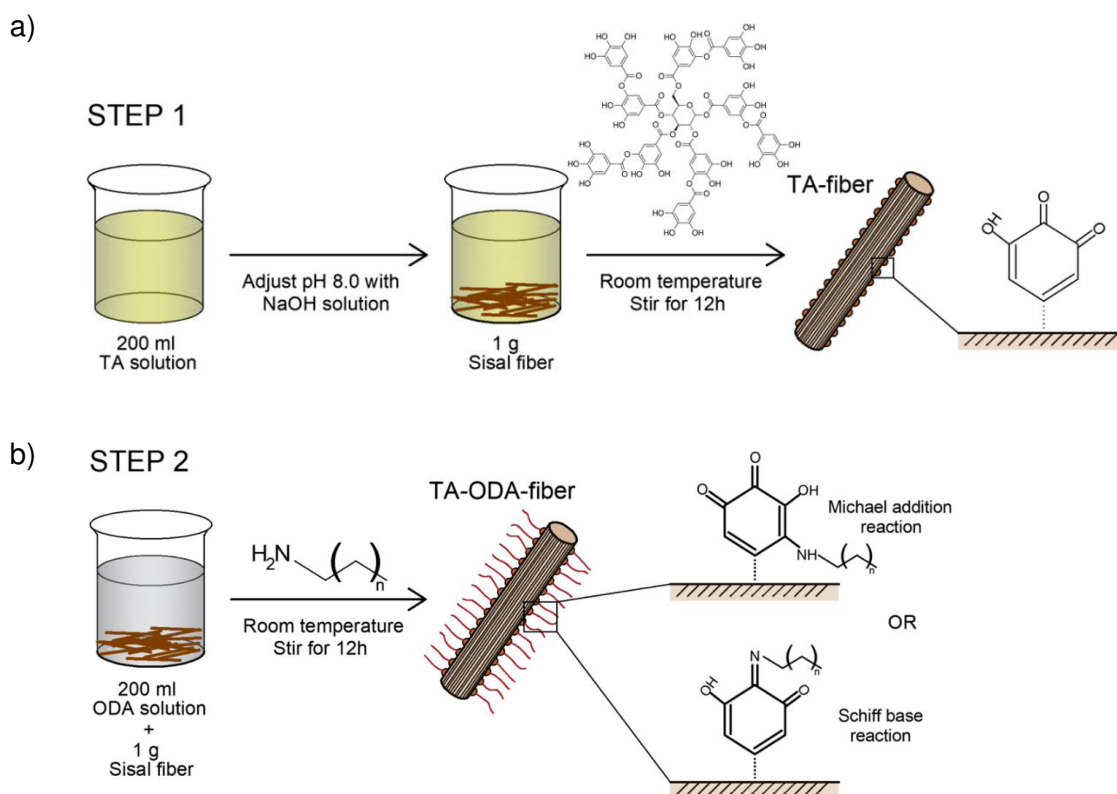


Figure 5.2 – Scheme of the suggested fiber surface modification consisting of two steps: (a) immersion in the tannic acid solution and (b) immersion in the octadecylamine solution.

5.2.2. Preparation of sisal fiber cementitious composite for pullout test

A low alkaline cementitious matrix was used based on earlier studies of a cement-based matrix with sisal fiber [20] (Table 5.2). The binder material was composed by 50 wt.% of CEM II/A-M (S-LL) 52.5 R, 30 wt.% of metakaolin, and 20 wt.% of fly ash. Firstly, the binder material was dry mixed with natural river sand (0-2 mm). Then, the water and superplasticizer were added to the dry components, and the materials were blended using a disperser IKA T50 digital Ultra-Turrax for 10 minutes.

Table 5.2 – Mixture composition of the cement-based matrix.

Components	Cement	Metakaolin	Fly Ash	Natural Sand	Water	Superplasticizer
Dosage (kg/m³)	190	114	76	536	246	1.12

The schematic configuration of the pullout specimens is shown in Figure 5.3. The mold consisted of 10 prismatic spaces to fill with dimensions of 8x10x25 mm³. In the center of each prism, single fibers were placed and stretched before casting. Then, the mold was filled with the matrix, and subsequently vibrated for 1 minute to remove possible voids in the matrix. After 24 hours, the pullout specimens were demolded, sealed in plastic bags, and stored in a climatic chamber with standard conditions of temperature and humidity for 28 days until the pullout tests.

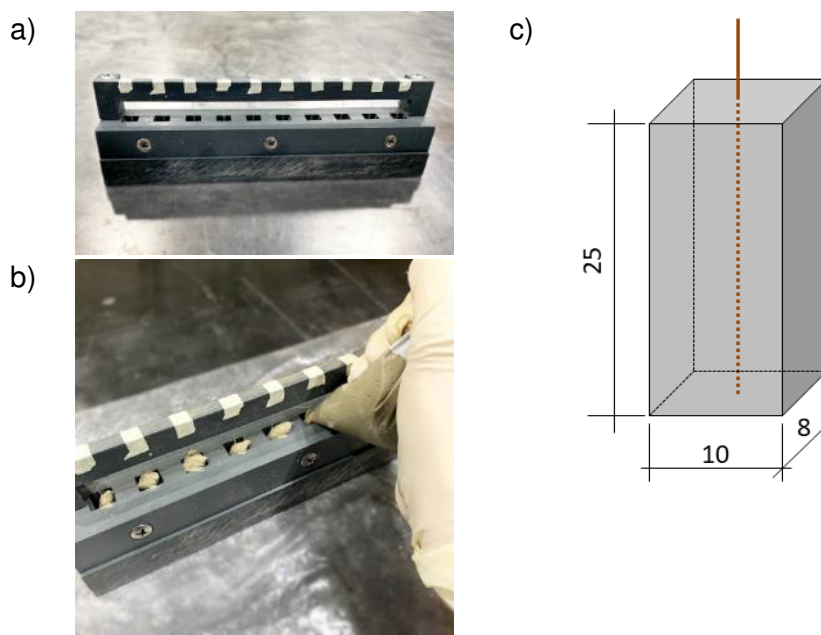


Figure 5.3 – Preparation of pullout samples: (a) mold and (b) casting of the specimens. (c) Schematic configuration of the pullout sample (dimensions in mm).

5.2.3. Fiber characterization

5.2.3.1. Scanning electron microscope (SEM) analysis

The longitudinal surface morphology of natural and modified sisal fibers was investigated using an Environmental Scanning Electron Microscope (ESEM) model Quanta 250 FEG, FEI. The ESEM was operated under low vacuum mode with an accelerating voltage of 5 to 7 kV. The fiber samples were placed in the sample holder with adhesive tape. It was not necessary any additional sample coating before the analysis. Furthermore, the instrument was equipped with mapping analysis which was used to specify the elemental composition of the original and modified fibers and their distribution on the surface of the fibers.

The cross-sectional surface aspect of natural and modified sisal fibers was assessed using a Scanning Electron Microscope (SEM) model TM3030Plus (Hitachi) operated under high vacuum mode with an accelerating voltage of 15 kV. The fiber samples were pre-coated with gold to make the fiber conductive.

5.2.3.2. Thermogravimetric analysis

The thermogravimetric analysis (TGA) was used to investigate the thermal stability of natural and modified sisal fibers. The evaluation was carried out by an STA 409 cell thermal analyzer (Netzsch, Germany). About 50 mg of fibers were previously prepared for the analysis by cutting with a scissor into small fibers of approximately 1 mm length. The samples were heated from 0 to 800 °C with a rate of 10 K/min in a nitrogen environment with a constant gas flow of 60 ml/min. The mass change was recorded for every 2.5 °C temperature increase.

5.2.3.3. Water absorption measurement

The water absorption test was performed to quantify the change in hydrophilicity of natural and modified sisal fibers. It was adopted the same procedure presented in Section 3.3.2.4. The moisture content (MC) was defined as an increase in weight percentage according to Equation 5.1 as follows:

$$MC (\%) = ((w_{sat} - w_{dry}) / w_{dry}) \times 100 \quad (\text{Eq. 5.1})$$

Where w_{sat} and w_{dry} correspond to the saturated and dried fiber weights, respectively.

5.2.3.4. Water contact angle

To investigate natural and modified sisal fiber wettability, static contact angle measurement was performed. There are several methods of tests reported in the literature, including the most applied Sessile drop technique and Wilhelmy Plate Method [21]. In the last method cited, the measurement is highly dependent on the fiber length put into the liquid and is not appropriate for natural fibers with irregular dimensions [21]. In this way, the sessile drop technique was adopted for the contact angle evaluation. To obtain a horizontal plane, samples were prepared as a flat surface of about 1 mm of aligned fibers composed of four alternate layers of fibers on a glass slide.

For the test, a DSA100 Drop Shape Analyzer system solution was used. A single droplet of distilled water with a total volume of 5 μl was placed on the sample surface with a pipette at a rate of 100 $\mu\text{l}/\text{min}$, and images were taken at each 1s. For each sample, 5 measurements were made. After the tests, the images were post-processed using ImageJ software, and the angles corresponding to 10, 20, and 30 seconds of exposure time were calculated. The static contact angles were measured on both sides of the water drop profile, and the final value corresponds to the average of these results.

5.2.3.5. Fourier-transform infrared spectroscopy

The infrared absorption spectrum of natural and modified sisal fiber was obtained from the chemical compositions of the fibers. The analysis was performed on a Bruker FTIR Spectrometer Alpha II equipment using an ATR accessory (Bruker ATR module) in the range of 400-4000 cm^{-1} frequency, with a resolution of 2 cm^{-1} . The obtained spectrum was an average of 32 scans. Each group was measured three times.

5.2.3.6. Mechanical properties

To evaluate the influence of the modification on the mechanical properties of

the fibers, uniaxial tensile tests were performed following the recommendations of ASTM C1557 [22]. The tensile strength tests were carried out using a Zwick Roell 1445 testing machine equipped with a 50 N load cell (Figure 5.4.a), at a displacement rate of 0.1 mm/min. A pre-load of 0.2 N was applied to ensure that the fibers were completely stretched at the beginning of the test. At least 10 specimens were tested for each condition. The preparation of the samples consisted in gluing the single fiber to a stiff paper frame (120 g/cm²), for a better alignment in the machine, with a free length of 20 mm. Then, the samples were clamped by the grips of the test set-up, and both lateral edges of the paper frame were cut to allow the fiber deformation during loading (Figure 5.4.b).

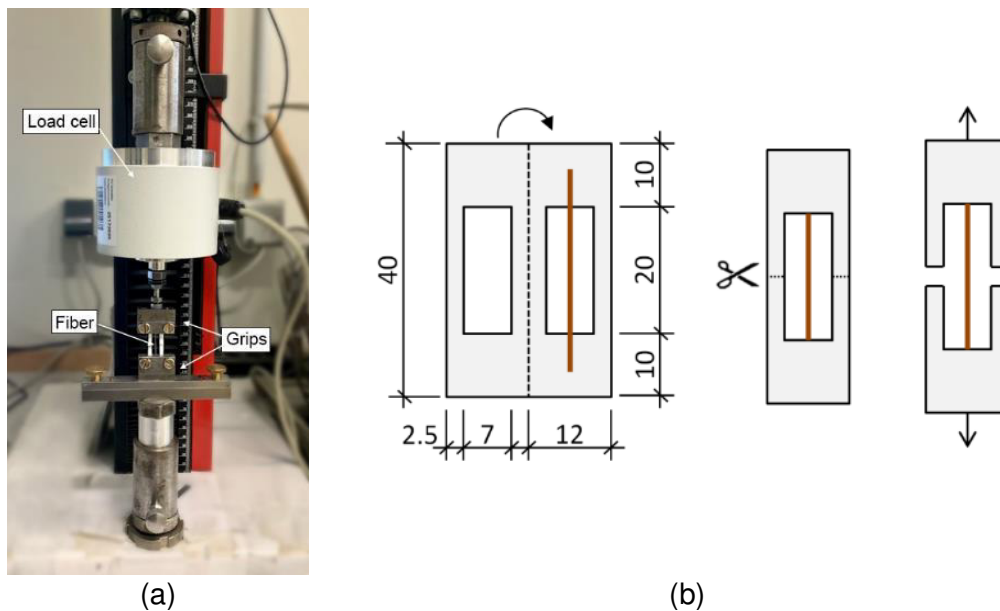


Figure 5.4 – (a) Single-fiber setup arrangement and (b) schematic configuration of the sample preparation (dimensions in mm).

In order to calculate the tensile strength of the fibers, their cross-sectional areas were measured using an optical microscope. An adjacent piece of each tested fiber was kept before the sample preparation, and then the area was obtained from the images using ImageJ software.

5.2.4. Fiber-matrix bond evaluation

Single-fiber pullout tests were performed to evaluate the influence of fiber modification in the bond with the cementitious matrix. Tests were performed using a Zwick Roell 1445 testing machine, equipped with a 50 N load cell, at a displacement rate of 1 mm/min. Figure 5.5 depicts the equipment used in the pullout tests. The bottom part of the test setup consisted of a clamp system where the matrix

was fixed, and the free end of the fiber was tightened to the top part. At least 10 specimens were tested for each parameter combination. The fiber cross-sectional area of each fiber was estimated from optical microscope images, as described in Section 5.2.3.1.

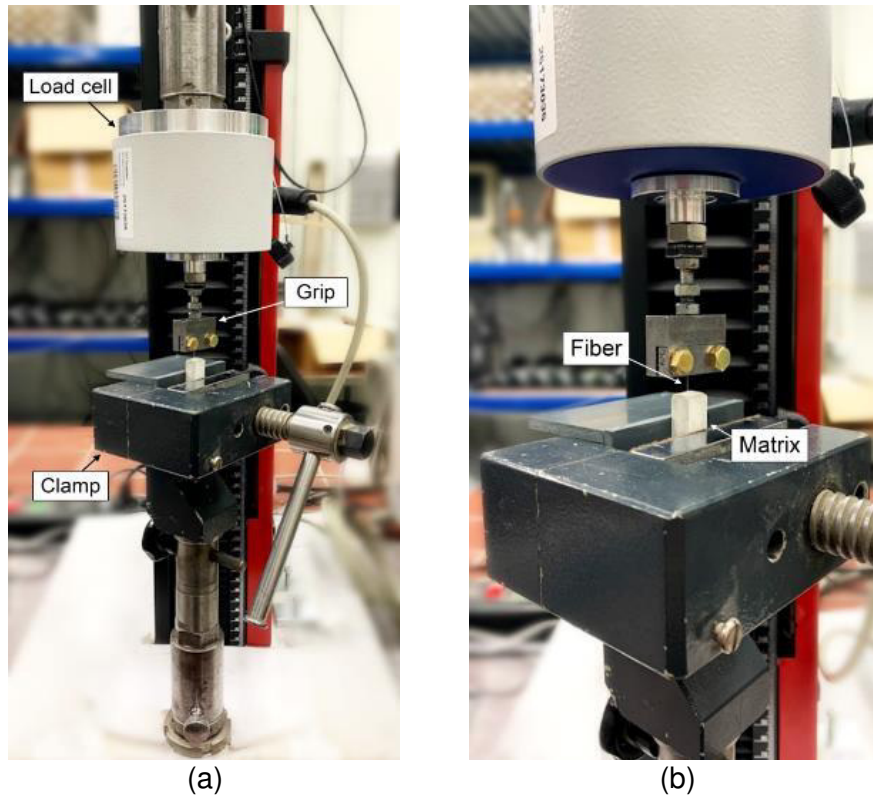


Figure 5.5 – (a) General overview and (b) detail of the single-fiber pullout test arrangement.

The average interfacial shear stress (τ) was obtained with Equation 5.2, as follows:

$$\tau = \frac{P_{max}}{2\pi r L_c} \quad (\text{Eq. 5.2})$$

Where P_{max} is the load immediately before the debonding initiation, r is the equivalent radius obtained from the fiber cross-sectional area and L_c is the embedded length, equal to 25 mm.

5.2.5. Fiber durability evaluation

As cement-based matrices are alkaline in nature, it is important to enhance sisal fiber's alkaline resistance to make them suitable for use as reinforcement in

cementitious composites. To evaluate the influence of surface modification in an alkaline aggressive environment, natural sisal and modified fibers were exposed to two different solutions: NaOH and Pore solutions. A strongly alkaline 1N NaOH solution (13.6 pH) was adopted, following the recommendations of ASTM D6942 [23]. Although this alkali concentration is higher than usual cement-based matrices (pH of approximately 12.7 at the fresh state [24]), stronger pH provides an increased degradation in a short time of exposure. On the other hand, a cement pore solution was prepared with a Portland cement CEM I 32.5 R. For this, 1.25 kg of cement was added to 6.5 l of water and mixed into a bucket. The mixture was then stirred each 1h for 24h and finally, the slurry was filtered to remove all the visible particles. The resulting alkaline pore solution presented a 12.8 pH.

The durability evaluation procedure started with the immersion of 50 mm length fibers in the alkaline solutions for 28 days. After completion of the exposure period, fibers were washed several times with distilled water to remove the excess alkali from the fiber surface and air-dried for 24 hours before the mechanical evaluation. Single fiber tensile tests were performed to assess the influence of surface modification on the durability of the fibers in terms of residual mechanical strength. For each fiber type and aggressive solution, 10 fibers were tested. The direct tensile tests followed the configuration presented in Section 5.2.3.6.

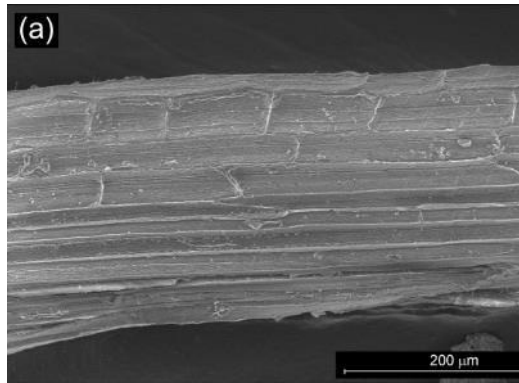
5.3. Results and discussion

5.3.1. Fiber characterization

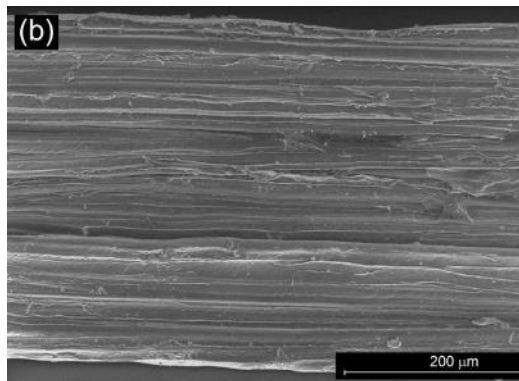
5.3.1.1. Scanning electron microscopy (SEM) analysis

Micrographs of the longitudinal and cross-sectional aspects of natural sisal and surface-modified sisal fibers are shown in Figures 5.6 and 5.7. From Figure 5.6.a, it is clear that natural sisal is characterized by fibrils along the axis, which is composed of cellulose microfibrils covered by a matrix of hemicellulose and lignin, bonding the microfibrils together. It was expected that the modification of the fibers in alkaline media of TA and ODA solutions resulted in the removal of some superficial components of the fiber, leading to a rougher surface.

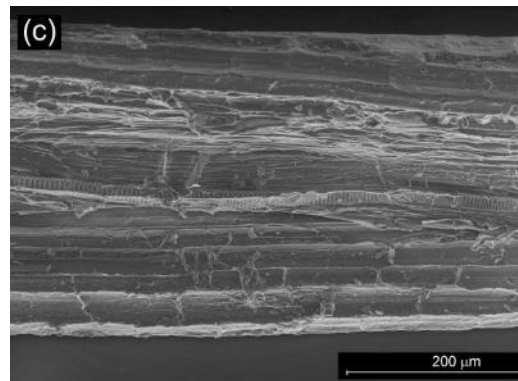
Natural Sisal



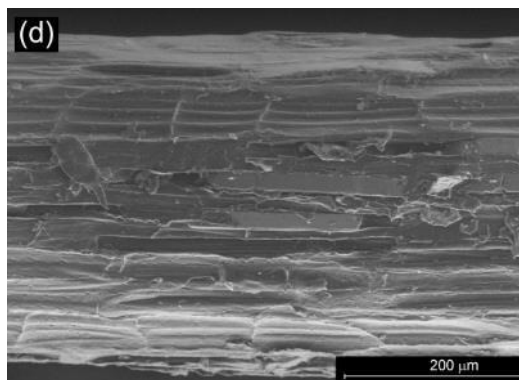
TA5-ODA1



TA5-ODA3.75



TA5-ODA5



TA10-ODA3.75

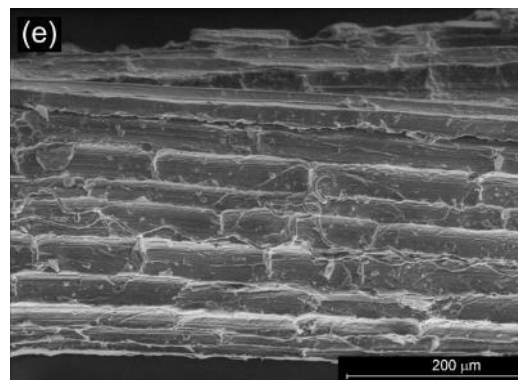
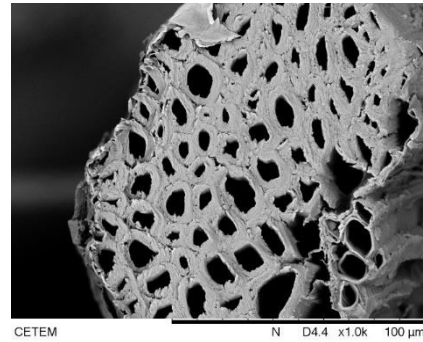
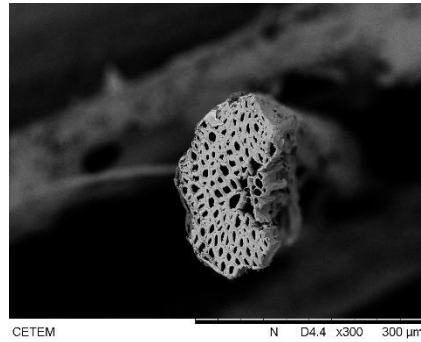


Figure 5.6 – SEM images of the longitudinal aspect of (a) natural sisal, and (b) TA5-ODA1, (c) TA5-ODA3.75, (d) TA5-ODA5, (e) TA10-ODA3.75 modified sisal fibers.

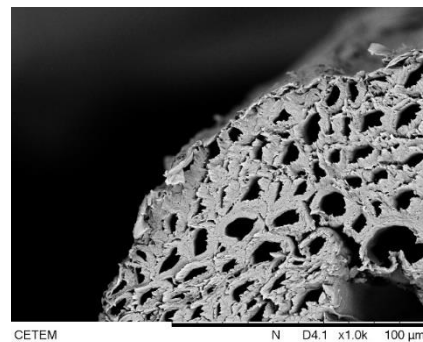
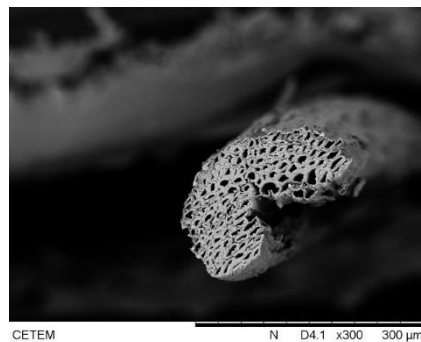
From Figure 5.6.b it was possible to notice that, for a low concentration of ODA solution (1 g/L), the fibers showed an irregular surface. The fiber degradation was even more evident with the increase in the ODA concentration (Figure 5.6.c), where some fibrils are unattached and exposed, evidencing the partial removal of hemicellulose and lignin. The same pattern was observed from the cross-sectional aspect in Figure 5.7.c. For the highest ODA concentration

(TA5-ODA5), it is possible to note that some fibrils are disconnected from the fiber, evidencing fiber degradation.

a) Natural
Sisal



b) TA5-ODA1



c) TA5-ODA5

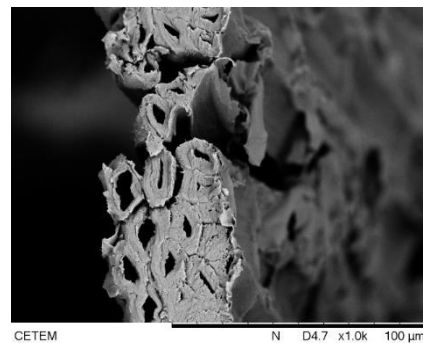
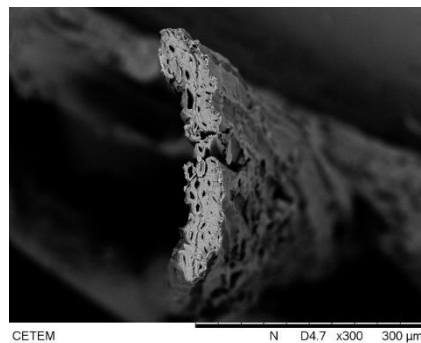


Figure 5.7 – SEM images of the cross-sectional aspect of (a) natural sisal, and (b) TA5-ODA1, (c) TA5-ODA5 modified sisal fibers.

The evaluation of a higher dosage of ODA concentration, 5 g/L, showed that there is a presence of some scaly layers above the surface of the modified fibers, indicating the deposition of compounds as a result of the reaction of the tannic acid quinones with the amine groups of octadecylamine. In this sense, the higher dosage of ODA solution concentration resulted in a more pronounced reaction considering the same period of exposure. It was also confirmed by the enhancement in the cross-sectional area, presented in Table 5.3. Up to the ODA concentration of 3.75 g/L, there was a reduction in the area, evidencing superficial fiber degradation.

However, for the higher concentration of 5 g/L, an increase in this value was reached, which can be related to the formation of the new layer above the fiber degraded surface structure.

Table 5.3 – Cross-sectional area of natural sisal and modified fibers.

	Cross-sectional area (mm ²)
Natural Sisal	0.030 ± 0.008
TA5-ODA1	0.027 ± 0.005
TA5-ODA2.5	0.033 ± 0.008
TA5-ODA3.75	0.023 ± 0.008
TA5-ODA5	0.032 ± 0.007
TA10-ODA3.75	0.027 ± 0.009

The increase of the TA solution concentration from 5 to 10 g/L, on the other hand, did not present a considerable modification in terms of the fiber cross-sectional area. However, from the longitudinal aspect image (Figure 5.6.e), it was clear that there was some deposition of new layers on the fiber, and some new spots compared to the 5 g/L concentration (Figure 5.6.c). The irregular surface on the modified fibers leads to increased surface roughness, which would contribute to the fiber-matrix mechanical bond.

In order to study the presence of different elements and their distribution on the fiber surface, mapping analysis was conducted for original and modified sisal fibers and the images obtained are presented in Figure 5.8. As detected, the original natural sisal fibers indicate a distribution of carbon, oxygen, and calcium elements on their surface in which the two first elements are attributed to sisal fiber chemical composition, and the last one is likely to correspond to fiber impurities. In modified fibers, there are two new elements including nitrogen and sodium elements in comparison to original natural sisal fibers. The presence of nitrogen and sodium elements in modified samples can be traced back to the use of TA-ODA and sodium hydroxide during the modification process, respectively. It clearly proves success in introducing ODA as a nitrogen-containing material to the surfaces of sisal fibers. Furthermore, the distribution of the mentioned elements is mostly uniform over the modified fiber length. Note that several selected modified samples were tested by mapping analysis. However, the results are reported only for sample TA10-

ODA3.75 with a proper amount of both TA and ODA since the nitrogen element could not be detected for the other samples due to the instrument's limitations.

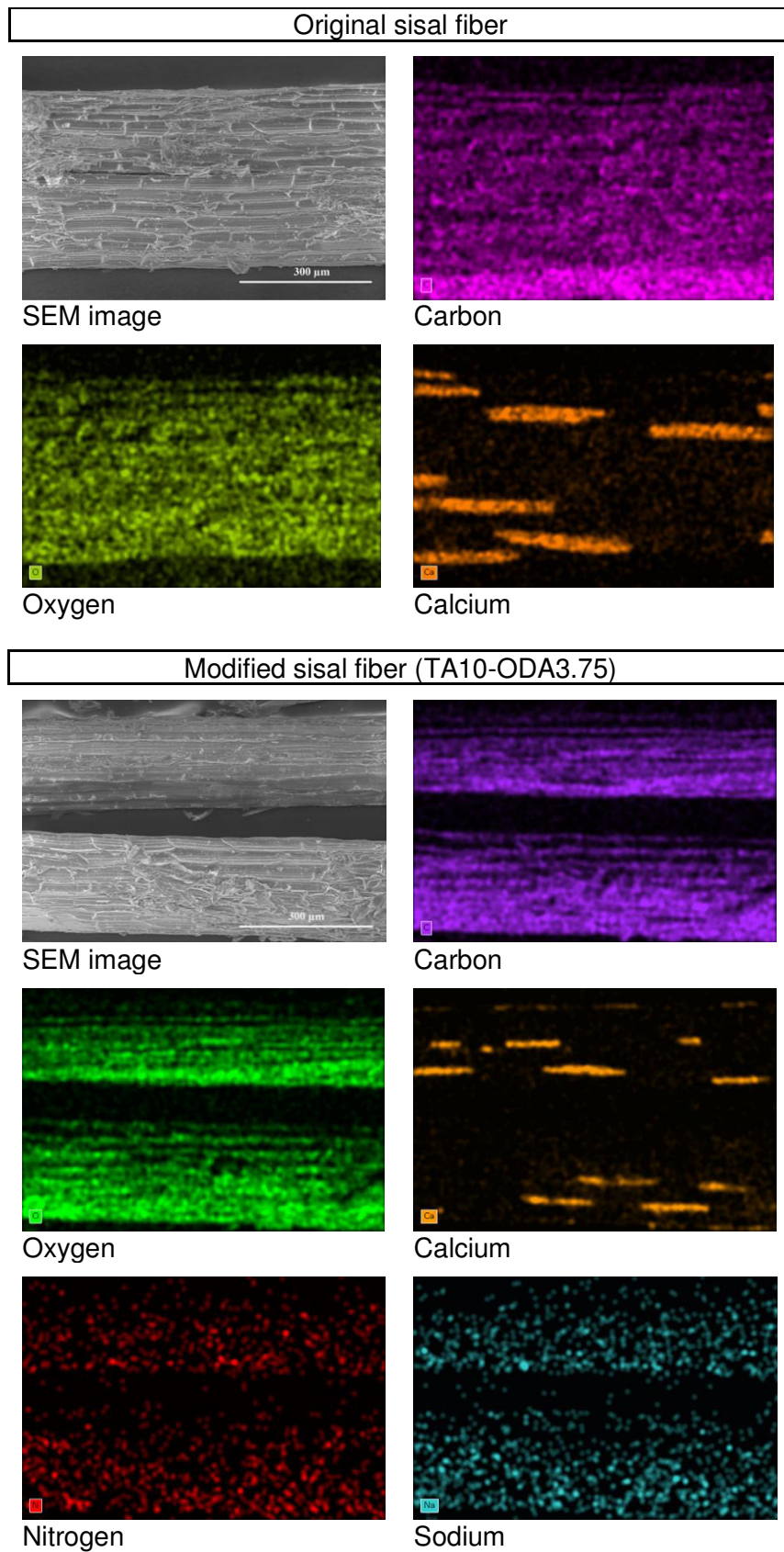


Figure 5.8 – Mapping images of original and modified (TA10-ODA3.75) sisal fibers.

Even though the coating mechanism involving these two steps is not completely understood [9,10], it is expected that it follows the subsequent explanation. TA polymeric chains undergo an oxidation process in presence of available dissolved oxygen through the possible formation of phenolate ion intermediaries under mild alkaline conditions (pH around 8) [25]. The oxidation step leads to generate quinones followed by oligomerization and a reduced solubility likely triggering to surface deposition on fiber [19]. The produced quinone compounds can react with the amine groups of the octadecylamine through Schiff-base formation and/or Michael-type addition [9,26] to create the ultimate hydrophobic coatings on the surface of sisal fibers as observed from surface roughness in SEM images.

5.3.1.2. Thermogravimetric analysis

The TGA and DTG results for natural and modified sisal fibers are presented in Figure 5.9. The curves exhibited that both the natural and modified fibers with different concentrations of ODA solution have mass losses in three stages. The first mass degradation was observed between 50 °C to 150 °C, which is related to moisture evaporation. In this range, there is the loss of adsorbed water in the fiber through intra and intermolecular dehydration reactions [27]. The second stage of mass loss was characterized by a peak at around 270 °C, and is mainly associated with hemicellulose decomposition and a small quantity of lignin and cellulose in the fiber. The third stage was characterized by the most pronounced peak in the DTG curves and originated from 300 °C to 400 °C. In this interval of temperature, there is the thermal decomposition of cellulose. This result was in accordance with several previous research works that evaluated the thermal stability of sisal fibers [27–29].

Besides, the residue values of various samples at 800 °C are clearly proportional to ODA concentration. In fact, as was observed in SEM images, higher amounts of coatings can be formed by increasing reactions between TA and amine molecules leading to the greatest residue for sample TA5-ODA5. As can be seen in Figure 5.9.b, no differences were observed in the positions of the peaks. The first peak occurred at 94.6 ± 4.1 °C, while the second and third peaks were at 291.6 ± 2.6 °C and 351.6 ± 1.8 °C, respectively. Thus, there is no negative effect on the

thermal stability of sisal fibers with the modification. Furthermore, it was observed a decrease in the intensity of the peaks with the increase in ODA concentration. It reveals that higher deposition of TA coating layer on the sisal fibers causes diminished weight loss rates compared to natural sisal fibers.

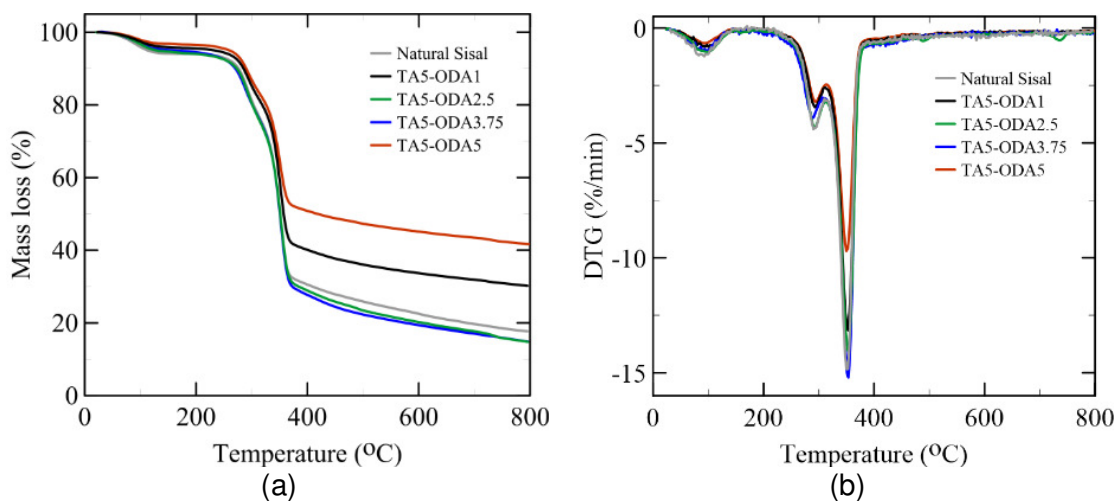


Figure 5.9 – (a) TGA and (b) DTG curves of natural sisal and sisal fibers modified with polyphenols.

5.3.1.3. Water absorption and contact angle measurements

Figure 5.10 presents the moisture absorption tendency of natural and modified sisal fibers. It is possible to notice that natural sisal fibers can absorb water at around 100% of their weight in the natural form. Nevertheless, all modified fibers became more hydrophobic, as they presented a reduction in the moisture content, considering the first 24 hours of exposure. The average reduction in the moisture content for the modified fibers was about 40% compared to the natural fibers. These fibers are characterized by the presence of a large number of hydroxyl groups, resulting in an overall hydrophilic nature. The movement of water through the fibers and the fiber dimensional variation because of the water uptake may result in microcracks in the region of the fiber-matrix interface and, consequently, poor interfacial bond. In this sense, it is important to reduce this level of water uptake to avoid degradation of the fiber-matrix interface.

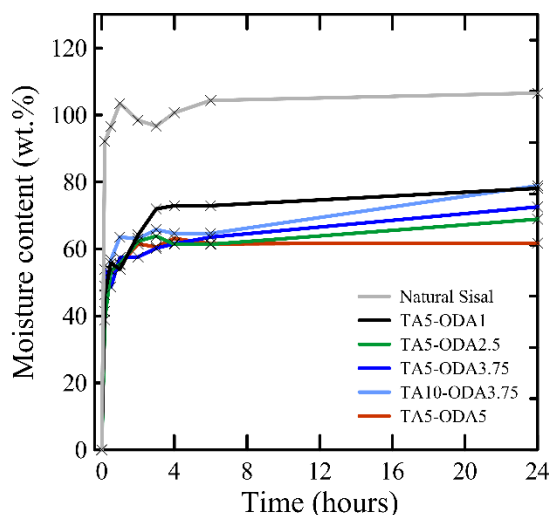


Figure 5.10 – Moisture content of natural sisal fiber and fibers modified with polyphenol.

This behavior can be also observed from the contact angle images and values of natural and modified sisal fibers, reported in Figure 5.11 and Table 5.4. As shown in Figure 5.11, when a droplet was placed individually on the surface of natural sisal, the water was completely absorbed after 20 seconds, and it was no longer possible to see the droplet of water. The large number of hydroxyl groups in the fiber surface are responsible for the good wettability with water, with a corresponding decrease in the contact angle value. This is considered critical for the fiber-matrix interface, as the cementitious matrix is a water-based material. On the contrary, for the modified fibers the droplet remained spherical and stable on the surface of the fibers even after 30 s of exposure. Higher contact angle values are related to a more hydrophobic nature of the material, evidencing a lower affinity of water molecules toward the fibers. This phenomenon confirms the formation of a hydrophobic layer on the modified fiber surface, which is consistent with the findings of the moisture absorption evaluation presented in Figure 5.10. Introducing amine groups with long hydrophobic tails is in charge of such hydrophobic behavior which was already stated in the literature [9,30].

Regarding the ODA solution for the fiber modification, the increase in the concentration did not result in a considerable decrease in the water uptake. Even for low ODA concentration (TA5-ODA1), the modified fiber presented a better performance compared to the natural fiber. The same behavior was observed for the increase in TA solution concentration, which also presented a slight influence on the water absorption capacity of the modified fibers. In addition, the lowest water

contact angle belonged to sample TA5-ODA5 with a maximum concentration of ODA. It might be described by the alterations in the combined influences of the surface phenomena and chemical compositions during the TA modification process.

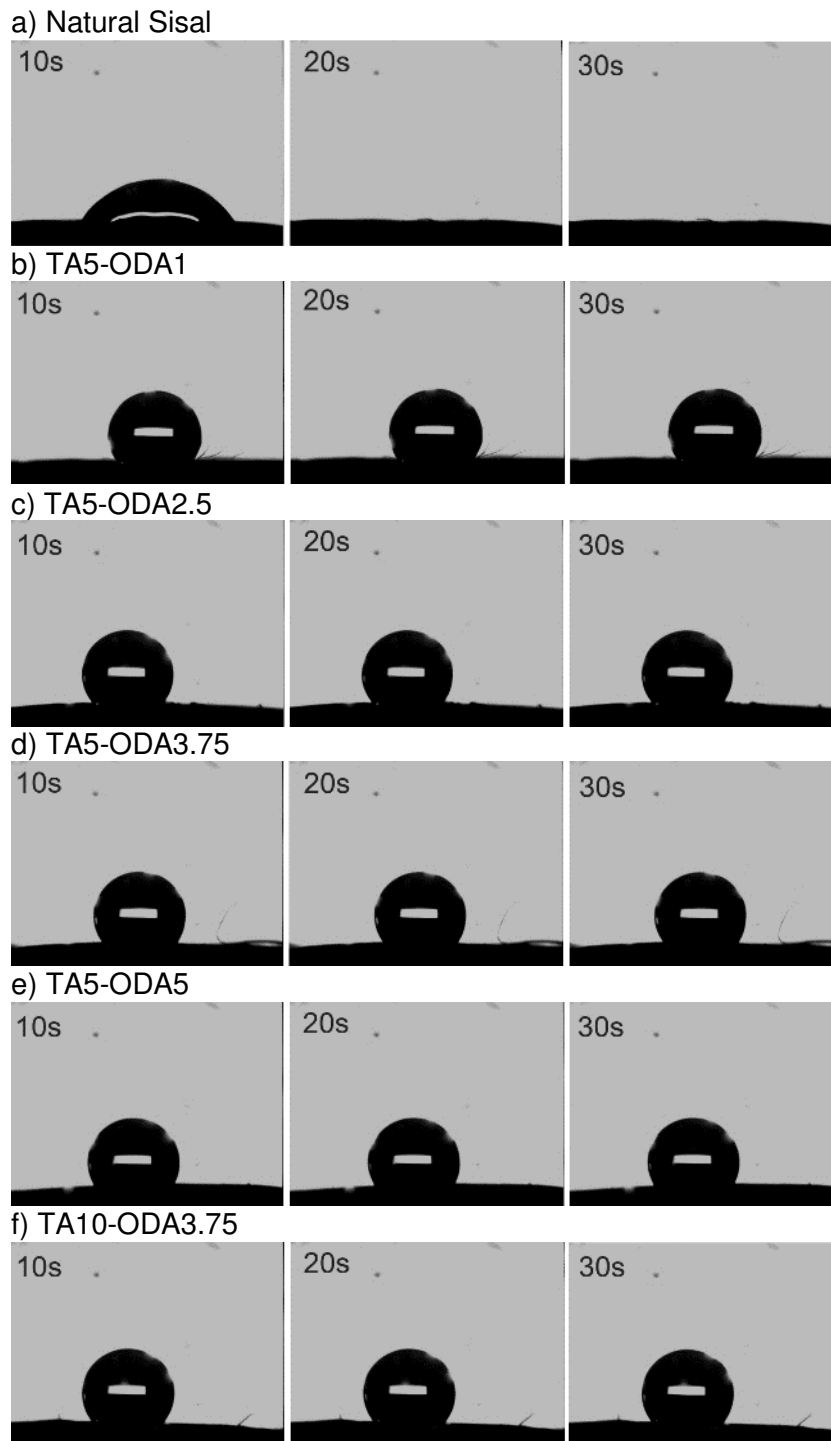


Figure 5.11 – Water contact angle test at 10, 20, and 30 s for (a) natural sisal and (b-f) fibers modified with polyphenols.

Table 5.4 – Water contact angle data of natural sisal and sisal fibers modified with polyphenols.

Fiber	Water contact angle (degree)		
	10s	20s	30s
Natural Sisal	56.6 ± 0.9	Completely absorbed	Completely absorbed
TA5-ODA1	122.9 ± 1.9	123.1 ± 2.6	121.9 ± 3.1
TA5-ODA2.5	125.8 ± 4.0	126.5 ± 4.9	125.6 ± 3.5
TA5-ODA3.75	124.9 ± 2.2	125.7 ± 3.3	124.4 ± 2.7
TA5-ODA5	113.2 ± 5.4	113.7 ± 7.6	113.3 ± 5.6
TA10-ODA3.75	126.4 ± 2.5	125.9 ± 3.7	125.3 ± 3.9

It is well-known that alkyl amine compounds such as ODA possess moderate basic properties providing alkaline conditions in water-soluble form. Apart from generating a layer of TA/ODA along with surface roughness seen in SEM images, hence, it is possible to hemicellulose removal under an alkaline medium similar to fiber modification by sodium hydroxide which led to more hydrophilic properties because of the improved number and accessibility of free hydroxyl groups on the fiber surface [31,32]. This is in line with the obtained results by Chen et al. [33], who achieved lower water contact angle values for bamboo fibers modified with a low concentration of sodium hydroxyl. Therefore, the combination of effects of forming surface roughness, introducing an alkyl long chain on the fiber surface, and increasing the number of hydroxyl groups through alkaline hydrolysis might be responsible for the reduction in water contact angle for the sample with the highest ODA concentration.

5.3.1.4. Fourier-transform infrared spectroscopy

The FTIR spectra of natural sisal and modified fibers are shown in Figure 5.12. Peak positions in the FTIR spectra are correlated with chemical stretching mode vibrations and the chemical composition changes in the sisal fiber surface by the modification process can be characterized [5]. From Figure 5.12, the spectra of natural sisal show the vibration modes in agreement with the literature [5,34]. Lignocellulosic fibers are mainly composed of cellulose, hemicellulose, and lignin, consisting of peaks in the region between 800 and 2000 cm^{-1} . The spectrum of the natural sisal exhibited C=O stretching of carboxylic acid or ester of hemicelluloses

[5,34], C=C benzene stretching ring of lignin [5,34,35], and C–OH stretching absorption of lignin [5,35] at around 1734 cm^{-1} , 1608 cm^{-1} , and 1026 cm^{-1} wavenumber, respectively. Additionally, a distinct broad peak centered at around 3315 cm^{-1} represents the stretching vibration of the hydroxyl group from moisture due to the intramolecular hydrogen bonding in the cellulose [36].

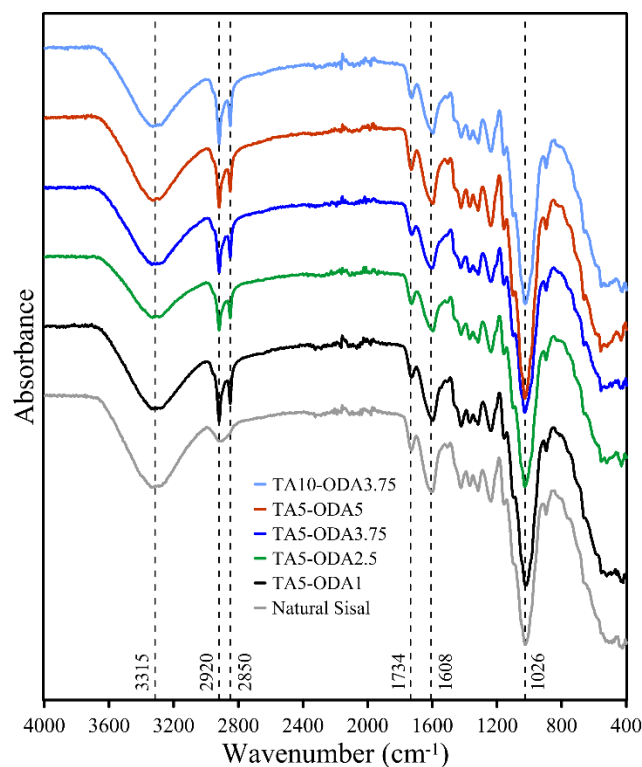


Figure 5.12 – Infrared spectroscopy of natural sisal and sisal fibers modified with polyphenols.

After fiber modification with polyphenols, the vibrational modes did not suffer significant changes, and the main bands appeared approximately in the same range of wavenumbers. This indicates that the chemical structure of the sisal fiber was not significantly affected by the fiber modification. However, new peaks at around 2920 and 2850 cm^{-1} appeared in all polyphenol-modified fibers. According to the literature [9,26], the appearance of these peaks suggests the octadecylamine attachment, attributed to the C–H stretching vibrations of $-\text{CH}_2$ or $-\text{CH}_3$.

5.3.1.5. Mechanical properties

Figure 5.13 shows the uniaxial tensile test results of natural and modified sisal fibers, in terms of tensile strength and Young's modulus. The tested natural sisal

fiber reached 441.10 ± 9.27 MPa of tensile strength and Young's modulus of 12.84 ± 1.48 , which is in accordance with previous results [37,38]. On the other hand, by increasing ODA concentration, there is a decrease in the tensile strength and Young's modulus of the modified fibers. This fact may be attributed to fiber damage caused by the exposure of the fibers to an alkaline solution during fiber modification. As the ODA solution provides an alkaline environment, it degrades the fiber through an alkaline hydrolysis process and results in the deterioration of the fiber's mechanical properties.

However, it is important to notice that the surface modification with a low concentration of ODA solution (1 g/L) was already efficient to reduce the water uptake (Section 5.3.1.3) with lower degradation of the fiber mechanical parameters, which can be considered an ideal situation. Regarding the TA concentration evaluation, the increase from 5 to 10 g/L resulted in a slight improvement in the mechanical properties, changing from 246.7 ± 26.7 MPa and 9.4 ± 1.7 GPa (TA5-ODA3.75) to 319.6 ± 43.6 MPa and 13.4 ± 1.1 GPa (TA10-ODA3.75), in terms of tensile strength and Young's modulus, respectively. Indeed, increasing TA concentration could likely mitigate the effect of alkaline hydrolysis of ODA since more numbers of ODA molecules would be consumed by reacting with the TA polymeric layer.

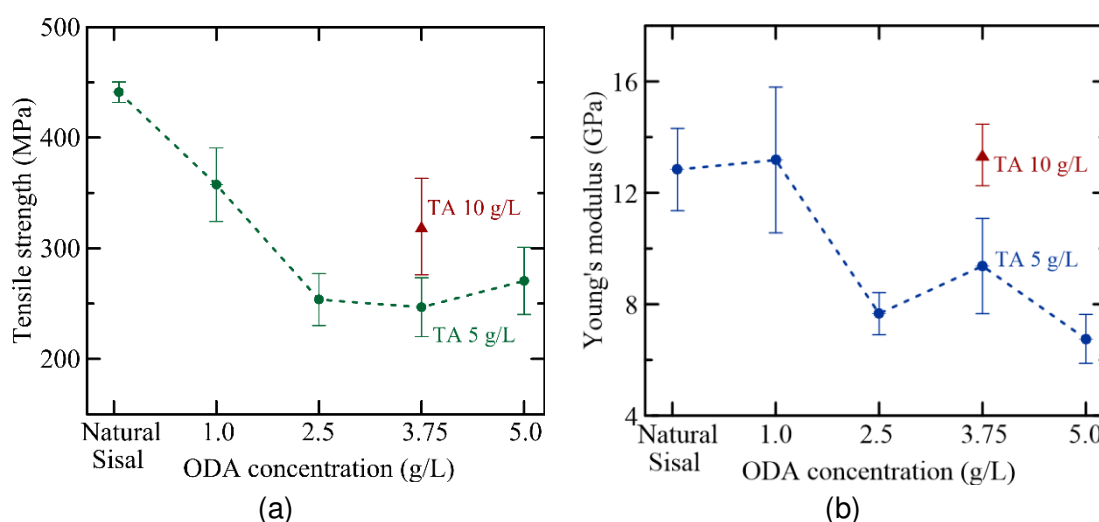


Figure 5.13 – (a) Tensile strength and (b) Young's modulus of natural sisal and sisal fibers modified with polyphenols.

The representative tensile stress-strain curves of natural and modified sisal fibers are shown in Figure 5.14. It is possible to notice that there is a more evident

mechanical performance deterioration for higher ODA concentrations (5 g/L), characterized by a change in the stress-strain curve pattern. Natural sisal is characterized by a relatively linear curve, with the maintenance of the Young's modulus until its rupture. However, for the TA5-ODA5 modified fiber, the curve changed to nonlinear behavior, with a more pronounced slope at the beginning of loading followed by a reduction in the curve slope with increased fracture strain. It is well known that the tensile strength and Young's modulus of natural fibers are directly related to the cellulose content in the fiber composition [39]. Thus, the mechanical properties observed for the TA5-ODA5 modified fiber could be related to the cellulose content decrease, resulting in reduced tensile strength and Young's modulus compared to the natural fiber.

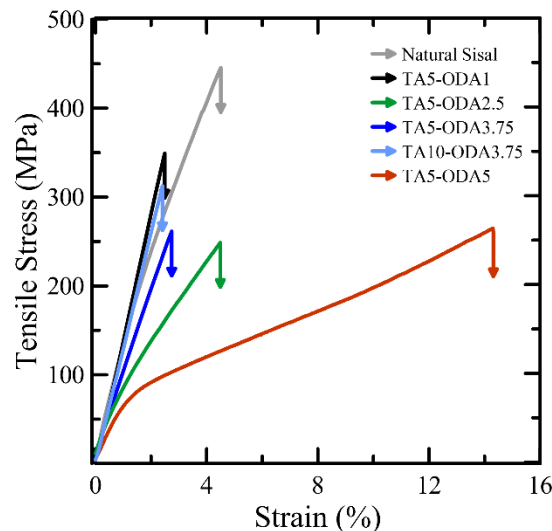


Figure 5.14 – Representative direct tensile test stress-strain curves of natural sisal and sisal fibers modified with polyphenols.

5.3.2. Fiber-matrix bond evaluation

It is expected that the fiber surface modification with polyphenol results in a better interfacial interaction of the fibers with cement-based matrices, based on the decrease of water movement along with the fiber structure (Section 5.3.1.3) and the increase in the mechanical and chemical adhesion. Hence, a quantitative analysis of the influence of the fiber surface modification was performed throughout pullout tests. The resulting typical load-slip curves are presented in Figure 5.15.

The typical sisal fiber pullout mechanism is characterized by the complete pullout of the fiber from the matrix, as evidenced by previous research [20,40]. There is an initial portion, characterized by an elastic-linear range with a rapid rate

of load ascent until reaches the peak debonding load. At this point, it is observed a degree of nonlinearity which is related to the initiation of the fiber debonding. Before debonding, the pullout behavior is associated with the adhesion strength, as a result of the mechanical and chemical fiber-matrix bond. Nonetheless, in the post-peak region, the pullout behavior is governed by the frictional shear strength, mainly related to mechanical adhesion. In this region, the natural sisal fiber is characterized by a slip-softening behavior, presenting a load drop until the complete fiber pullout. However, the surface modification may change the pullout performance in terms of alterations in the chemical and mechanical interaction of the modified fiber with the matrix.

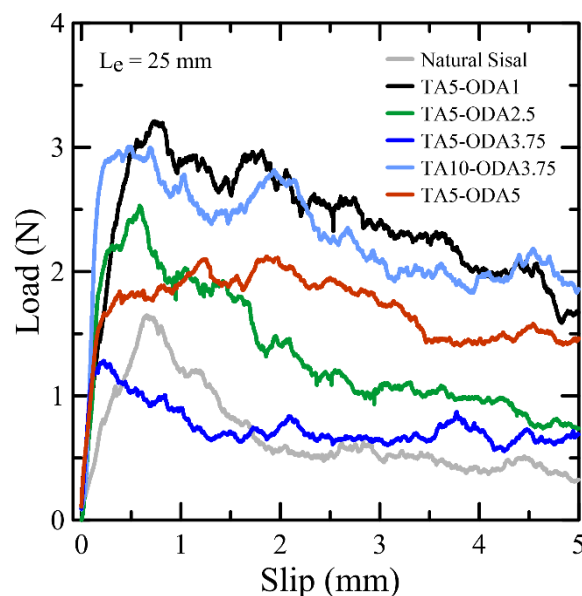


Figure 5.15 – Typical pullout curves of natural sisal and sisal fibers modified with polyphenols.

As shown in the curves in Figure 5.15, all the samples presented a slip behavior, independent of the fiber surface modification. However, there is a change from slip softening to slip hardening in the TA5-ODA5 sample. This post-peak modification may be related to the increase in the surface roughness of the fiber observed in the SEM images, which contributes to an enhanced frictional bond in the debonding stage. In addition, the maximum pullout load values of the modified samples were enhanced for low ODA concentrations (1 and 2.5 g/L) compared to natural sisal samples. Nonetheless, a reduction was seen in maximum pullout load values for the samples with a high concentration of ODA (3.75 and 5 g/L). Imparting hydrophobic properties to sisal fibers through introducing long-chain

alkyl groups of ODA can successfully decrease their wettability and moisture content as stated in section 5.3.1.3, which causes lower water absorption and swelling capacity.

It possibly triggers moderated volume changes during mixing with fresh cement suspension and drying step along with lower delamination at the fiber-matrix interface which can be considered as the reason for the improvement in interfacial properties. In higher concentrations of ODA, more reactions between TA and ODA can take place to completely cover the entire surface of the modified fibers through an alkyl long chain with hydrophobic features diminishing feasible reactions with cement hydrates as water-based materials as well as fiber-matrix interactions. Moreover, a combination of TA layer deposition including numerous hydroxyl groups, hydrophobic ODA insertion on the fiber surface, and creating surface roughness can be effective in the improvement of maximum pullout load for sample TA10-ODA3.75 with increasing TA concentration.

From the curves in Figure 5.15, it was also possible to obtain some fiber/matrix interfacial characteristics, as presented in Table 5.5. These parameters are expressed in terms of: (i) *peak debonding load*, which is related to the maximum load before the fiber debonding proceeds; (ii) *interfacial bond strength*, obtained from Equation 5.2 considering the value peak debonding load, to exclude the influence of the fiber cross-sectional area; and (iii) *energy until 1 mm*, obtained as the area above the load-slip curve until the relative displacement of 1 mm.

Table 5.5 – Summary of pullout properties of natural sisal and sisal fibers modified with polyphenols.

	Peak debonding load (N)	Interfacial bond strength (MPa)	Energy until 1 mm (N.mm)
Natural Sisal	2.08 ± 0.61	0.14 ± 0.04	1.67 ± 0.59
TA5-ODA1	2.79 ± 0.56	0.18 ± 0.04	2.14 ± 0.45
TA5-ODA2.5	2.51 ± 0.41	0.16 ± 0.03	1.88 ± 0.26
TA5-ODA3.75	1.19 ± 0.32	0.08 ± 0.02	1.00 ± 0.31
TA5-ODA5	1.82 ± 0.21	0.12 ± 0.01	1.60 ± 0.17
TA10-ODA3.75	3.21 ± 0.57	0.21 ± 0.04	2.63 ± 0.49

It was found that, by increasing the ODA solution concentration to 2.5 g/L, there is an improvement in the pullout properties compared to the natural fiber. The

first step of the fiber modification with tannic acid results in the formation of some hydrophilic groups, which partially react with the octadecylamine, but some of them remain on the surface of the fiber. These hydroxyl groups have a good affinity to hydrophilic cementitious media, forming strong hydrogen bonds between each other. On the other hand, the increase in the ODA solution concentration may result in a decrease in the free hydroxyl groups in the fiber surface, contributing to a decrease in the chemical fiber-matrix adhesion, reaching lower peak debonding load values.

5.3.3. Fiber durability evaluation

Figure 5.16 depicts the results of the direct tensile tests assessed after the exposure time of natural and modified sisal fibers exposed to 1N NaOH solution and cement pore solution. The graphs are presented in terms of normalized average tensile strength, after 10 tests for each batch. Values higher than 1 indicate that the fibers have greater stability in the alkaline environment compared to the reference.

As was expected, in general natural and modified fibers presented higher degradation in 1 N NaOH solution, as this solution represents an extremely alkali environment with a higher pH than the cement-based matrices mentioned in Section 5.2.5. Natural sisal retains only 47% of its original tensile strength in NaOH solution, while modified fibers presented better tensile strength retention compared to natural sisal. In cement pore solutions, the strength loss of natural sisal was less expressive, except for the TA5-ODA1 and TA5-ODA5, presenting a similar level of strength loss in both alkaline environments.

It is important to highlight the greater stability that TA5-ODA2.5 modified fiber presented, with no modification in the tensile strength even after the alkaline exposure to NaOH solution. It is expected that the surface coating with 2.5 g/L ODA produced a protective coating on the fiber surface, which may reduce the deposit of ions on the fiber surface directly, retarding the fiber degradation. On the contrary, the lower and higher dosages of ODA (TA5-ODA1 and TA5-ODA5, respectively) presented increased mechanical degradation after NaOH solution exposure. These results can be attributed to the fact that the TA5-ODA1 fiber modification protocol was not sufficient to enhance fiber resistance to deterioration. As mentioned in Section 5.3.1.1, the maintenance of the surface aspect of this fiber

reveals that this dosage did not considerably change the fiber structure. On the other hand, higher dosages of ODA (5 g/L) resulted in increased degradation of the fiber structure during the modification process (Sections 5.3.1.1 and 5.3.1.5). As a result, the new fiber structure seems to be more susceptible to alkaline attack, which can be related to the direct attack of minerals on the cellulose chain exposed in the new structure at a faster rate.

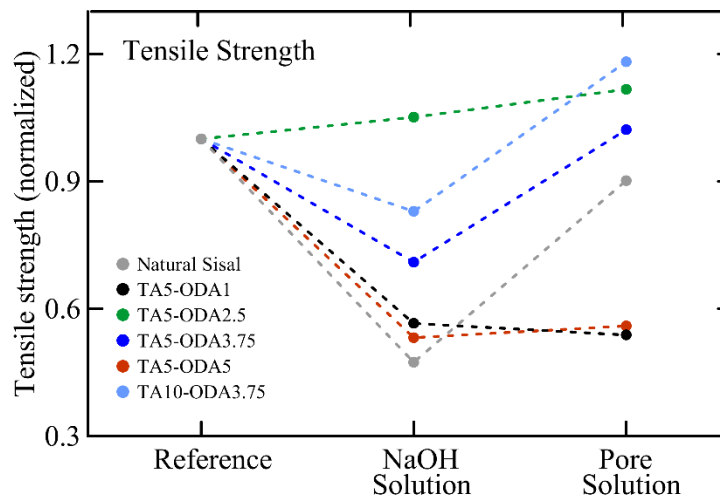


Figure 5.16 – Normalized tensile strength of natural sisal and sisal fibers modified with polyphenols before and after exposure to NaOH and Pore solutions.

5.4. Comparative evaluation of the proposed fiber modifications

Chapters 3, 4, and 5 dealt with the evaluation of different fiber modifications regarding the influence on the physical and mechanical properties of sisal fibers, in order to make them more suitable for use as reinforcement in cement-based matrices. Thus, Figure 5.17 presents a summary of some of the properties evaluated in terms of alkali treatment, polymeric fiber coating, and surface modification with polyphenols. The properties considered in the graphs are presented as normalized values concerning the results found for natural sisal fiber, without any treatment. Finally, Figure 5.18 presents an overview of the comparative performance of the different fiber treatments proposed in this study, considering the best results obtained in each one of the proposed fiber modifications.

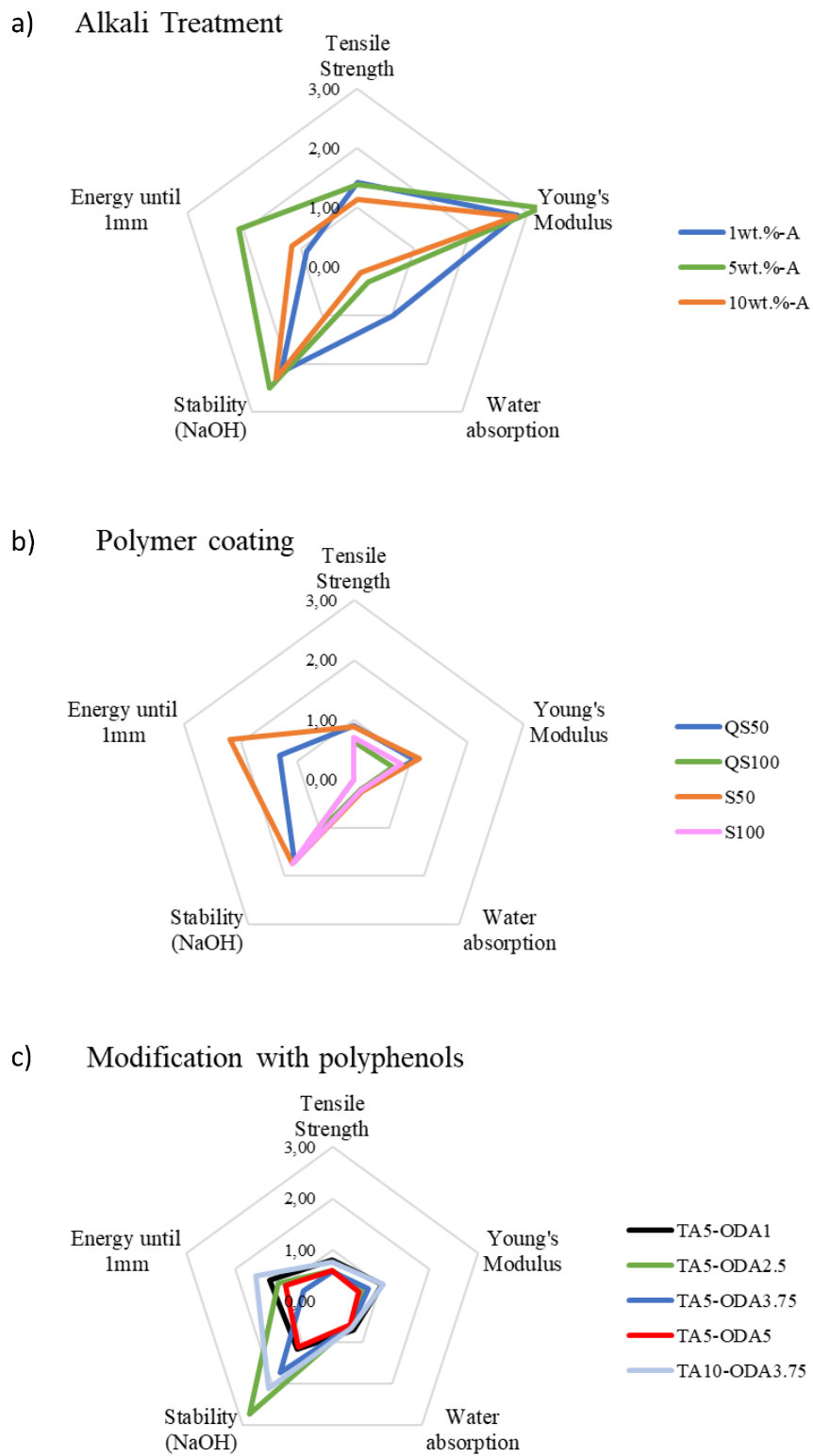


Figure 5.17 – Comparative graphs of fiber physical and mechanical properties considering the (a) alkali treatment, (b) polymer coating, and (c) modification with polyphenols.

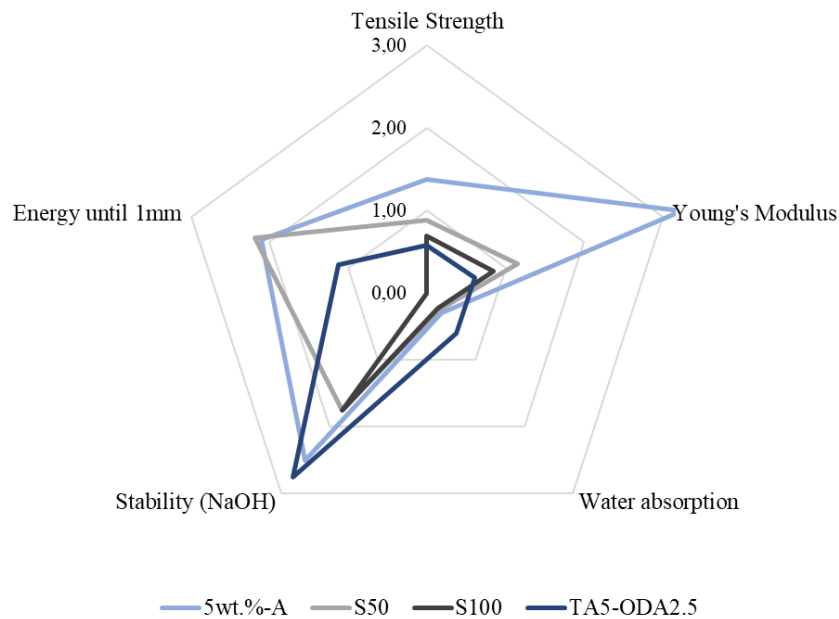


Figure 5.18 – Comparative graph of fiber physical and mechanical properties considering the best results obtained for each treatment evaluated in this study.

The mechanical properties considered for comparison were tensile strength and Young's modulus, obtained from the single fiber direct tensile tests. These properties are important to validate if the treatment has not degraded the fiber excessively. Therefore, low values indicate fiber degradation, while higher values represent an increase in tensile strength values and Young's modulus compared to natural sisal fiber. Thus, there is prominence regarding the improvement of these properties in the case of alkali treatment with 5wt.% NaOH solution (Figure 5.18). On the other hand, the fiber-matrix adhesion was evaluated through the total energy value until 1 mm of fiber displacement in the pullout tests. Thus, higher values indicate better performance, improving the properties of chemical and mechanical interlock with the matrix compared to natural sisal fiber. In this sense, the alkaline treatment with 5wt.% is again considered the best one, followed by the S50 polymeric coating sample.

Water absorption capacity was also pointed out as a relevant property for improving the behavior of sisal fibers in cementitious matrices. In this case, lower values indicate better performance, as a reduction in the trend for water absorption tendency is expected. In this case, all treatments were considerably efficient, with reasonably worse results for polyphenol modification. Finally, stability after exposure of fibers to alkaline solution was also considered in the comparative

analysis. Higher values indicate greater fiber stability, which was promising in all treatments, especially for alkaline treatment and polyphenol modification.

5.5. Conclusions

In this work, a new surface modification of sisal fibers is proposed by a polyphenol chemistry approach. The process consisted of a two-step procedure, including the use of tannic acid and octadecylamine solutions. The following conclusions were drawn:

- The as-obtained TA-ODA coated fiber shows a more hydrophilic surface, confirmed by water absorption and contact angle measurements. This result could be related to the TA deposition and posterior reaction with the octadecylamine amine groups, creating a new hydrophobic layer;
- The SEM images confirm the creation of the new layer, changing the superficial aspect of the modified fibers. Also, this new layer presents a higher roughness, which could be responsible for the enhancement in the pullout response of modified fibers;

Based on mapping results, nitrogen and sodium elements as a consequence of TA/ODA surface treatment along with using sodium hydroxide appeared on the surface of the modified fibers, confirming the prosperous functionalization of sisal fibers through introducing nitrogen-containing material i.e. ODA.;

- The solutions used for fiber modification are highly alkaline, which results in the degradation of some fiber constituents. From the TGA curves, the peaks remained in the same positions but with decreased intensity, evidencing the partial removal of hemicellulose and lignin. These findings are in accordance with the SEM images, especially for the TA5-ODA5 modified fiber with increased surface degradation. However, this had a consequence on the mechanical behavior of modified fibers, with a considerable degradation of the mechanical properties;
- The TA5-ODA1 was found to be a good alternative, with almost no fiber mechanical degradation, improved water absorption capacity,

and pullout behavior. However, this modified fiber did not present good stability when exposed to an alkaline environment, as mentioned in the fiber durability evaluation;

- Even though TA5-ODA2.5 modified fiber presented a slight mechanical properties degradation, it showed the best results in terms of pullout behavior improvement, reduction in the water affinity, and enhanced durability in aggressive alkaline environments.

To conclude, the proposed fiber modification approach could provide a simple and efficient procedure to achieve a more hydrophobic surface, with increased adhesion to cementitious matrices by the improvement in mechanical and chemical bonds. Also, the new superficial layer is responsible for stability enhancement in alkaline environments and maximizing the performance of sisal fibers in cement-based matrices.

5.6. References

- 1 BARRA, B.; PAULO, B.; ALVES, C.; SAVASTANO JUNIOR, H.; GHAVAMI, K. Effects of methane cold plasma in sisal fibers. **Key Engineering Materials**, v.517, p.458-468, 2012.
- 2 GAÑAN, P.; GARBIZU, S.; LLANO-PONTE, R.; MONDRAGON, I. Surface modification of sisal fibers: Effects on the mechanical and thermal properties of their epoxy composites. **Polymer Composites**, v.26, n.2, p.121-127, 2005.
- 3 SILVA, C. C.; LIMA, A. de F.; MORETO, J. A.; DANTAS, S.; HENRIQUE, M. A.; PASQUINI, D.; RANGEL, E. C.; SCARMÍNIO, J.; GELAMO, R. V. Influence of plasma treatment on the physical and chemical properties of sisal fibers and environmental application in adsorption of methylene blue. **Materials Today Communications**, v.23, p.101140, 2020.
- 4 KABIR, M. M.; WANG, H.; LAU, K. T.; CARDONA, F. Chemical treatments on plant-based natural fibre reinforced polymer composites: An overview. **Composites Part B: Engineering**, v.43, n.7, p.2883-2892, 2012.
- 5 SANJAY, M. R.; SIENGCHIN, S.; PARAMESWARANPILLAI, J.; JAWAID, M.; PRUNCU, C. I.; KHAN, A. A comprehensive review of techniques for natural fibers as reinforcement in composites: Preparation, processing and characterization. **Carbohydrate Polymers**, v.207, p.108-121, 2019.
- 6 FERREIRA, S. R. **Effect of surface treatments on the structure, mechanical, durability and bond behavior of vegetable fibers for cementitious composites**. Rio de Janeiro, 2016. 259p. Tese de Doutorado –

- COPPE, Universidade Federal do Rio de Janeiro.
- 7 FERREIRA, S. R.; SILVA, F. de A.; LIMA, P. R. L.; TOLEDO FILHO, R. D. Effect of hornification on the structure, tensile behavior and fiber matrix bond of sisal, jute and curauá fiber cement based composite systems. **Construction and Building Materials**, v.139, p.551-561, 2017.
 - 8 SGU, S.; YANG, L.; HUANG, W.; BU, Y.; CHEN, D.; HUANG, J.; ZHOU, Y.; XU, W. Fabrication of hydrophobic cotton fabrics inspired by polyphenol chemistry. **Cellulose**, v.24, n.6, p.2635-2646, 2017.
 - 9 HU, Z.; BERRY, R. M.; PELTON, R.; CRANSTON, E. D. One-Pot Water-Based Hydrophobic Surface Modification of Cellulose Nanocrystals Using Plant Polyphenols. **ACS Sustainable Chemistry and Engineering**, v.5, n.6, p.5018-5026, 2017.
 - 10 REZAIIE, A. B.; LIEBSCHER, M.; RANJBARIAN, M.; SIMON, F.; ZIMMERER, C.; DRECHSLER, A.; FRENZEL, R.; SYNITSKA, A.; MECHTCHERINE, V. Enhancing the interfacial bonding between PE fibers and cementitious matrices through polydopamine surface modification. **Composites Part B**, v.217, p.108817, 2021.
 - 11 ZHOU, M.; LI, Y.; HE, C.; JIN, T.; WANG, K.; FU, Q. Interfacial crystallization enhanced interfacial interaction of Poly (butylene succinate)/ramie fiber biocomposites using dopamine as a modifier. **Composites Science and Technology**, v.91, p.22-29, 2014.
 - 12 LI, Y.; CHEN, Q.; YI, M.; ZHOU, X.; WANG, X.; CAI, Q.; YANG, X. Effect of surface modification of fiber post using dopamine polymerization on interfacial adhesion with core resin. **Applied Surface Science**, v.274, p.248-254, 2013.
 - 13 SINGH, A. S.; HALDER, S.; WANG, J.; IMAM, M. A.; CHEN, P. Tannic acid intermediated surface functionalization of bamboo micron fibers to enhance mechanical performance of hybrid GFRP. **Composites Part B: Engineering**, v.177, p.107322, 2019.
 - 14 LIN, T. C.; LEE, D. J. Cotton fabrics modified with tannic acid/long-chain alkylamine grafting for oil/water separation. **Journal of the Taiwan Institute of Chemical Engineers**, v.127, p.367-375, 2021.
 - 15 SHAH, I.; JING, L.; FEI, Z. M.; YUAN, Y. S.; UMAR, M.; KANJANA, N.. A Review on Chemical Modification by using Sodium Hydroxide (NaOH) to Investigate the Mechanical Properties of Sisal, Coir and Hemp Fiber Reinforced Concrete Composites. **Journal of Natural Fibers**, v.19, n.4, p.1-19, 2021.
 - 16 KLERK, M. D.; KAYONDO, M.; MOELICH, G. M.; VILLIERS, W. I.; COMBRINCK, R.; BOSHOFF, W. P. Durability of chemically modified sisal fibre in cement-based composites. **Construction and Building Materials**, v.241, p.117835, 2020.
 - 17 WEI, J.; MEYER, C. Improving degradation resistance of sisal fiber in concrete through fiber surface treatment. **Applied Surface Science**, v.289, p.511-523, 2014.

- 18 ZHAO, L.; ZHU, S.; WU, H.; LIANG, H.; LIU, C.; LIU, W.; ZHOU, W.; SONG, Y. The improved resistance against the degradation of sisal fibers under the environment of cement hydration by surface coating of graphene oxide (GO) based membranes. **Construction and Building Materials**, v.305, p.124694, 2021.
- 19 SILEIKA, T. S.; BARRETT, D. G.; ZHANG, R.; LAU, K. H. A.; MESSERSMITH, P. B. Colorless multifunctional coatings inspired by polyphenols found in tea, chocolate, and wine. **Angewandte Chemie - International Edition**, v.52, n.41, p.10766-10770, 2013.
- 20 CASTOLDI, R. de S.; SOUZA, L. M. S.; SILVA, F. de A. Comparative study on the mechanical behavior and durability of polypropylene and sisal fiber reinforced concretes. **Construction and Building Materials**, v.211, p.617-628, 2019.
- 21 ZHANG, H.; XIE, J.; AN, S.; QIAN, X.; CHENG, H.; ZHANG, F.; LI, X. A novel measurement of contact angle on cylinder-shaped lignocellulosic fiber for surface wettability evaluation. **Colloids and Surfaces A: Physicochemical and Engineering Aspects**, v.540, p.106-111, 2018.
- 22 AMERICAN SOCIETY FOR TESTING AND MATERIALS. **ASTM C1557**: Standard Test Method for Tensile Strength and Young's Modulus of Fibers. United States, 2020.
- 23 AMERICAN SOCIETY FOR TESTING AND MATERIALS. **ASTM D6942**: Standard Test Method for Stability of Cellulose Fibers in Alkaline Environments. United States, 2019.
- 24 KUNDU, S. P.; CHAKRABORTY, S.; MAJUMDER, S. B.; ADHIKARI, B. Effectiveness of the mild alkali and dilute polymer modification in controlling the durability of jute fibre in alkaline cement medium. **Construction and Building Materials**, v.174, p.330-342, 2018.
- 25 REZAIIE, A. B.; LIEBSCHER, M.; DRECHSLER, A.; SYNITSKA, A.; MECHTCHERINE, V. Tannic acid/ethanolamine modification of PE fiber surfaces for improved interactions with cementitious matrices. **Cement and Concrete Composites**, v.131, p.104573, 2022.
- 26 WANG, L.; HUI, L.; SU, W. Superhydrophobic modification of nanocellulose based on an octadecylamine/dopamine system. **Carbohydrate Polymers**, v.275, p.118710, 2022.
- 27 MARTIN, A. R.; MARTINS, M. A.; SILVA, O. R. R.; MATTOSO, L. H. C. Studies on the thermal properties of sisal fiber and its constituents. **Thermochimica Acta**, v.506, n.1-2, p.14-19, 2010.
- 28 HAJIHA, H.; SAIN, M.; MEI, L. H. Modification and Characterization of Hemp and Sisal Fibers. **Journal of Natural Fibers**, v.11, n.2, p.144-168, 2014.
- 29 SILVA, C. C.; LIMA, A. de F.; MORETO, J. A.; DANTAS, S.; HENRIQUE, M. A.; PASQUINI, D.; RANGEL, E. C.; SCARMÍNIO, J.; GELAMO, R. V. Influence of plasma treatment on the physical and chemical properties of sisal fibers and environmental application in adsorption of

- methylene blue. **Materials Today Communications**, v.23, p.101140, 2020.
- 30 XIONG, K.; QI, P.; YANG, Y.; LI, X.; QIU, H.; LI, X.; SHEN, R.; TU, Q.; YANG, Z.; HUANG, N. Facile immobilization of vascular endothelial growth factor on a tannic acid-functionalized plasma-polymerized allylamine coating rich in quinone groups. **RSC Advances**, v.6, n.21, p.17188-17195, 2016.
- 31 RAY, D.; SARKAR, B. K. Characterization of alkali-treated jute fibers for physical and mechanical properties. **Journal of Applied Polymer Science**, v.80, n.7, p.1013-1020, 2001.
- 32 HARMSSEN, P.; HUIJGEN, W.; LÓPEZ, L.; BAKKER, R. Literature Review of Physical and Chemical Pretreatment Processes for Lignocellulosic Biomass. **Food and Biobased Research**, p.1-49, 2010.
- 33 CHEN, H.; ZHANG, W.; WANG, X.; WANG, H.; WU, Y.; ZHONG, T.; FEI, B. Effect of alkali treatment on wettability and thermal stability of individual bamboo fibers. **Journal of Wood Science**, v.64, n.4, p.398-405, 2018.
- 34 FERREIRA, S. R.; SILVA, F. de A.; LIMA, P. R. L.; TOLEDO FILHO, R. D. Effect of fiber treatments on the sisal fiber properties and fiber-matrix bond in cement based systems. **Construction and Building Materials**, v.101, p.730-740, 2015.
- 35 SIVA, J.; RAJU, N.; VICTOR, M.; KUMARAN, P. Comprehensive characterization of raw and alkali (NaOH) treated natural fibers from *Symphirema involucratum* stem. **International Journal of Biological Macromolecules**, v.186, p.886-896, 2021.
- 36 BARRETO, A. C. H.; ROSA, D. S.; FECHINE, P.B.A.; MAZZETTO, S. E. Properties of sisal fibers treated by alkali solution and their application into cardanol-based biocomposites. **Composites Part A: Applied Science and Manufacturing**, v.42, n.5, p.492-500, 2011.
- 37 BELAADI, A.; BEZAZI, A.; BOURCHAK, M.; SCARPA, F. Tensile static and fatigue behaviour of sisal fibres. **Materials and Design**, v.46, p.76-83, 2013.
- 38 SILVA, F. de A.; CHAWLA, N.; TOLEDO FILHO, R. D. Mechanical behavior of natural sisal fibers. **Journal of Biobased Materials and Bioenergy**, v.4, n.2, p.106-113, 2010.
- 39 KOMURAIHAH, A.; KUMAR, N. S.; PRASAD, B. D. Chemical Composition of Natural Fibers and its Influence on their Mechanical Properties. **Mechanics of Composite Materials**, v.50, n.3, p.359-376, 2014.
- 40 SILVA, F. de A.; MOBASHER, B.; SORANAKOM, C.; TOLEDO FILHO, R. D. Effect of fiber shape and morphology on interfacial bond and cracking behaviors of sisal fiber cement based composites. **Cement & Concrete Composites**, v.33, n.8, p.814-823, 2011.

6 Tensile creep behavior of sisal fibers under different environmental conditions

The mechanical behavior and deformation mechanisms of sisal fiber when subjected to quasi-static tensile stresses are well known. However, much aspects about the time-dependent behavior of these fibers under sustained load is still unknown. This chapter reports a study of the time-dependent behavior of sisal fibers subjected to uniaxial tensile sustained load in various environments. To simulate potential in-service conditions, the fibers were tested under water, and also submersed in different alkaline environments, represented by 0.5M and 1M NaOH solutions. The investigated stress levels were 8, 16, and 33% of the ultimate tensile strength of these fibers, corresponding to 1, 2, and 4 N, respectively. Moreover, the effect of different modifications on the fiber creep behavior was also investigated. Alkaline treatment, styrene-butadiene polymer coating with different polymer content (50% and 100% v/v), and functionalization with tannic acid were adopted. After the time-dependent tests, pristine and modified fibers were tested under quasi-static uniaxial tensile tests to assess the effect of fiber modifications on fiber durability, in terms of mechanical response. The experimental investigations revealed that sisal fibers exhibited a logarithmic creep behavior, with a high constant rate in the primary creep, followed by a constant rate in the secondary creep. The sisal fiber under sustained load showed significant creep, and the time-dependent strain level was dependent on the load level. It was also found that the high humidity environment changes the global rate of fiber deformation, reaching higher levels of time-dependent strain. Furthermore, all applied treatments were efficient to reduce the level of fiber creep strain, with the best results obtained for the TA functionalized fibers. In general, when compared to the as-received fibers, modified sisal fibers showed improved maintenance of the mechanical properties after sustained-load tests under aggressive environments.

The creep test device was developed at TU Dresden, Germany. However, some minor adjustments were made at PUC-Rio to enable better performance of

the experimental arrangement. So, the creep tests and the fiber mechanical characterization were performed at PUC-Rio.

6.1. Introduction

The use of sustainable materials is becoming a priority in several areas of society, including the construction sector [1–3]. In this context, the use of natural fibers as reinforcement in composites is gaining attention in the current panorama [4,5]. An important aspect to be investigated for a reliable structural use of natural fiber composites as a building material is the time-dependent behavior [6]. The creep fracture of the material usually occurs at a lower load level than the static ultimate load. Also, the composite exposure to a sustained load for a long time is likely to cause a reduction in the ductility capacity. Thus, creep is an essential property to be considered in the medium to long-term behavior of sisal fiber composites [6]. Even though composite creep is of special interest, it is known that fiber creep contributes as one of the mechanisms causing the time-dependent crack widening of composites under sustained load [6,7].

The creep behavior of single natural fibers is still poorly understood [8–10]. Many efforts have been concentrated on the tensile properties of sisal fibers under quasi-static loading [11–15]. However, considering the composition of natural fibers, it is expected that they present significant viscoelastic behavior, comparable to polymeric materials [10]. When loaded, natural fiber exhibits instantaneous and time-dependent strain. With the increase in stress, there is sufficient energy to break the bonds of the macromolecular structure of the fiber amorphous compounds, and the molecules tend to align in the stress direction. Then, it is expected that the creep compliance is reduced, and the time-dependent strain reaches a plateau, called secondary creep [9]. In this range, it is considered that part of the total strain is non-recoverable after the removal of the applied stress [9]. So, it is important to consider the viscoelastic behavior of sisal fibers as this could influence the time-dependent behavior of natural fiber composites, which is important to ensure the reliability of the designed structures in terms of long-term applications.

To the best of the authors' knowledge, there are only a few studies that mention the creep performance of natural fibers, and no information on the creep behavior of sisal fiber is available in the literature. According to Yu et al. [16],

bamboo fibers showed time dependency creep deformation, which is also influenced by fiber moisture content. They exhibit increases in creep compliance with increasing moisture content. The same behavior was evidenced by previous authors for different fibers, such as hemp fibers [10,17], jute fibers [8], and *Raffia vinifera* fibers [18]. Cisse et al. [9] mentioned that hemp fibers exhibited significant time-dependent strain when submitted to a tensile load. In addition, a characteristic logarithmic function was found as a result, with a high strain rate during the primary creep and a lower and constant rate during the secondary creep.

Some works [6,7,19–21] have been published on the time-dependent behavior on the single fiber level in terms of composite and pull-out evaluation, for different types of fibers. Furthermore, information on this behavior in terms of single fiber tensile creep is still limited, especially regarding sisal fibers. This paper reports the time-dependent response of sisal on the uniaxial single fiber tensile creep. Fibers were tested at different loads and environmental conditions, to find the effect of the load over time in sisal fibers and the influence of fiber modification on their creep performance. A quasi-static single fiber tensile test investigation was also performed after the creep tests to gain further insight into the mechanical degradation of the fiber.

6.2. Experimental methods

6.2.1. Materials and processing

Natural sisal and modified sisal fibers were evaluated. The natural sisal fibers used in this study were the same detailed in Chapter 3. Also, the fibers were cleaned before all treatments, as mentioned in Section 3.2.2. Alkaline treatment, polymer coating, and surface tannic acid functionalization were the modifications adopted, based on the results presented in Chapters 3, 4, and 5. For the alkaline fiber modification, sodium hydroxide (NaOH), reagent grade $\geq 97\%$, pellets were used, supplied by Isofar Company. Two different XSBR polymers were used in the polymer coating process, the Litex™ S 9076 (soft stiff, solid content 47% and viscosity < 300 mPa.s) and the Litex™ S 10656 (medium stiff, solid content 50% and viscosity < 500 mPa.s), all purchased from Synthomer. Finally, the surface functionalization was performed with tannic acid (ACS reagent) and octadecylamine ($\geq 99.0\%$, GC) components, both purchased from Sigma-Aldrich.

6.2.2. Sisal fiber modification

As mentioned before, three distinct modifications were proposed for natural sisal fibers. These modifications were previously used in the literature and were successfully adopted to enhance sisal fiber hydrophobicity, and resistance to alkali attack, and to improve sisal fiber adhesion toward cement-based matrices [12,22,23]. The modification parameters adopted for each fiber modification proposed are summarily described in the following sections. Detailed information can be found in the previous Chapters 3, 4, and 5.

6.2.2.1. Alkaline treatment (ALK)

The sisal fibers were immersed in a 5 wt.% of NaOH aqueous solution at a laboratory-controlled temperature of 22 ± 3 °C for 60 minutes. To minimize the fiber shrinkage as a result of the solution absorption/desorption process, fibers were kept stretched during the immersion. After the exposure interval, fibers were washed with distilled water to remove the excess of alkali on the surface. Also, to neutralize the alkali reaction, fibers were immersed in 1 wt.% acetic acid (CH_3COOH) solution, washed with distilled water, and then air-dried.

6.2.2.2. Polymer coating (S50 and S100)

The fiber's surface was impregnated with two different polymer aqueous emulsions, with 50 (S50) and 100% v/v (S100) S polymer solution concentrations. The polymer impregnation process was performed in a special apparatus developed by the author, to better distribute the polymer on the fiber surface. The apparatus is detailed and described elsewhere (Chapter 4). After the impregnation process, fibers were put in an oven (140 ± 5 °C) for 4 minutes, to assure polymer cross-linking.

6.2.2.3. Tannic acid functionalization (TA)

Initially, the process consisted in dissolving 1 g of tannic acid in 200 mL of deionized water (5 g/L). The pH of the solution was adjusted to 8 by adding 0.55M NaOH solution and then 1 g of sisal fibers was added to the solution. The mixture was kept in mechanical stirring for 12 hours. After this period, fibers were washed

with deionized water. Subsequently, it was prepared 200 mL of octadecylamine solution with 120 mL of isopropanol, 80 mL of deionized water, and 0.5 g of octadecylamine (2.5 g/L). The fibers were then added to the solution, and the mixture was mechanically stirred for 12 hours. Finally, the resulting functionalized fibers were washed and then air-dried.

6.2.3. Single fiber tensile test

Quasi-static single fiber tensile tests were performed before and after the time-dependent tensile tests, to understand the influence of the loading level and environmental conditions on sisal fibers. In addition, single fiber quasi-static tensile tests were conducted to evaluate the effect of fiber modifications on the creep performance under the same environmental conditions to which natural sisal fiber was submitted.

6.2.3.1. Quasi-static test

The quasi-static single fiber tensile tests were performed following the recommendations of ASTM C1557 [24]. A universal testing machine with 100 kN load capacity (Instron EMIC 23-100), equipped with a 1 kN load cell, was used for the tests (Figure 6.1). Single fibers were firstly glued to a stiff paper frame (120 g/cm²) to guide the alignment in the testing machine, with a free gauge length of 20 mm. Then, the sample was placed in the grips of the testing machine, and the lateral edges of the paper frame were cut with scissors, to allow fiber deformation during load application. The fibers were loaded until failure at a deformation-controlled mode with a displacement rate of 0.1 mm/min. A pre-load of 0.2 N was applied to ensure that the fibers were completely stretched at the beginning of the tests. An adjacent piece of each tested fiber was analyzed in an optical microscope to determine the cross-sectional area, which was used to calculate the tensile stresses. The effective cross-sectional area was determined by neglecting the lumen area. Average tensile strength and Young's modulus were obtained from the results of 10 replicates. For the wet state, the fibers were soaked in water for 16 h before testing.

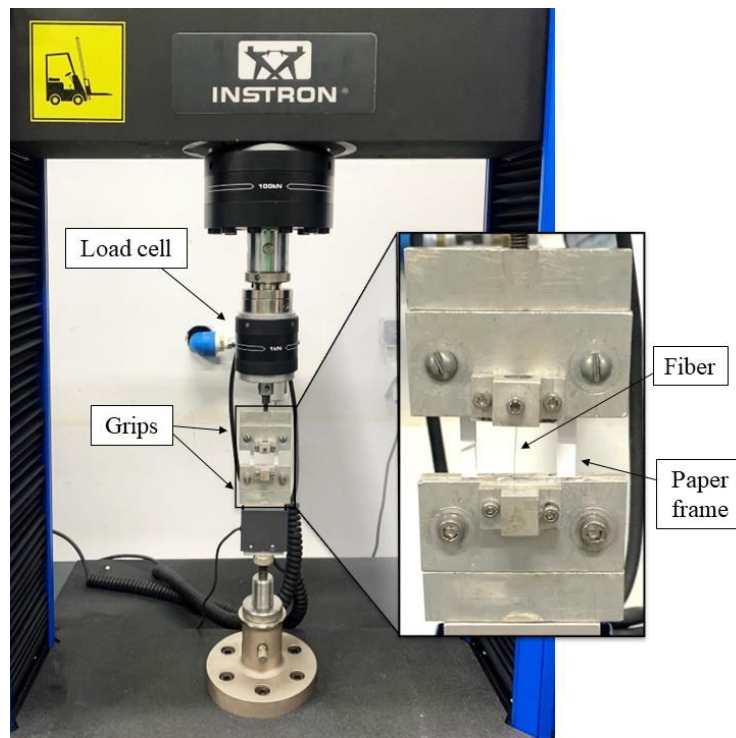


Figure 6.1 – Setup for quasi-static single fiber tensile test.

6.2.3.2. Time-dependent test

The time-dependent tests were proposed to evaluate the single fiber creep response under different conditions. The main idea was to simulate the conditions of the fibers used as reinforcement in cement-based matrices. The variables adopted were the fiber type, sustained load level, and environmental exposure conditions. Figure 6.2 presents a summary of the variables and identification of the samples tested. The details of the procedure adopted for each test will be discussed subsequently. As mentioned before, different treated fibers (ALK, S50, S100, and TA named fibers) were adopted to evaluate the influence of the modifications in the sisal fiber performance subjected to the conditions when used as reinforcement in concrete elements. These different approaches have been proposed in the literature to decrease water absorption tendency and enhance fiber stability in alkaline media.

The reference environmental condition (REF) is related to the air exposure, representing the dry fiber before inclusion in the matrix, to compare to the wet condition (W). It is well known that the hydroxyl groups present in the natural fiber structure are responsible for their highly hydrophilic nature of them [12,23,25]. So, the wet condition simulates the saturated fiber after the water absorption during the

mixture/casting process and the structure service life. Also, the alkaline solution was adopted to simulate the alkaline environment of concrete. In aggressive alkaline media, some natural fiber constituents (lignin, hemicellulose, and cellulose) are gradually destroyed, leading to the loss of reinforcing capacity [13,26,27]. Two different strong alkaline solutions (1M and 0.5M NaOH) were adopted, representing severe alkaline conditions in comparison to typical cement-based matrix alkalinity. In this sense, 28 days of exposure to these alkaline solutions represent an accelerated degradation process.

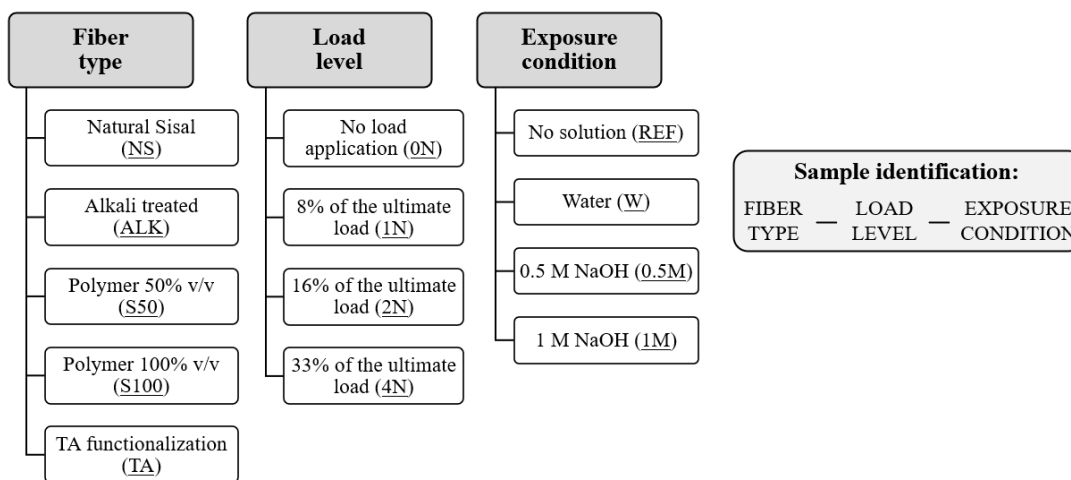


Figure 6.2 – Summary of experimental conditions for time-dependent fiber tests and explanation of the sample identification in this study.

In terms of the load application, the same reasoning was adopted. No load condition simulates the fiber before inclusion in the matrix, and the loaded conditions try to reproduce the fiber when subjected to load transfer inside the matrix. The sisal fiber ultimate load of 12.06 ± 1.57 N was considered, based on the results obtained in previous study [28]. In this sense, 1, 2 and 4 N were adopted as load levels, corresponding to approximately 8, 16, and 33% of the natural sisal fiber ultimate load, respectively.

The experimental arrangement used to perform the time-dependent tests is shown in Figure 6.3.

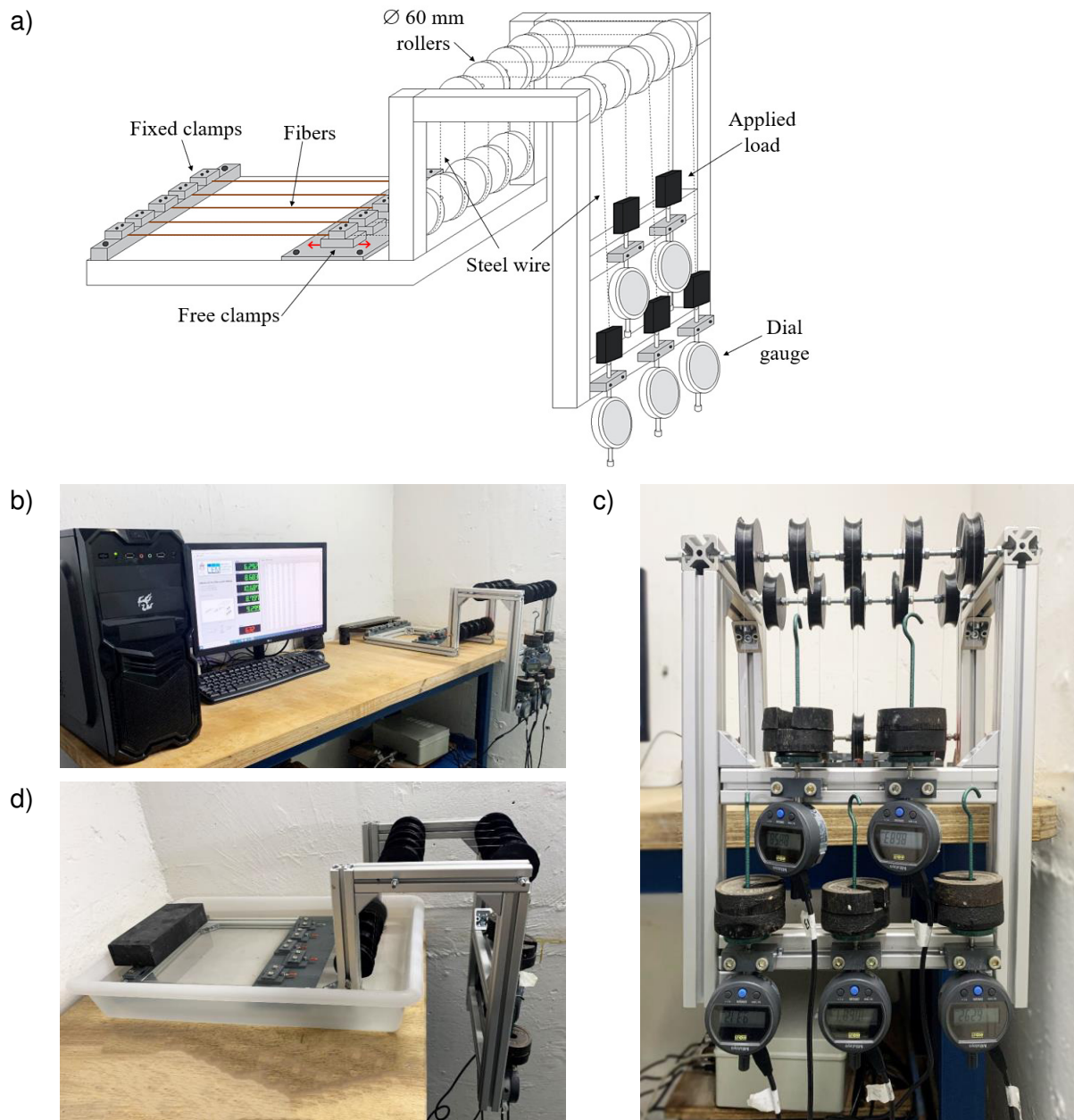


Figure 6.3 – Time-dependent tests: (a) Schematic configuration, (b) setup overview, (c) load application device, and (d) detail of the fibers during tests.

For the frame, it was important to find a material resistant to alkaline attack. The same prescription applies to the rollers, which were produced in a 3D printer using polymeric material. It was designed to fix the fibers in two opposite edges to keep the single fibers stretched. In the fixed clamps, the fibers were attached, and movement was not allowed on this edge. On the opposite edge, the fibers were fixed in free clamps that allow horizontal movement and, consequently, fiber deformation under sustained load. The initial free length of the fibers adopted was 22 ± 4 cm. A device was produced to allow load application as a sustained load, detailed in Figure

6.3.c. To connect the clamped fibers to the deformation acquisition and load application devices, a steel wire was used between the free clamps and the devices. The loads were kept constant for 28 days. For each sample batch, 5 fibers were kept under sustained load in the respective environmental condition for 28 days. During the tests, the arrangement was kept in a controlled temperature and humidity room.

Digital dial gauges (Mitutoyo accuracy of 0.001 mm) were assumed to measure the fiber displacement with time, which was used to calculate the associated strain based on the initial length. A system was developed to allow automatic recording of the fiber length variation, using Arduino Uno hardware and data acquisition was performed on the LabView platform. It was programmed to perform the displacement recording at intervals of 10 min or with 0.001 mm of displacement variation. The fiber elongation was measured, and the strain was calculated as the fiber elongation divided by the initial fiber free length. The program interface developed in LabView is presented in Appendix B.

6.3. Results and discussion

6.3.1. Quasi-static behavior of natural and modified sisal fiber

Natural sisal fiber and fibers modified with different treatments were first tested under quasi-static loading conditions. It is important to investigate their quasi-static behavior under tensile stresses to better understand the influence of fiber modification on the time-dependent performance of sisal fibers. Figure 6.4 shows the quasi-static tensile stress versus strain curves of natural and modified sisal fibers.

The natural sisal fiber presented a linear behavior until the fiber failure, with a sudden drop in stress value after reaching the fiber strength. The ultimate tensile strength and Young's modulus of natural sisal fiber are 445.56 ± 9.32 MPa and 9.52 ± 1.42 GPa, respectively. Even though natural fibers present considerable variability in terms of mechanical properties [29], these results are in the range of those found in the literature [30–32]. From the curves, it is clear that fiber modification influenced the fiber mechanical properties. Modified fibers continued to exhibit an elastic behavior until failure, but different stress and strain levels were found. The alkali-treated sisal fibers presented an increased Young's modulus

(11.34 ± 1.03 GPa) compared to natural sisal fiber. However, a slight decrease of ~20% in the fiber tensile strength was found, probably as a result of the partial degradation of some fiber components in the alkaline solution exposure [12]. A similar trend was found for the S100 and TA fibers, however, attributed to different fiber mechanisms depending on the modification procedure.

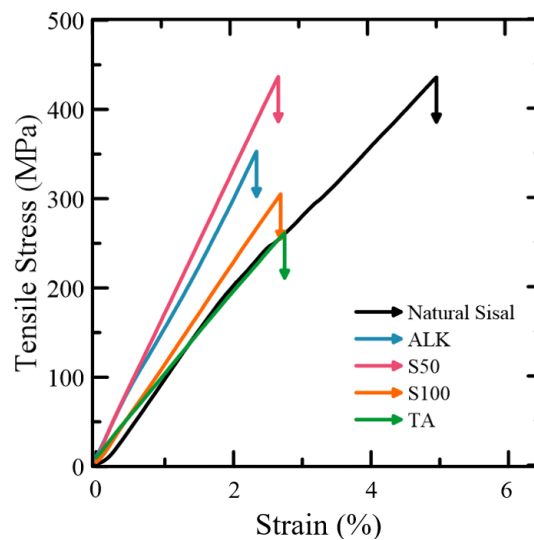


Figure 6.4 – Quasi-static direct tensile test results of natural and modified sisal fibers.

It was expected that the polymer film of SBR formed on the fiber surface could absorb part of the stress applied to the fiber, resulting in enhanced stress-strain capacity [31,33], which is in accordance with the results found for the S50 polymer-coated fiber. However, the higher polymer emulsion (S100) presented a decrease in the ultimate limit strength capacity, attributed to the poor interlock between the thicker layer of polymer and the fiber surface, previously observed in Chapter 4. On the other hand, the TA-treated fiber also presented a decrease in the tensile strength and Young's modulus, which could be also attributed to the alkaline fiber damage (Chapter 5), as the fibers are submerged in alkaline solutions during the TA modification procedure.

To better describe the effect of moisture on the tensile behavior of sisal fibers, saturated sisal fibers were also submitted to quasi-static single-fiber direct tensile tests. The resulting tensile stress versus strain curves for air dried and saturated sisal fiber are presented in Figure 6.5. It is clear that fibers under a high humidity factor present enhanced strain capacity and reduced Young's modulus compared to natural sisal fibers. According to previous authors [10,16,34], the water presence

causes swelling of the fibers, breaking the inter- and intramolecular hydrogen bonds in the fiber structure, and inducing an increase in the free volume between macromolecules. Consequently, there is an increase in molecule mobility and additional strain on the fiber macro scale [17,34].

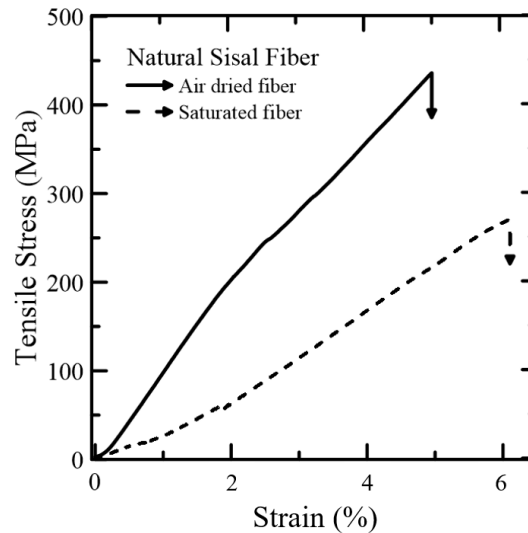


Figure 6.5 – Quasi-static direct tensile test results of air-dried and saturated natural sisal fiber.

6.3.2. Time-dependent behavior of natural and modified sisal fiber

6.3.2.1. Natural sisal fiber

The creep tests on natural sisal fiber were performed to investigate the possible influence on the macroscopic behavior of natural fiber composites when exposed to a sustained load. A sustained load was applied to single fibers individually which were submitted to different exposure conditions. The typical resulted curves of the time-dependent single fiber tests are presented in Figure 6.6. The creep curves are characterized as a logarithmic function of time, with a high strain rate on the primary creep and a lower rate during the second step [9]. The sudden increase of strain in the first minutes is related to the instantaneous strain response. In the secondary step, fibers presented the time-dependent strain, in which the strain level is dependent on the magnitude of the applied stress. The higher the sustained load, the higher the time-dependent strain level. The fracture did not occur for the specimens tested in the dried condition (no solution), reaching 0.72 ± 0.09 % strain at 33% of the stress level (4 N). The time-dependent strain levels obtained

for natural sisal in the “no solution” condition are similar to those obtained by previous research [34].

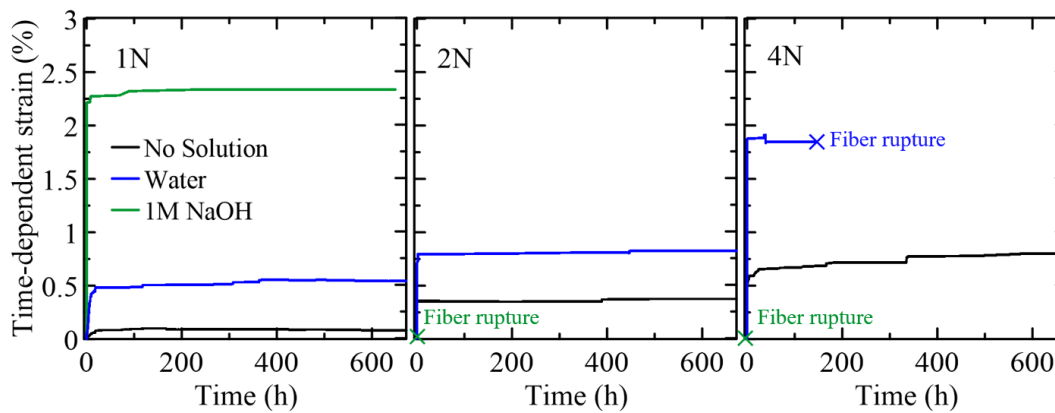


Figure 6.6 – Time-dependent strain test results of natural sisal fibers under “no solution”, water, and 1M NaOH conditions.

Creep behavior was also investigated in saturated conditions (water). The time-dependent strain considerably increases with the water presence, compared to the air-exposed fibers (no solution). According to the literature review, it is expected that the humidity presence accelerates the creep behavior of natural fibers [17,36,37]. As shown in Section 6.3.1, saturated fibers presented enhanced strain capacity compared to the natural sisal fibers, which agrees with the results found in the creep tests. Then, wet fibers under prolonged stress will elongate further than dry fibers under similar stress conditions. For the considered creep time, the time-dependent strains of about 0.5% and 1% were reached for 1 N and 2 N load levels. In this sense, humidity improves the deformability of natural fibers [10]. However, for the higher stress level, the fiber failure occurred directly after the last strain value was recorded. The moisture absorption causes fiber swelling, a dimensional change in the fiber structure which is related to the breaking of the inter and intramolecular hydrogen bonds between the macromolecules [38]. In this high humidity environment, a saturation of the hydroxyl groups can be reached, inducing an increase in the free volume between macromolecules in the amorphous components and resulting in enhanced molecule mobility [17].

In the alkaline solution, the fiber loaded with 1 N presented an increased level of strain compared to the “no solution” and water exposure conditions. This result indicates that fiber can lengthen by up to 2.3% after 28 days at a load as low as 8%

of its capacity in this exposure condition, representing an enhancement of approximately 23 times the fiber strain in the air environment. The exposure of lignocellulosic fiber to an alkaline environment results in hydrogen bond breakage and removal of the amorphous components, hemicellulose, and lignin [12,39]. Consequently, the deformation of individual cellulose microfibrils is facilitated, as a result of the absence of interlocking hydrogen bonding [39].

However, it is alarming that the time-dependent fiber tensile test in the alkaline solution results in fiber failure for 2 and 4 N load levels. This indicates that the alkaline solution combined with higher load level results in improved fiber degradation, leading to fiber failure. After the degradation of the amorphous components, the cellulose fibrils are completely exposed to the alkaline attack, accelerating the fiber degradation [12,40]. Consequently, the combination of cellulose fragility and high load application resulted in fiber embrittlement and rupture. Moreover, it is important to highlight that the 1M NaOH solution adopted in this study represents a more severe condition, with a higher alkaline level than a typical cementitious matrix.

To further analyze the results, the creep compliance C_c was obtained as a relation to the creep strain ε_c in function of the applied stress σ [20]. The average time-dependent strain at the end of 28 days was considered. Figure 6.7 shows the calculated C_c values.

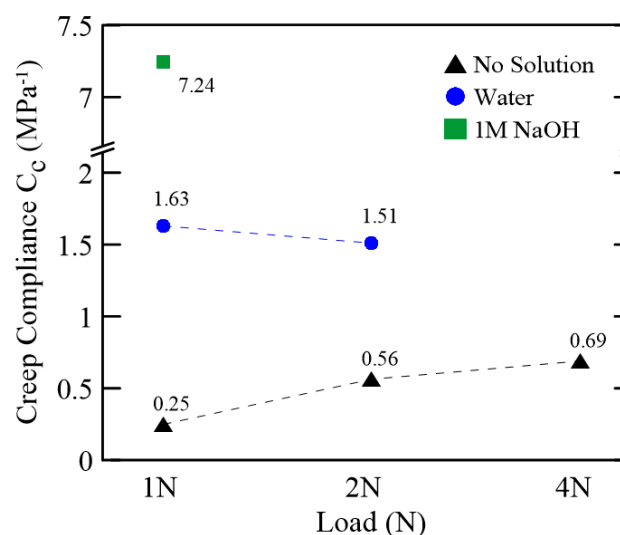


Figure 6.7 – The creep compliance C_c of single sisal fibers at different load levels and exposure conditions.

The creep compliance for the “no solution” condition increased with the increase of the load applied. A different pattern was noted for the fiber under water, where it was not observed significant change in the creep compliance level with the load increase. In this case, the strain is influenced by other variables, including the moisture presence, which increases the fiber elongation and, consequently, the creep compliance. As expected, a higher level of creep compliance was reached by the alkaline exposed fiber, where the moisture presence and fiber degradation markedly influence the strain capacity of the fiber.

6.3.2.1.1. Mathematical model

To describe the creep behavior of sisal fibers, the four-element Burgers model was used. This method is a combination of the Maxwell and Kelvin models, by the association in series and parallel of springs and dashpots, characterized by their respective Young’s Modulus E and coefficient of viscosity η . The four-element Burgers model is illustrated in Figure 6.8, as well as its mathematical expression in Equation 6.4.

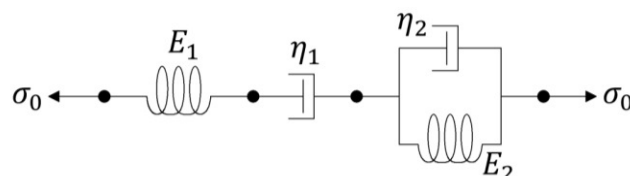


Figure 6.8 – Four-element Burgers Model.

$$\varepsilon(t) = \underbrace{\frac{\sigma_0}{E_1}}_{(I)} + \underbrace{\frac{\sigma_0}{E_2} \left(1 - e^{-t \frac{E_2}{\eta_2}}\right)}_{(II)} + \underbrace{\frac{\sigma_0}{\eta_1} t}_{(III)} \quad \text{Eq. 6.4}$$

Figure 6.9 represent the time-dependent experimental and Burgers model adjustment curves. It is assumed that the fiber is subjected to a constant unidirectional stress σ_0 , resulting in the creep strain $\varepsilon(t)$, where t is the time, E_1 and E_2 are the elastic moduli of the Maxwell and Kelvin springs, and η_1 and η_2 are viscosities of the Maxwell and Kelvin dashpots. In Equation 6.4, the term indicated as (I) is the instantaneous deformation, as a result of minor changes in bond lengths and angles. The next term, (II), is the early-stage creep strain, in which molecular chain relaxations and extensions are expected. The viscous slippage of molecular

chains is considered in term (III), related to the long-term creep strain [41]. From the experimental data and numerical model, it is possible to obtain the creep parameters by applying the least squares method via *Matlab* software. The obtained parameters are presented in Table 6.1.

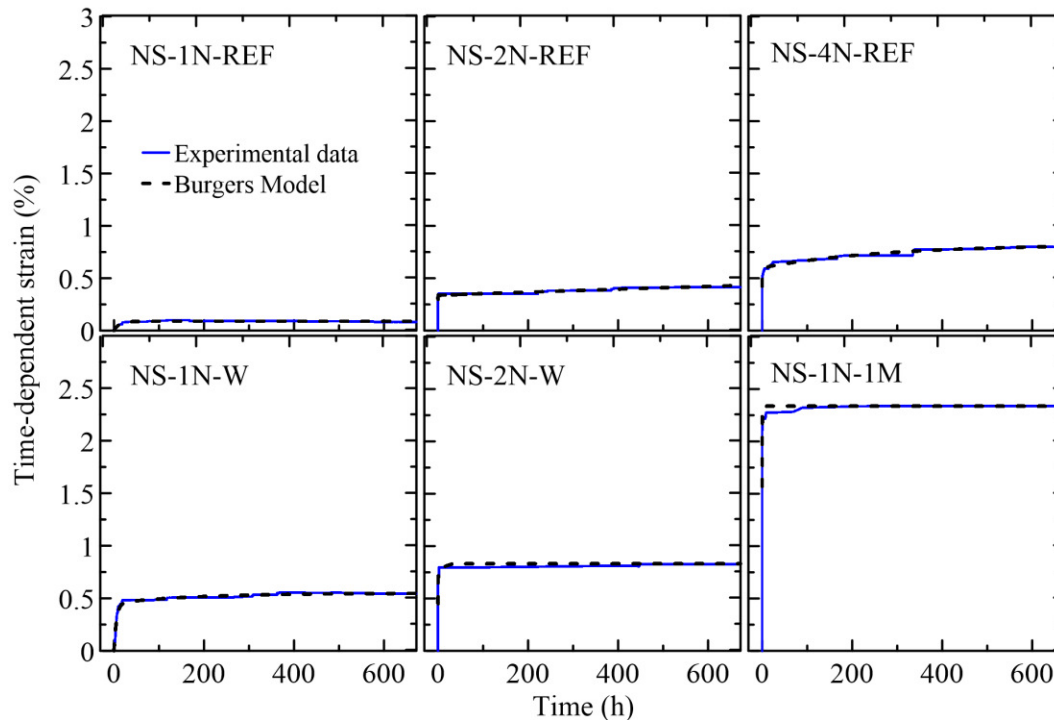


Figure 6.9 – Typical time-dependent experimental and four-element Burgers model adjustment curves of natural sisal fibers in “no solution”, water, and 1M NaOH conditions.

To the best of the author’s knowledge, no study has been conducted on the development of the mathematical modeling of natural fibers. Moreover, by comparing the creep parameters obtained for the reference fibers, there is a nonlinearity of these parameters’ values with the increase of the applied tension σ_0 . The same is concluded for the correlation between the parameters for the reference fiber and the fiber under water, for the 31.8 and 63.7 MPa applied stress. By observing the obtained correlation coefficients R^2 presented in Table 6.1, the four-element Burgers Model is considered adequate to simulate the creep behavior of sisal fibers. With regard to the curves presented in Figure 6.9, there is a visual overlapping of the experimental and adjusted curves, also validating the chosen model.

Table 6.1 – Summary of the Four-element Burgers Model parameters for natural sisal fibers.

Sample identification	σ_0 (MPa)	E_1 (MPa)	E_2 (MPa)	η_1 (MPa.s)	η_2 (MPa.s)	R^2
NS-1N-REF		1830.1	1843.7	3.37×10^4	6.21×10^7	0.8232
NS-1N-W	31.8	279.9	283.2	2.06×10^4	2.89×10^8	0.9731
NS-1N-1M		67.2	68.5	4.61×10^4	7.64×10^7	0.9331
NS-2N-REF		224.8	1177.3	4.07×10^5	3.52×10^8	0.8587
NS-2N-W	63.7	382.67	382.7	7.55×10^5	1.70×10^8	0.8446
NS-4N-REF	127.3	481.3	1244.5	9.98×10^5	1.92×10^8	0.8642

6.3.2.2. Modified sisal fiber

Fibers modified with different treatments were also tested in similar loading conditions of natural sisal. In summary, all treatments were able to reduce the water affinity of the sisal fiber and enhance fiber-cementitious matrix adherence. Thus, this study aims to evaluate the efficiency of these modifications in the behavior under sustained load in aggressive environments, simulating the conditions when used as reinforcement in cement-based composites.

The time-dependent deformation curves are presented in Figure 6.10. Firstly, fibers were tested under 1M NaOH alkaline solution with a sustained load of 1 N. In this case, all types of fibers were loaded for 28 days (672 hours), and no collapses were recorded. After this time, all samples reached the secondary or steady creep state [8], with a nearly constant creep rate. However, the time-dependent strain level of the single fibers was dependent on the fiber modification. The results of the natural sisal fiber for the 1N-1M NaOH condition show a time-dependent strain of approximately 2.4% after 28 days. On the other hand, the time-dependent strain level decreases with all treated fibers. For the polymer-impregnated fibers (S100 and S50) and the TA-ODA modified fiber (TA) it was reduced to approximately $0.6 \pm 0.1\%$, representing a decay of around 4 times compared to the natural sisal.

As mentioned before, the humidity presence results in enhanced fiber elongation. Thus, the presence of a hydrophobic layer around the fiber surface, with a polymer or a structure formed from the fiber functionalization with the octadecylamine, resulted in the decrease of the time-dependent strain compared to the natural sisal. Also, these layers formed a protective barrier against alkali-attack, avoiding excessive degradation of the fiber structure and, consequently, fiber

deformation. Moreover, the best result was observed for the alkali-treated fiber, with a very low time-dependent strain level. It was reported that, during the alkaline modification with the fiber stretched, there is a controlled degradation of amorphous compounds of the fiber, breaking some chemical bonds and, consequently, allowing the alignment of the microfibrils along the fiber axis [12]. Therefore, it could explain the reduction in the instantaneous and time-dependent strain level, as the molecules are already aligned in the stress direction before the creep test.

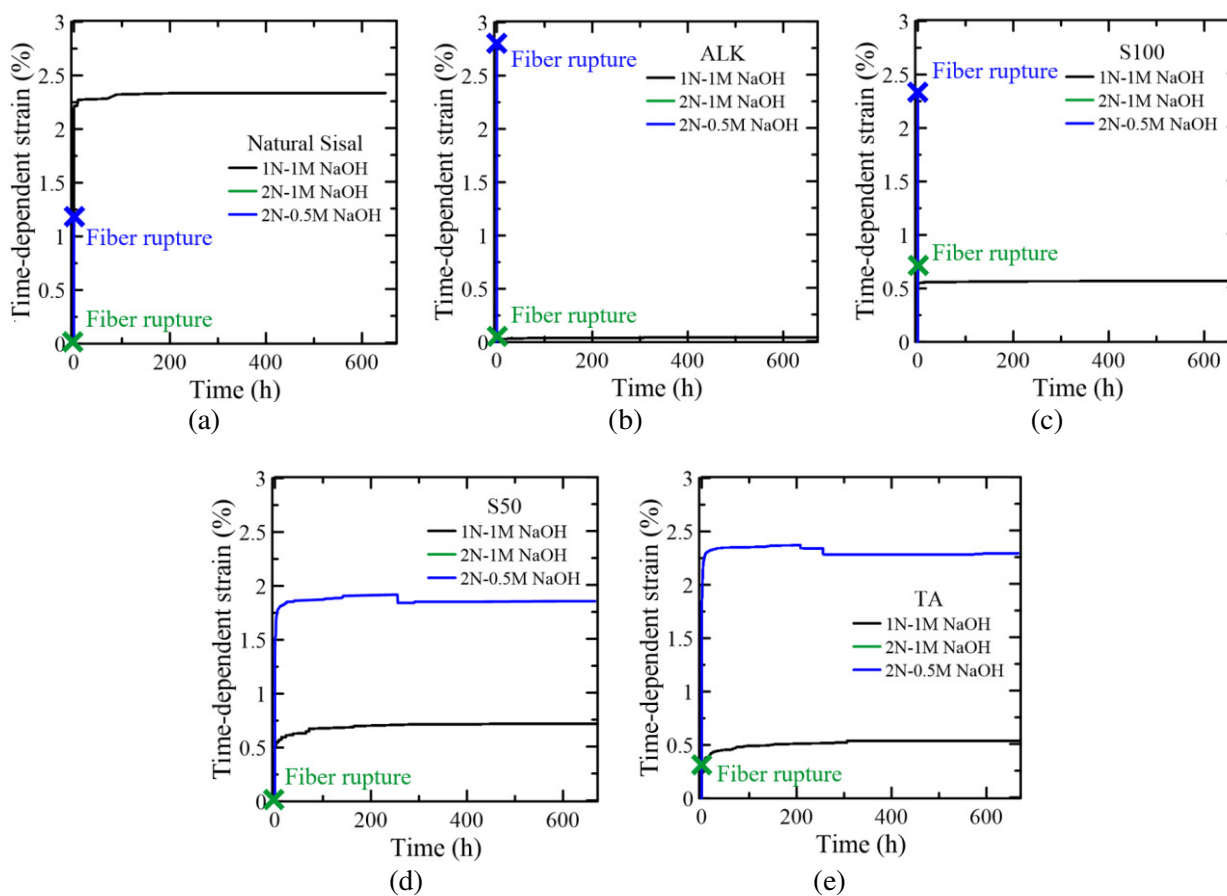


Figure 6.10 – Time-dependent strain test results of natural and modified sisal fibers in different environmental conditions.

The second environmental condition was composed of the same alkaline solution (1M NaOH), however with a load level of 2 N. The enhancement in the loading level resulted in larger instantaneous deformation, leading to fiber breakage. In this sense, it was not possible to compare the behavior of natural and treated fibers under this load condition, which is more similar to the estimated maximum load transfer to the fiber at service during composite loading. It could be related to the combination of the enhanced load with the excessive alkali

degradation of the fiber under this highly alkaline solution, leading to a higher fiber deformation and resulting in rupture. As 1M NaOH is considered an extremely aggressive alkaline solution, it was suggested a lower alkali concentration solution (0.5 M NaOH) to allow the comparison with the 2N load level.

As can be seen from the results for 2N-0.5M NaOH condition, natural sisal, alkali-treated, and S100 polymer modified fiber presented a similar behavior, with a rapid increase in the instantaneous deformation leading to fiber rupture. In the case of the alkali-treated fiber, there is no formation of the protective layer around the fiber. Consequently, fiber is susceptible to humidity absorption and volume variation, which could be related to enhanced fiber deformation, culminating in fiber rupture. On the other hand, it is shown in Chapter 4 that the S100 polymer coating has a lower adherence to the fiber structure, and it is not completely bonded to the fiber surface. Therefore, it allows the penetration of alkaline solution in the sisal fiber structure, resulting in enhanced fiber strain and rupture in this condition.

Nonetheless, there is an obvious effect of S50 and TA fiber modification. In these cases, fibers were loaded with 2N in the aggressive solution of 0.5M NaOH, and no rupture was recorded after 28 days. This behavior can be directly related to the superficial protection of the fiber surface. As there is a barrier against humidity absorption, the stability in this aggressive environment is increased, leading to the enhancement of the fiber creep behavior. It is also important to highlight that the creep strains of S50 and TA fibers were higher than that of 1N-1M NaOH condition. It indicates that the load level has more influence over the fiber deformation than the alkalinity of the solution, leading to a higher level of time-dependent strain.

6.3.2.3. Residual mechanical properties

After the creep tests, the fibers were subjected to quasi-static single fiber tensile tests, to evaluate the influence of fiber modifications on the conservation of the mechanical properties of sisal fiber after loading and aggressive environment exposure. The results of the quasi-static single fiber tensile tests are summarized in Table 6.2.

Table 6.2 – Summary of the mechanical properties of the studied fibers after the creep tests.

Fiber	Sample identification	Tensile Strength (MPa)	Young's modulus (GPa)	Ultimate strain (%)
Natural Sisal	NS-0N-REF	445.6	9.52	4.5
	NS-0N-1M	212.8	5.95	3.3
	NS-1N-1M	167.2	5.04	3.4
	NS-2N-1M		Fiber rupture	
	NS-2N-0.5M		Fiber rupture	
ALK	ALK-0N-REF	357.8	11.34	3.0
	ALK-0N-1M	205.5	6.32	3.0
	ALK-1N-1M	205.7	8.15	2.6
	ALK-2N-1M		Fiber rupture	
	ALK-2N-0.5M		Fiber rupture	
S50	S50-0N-REF	436.6	16.11	2.7
	S50-0N-1M	296.7	9.89	3.0
	S50-1N-1M	238.6	6.78	3.7
	S50-2N-1M		Fiber rupture	
	S50-2N-0.5M	234.8	6.71	3.6
S100	S100-0N-REF	305.1	11.31	2.7
	S100-0N-1M	182.0	5.25	3.5
	S100-1N-1M	162.8	5.37	3.2
	S100-2N-1M		Fiber rupture	
	S100-2N-0.5M		Fiber rupture	
TA	TA-0N-REF	261.4	9.19	0.027
	TA-0N-1M	173.4	6.93	0.023
	TA-1N-1M	143.2	6.48	0.021
	TA-2N-1M		Fiber rupture	
	TA-2N-0.5M	183.3	6.04	0.028

Comparing the fibers with no load and no aggressive solution (0N-REF) with the non-loaded and loaded conditions in an alkaline environment (0N-1M and 1N-1M), it was clear that, for all tested fibers, the alkaline exposure resulted in degradation in the ultimate fiber tensile strength and Young's modulus. Thus, fibers became less resistant and more susceptible to deformation. However, the level of this degradation varied depending on the fiber type.

To clearly visualize these variations, Figure 6.11 shows the normalized mechanical properties in terms of tensile strength, Young's modulus, and ultimate strain. The normalized values correspond to the ratio between the results of the loaded/alkaline solution conditions considered, and the values obtained for the reference condition, with no load application and no solution exposure (0N-REF). Higher ratios mean that the fibers maintained similar mechanical properties values compared to the reference fibers. On the opposite, lower values represent higher fiber degradation.

In terms of the normalized tensile strength (Fig. 6.11.a), it is clear that all treatments resulted in a higher level of maintenance of the tensile strength after the degradation tests. After exposure to 1M NaOH with no load application, natural sisal preserved only 48% of its tensile strength compared to the reference, while it was 57%, 60%, 68%, and 66% for the ALK, S100, S50, and TA modified fibers, respectively. In the same alkaline solution in a loaded condition with 1N, the same trend was observed, changing from 38% for the natural sisal to $55 \pm 2\%$ for the treated fibers. In general, the best results were reached by the TA-modified fiber, which presented a reduction of only 30% in the tensile strength after exposure to 2N-0.5M NaOH.

For the Young's modulus analysis, a similar behavior was reached for all samples, with the decrease of the Young's modulus after the degradation tests (Figure 6.11.b). However, the Young's modulus degradation level was not so expressive in the natural sisal. The lower results were reached by the S100 and S50 polymer coated fiber, for 0N-1M NaOH and 1N-1M NaOH, respectively. The TA-modified fiber also presented the best results in terms of Young's modulus, with a reduction of around only 23% when submitted to 1M NaOH. In terms of ultimate strain, it followed an increase in opposition to the Young's modulus (Figure 6.11.c). It is expected that fiber with lower rigidity presents enhanced deformation capacity, with increased ultimate strain capacity. Consequently, the higher values of normalized ultimate strain were obtained by the S50 and S100 polymer-coated fibers.

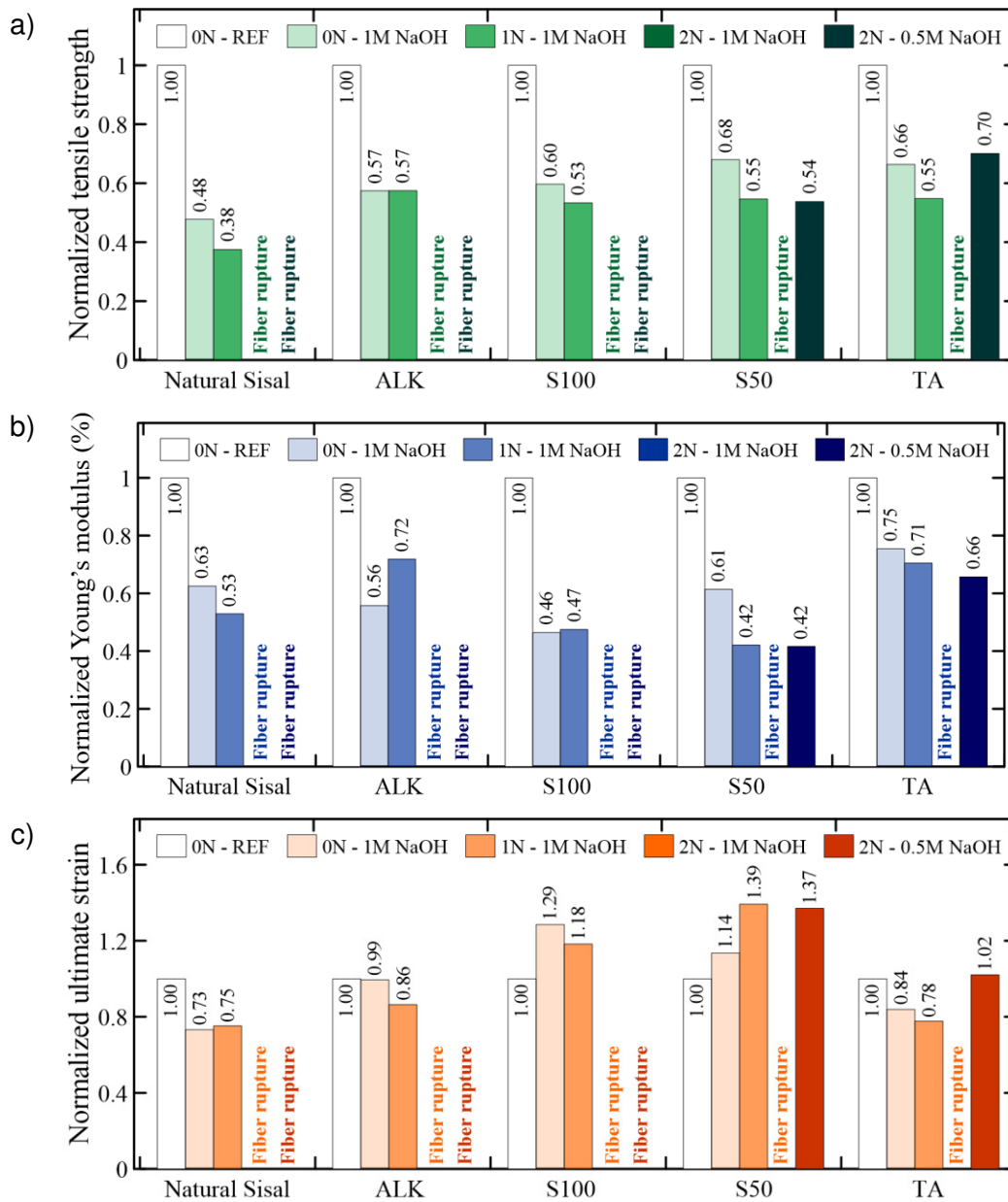


Figure 6.11 – Normalized mechanical properties of the studied fibers after the creep tests: (a) tensile strength, (b) Young's modulus, and (c) ultimate strain.

6.4. Conclusions

An experimental investigation was performed on the time-dependent behavior on the single fiber level. Natural and modified sisal fibers were tested in different load and environmental conditions. A clear fiber modification influence was found with the tensile response of the fibers. The following conclusions can be made:

- The humidity presence significantly influences the creep behavior of sisal fibers. The fiber water uptake increases the creep strain level of the natural fibers;
- Load level has more influence on the time-dependent strain level than the alkaline solution aggressivity;
- All single fiber tensile specimens loaded at 16% of the quasi-static capacity in 1M NaOH alkaline solution broke over time. This was attributed to the extremely alkaline environment of the fibers, which resulted in an excessive fiber degradation;
- Improvements in the characteristic properties in creep of sisal fiber were obtained with fiber modification, presenting a lower creep strain level when compared to as-received sisal;
- All treatments resulted in a higher level of maintenance of the tensile strength after the degradation tests. The best results were obtained for the TA-modified fiber, followed by the S50 polymer-coated fiber.

Thus, this study enables to the understanding of the creep behavior of sisal fibers in order to predict the performance of sisal fiber composites. However, the single-fiber tensile creep test cannot represent true conditions in composite materials, in all their complexity. Thus, the creep behavior of composite materials reinforced with these fibers should be investigated and correlated to the results obtained. However, the results showed that the time-dependent tensile of sisal fibers should be considered as a source of the composite crack widening over time.

6.5. References

- 1 SHAHINUR, S.; HASAN, M. Natural Fiber and Synthetic Fiber Composites: Comparison of Properties, Performance, Cost and Environmental Benefits. In:___ **Encyclopedia of Renewable and Sustainable Materials**. Elsevier, 2019. p.794-802.
- 2 ASPRONE, D.; DURANTE, M.; PROTA, A.; MANFREDI, G. Potential of structural pozzolanic matrix-hemp fiber grid composites. **Construction and Building Materials**, v.25, n.6, p.2867-2874, 2011.
- 3 TOWNSEND, T. World natural fibre production and employment. In:___ **Handbook of Natural Fibres**. Elsevier, 2020. p.15-36.
- 4 CHAKRABORTY, S.; KUNDU, S. P.; ROY, A.; ADHIKARI, B.; MAJUMDER, S. B. Polymer modified jute fibre as reinforcing agent

- controlling the physical and mechanical characteristics of cement mortar. **Construction and Building Materials**, v.49, p.214-222, 2013.
- 5 AKINYEMI, B. A.; ADESINA, A. Utilization of polymer chemical admixtures for surface treatment and modification of cellulose fibres in cement-based composites: a review. **Cellulose**, v.28, p.1241-1266, 2021.
- 6 TAKEMURA, K.; MIYAMOTO, S.; KATOGLI, H. Effect of surface treatment on creep property of jute fiber reinforced green composite under environmental temperature. **Key Engineering Materials**, v.525-526, p.53-56, 2012.
- 7 BABAFEMI, A. J.; BOSHOFF, W. P. Tensile creep of macro-synthetic fibre reinforced concrete (MSFRC) under uni-axial tensile loading. **Cement and Concrete Composites**, v.55, p.62-69, 2015.
- 8 JGASSAN, J.; BLEDZKI, A. K. Influence of fiber surface treatment on the creep behavior of jute fiber-reinforced polypropylene. **Journal of thermoplastic composite materials**, v.12, p.388-398, 1999.
- 9 CISSE, O.; PLACET, V.; GUICHERET-RETEL, V.; TRIVAUDEY, F.; BOUBAKAR, M. L. Creep behaviour of single hemp fibres. Part I: viscoelastic properties and their scattering under constant climate. **Journal of Materials Science**, v.50, n.4, p.1996-2006, 2015.
- 10 PLACET, V.; CISSE, O.; GUICHERET-RETEL, V.; TRIVAUDEY, F.; BOUBAKAR, L. Viscoelastic behaviour of single hemp fibre under constant and cyclic humidity environment - Experiment and modelling. **ICCM International Conferences on Composite Materials**, 2015.
- 11 NODA, J.; TERASAKI, Y.; NITTA, Y.; GODA, K. Tensile properties of natural fibers with variation in cross-sectional area. **Advanced Composite Materials**, v.25, n.3, p.253-269, 2016.
- 12 CASTOLDI, R. de S.; SOUZA, L. M. S.; SOUTO, F.; LIEBSCHER, M.; MECHTCHERINE, V.; SILVA, F. de A. Effect of alkali treatment on physical-chemical properties of sisal fibers and adhesion towards cement-based matrices. **Construction and Building Materials**, v.345, p.128363, 2022.
- 13 CASTOLDI, R. de S.; SOUZA, L. M. S.; SILVA, F. de A. Comparative study on the mechanical behavior and durability of polypropylene and sisal fiber reinforced concretes. **Construction and Building Materials**, v.211, p.617-628, 2019.
- 14 SILVA, F. de A.; CHAWLA, N.; TOLEDO FILHO, R. D. An experimental investigation of the fatigue behavior of sisal fibers. **Materials Science and Engineering A**, v.516, n.1-2, p.90-95, 2009.
- 15 THOMASON, J. L.; CARRUTHERS, J.; KELLY, J.; JOHNSON, G. Fibre cross-section determination and variability in sisal and flax and its effects on fibre performance characterisation. **Composites Science and Technology**, v.71, n.7, p.1008-1015, 2011.
- 16 YU, Y.; JIANG, Z.; FEI, B.; WANG, G.; WANG, H. An improved microtensile technique for mechanical characterization of short plant fibers:

- A case study on bamboo fibers. **Journal of Materials Science**, v.46, n.3, p.739-746, 2011.
- 17 GUICHERET-RETEL, V.; CISSE, O.; PLACET, V.; BEAUGRAND, J.; PERNES, M.; BOUBAKAR, M. L. Creep behaviour of single hemp fibres. Part II: Influence of loading level, moisture content and moisture variation. **Journal of Materials Science**, v.50, n.5, p.2061-2072, 2015.
- 18 SIKAME TAGNE, N. R.; NDAPEU, D.; NKEMAJA, D.; TCHEMOU, G.; FOKWA, D.; HUISKEN, W.; NJEUGNA, E.; FOGUE, M.; DREAN, J. Y.; HARZALLAH, O. Study of the viscoelastic behaviour of the *Raffia vinifera* fibres. **Industrial Crops and Products**, v.124, p.572-581, 2018.
- 19 BOSHOFF, W. P.; MECHTCHERINE, V.; VAN ZJIL, G. P. Characterising the time-dependant behaviour on the single fibre level of SHCC: Part 2: The rate effects on fibre pull-out tests. **Cement and Concrete Research**, v. 39, n.9, p.787-797, 2009.
- 20 BOSHOFF, W. P.; MECHTCHERINE, V.; VAN ZJIL, G. P. Characterising the time-dependant behaviour on the single fibre level of SHCC: Part 1: Mechanism of fibre pull-out creep. **Cement and Concrete Research**, v. 39, n.9, p.779-786, 2009.
- 21 TAKEMURA, K. Effect of surface treatment to tensile static and creep properties for jute fiber reinforced composite. **High Performance Structures and Materials III**, v.85, p.143-149, 2006.
- 22 CASTOLDI, R. de S.; SOUZA, L. M. S., SILVA, F. de A. Effect of Alkali Treatment to Improve Fiber-Matrix Bonding and Mechanical Behavior of Sisal Fiber Reinforced Cementitious Composites. **RILEM-fib International Symposium on Fibre Reinforced Concrete**. p.51-60, 2021.
- 23 CASTOLDI, R. de S.; SOUZA, L. M. S., SILVA, F. de A. Mechanical evaluation of the stability of mercerized sisal fibers on alkaline environment. **Proceedings of the 5th International Conference on Natural Fibers - Materials of the Future**. p.140-142, 2021.
- 24 AMERICAN SOCIETY FOR TESTING AND MATERIALS. **ASTM C1557**: Standard Test Method for Tensile Strength and Young's Modulus of Fibers. United States, 2020.
- 25 BECKERMANN, G. W.; PICKERING, K. L. Engineering and evaluation of hemp fibre reinforced polypropylene composites: Fibre treatment and matrix modification. **Composites Part A: Applied Science and Manufacturing**, v.39, n.6, p.979-988, 2008.
- 26 VEIGAS, M. G.; NAJIMI, M.; SHAFEI, B. Cementitious composites made with natural fibers: Investigation of uncoated and coated sisal fibers. **Case Studies in Construction Materials**, v.16, e00788, 2022.
- 27 KLERK, M. D.; KAYONDO, M.; MOELICH, G. M.; VILLIERS, W. I.; COMBRINCK, R.; BOSHOFF, W. P. Durability of chemically modified sisal fibre in cement-based composites. **Construction and Building Materials**, v.241, p.117835, 2020.
- 28 CASTOLDI, R. de S.; SOUZA, L. M. S.; SILVA, F. de A. Comparative

- study on the mechanical behavior and durability of polypropylene and sisal fiber reinforced concretes. **Construction and Building Materials**, v.211, p.617-628, 2019.
- 29 F. de A. Silva, N. Chawla, R.D. de T. Filho, Tensile behavior of high performance natural (sisal) fibers. **Composites Science and Technology**, v.68, n.15-16, p.3438-3443, 2008.
- 30 TEIXEIRA, F. P.; GOMES, O. da F. M.; SILVA, F. de A. Degradation Mechanisms of Curaua, Hemp, and Sisal Fibers Exposed to Elevated Temperatures. **BioResources**, v.14, n.1, p.1494-1511, 2019.
- 31 FERREIRA, S. R.; SENA NETO, A. R.; SILVA, F. de A.; SOUZA JUNIOR, F. G.; TOLEDO FILHO, R. D. The influence of carboxylated styrene butadiene rubber coating on the mechanical performance of vegetable fibers and on their interface with a cement matrix. **Construction and Building Materials**, v.262, p.120770, 2020.
- 32 BELAADI, A.; BEZAZI, A.; BOURCHAK, M.; SCARPA, F. Tensile static and fatigue behaviour of sisal fibres. **Materials and Design**, v.46, p.76-83, 2013.
- 33 FIDELIS, M. E. A.; TOLEDO FILHO, R. D.; SILVA, F. de A.; MOBASHER, B.; MÜLLER, S.; MECHTCHERINE, V. Interface characteristics of jute fiber systems in a cementitious matrix. **Cement and Concrete Research**, v.116, p.252-265, 2019.
- 34 SEDLACHEK, K. M. **The effect of hemicelluloses and cyclic humidity on the creep of single fibers**. Atlanta, 1995. 245p. Thesis - Institute of Paper Science and Technology.
- 35 SILVA JUNIOR, I. B. **Propriedades mecânicas e fluência de compósitos cimentícios têxteis reforçados com fibras de sisal**. Rio de Janeiro, 2020. 148p. Dissertação de Mestrado – Programa de Pós-Graduação em Engenharia Civil, PUC-Rio.
- 36 HABEGER, C. C.; COFFIN, D. W.; HOJJATIE, B. Influence of humidity cycling parameters on the moisture-accelerated creep of polymeric fibers. **Journal of Polymer Science, Part B: Polymer Physics**, v.39, n.17, p.2048-2062, 2001.
- 37 OLSSON, A.-M.; SALMÉN, L.; EDER, M.; BURGERT, I. Fibre morphological effects on mechano-sorptive creep. **Wood Science and Technology**, v.44, n.4, p.475-483, 2010.
- 38 FERREIRA, S. R.; SILVA, F. de A.; LIMA, P. R. L.; TOLEDO FILHO, R. D. Effect of hornification on the structure, tensile behavior and fiber matrix bond of sisal, jute and curauá fiber cement based composite systems. **Construction and Building Materials**, v.139, p.551-561, 2017.
- 39 GODA, K.; SREEKALA, M. S.; GOMES, A.; KAJI, T.; OHGI, J. Improvement of plant based natural fibers for toughening green composites-Effect of load application during mercerization of ramie fibers. **Composites Part A: Applied Science and Manufacturing**, v.37, n.12, p.2213-2220, 2006.

- 40 WEI, J.; MEYER, C. Degradation mechanisms of natural fiber in the matrix of cement composites. **Cement and Concrete Research**, v. 73, p.1-16, 2015.
- 41 XU, Y.; WU, Q.; LEI, Y.; YAO, F. Creep behavior of bagasse fiber reinforced polymer composites. **Bioresource Technology**, v.101, n.9, p.3280-3286, 2010.

7 Conclusions and suggestions

7.1. Conclusions

In this study, the potential of sisal fibers to be used as reinforcement in cement-based matrices was exploited, presenting alternatives to overcome the aforementioned limitations, which include excessive fiber water absorption, low adhesion to cement-based matrices, and susceptibility to alkaline degradation. After the literature review, the possible scientific gaps were reported, and an experimental program was structured to meet the thesis objectives. To address the potential degradability and low performance of the natural fiber, three different fiber modifications were proposed: (i) alkaline treatment, (ii) polymer coating, and (iii) surface modification with polyphenols. From the obtained results, notable improvements were observed for all proposed treatments compared to the non-treated fiber.

The first approach proposed was the alkaline treatment, which is a well-known treatment to enhance the physical and mechanical properties of natural fibers. Even though there are several studies on alkali treatment, this thesis aimed to determine the optimum variables for the treatment procedure, including alkaline solution concentration and the effect of load applied during the treatment, focusing on the use of these fibers as reinforcement for cement-based matrices. It was found that the alkali treatment was efficient in reducing the proportion of hydrophilic constituents of the fiber, resulting in a considerable decrease in the water uptake tendency, reaching about 70% lower moisture absorption for the 5wt.% NaOH solution concentration. The fiber surface became rougher, achieving an improved mechanical interlock with the cementitious matrix, with a 118% increase in the peak debonding load. Also, the stretch of the fibers during the treatment procedure resulted in greater improvement in fiber strength and stiffness, as it avoids fiber shrinkage and improves the orientation of the fibrils.

The coating of the sisal fiber with XSBR polymers was also efficient in reducing the water absorption tendency of the fibers, with 80% less moisture

content when compared to natural sisal fibers, after exposure to humidity for 2 hours. It was reported a formation of a new layer around the fibers, was confirmed by the scanning electron microscope (SEM) and atomic force microscope (AFM) image analyses, which worked as a barrier to the moisture penetration. The low emulsion polymers also penetrated the fiber lumens, resulting in stiffer fibers. Furthermore, the interfacial adhesion between the fiber surface and the cementitious matrix was improved, as a result of the new chemical and mechanical interactions between the new polymeric layer and the cementitious matrix. Also, avoiding the swelling of the fibers is determinant to reach a denser fiber-matrix interface, with improved adhesion properties. The best results were found for the S50 fiber, changing the interfacial bond strength from ~ 2 MPa for natural sisal to ~ 5 MPa for the polymer-coated fiber.

The new facile approach for sisal fiber surface functionalization based on polyphenol chemistry was also efficient in enhancing fiber-matrix bonding as well as water absorption reduction. A two-step procedure was proposed, including the use of tannic acid (TA) and octadecylamine (ODA) solutions. A new hydrophobic layer was obtained in the fiber surface, as a result of the TA deposition and posterior reaction with ODA amine groups. Specifically, a $\sim 40\%$ decrease was recorded in the moisture absorption capacity of functionalized sisal fibers. Even though TA5-ODA2.5 modified fiber presented a slight mechanical properties degradation, it showed the best results in terms of pullout behavior improvement and reduction.

The investigations also included fiber creep tests to evaluate the influence of the treatments on the long-term performance of sisal fibers. Further insights were also reported on the effect of different aggressive environments and load levels. This was accompanied by quasi-static tensile tests, performed before and after the exposure period, in order to evaluate the fiber degradation in terms of mechanical performance. It was shown that the humidity presence significantly increases the creep of sisal fiber, which is reduced by the previous adequate treatment of the fiber. Also, the proposed treatments were efficient to decrease fiber degradation after the time-dependent tests. These results provide information about the time-dependent behavior of sisal fibers under sustained load, an important property to be considered to enable the reliable structural use of natural fiber composites as a building material.

In general, the outcome of this study provided reliable information on how sisal fibers can be modified to reach adequate performance to be considered as an alternative to synthetic fibers for cementitious composites, especially where the price and availability issues limit access to synthetic fibers.

7.2. Suggestions for future works

Notwithstanding this study has presented novel results regarding the sisal fiber performance and durability in an alkaline environment, it is evident that, in parallel, it demonstrates new demands for specific investigations that may be explored in future works.

Although the performance enhancement of sisal fibers was reached after the fiber treatments, which was the fundamental motivation of this study, no consideration was reported about the influence of fiber modification on the composite level performance. The results found for the fiber and fiber-matrix interface level could not represent the totally accurate conditions as a real reinforcement embedded into composite materials. Since the study has contributed to an advance of knowledge on the fiber modification and durability of sisal fibers, these results can be used as input data by researchers eventually interested in performing analytical and experimental analysis at the composite level and continuing to evaluate their potential to be employed in field applications.

Appendix A

Different fiber treatments proposed by previous authors

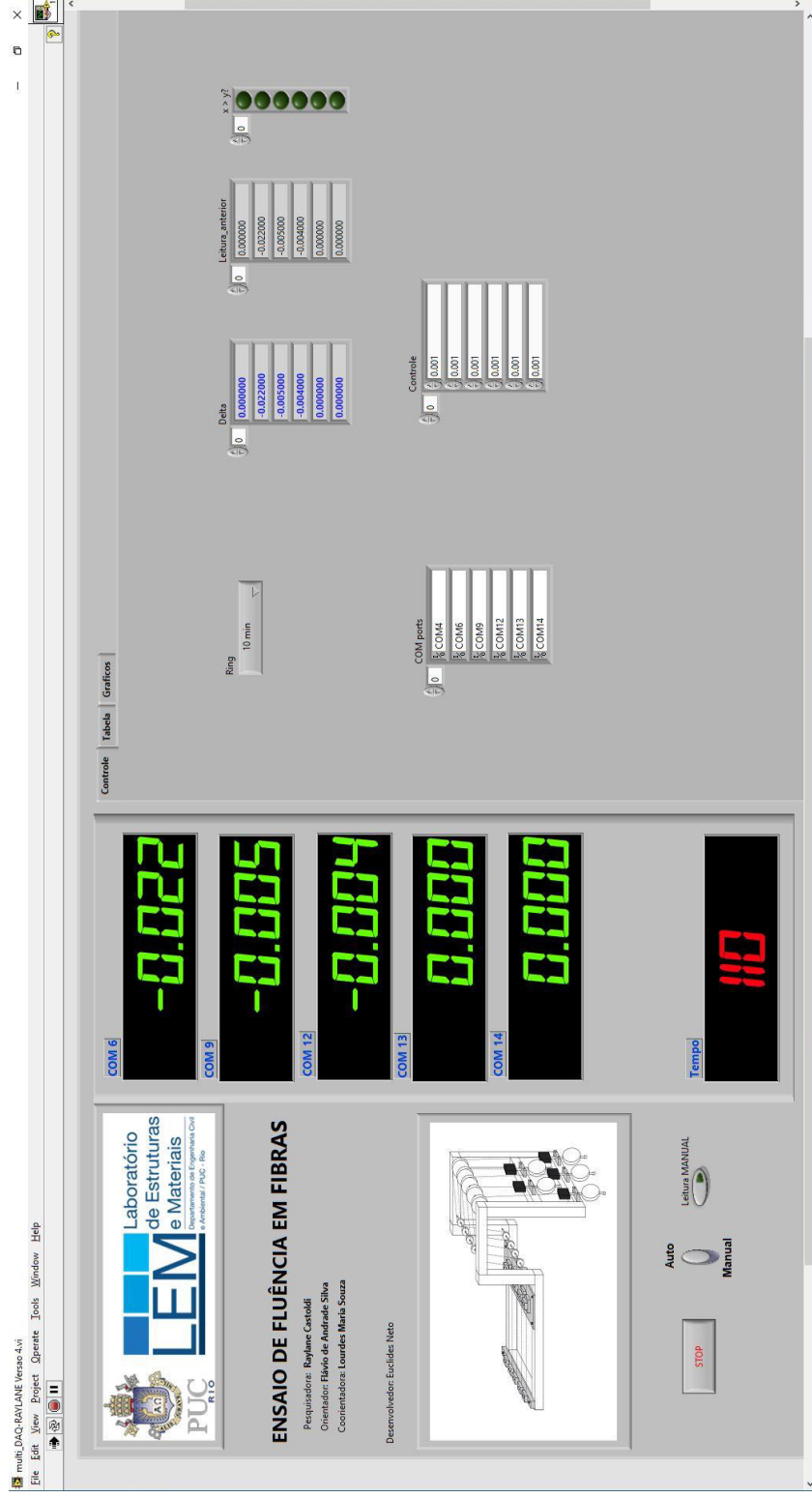
Fiber	Treatment	Chemical used	Tensile strength	Young's Modulus	Elongation at break	Interfacial Strength	Ref.
Sisal, curauá and jute	Hornification	10 cycles	470, 815, 324 MPa	17.6, 81.4, 33.46 GPa	0.05, 0.019, 0.008 mm/mm	0.42, 0.32, 0.42 MPa	[1]
Sisal	Hornification	10 cycles	470 MPa	17.6 GPa	-	0.42 MPa	[2]
Sisal, curauá and jute	Hornification	10 cycles	470, 815, 543 MPa	17.6, 81.4, 38.41 GPa	0.05, 0.019, 0.01 mm/mm	0.42, 0.32, 0.42 MPa	[3]
Sisal	Hornification	10 cycles	470 MPa	17.6 GPa	0.043 mm/mm	0.42 MPa	[4]
Pine, unbleached eucalyptus	Hornification	4 cycles	-	-	-	-	[5]
	Hornification	10 cycles	474 MPa	18.05 GPa	0.05 mm/mm	0.42 MPa	
	Alkali treatment	Ca(OH) ₂	708 MPa	22.66 GPa	0.03 mm/mm	0.39 MPa	[6]
Sisal	Polymer impregnation	Styrene butadiene	722 MPa	23.98 GPa	0.03 mm/mm	0.49 MPa	
	Horn. + polymer impreg.	Water + Styr. butad.	727 MPa	25.04 GPa	0.05 mm/mm	0.86 MPa	
Sisal	Hornification	10 cycles	353 MPa	15.72 GPa	1 mm/mm	0.21 MPa	[7]
Sisal, refugo, field brush	Hornification	10 cycles	353, 272, 322 MPa	-	-	0.28, 0.25, 0.19 MPa	[8]
Sisal	Na ₂ CO ₃	Na ₂ CO ₃	217, 137 MPa	27.4, 22.4 GPa	0.05, 0.035 mm/mm	-	[9]
Jute	Polymer impregnation	Styrene butadiene	281 MPa	34 GPa	-	0.37 MPa	[10]
	Mercerisation	NaOH	5, 5.9 MPa	7, 7.9 GPa	-	-	[11]
Flax, hemp	Acetylation	Acetic acid + H ₂ SO ₄	6.4, 4.4 MPa	7.5, 7.4 GPa	-	-	
Curauá	Alkalization	Ca(OH) ₂	697 MPa	39 GPa	2.01%	0.59 MPa	[12]
Curauá	Alkalization	Ca(OH) ₂	-	-	-	2.22 N	[13]
Bagasse	Silane	RSi(OR') ₃	-	-	-	-	[14]
Jute	Alkalization	NaOH	-	-	-	-	[15]
	Biopolymeric treatment	Cellulose acetate	475 MPa	15.2 GPa	3.37%	0.1 MPa	
Sisal		Cassava starch	415 MPa	13.09 GPa	3.97%	-	[16]
		Hydrophobic starch	467 MPa	14.93 GPa	6.30%	-	
Sisal	Acetate treatment	Acetate polymer	475 MPa	15.2 GPa	0.034 mm/mm	0.1 MPa	[17]
Coir	Alkalization	NaOH	-	-	-	-	[18]

- 1 S. R. FERREIRA, F. DE ANDRADE SILVA, P. R. L. LIMA, R. D. TOLEDO FILHO, Effect of Natural Fiber Hornification on the Fiber Matrix Interface in Cement Based Composite Systems. **Key Engineering Materials**, v.668, p.118-125,2015.
- 2 FERREIRA, S. R.; LIMA, P. R. L.; SILVA, F. de A.; TOLEDO FILHO, R. D. Effect of Sisal Fiber Hornification on the Fiber-Matrix Bonding Characteristics and Bending Behavior of Cement Based Composites. **Key Engineering Materials**, v. 600, p.421-432, 2014.
- 3 FERREIRA, S. R.; SILVA, F. de A.; LIMA, P. R. L.; TOLEDO FILHO, R. D. Effect of hornification on the structure, tensile behavior and fiber matrix bond of sisal, jute and curauá fiber cement based composite systems. **Construction and Building Materials**, v.139, p.551-561, 2017.
- 4 S. FERREIRA, P. LIMA, F. SILVA, R. TOLEDO FILHO, Effect of sisal fiber hornification on the adhesion with portland cement matrices. **Revista Matéria**, v.17, n.2, p.1024-1034, 2012.
- 5 J.E.M. BALLESTEROS, S.F. SANTOS, G. MÁRMOL, H. SAVASTANO, J. FIORELLI, Evaluation of cellulosic pulps treated by hornification as reinforcement of cementitious composites. **Construction and Building Materials**, v.100, p.83-90, 2015.
- 6 FERREIRA, S. R.; SILVA, F. de A.; LIMA, P. R. L.; TOLEDO FILHO, R. D. Effect of fiber treatments on the sisal fiber properties and fiber-matrix bond in cement based systems. **Construction and Building Materials**, v.101, p.730-740, 2015.
- 7 R. DE JESUS SANTOS, P.R.L. LIMA, Effect of Treatment of Sisal Fiber on Morphology, Mechanical Properties and Fiber-Cement Bond Strength. **Key Engineering Materials**, v. 634, p.410-420, 2014.
- 8 LIMA, P. R. L.; SANTOS, R. J.; FERREIRA, S. R.; TOLEDO FILHO, R. D. Characterization and treatment of sisal fiber residues for cement-based composite application. **Engenharia Agrícola**, v.34, n.5, p.812-825, 2014.
- 9 WEI, J.; MEYER, C. Improving degradation resistance of sisal fiber in concrete through fiber surface treatment. **Applied Surface Science**, v.289, p.511-523, 2014.
- 10 FIDELIS, M. E. A.; TOLEDO FILHO, R. D.; SILVA, F. de A.; MOBASHER, B.; MÜLLER, S.; MECHTCHERINE, V. Interface characteristics of jute fiber systems in a cementitious matrix. **Cement and Concrete Research**, v.116, p.252-265, 2019.
- 11 SNOECK, D.; SMETRYNS, P.-A.; BELIE, N. D. Improved multiple cracking and autogenous healing in cementitious materials by means of chemically-treated natural fibres. **Biosystems Engineering**, v.139, p.87-99, 2015.
- 12 ZUKOWSKI, B.; SILVA, F. de A.; TOLEDO FILHO, R. D. Design of strain hardening cement-based composites with alkali treated natural curauá fiber. **Cement and Concrete Composites**, v.89, p.150-159, 2018.
- 13 ZUKOWSKI, B.; SANTOS, E. R. F.; MENDONÇA, Y. G. dos S.; SILVA, F. de A.; TOLEDO FILHO, R. D. The durability of SHCC with alkali treated curauá fiber exposed to natural weathering. **Cement and Concrete Composites**, v.94, p.116-125, 2018.
- 14 K. BILBA, M.A. ARSENE, Silane treatment of bagasse fiber for reinforcement of cementitious composites. **Composites Part A: Applied**

- Science and Manufacturing**, v.39, n.9, p.1488-1495, 2008.
- 15 KUNDU, S. P.; CHAKRABORTY, S.; ROY, A.; ADHIKARI, B.; MAJUMDER, S. B. Chemically modified jute fibre reinforced non-pressure (NP) concrete pipes with improved mechanical properties. **Construction and Building Materials**, v.37, p.841-850, 2012.
- 16 LIMA, P. R. L.; SANTOS, H. M.; CAMILLOTO, G. P.; CRUZ, R. S. Effect of Surface Biopolymeric Treatment on Sisal Fiber Properties and Fiber-Cement Bond. **Journal of Engineered Fibers and Fabrics**, v.12, n.2, p.59-71, 2018.
- 17 CRUZ, H. M.; LOPES, P. Cellulose acetate treatment of sisal fiber for cement based composites. **Materials Science**, 2015.
- 18 L. YAN, N. CHOUW, L. HUANG, B. KASAL, Effect of alkali treatment on microstructure and mechanical properties of coir fibres, coir fibre reinforced-polymer composites and reinforced-cementitious composites. **Construction and Building Materials**, v.112, p.168-182, 2016.

Appendix B

Program interface developed in LabView to automatically record the fiber deformation



multi-DAC-RAMLANE Versão 4.01

File Edit View Project Operate Tools Window Help



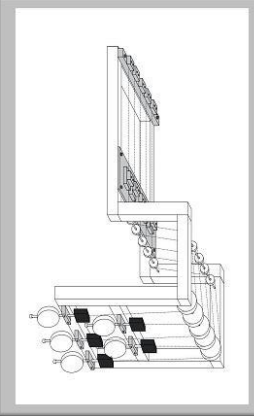
ENSAIO DE FLUÊNCIA EM FIBRAS

Pesquisadora: Raylane Castoldi
 Orientador: Flavio de Andrade Silva
 Coordenadores: Lourdes Maria Souza
 Desenvolvedor: Euclides Neto

STOP

Auto
Manual

Leitura MANUAL



COM 6

-0.0222

COM 9

-0.0005

COM 12

-0.0004

COM 13

0.0000

COM 14

0.0000

Tempo

87

Control | Tabela | Graficos

COM 6	COM 9	COM 12	COM 13	COM 14	TEMPO
-0.022000	-0.000500	-0.003500	0.000000	0.000000	25.000000
15.104600	-0.000800	-0.003500	0.000000	0.000000	39.000000
5.929300	-0.000800	-0.003500	0.000000	0.000000	41.000000
-0.021000	-0.000800	-0.003500	0.000000	0.000000	43.000000
-0.021000	13.665300	-0.003500	0.000000	0.000000	53.000000
-0.021000	8.095800	-0.003500	0.000000	0.000000	57.000000
-0.022000	-0.003500	-0.003500	0.000000	0.000000	59.000000
-0.022000	-0.003500	5.995300	0.000000	0.000000	69.000000
-0.022000	-0.003500	-0.004000	0.000000	0.000000	71.000000

multi_DAQ-PAN/ANLE Versão 4.xi

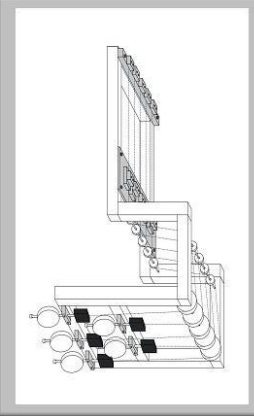
File Edit View Project Operate Tools Window Help

Logo: PUC RIO, LEM de Estruturas e Materiais, Departamento de Engenharia Civil e Ambiental / PUC - Rio

ENSAIO DE FLUÊNCIA EM FIBRAS

Pesquisador: Raylane Castoldi
Orientador: Flavio de Andrade Silva
Coordenadores: Lourdes Maria Souza

Desenvolvedor: Euclides Neto



STOP

Auto
Manual

Leitura MANUAL

COM 6: -0.0222
COM 9: -0.0005
COM 12: -0.0005
COM 13: 0.0000
COM 14: 0.0000

Tempo: 122

Controle | Tabela | Graficos

XY COM6: Amplitude vs Time (Plot 0)

XY COM9: Amplitude vs Time (Plot 0)

XY COM12: Amplitude vs Time (Plot 0)

XY COM13: Amplitude vs Time (Plot 0)

XY COM14: Amplitude vs Time (Plot 0)